Modelling and Control of Kinematically Complex Robotic Systems

Modellering og regulering av roboter med komplekse kinematiske strukturer

Philosophiae Doctor (PhD) Thesis

Cong Dung Pham

Department of Mathematical Sciences and Technology
Faculty of Environmental Science and Technology
Norwegian University of Life Sciences

Ås 2015

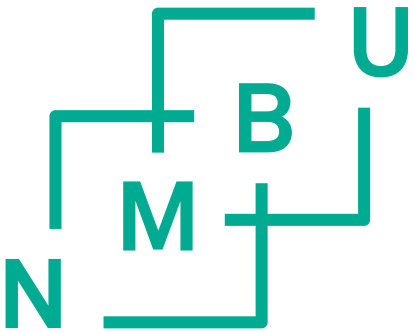

Thesis number 2015:80
ISSN 1894-6402
ISBN 978-82-575-1316-0

Summary

This thesis is concerned with modelling and control of kinematically complex robotic systems.

The thesis is divided into four main parts. Part I is concerned with a large class of robotic systems, namely vehicle-manipulator systems. One application of such systems is teleoperation in a distant environment. We are mainly concerned with efficient and intuitive teleoperation of vehicle-manipulator systems. The main contribution of this part is a control allocation approach to teleoperation which results is smoother and more efficient control, as well as faster and more intuitive operation.

Part II deals with robotics-assisted minimally invasive surgery (RAMIS). Specifically we address the constraints imposed by the entry point of RAMIS, which are commonly referred to as the Remote Center of Motion (RCM). The manipulator kinematics with velocity constraints are presented analytically.

In Part III, we present a detailed study on the effects of passive joints on manipulators. Both serial and parallel manipulators are investigated. We find that, for serial manipulators, we can deal with passive joints in controller while we have to consider the effects of the passive joints in the design of parallel manipulators.

In Part IV, we propose a new agricultural platform that is developed by our group. CAN and CANopen have been implemented, which makes the robot very versatile. It also makes it easy to expand and adapt the robot for many different applications.

Sammendrag

Denne oppgaven omhandler modellering og regulering av roboter med komplekse kinematiske strukturer. Oppgaven er delt inn i fire hoveddeler.

Del I omhandler en stor gruppe robotsystemer kalt kjøretøy-manipulator systemer. En anvendelse av slike systemer er fjernstyring. Vi er først og fremst interessert i effektiv og intuitiv fjernstyring av kjøretøy-manipulator systemer. Det største bidraget i denne delen er en «control allocation» tilnærming til fjernstyring som resulterer i en jevnere og mer effektiv regulering av roboten, så vel som raskere og mer intuitiv styring.

Del II omhandler robotisert kikkhullskirurgi (RAMIS). Vi adresserer spesifikt de kinematiske begrensninger som følger av RAMIS, som er ofte referert til som «Remote Center of Motion» (RCM). Manipulatorens kinematikk med hastighetsbegrensninger presenteres analytisk.

I del III presenterer vi en detaljert studie av effekten av passive robotledd. Både manipulatorarmer og parallelle strukturer blir undersøkt. Vi konkluderer at for manipulatorarmer kan vi håndtere passive ledd i styringssystemet, mens vi må håndtere virkningene av passive ledd i designet av parallelle manipulatorer.

I del IV foreslår vi en ny landbruksplattform som er utviklet av vår forskergruppe. CAN og CANopen er implementert, noe som gjør roboten veldig allsidig. Det gjør det også enkelt å utvide og tilpasse roboten for mange forskjellige bruksområder.

Contents

Preface

This thesis is submitted in partial fulfilment of the requirements for the degree of Doctor of Philosophy at the Norwegian University of Life Sciences. The research presented in this thesis is the results of my doctoral studies in the period February 2012 through September 2015.

During my PhD, I was fortunate enough to cooperate with some very good Professors from several research institutions: Prof. Jan Tommy Gravdahl from Norwegian University of Science of Technology; Prof Fernando Lizarralde and Prof. Liu Hsu from Federal University of Rio Janeiro; Prof. Rolf Johansson from Lund University.

I also visited Federal University of Rio Janeiro in two months in 2013. It is a great opportunity and experiment for me.

Publications

The material presented in this thesis is based on the papers listed below. The chapters in which the papers occur are included for each paper. The papers that are included are market with an asterisk. The main contributions are found in Part I and Part II.

Part I - Control Allocation for Teleoperation of Kinematically Dissimilar Robots

1. **Control Allocation for Mobile Manipulators with On-board Cameras***
   C. D. Pham and P. J. From
   IEEE International Conference on Intelligent Robots and Systems, Tokyo, Japan, 2013.
   Chapter 2.

2. **Evaluation of Subjective and Objective Performance Metrics for Haptically Controlled Robotic Systems***
   C. D. Pham, P. H. N. Trinh and P. J. From
   Modeling, Identification and Control, 2014.
   Chapter 3.

3. **Comparison of Mental and Theoretical Evaluations of Remotely Controlled Mobile Manipulators**
   C. D. Pham, P. H. N. Trinh and P. J. From
   19th World Congress of the International Federation of Automatic Control, Cape Town, South Africa, 2014.
   This paper is partially covered by Pham et al. [2014c], see Chapter 3.

4. **A Control Allocation Approach to Haptic Control of Underwater Robots**
   C. D. Pham, C. Spiten and P. J. From
   IEEE International Workshop on Advanced Robotics and its Social Impacts, Lyon, France, 2015.

Part II - Kinematically Constrained Serial Manipulators

5. **An Analytical Approach to Operational Space Control of Robotic Manipulators with Kinematic Constraints***
   C. D. Pham, F. Coutinho, F. Lizarralde, L. Hsu and P. J. From
   19th World Congress of the International Federation of Automatic Control, Cape Town, South Africa, 2014.
   Chapter 4.

6. **Abordagem analítica para controle no espaço operacional de manipuladores com restrições cinemáticas**
   F. Coutinho, P. J. From, **C. D. Pham**, F. Lizarralde
   XIX Congesso Brasileiro de Automatica, 2015.
   This paper is partially covered by Pham et al. [2014a], see Chapter 4.

7. **Dynamic Manipulability of Velocity-constrained Serial Robotic Manipulators***
   C. D. Pham and P. J. From
   IEEE International Conference on Robotics and Biomimetics, Bali, Indonesia, 2014.
   Chapter 5.

8. **Analysis of a Moving Remote Center of Motion for Robotics-Assisted Minimally Invasive Surgery***
   C. D. Pham, F. Coutinho, A. Leite, F. Lizarralde, P. J. From and R. Johansson
   IEEE/RSJ International Conference on Intelligent Robots and Systems, Hamburg, Germany, 2015.
   Chapter 6.

9. **Singularity Analysis of Robotic Manipulators with Velocity-Constraints for Minimally Invasive Surgery***
   C. D. Pham and P. J. From
   IEEE International Conference on Robotics and Biomimetics, Zhuhai, China, 2015.
   Chapter 7

Part III - Kinematic Analysis of Parallel Manipulators

10. **A Geometric Approach to the Design of Serial and Parallel Manipulators with Passive Joints***
    C. D. Pham, P. J. From and J. T. Gravdahl
    Applied Mathematics, 2014.
    Chapter 8.

11. **Fault Tolerance of Parallel Manipulators with Passive Joints**
    P. J. From, **C. D. Pham** and J. T. Gravdahl
    Proceedings in Applied Mathematics and Mechanics, 2014.
    This paper is partially covered by Pham et al. [2014b], see Chapter 8.

Part IV - Agricultural Robotics

Chapter 1

Introduction

1.1 Kinematically Complex Robotic Systems

Robots take many different forms. Some common examples are serial manipulators, parallel manipulators, mobile vehicles and mobile manipulators. The main groups of robots can be characterized by different kinematic structures. Kinematics thus represent one of the fundamental problems in robotics and is the starting point of all modelling and controller-design of any robot.

All of the platforms discussed in this thesis have very different kinematics and thus require different approaches to modelling and control. In this thesis we therefore discuss several topics on modelling and control of robots with different kinematic structures, and in particular robots that have complex kinematics that are challenging from a modelling and control point of view.

1.1.1 Robotics

Robotics has a long development history. The first industrial robot was Unimate, (Fig. 1.1a), a serial manipulator that was created by George Devol. It worked on a General Motors assembly line at the Inland Fisher Guide Plant in Ewing Township, New Jersey, in 1961 (Nof [1999]). A serial manipulator is an open-loop kinematic chain that consists of a sequence of rigid bodies (links) connected by joints. A serial manipulator is normally a link between a fixed base and an end effector tool. In general, a serial manipulator needs 6 degree of freedom to control both the position and orientation of its end effector in the three-dimensional space (Siciliano and Khatib [2008]).

Another important class of robots is parallel manipulators. A parallel manipulator is a closed-loop mechanism that contains an end effector, a fixed base and at least two kinematic chains connecting the end effector and the base (Siciliano and Khatib [2008]). One of the best known parallel manipulators is formed from six linear actuators that support a movable base for devices such as flight simulators, Fig. 1.2a. It was suggested by Stewart (Merlet [2012]).

An important branch in robotics is mobile robots that can move freely in an environment (From et al. [2014a]). One early mobile robot is Shakey, Fig. 1.3a, which, starting in 1966, was developed by Charlie Rosen's group at the Stanford Research Institute

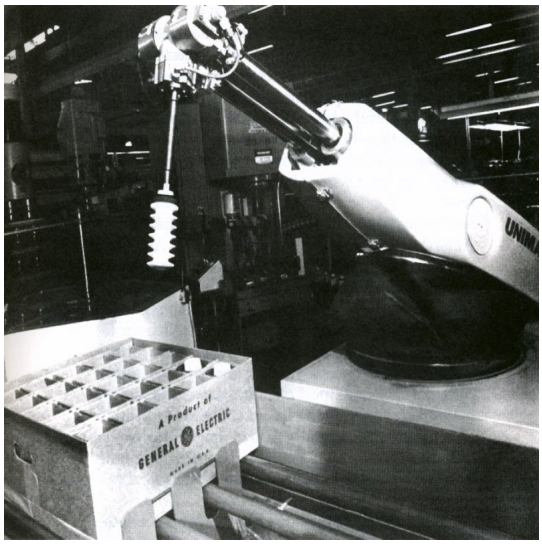

(a) The Unimate robot is a serial manipulator. It weights about two tons. The Unimate feature up to six fully programmable axes of motion. Courtesy of GE.

(b) The IRB 140 ABB serial manipulator is a six axes multipurpose industrial robot and handles a payload of 6kg with a reach of 810mm. Courtesy of ABB.

Figure 1.1: Two examples of serial manipulators

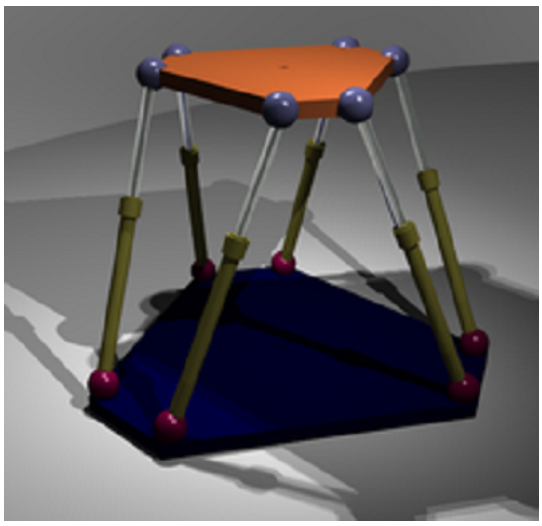

(a) The Stewart platform has six prismatic actuators. Devices placed on the top plate can be moved in the six degrees of freedom. Courtesy of Wikipedia.

(b) The ABB's IRB 360 FlexPicker is a high speed robotic picking and packing technology. Courtesy of ABB.

Figure 1.2: Two examples of parallel manipulators

(now called SRI). Shakey was the first mobile robot to reason about its actions. It used programs that gave it the ability for independent perception, world modeling, and action generation (Siciliano and Khatib [2008]). Recently mobile robots have become more common place in commercial and industrial settings.

To combine the advantages of mobile platforms and robotic manipulator arms and reduce their drawbacks, we have mobile manipulators that are robot systems built from

(a) The Shakey robot from SRI. It had a TV camera, a triangulating range finder, and bump sensors, and was connected to DEC PDP-10 and PDP-15 computers via radio and video links. Courtesy of SRI International.

(b) The BigDog is a rough-terrain robot from Boston Dynamics that walks, runs, climbs and carries heavy loads. BigDog is powered by an engine that drives a hydraulic actuation system. Courtesy of Boston Dynamic.

Figure 1.3: Two examples of mobile manipulators

a robotic manipulator arm mounted on a mobile platform. An example of mobile manipulator is PR2, Fig. 1.4a, that is build by Willow Garage.

1.1.2 Methods

In this section, we review the fundamental concepts of kinematics, Lie groups, configuration spaces, frames and finally kinematic modelling. Parts of this section is taken from From et al. [2014a].

1.1.2.1 Lie Groups

The kinematics of a mechanical system, such as a rigid body or a robotic manipulator, can be derived globally in terms of Lie groups and Lie algebra structures. More specifically, an element of the Lie group corresponds to a configuration of the mechanism while the velocity can be expressed as an element of the Lie algebra.

Formally, we can define a group $\mathcal{G}$ by identifying four important properties on the elements $g_1, g_2, g_3 \in \mathcal{G}$ given a group operation o:

Property 1.1 (Closure) A set G is closed under the group operation o if for all $g_1, g_2 \in \mathcal{G}$, then $g_1 \, o \, g_2 \in \mathcal{G}$.

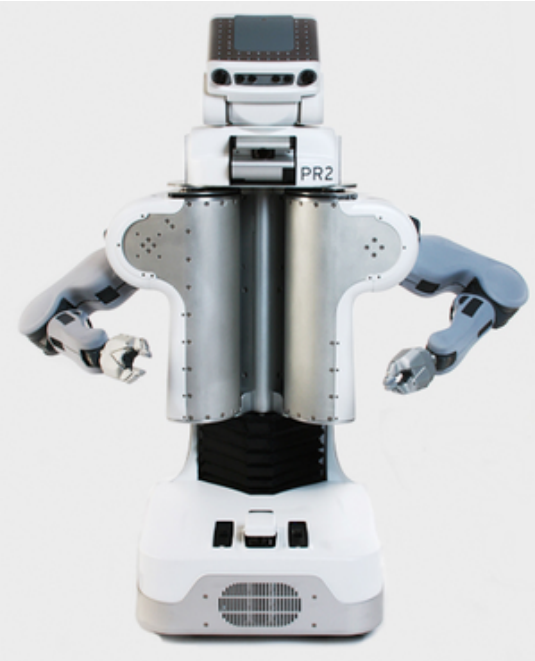

(a) The PR2 robot from Willow Garage. It has two 7-DOF arms mounted on an omnidirectional base. Courtesy of Willow Garage.

(b) The Kuka mobile manipulator consists of a five degree of freedom arm and an omnidirectional mobile platform. Courtesy of Kuka.

Figure 1.4: Two examples of mobile manipulators

Property 1.2 (Identity) A set $\mathcal{G}$ has an identity element if it is possible to find an element $e \in \mathcal{G}$ such that $g \, o \, e = e \, o \, g = g$ for every $g \in \mathcal{G}$.

Property 1.3 (Inverse) A set $\mathcal{G}$ is invertible if for each $g \in \mathcal{G}$, there exists a unique inverse $g^{-1} \in \mathcal{G}$ such that $g \, o \, g^{-1} = g^{-1} \, o \, g = e$.

Property 1.4 (Associativity) A set G is called associative if for all $g_1, g_2, g_3 \in \mathcal{G}$, then $(g_1 \, o \, g_2) \, o \, g_3 = g_1 \, o \, (g_2 \, o \, g_3)$.

Based on these properties we can formally define a group as:

Definition 1.1. *(Group) A set $\mathcal{G}$ with elements $g_1, g_2, g_3 \in \mathcal{G}$ together with a binary operation o, is called a group if it satisfies Property 1.1-Property 1.4 above.*

In robotics we are mainly interested in sets that are manifolds. A manifold is a smooth and in general curved surface embedded in the Euclidean space. We first need to define topological space.

Definition 1.2. *(Topological space) A set $\mathcal{M}$ is called a topological space if there exists a collection of open subsets of $\mathcal{M}$ for which the following axioms hold:*

1. *The union of a countable number of open sets is an open set.*
2. *The intersection of a finite number of open sets is an open set.*
3. *Both $\mathcal{M}$ and $\mathcal{O}$ are open sets.*

A manifold is defined in the following way:

Definition 1.3. *(Manifold) A topological space is a manifold if for every $x \in \mathcal{M}$, there exists an open set $U \in \mathcal{M}$ such that*

1. *$x \in \mathcal{M}$,*
2. *U is homeomorphic to $\mathbb{R}^n$,*
3. *n is fixed for all $x \in \mathcal{M}$.*

Further we want these manifolds to be differentiable, i.e., manifolds that can be represented by several coordinate charts and can be patched together in a smooth manner. We have the definition of Lie groups:

Definition 1.4. *(Lie Group) A Lie Group is a group $\mathcal{G}$ which is also a smooth manifold and for which the group operation and the inverse are smooth mappings.*

1.1.2.2 Some Important Lie Groups

There are several examples of Lie groups, many of which are widely used in robotics.

The Euclidean Space The Euclidean space $\mathbb{R}^n$ with addition as the group operator is a group. Given two elements $x = [x_1\ x_2\ \cdots\ x_n]^T \in \mathbb{R}^n$ and $y = [y_1\ y_2\ \cdots\ y_n]^T \in \mathbb{R}^n$ the group operation is given by

$$x\ o\ y = \begin{bmatrix} x_1 + y_1 \\ x_2 + y_2 \\ \vdots \\ x_n + y_n \end{bmatrix} \in \mathbb{R}^n \tag{1.1}$$

and the inverse of an element is given by

$$x^{-1} = \begin{bmatrix} -x_1 \\ -x_2 \\ \vdots \\ -x_n \end{bmatrix} \in \mathbb{R}^n\,. \tag{1.2}$$

In robotics, it presents the motion of a prismatic robotic joint with $n = 1$; if we choose $n = 2$ we get the group of linear transformations in the plane; and if we choose $n = 3$ we get the group of linear transformations in the 3-dimensional Euclidean space.

The General Linear Group The general linear group of order n consists of all $n \times n$ nonsingular real matrices and is denoted $GL(n, \mathbb{R})$. The manifold of $GL(n, \mathbb{R})$ is thus an open subset of $\mathbb{R}^{n\times n}$ defined by all matrices in $\mathbb{R}^{n\times n}$ except the ones that have determinant equal zero. The identity element is given by the $n \times n$ identity matrix and *Property 1.2* is satisfied. As we restrict ourselves to nonsingular matrices the inverse always exists and is given by the matrix inverse. Note that *Property 1.3* requires all matrix groups to be subgroups of $GL(n, \mathbb{R})$, i.e., that the inverse exists. As a result a matrix group of $n \times n$ matrices is always a subgroup of $GL(n, \mathbb{R})$.

The Special Orthogonal Group The special orthogonal group is a subgroup of the orthogonal group defined as

$$SO(n) = R \in GL(n, \mathbb{R}) | R^T R = I, det(R) = +1. \tag{1.3}$$

The special orthogonal group $SO(n)$ consists of all elements with determinant $+1$. An element of the special orthogonal group of dimension 3 is a rotation matrix and can be interpreted as pure rotational motion of a rigid body. As $R^T R = I$ we can conclude that the inverse of an element R is the same as the transpose, i.e., $R^{-1} = R^T$.

This is the group of rotations in the plane with $n = 2$. With $n = 3$, it presents the rotation motion in the 3-dimensional Euclidean space.

The Special Euclidean Group The special Euclidean group $SE(n)$ is the group of rigid body transformations on $\mathbb{R}^n$. We are especially interested in the special Euclidean group that acts on $\mathbb{R}^3$, denoted $SE(3)$. This is the set of rigid body transformations on $\mathbb{R}^3$ defined as the set of mappings $g : \mathbb{R}^3 \to \mathbb{R}^3$ given by $g(x) = Rx + p$ where $R \in SO(3)$ and $p \in \mathbb{R}^3$. The matrix representation of $SE(3)$ is typically given as

$$g = \begin{bmatrix} R & p \\ 0 & 1 \end{bmatrix}. \tag{1.4}$$

This presents both the translation with $p \in \mathbb{R}^3$ and the rotation with $R \in SO(3)$ of a rigid body.

1.1.2.3 Configuration Spaces

The configuration of a rigid body can be described by the positions of all the point masses that are part of the body. The positions of three fixed non-collinear points of the body are enough to determine the positions of all the other points. This lemma taken from Duindam [2006]

Lemma 1.1. *The space of all possible configurations of a rigid body in three dimensional space, relative to some reference frame, is the six-dimensional space $SE(3)$, which is topologically equivalent to the set $\mathbb{R}^1 \times \mathbb{R}^1 \times \mathbb{R}^1 \times \mathbb{S}^2 \times \mathbb{S}^1$.*

Proof: Suppose we have a rigid object with three non-collinear reference points on it. For the first point, p_1, we can put it freely in space so there are three degrees of freedom, $\mathbb{R}^3$. Because three point are on a rigid body so the distance between them are constant. The second point, p_2, have to be on a sphere with the center p_1 so there are two degrees of freedom, $\mathbb{S}^2$. For the last point must be both on a sphere with the center p_1 and a sphere with the center p_2. There is only one degree of freedom in positioning the last point, $\mathbb{S}^1$, (Duindam [2006]).

1.1.2.4 Reference Frames

A reference frame is a collection of points for which the distance between any two points is constant at all times. There are two types of reference frames:

- Inertial reference frames: This is chosen such that its points can be used as a reference for all other reference frames. An inertial reference frame is one whose points do not accelerate.
- Non-inertial reference frames: These can be attached on each rigid body in the system. These reference frames will then accelerate with respect to the inertial frame and are thus non-inertial. We will use these reference frames to observe the motion of each rigid body relative to the inertial frame.

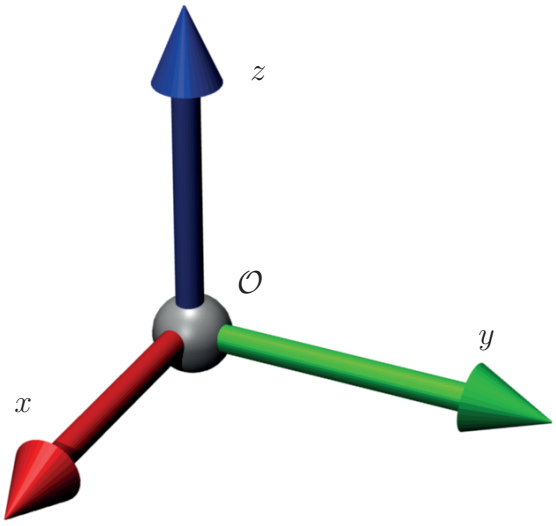

Figure 1.5: A reference frame

In a robotic system, we usually choose an inertial reference frame that is fixed, and several non-inertial reference frames that are attached to the robot.

1.1.2.5 Kinematics

The configuration of a rigid body in the three-dimensional space has six degrees of freedom (DoF) and can be presented as a vector in $\mathbb{R}^6$. The position variables of a rigid body can be presented as a vector:

$$\eta = \begin{bmatrix} x_{0b} \\ y_{0b} \\ z_{0b} \\ \phi \\ \theta \\ \psi \end{bmatrix}. \tag{1.5}$$

The configuration state can also be presented in matrix form in $SE(3)$:

$$g_{0b} = \begin{bmatrix} R_{0b} & p_{0b} \\ 0 & 1 \end{bmatrix} \in \mathbb{R}^{4\times 4}, \tag{1.6}$$

with rotation matrix $R_{0b} \in SO(3)$ and translation vector $p_{0b} \in \mathbb{R}^3$.

We just consider manipulators with 1-DoF joints, we denote by q_i the joint position of joint i. For a manipulator that has n joints, we have:

$$q = \begin{bmatrix} q_1 \\ q_2 \\ \vdots \\ q_n \end{bmatrix}. \tag{1.7}$$

For a mobile manipulator system, the configuration can be presented by:

$$\xi = \begin{bmatrix} \eta \\ q \end{bmatrix}, \tag{1.8}$$

where η is taken from (1.5) and represents the position of the vehicle and q is taken from (1.7) and gives the position of the manipulator arm.

The forward kinematics map of a manipulator gives the transformation from the base frame $\mathcal{F}_0$, inertially fixed to the base of the robot, to the end-effector frame $\mathcal{F}_e$, a non-inertial frame that is attached to the end effector, (From et al. [2014a]), and can be represented by

$$g_{0e} = \begin{bmatrix} R_{0e} & p_{0e} \\ 0 & 1 \end{bmatrix} \in \mathbb{R}^{4\times 4}, \tag{1.9}$$

where $R_{0e} \in SO(3)$ and $p_{0e} \in \mathbb{R}^3$.

The body velocity V_{0e}^B is the end-effector velocity as seen from the end-effector frame $\mathcal{F}_e$

$$V_{0e}^B = \begin{bmatrix} v_{0e}^B \\ \omega_{0e}^B \end{bmatrix}, \tag{1.10}$$

where the linear part v_{0e}^B and the rotational part ω_{0e}^B are the linear velocity and the angular velocity of the body frame $\mathcal{F}_e$ in the inertial frame $\mathcal{F}_0$ seen from the frame $\mathcal{F}_e$, respectively.

1.1.3 Challenges

For several kinematically complex robotic systems, there are still many problems to solve that apply in practical problems. Mobile manipulators, parallel manipulators and constrained manipulators are subjects that still get a lot of attention.

Firstly, the teleoperation of mobile manipulators is a very difficult task. In the nuclear disaster in Japan, there were no robots, especially mobile manipulators, that were good enough to be used in this kind of situations. More specifically, the operators find it difficult to focus on the main tasks when they have to control both the mobile base and the arm because the haptic device used to control the robot is kinematically different from the robot. This makes it challenging to map the motion of the haptic to a corresponding motion for the mobile manipulator. In this thesis, a new intelligent control allocation between the base and the manipulator arm is implemented in Pham

and From [2013], Pham et al. [2014d,c].

Secondly, control of constrained manipulators has been studied a long time but there are still many drawbacks with existing solutions. With existing solutions, constraints are not presented analytically and the original control law for non-constrained manipulators cannot be applied directly on these robots. An algorithm that helps to solve these challenges for constrained robts used in minimally invasive surgery is presented in Pham et al. [2014a], Pham and From [2014], Pham et al. [2015].

Thirdly, if the torque failure in one of the joints occur, a manipulator can collapse due to external forces. To guarantee robustness of robots, it is important to know the effects of these joint failures, i.e., what happens when an active joint becomes passive. We presented a robust approach to deal with this in Pham et al. [2014b], From et al. [2014b].

Finally, one of the main challenges to our world is supplying food to everyone. The population continues to increase, however the natural resource for agriculture is limited. Therefore we need to increase the productivity in agriculture and try to use as much land as possible. There are several plots of land that are not utilized today because it is not viable with the conventional and large machinery used in agriculture, either because the land is too small or too steep. It is not efficient and economically viable to produce food on these plots of land. Moreover, heavy agricultural machinery damages the soil permanently. We propose a robotic platform as a solution to these problems. It is a a low-cost, light-weight, and highly versatile agricultural robot presented in Grimstad et al. [2015c,b].

1.2 Part I - Control Allocation for Teleoperation of Kinematically Dissimilar Robots

Robotic manipulators are usually used to interact with its environment with dexterity and accuracy. A manipulator cannot move around so its workspace is small and limited. In contrast, mobile robots can freely move around. A system with a robot mounted on a mobile base has great potential because it combines two important properties: the mobility of the mobile base and the dexterity and manipulability of the manipulator arm Park and Khatib [2006], Seraji [1998], Farkhatdinov and Jee-Hwan [2008].

1.2.1 Kinematics of Mobile Manipulators

In this section we will describe briefly the kinematic relations of vehicle-manipulator (VM) systems, or mobile manipulators.

We start by choosing the reference frames of the system like in Fig. 1.6. We will attach a reference frame $\mathcal{F}_0$ to a fixed point (inertial reference frame) and a reference frame $\mathcal{F}_b$ to the vehicle. $\mathcal{F}_b$ also defines the base of the robot arm and is not inertial. We denote the configuration of the vehicle with respect to the inertial frame by g_{0b} like (1.9). The manipulator kinematics is given with respect to the base frame $\mathcal{F}_b$ (the vehicle), so we can use the standard formulation of the manipulator kinematics. The configuration

of the end effector of the robot is identified with the reference frame $\mathcal{F}_e$ and is defined with respect to the base frame by the homogeneous transformation matrix g_{be}. Finally the configuration of the end effector with respect to the inertial frame is given by $g_{0e} = g_{0b}g_{be}$ (From et al. [2014a]).

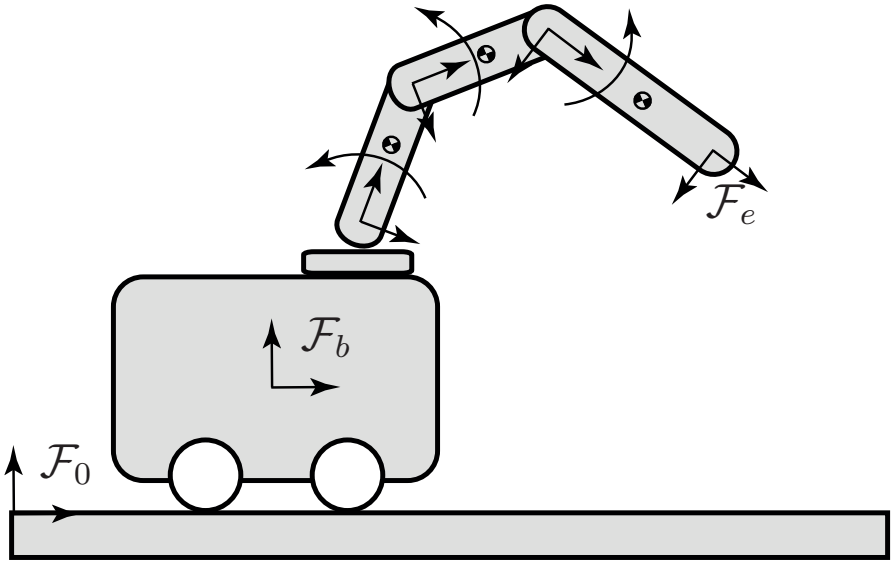

Figure 1.6: The coordinates of mobile manipulator

We can write the configuration of a vehicle-manipulator system as a vector

$$\xi = \begin{bmatrix} \eta \\ q \end{bmatrix} \in \mathbb{R}^{6+n} \tag{1.11}$$

where $\eta = [x_{0b}\, y_{0b}\, z_{0b}\, \phi_{0b}\, \theta_{0b}\, \psi_{0b}]$ and $q = [q_1\, q_2 \cdots q_n]^T$. In the case that the vehicle's configuration space is a subspace of the special Euclidean group, for example a wheeled vehicle in the plane, we can write the vehicle configuration as a vector in $\mathbb{R}^m$ and the configuration space of the vehicle-manipulator system as a vector in $\mathbb{R}^{m+n}$. The velocities of the VM system can be given in the inertial frame as

$$\dot{\xi} = \begin{bmatrix} \dot{\eta} \\ \dot{q} \end{bmatrix} \in \mathbb{R}^{6+n}. \tag{1.12}$$

1.2.2 Teleoperation

Teleoperation is a system where a user controls a robot in a distant environment. The user usually uses a haptic device, the master, to control a robot, the slave, from far away. There are three types of control architectures: i) direct control: the robot follows the user commands without any autonomy; ii) supervisory control: the user gives high level command and the robot uses its intelligence to perform tasks; iii) shared control: the robot follows the user commands with automated help (Siciliano and Khatib [2008]).

The master haptic moves in the master workspace, while the slave robot moves in the slave workspace. These workspaces are usually very different. In many cases, the

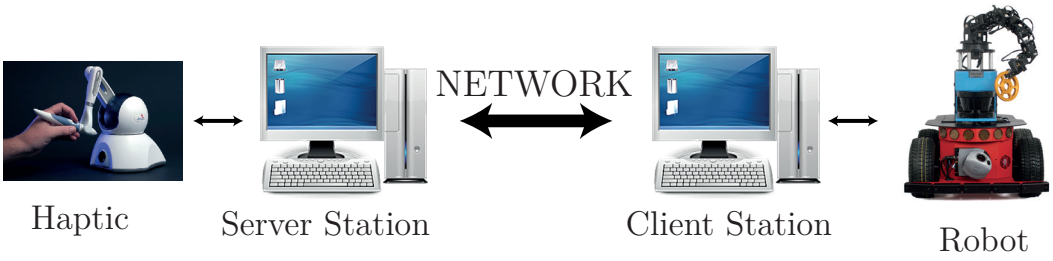

Figure 1.7: The teleoperation system scheme

master and slave robots are kinematically dissimilar mechanisms. So they require a non-trivial mapping from the master workspace to the slave workspace.

The first goal of a teleoperation system is that the slave follows the master. Normally a position-position or position-velocity architecture is applied to satisfy this requirement. The slave position or velocity are controlled by the master position.

Some systems provide not only motion information but also force feedbacks to the operator. The haptic can apply some forces to the operator who can feel the environment better. These systems are called bilateral. With position-force architecture, the user feels the interaction forces between the slave robot and the environment to get a better understanding of the environment (Siciliano and Khatib [2008]).

1.2.3 State-of-the-Art of Teleoperation Mobile Manipulators

There are some solutions to control mobile manipulators with one haptic device found in literature. The concept of operation modes is introduced to control either the mobile base (locomotion mode) or the manipulator (manipulation mode) with the haptic device.

Firstly, the operator can choose the operation mode manually, i.e., whether the vehicle or the arm is controlled. With the teleoperation system in Farkhatdinov and Jee-Hwan [2008], the operator remotely controls several different objects or several properties of the same robot using a switch to choose what object/property to control. Similarly, Farkhatdinov et al. [2008] use a switch to control either the speed of vehicle or the position of manipulator.

Secondly, Wrock and Nokleby [2011] presented an approach to choose what mode to control the VM system using the configuration of the slave manipulator. The system automatically switches between the two modes based on the slave manipulator. The mobile base just moves after the manipulator breaches it's workspace limit.

In contrast, Farkhatdinov and Jee-Hwan [2008] use the master manipulator position to automatic switch between two different operation modes. A predefined area in the master workspace is used to decide whether the vehicle or the manipulator are controlled. When the haptic is in this area, a position-to-position control scheme is applied for accurate control. On the other hand, a position-to-velocity control scheme is used for fast locomotion.

All of the switching between the operation modes described above is very apparent to the operator. It also results in a rather unintuitive control, especially when the operator sees the remote workspace through a camera fixed on the mobile base. A more intuitive

way to control mobile manipulators is thus desireable from the operator's point of view.

1.2.4 Contribution

We suggest an approach to control mobile manipulators presented in the following papers:

- **Control Allocation for Mobile Manipulators with On-board Cameras***
  C. D. Pham and P. J. From
  IEEE International Conference on Intelligent Robots and Systems, Tokyo, Japan, 2013.

- **Evaluation of Subjective and Objective Performance Metrics for Haptically Controlled Robotic Systems***
  C. D. Pham, P. H. N. Trinh and P. J. From
  Modeling, Identification and Control, 2014.

- **Comparison of Mental and Theoretical Evaluations of Remotely Controlled Mobile Manipulators**
  C. D. Pham, P. H. N. Trinh and P. J. From
  19th World Congress of the International Federation of Automatic Control, Cape Town, South Africa, 2014.

- **A Control Allocation Approach to Haptic Control of Underwater Robots**
  C. D. Pham, C. Spiten and P. J. From
  IEEE International Workshop on Advanced Robotics and its Social Impacts, Lyon, France, 2015.

The method proposed reduce the differences between the two modes, i.e., whether the mobile base or manipulator is controlled, allowing for smoother and more efficient control, as well as faster and more intuitive operation. The operator now just focuses on the main task, and does not need worry about whether the base or the arm is controlled, this is handled automatically by the controller. The theory is verified through experiments on a small mobile manipulator.

1.3 Part II - Kinematically Constrained Serial Manipulators

Minimally invasive surgery (MIS) is a surgical procedure performed through a small opening in the patient's body called the trocar, or the incision point. Because the incisions are small, MIS leads to less patient trauma, shorter recovery times and lower overall risk compared to conventional open surgery. However, MIS also has some disadvantages for the surgeon, like losing the degrees of freedom and the reversed kinematics of the surgery. Robotics can help to deal with this problem and improve the quality of MIS.

Robotics-assisted minimally invasive surgery (RAMIS) is a similar setup to MIS where a robot controls the tool. In RAMIS, the end effector is attached to a long and thin shaft used to penetrate the skin through the incision point. To avoid damaging the patients' tissues at the incision point, it is common to require that the lateral displacements at this point is kept to a minimal. The only commercially available RAMIS is the da Vinci surgical system (Fig. 1.8) that can provide the surgeon with the precision, dexterity and control of traditional open surgery, while only requiring $1-2$ cm incision points (Gomes [2011]).

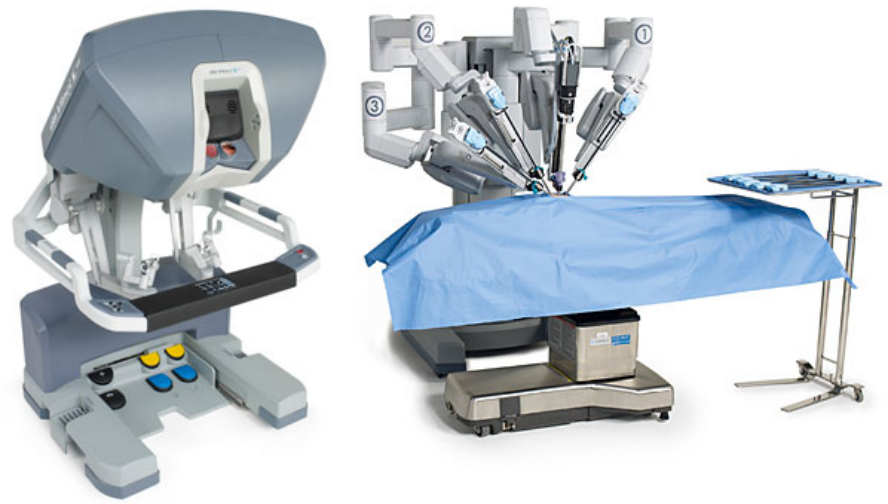

Figure 1.8: The da Vinci Surgical System. Courtesy of Intuitive Surgical, Inc.

1.3.1 Kinematics

In this section, we briefly review Jacobian, manipulability and kinematic solutions in RAMIS.

1.3.1.1 Jacobian

The standard body Jacobian matrix gives the mapping from the joint velocities $\dot{q}$ to the end-effector velocities V_{0e}^B in body coordinates which is the mapping (From et al. [2014a])

$$V_{0e}^B = J_{0e}^B(q)\dot{q}. \tag{1.13}$$

The body Jacobian matrix $J_{0e}^B(q)$ is found by representing the twist of each joint i in the end-effector frame, i.e.,

$$\begin{aligned} J_{0e}^B(q) &= \begin{bmatrix} X_1^\dagger & X_2^\dagger & \cdots & X_n^\dagger \end{bmatrix} \\ &= \begin{bmatrix} \mathrm{Ad}_{g_{1e}}^{-1} X_1^1 & \mathrm{Ad}_{g_{2e}}^{-1} X_2^2 & \cdots & X_n^n \end{bmatrix} \in \mathbb{R}^{6\times n}, \end{aligned} \tag{1.14}$$

where X_i^i is the constant twist in frame $\mathcal{F}_i$ and $\mathrm{Ad}_{g_{ie}}^{-1}$ is the Adjoint matrix that transforms X_i^i from frame $\mathcal{F}_i$ to $X_i^\dagger$ represented in the end-effector frame $\mathcal{F}_e$.

1.3.1.2 Manipulability

One of the most important evaluation criteria in controlling manipulators is that we need to know how easy it is for the manipulator to change the position and orientation of the end effector, i.e, how much energy is required. The manipulability index, introduced in Yoshikawa [1985b], gives us this information by calculating the distance to singular configuration.

Given the manipulability Jacobian $J_M \in \mathbb{R}^{r\times n}$, the (kinematic) manipulability matrix is given by

$$W = J_M J_M^{\mathsf{T}}, \tag{1.15}$$

and the manipulability measure as

$$w = \sqrt{\det\left|J_M J_M^{\mathsf{T}}\right|}. \tag{1.16}$$

For non-redundant robots where $r = n$, the manipulability measure is given simply by

$$w = \left|\det J_M\right|. \tag{1.17}$$

1.3.1.3 Kinematic Solutions in Robotics-Assisted Minimally Invasive Surgery

Robotics-Assisted Minimally Invasive Surgery is a redundant robot manipulator. We want to control the motion at the end effector while the incision point does not allow any lateral motions. An example of the system is shown in Fig. 1.9. The frame at the incision point is denoted $\mathcal{F}_c$. The frame of the joint located before the incision point and the joint that is located after the incision point is denoted by $\mathcal{F}_a$ and $\mathcal{F}_b$, respectively.

Normally, a hole constraint is applied at $\mathcal{F}_c$ that does not allow any lateral motions to prevent the damage to patients.

The desired end-effector motion is given by the frame $\mathcal{F}_e$. We will denote the velocity variables in the following way

$$V_{0e}^B = \begin{bmatrix} v_x^e & v_y^e & v_z^e & \omega_x^e & \omega_y^e & \omega_z^e \end{bmatrix}^{\mathsf{T}} \tag{1.18}$$

and similarly for the other frames. V_{ij}^B is thus the velocity in body coordinates of a rigid body with frame $\mathcal{F}_j$ with respect to the frame $\mathcal{F}_i$. V_{ij}^B is an element of the Lie algebra $se(3)$ of the Special Euclidean Group SE(3), and is found as $V_{ij}^B = g_{ij}^{-1}\dot{g}_{ij}$ where g_{ij} is the homogeneous transformation matrix describing the location of $\mathcal{F}_j$ in $\mathcal{F}_i$.

For RAMIS the Jacobian takes a rather different form compared to (1.14):

$$\bar{J}_a^B = \begin{bmatrix} \sum \alpha_i X_i^\dagger & \sum \alpha_j X_j^\dagger & \cdots & \sum \alpha_k X_k^\dagger \end{bmatrix} \in \mathbb{R}^{m\times 6}, \tag{1.19}$$

for some $(n-m)$-dimensional constraint. This Jacobian takes in to account the constraints of the incision point, and is denoted the Constrained Jacobian. Here the bar in $\bar{J}_a^B$ distinguishes the Constrained Jacobian Matrix from the standard Jacobian J_a^B. $X_i^\dagger$ are the manipulator twists while α_i are configuration-dependent functions of the

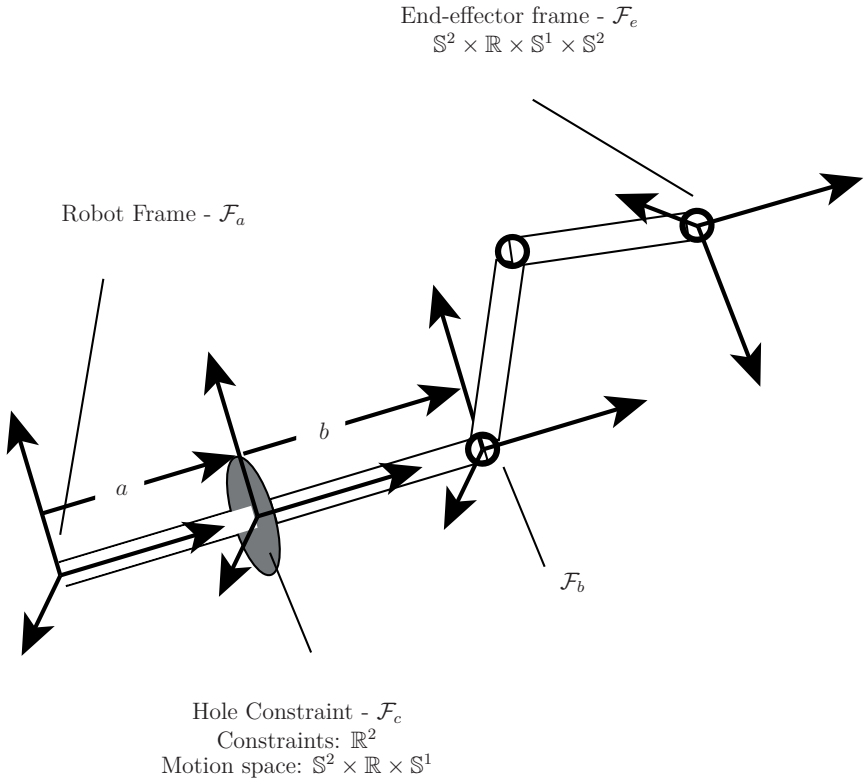

Figure 1.9: An example of constraints manipulators: a hole constraint which prevents any lateral motion of a specific point on the manipulator chain. The constrained link is constrained at the point $\mathcal{F}_c$ which, in turn, results in a reduced motion space at $\mathcal{F}_a$. The motion spaces of the different frames are subgroups of $SE(3)$ defined by linear motion $\mathbb{R}$, circular motion $\mathbb{S}$, and the sphere $\mathbb{S}^2$.

manipulator and constraint kinematics.

The Constrained Jacobian Matrix for a hole-shaped constraint can for example be found as

$$\bar{J}_a^B = \begin{bmatrix} X_1^\dagger - \frac{1}{a}X_5^\dagger & X_2^\dagger + \frac{1}{a}X_4^\dagger & X_3^\dagger & X_6^\dagger & X_7^\dagger & X_8^\dagger \end{bmatrix} \in \mathbb{R}^{6\times 6}\,. \tag{1.20}$$

1.3.2 State-of-the-Art of Robotics-Assisted Minimally Invasive Surgery

We can divide the different kinds of constrained robotics in two groups:

- Physical constrained systems;
- Virtual constraints.

Parallel manipulators or closed-chain mechanisms are systems with physical constraints. This constraint is from the systems itself, i.e., the hardware of the system. The second group can be guided robot systems or software-based constraints, and are denoted virtual or artificial constraints.

1.3.2.1 Hardware-based Solutions

The constraints imposed by the entry point of RAMIS are commonly referred to as the Remote Center of Motion (RCM). The RCM can be obtained mechanically by using a parallel device that keeps the RCM fixed, such as in the DaVinci robot from Inuitive Surgical (Guthart and Salisbury Jr [2000]). This is a safe solution, but not flexible when it comes to changing the RCM during surgery.

1.3.2.2 Software-based Solutions

There is a wide variety of approaches to deal with software-based constrained systems. When the manipulator position is constrained by the task geometry, the force control (Mason [1981]) or hybrid position/force control (Raibert and Craig [1981]) can be used to satisfy the constraint.

One of the first theories for obstacle avoidance of manipulators was potential field (Khatib [1986]). Normally two types of potential fields are applied to the robot: i) an attractive potential U_a that pushes the robot end effector towards its desired position and a repulsive field U_{ri} that pushes each link of the robot and the robot end effector away from the obstacles.

The potential field in principle guarantees that the robot does not hit the obstacles, as the artificial force pushes the robot away from the obstacle with a higher force as the distance to the obstacle reduces. Although the strength of the potential field can be tuned, the formulation does not allow for exact positioning of the robot with respect to the obstacles.

The obstacle avoidance for redundant manipulators has also been given a lot of attention. One approach is to let end-effector velocities be controlled with the first priority while the constraint is given the second priority task that is controlled in null-space of the Jacobian matrix (Maciejewski and Klein [1985], Nakamura et al. [1987]). The Jacobian contained two parts: i) end-effector Jacobian; and ii) obstacle avoidance Jacobian. This method could not guarantee satisfying the constraint. It also did not treat the end effector and the constraint in the same way.

More specifically, when inserting the robotic tool into the patient it is crucial to avoid any lateral motion. Early results solved the motion constraints as a general optimization problem, for example in Funda et al. [1996]. In Ortmaier and Hirzinger [2000], the RCM kinematics was derived and used to estimate the position of the entry point for a robot with passive joints. The passive joints guarantee that no forces are exerted to the entry point. In Locke and Patel [2007] the kinematic model was used to derive an optimization technique that allows isotropy of the surgical tool to be evaluated subject to the RCM constraint. Trocar kinematics was also discussed in Mayer et al. [2004].

Another approach combined hybrid force/position control and Natural Admittance Control (NAC) that used to control RAMIS (Deal et al. [2012]). With this controller, the portal constraints was guaranteed and at the same time allows for compliant behavior at the end-effector. The resulting controller divided the control efforts into a 2-DoF stiff control at the entry point and a 4-DoF NAC controller at the end effector. Generally,

robot dynamics may be expressed as:

$$Q + Jw = M(q)\ddot{q} + C(q, \dot{q})\dot{q} + g(q), \tag{1.21}$$

where Q is a vector of motor efforts, J is the Jacobian matrix, $M(x)$ is the inertia matrix, $C(q, \dot{q})$ is the Coriolis and centripetal matrix and $g(q)$ is the potential forces. The hybrid position/NAC controller was then given by:

$$Q_{hybrid} = Q_{vel,pos} + Q_{vel,nac} + Q_g + Q_{nac,phys} + Q_{nac,virt}, \tag{1.22}$$

where the contributions are due to desired velocity, $Q_{vel,pos}$, due to ideal joint velocities, $Q_{vel,nac}$,due to gravitational loads, Q_g, due to physical forces/moments acting on the tool tip (interaction efforts), $Q_{nac,phys}$, and due to emulation of virtual forces/torques attributable to virtual springs and dampers acting on the endpoint, but instantiated through computed motor efforts, $Q_{nac,virt}$.

We note that none of these approaches can control both RCM and end effector at the same time.

1.3.3 Contribution

The proposed approach is presented in the following papers:

- **An Analytical Approach to Operational Space Control of Robotic Manipulators with Kinematic Constraints***
  C. D. Pham, F. Coutinho, F. Lizarralde, L. Hsu and P. J. From
  19th World Congress of the International Federation of Automatic Control, Cape Town, South Africa, 2014.

- **On the Dynamic Manipulability of Velocity-constrained Serial Robotic Manipulators***
  C. D. Pham and P. J. From
  IEEE International Conference on Robotics and Biomimetics, Bali, Indonesia, 2014.

- **Analysis of a Moving Remote Center of Motion for Robotics-Assisted Minimally Invasive Surgery***
  C. D. Pham, F. Coutinho, A. Leite, F. Lizarralde, P. J. From and R. Johansson
  IEEE/RSJ International Conference on Intelligent Robots and Systems, Hamburg, Germany, 2015.

- **Singularity Analysis of Robotic Manipulators with Velocity-Constraints for Minimally Invasive Surgery***
  C. D. Pham and P. J. From
  IEEE International Conference on Robotics and Biomimetics, Zhuhai, China, 2015.

We present an analytical representation of manipulator kinematics with velocity constraints on the chain. The constraint Jacobian allows us to treat constrained manipulators in the same way as non-constrained manipulators so we can apply conventional control schemes such as compliant and hybrid control on the constrained manipulator. This also helps us to analyse the mobility and singularities of constrained manipulators. Moreover, RCM velocities can also be controlled at the same time as the end-effector velocities. None of the previous work can do this. We applied the approach on a Motoman DIA10 dual-arm robot with a Phantom Omni haptic device to verify the theory.

1.4 Part III - Kinematic Analysis of Serial and Parallel Manipulators

Manipulators are used in many remote and harsh environments where humans cannot or do not want to operate. The need for a rigorous theory on what happens when joint failure occurs is thus important to be able to cope with unforeseen events such as actuation failure. We therefore need to know the passive joints' effect on serial and parallel manipulators when external forces are present.

1.4.1 Joint Failure

There are two main types of joint failure:

- Locked joint: the velocity of the effected joint is zero (Maciejewski and Balakrishnan [1998]).
- Joint force/torque failure, also called free-swinging joint faults (FSJF) (English and Maciejewski [1998]). This failure happens when an active joint loses its force/torque from a fault in joint motor/gears. The failed joints will become passive and can move freely.

1.4.2 Kinematics of Parallel Manipulators

For a robotic mechanism with several sub-chains $j = 1...k$, for example a parallel manipulator with three sub-chains in Fig. 1.10, we will write the twist of joint i as $\mathcal{G}_i$ and the *twist system* of chain j as

$$\overline{\mathcal{M}}_j = (\mathcal{G}_1, \mathcal{G}_2, \ldots, \mathcal{G}_n) = (\overline{\mathcal{M}}_{j1}, \overline{\mathcal{M}}_{j2}, \ldots, \overline{\mathcal{M}}_{jn}). \tag{1.23}$$

where we use the second notation $\mathcal{M}_{ji}$ when we need to clarify what chain the joints belong to in a parallel mechanism, i.e., joint i at chain j. We use the same notation for the joint positions, i.e. θ_{ji} [1]. The twist system describes the motion of the end effector for the open chain.

[1] In this part of thesis use θ instead of q to denote the joint positions.

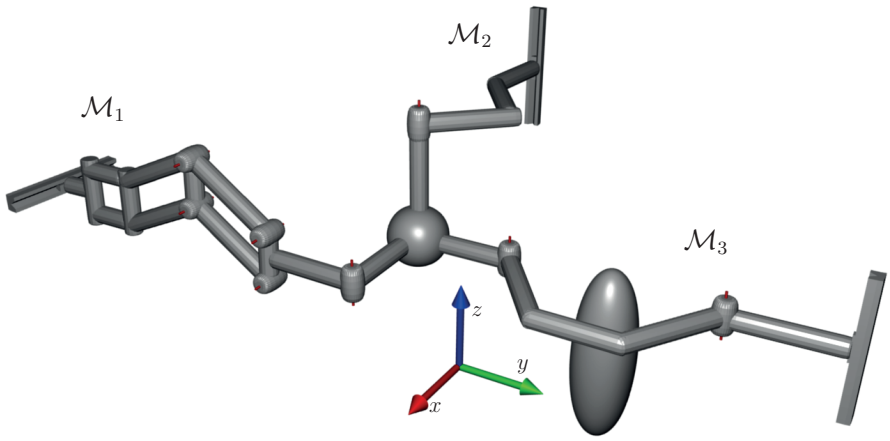

Figure 1.10: An example of parallel manipulator with three sub-chains.

Let the parallel manipulator

$$\mathcal{M} = \mathcal{M}_1 || \mathcal{M}_2 || \cdots || \mathcal{M}_k \tag{1.24}$$

consist of k serial manipulator sub-chains that share a common base and a common end effector.

We are interested in the *passive motion*, i.e. the motion due to the passive joints when the active joints are fixed. We denote this by

$$\mathcal{M}_P = \mathcal{M}_{P1} || \mathcal{M}_{P2} || \cdots || \mathcal{M}_{Pk} \tag{1.25}$$

where $\mathcal{M}_{Pj}$ consists of only the passive joints of chain j.

Although only the passive joints are considered, the twists of the passive joints depend on the configuration of the active joints. The twist of joint i is given by

$$\mathcal{G}_i' = \mathrm{Ad}_{g_{b(i-1)}} \mathcal{G}_i \tag{1.26}$$

where $g_{bi} \in SE(3)$ is the transformation from the base to joint i. We will assume it implicitly understood that the twists, as written in (1.23), are transformed according to (1.26), and thus write $\mathcal{G}$ for $\mathcal{G}'$. Similarly when we write $\mathrm{Ad}_g \overline{\mathcal{M}}$, we mean

$$\mathrm{Ad}_{g(\theta)} \overline{\mathcal{M}} := \{\mathcal{G}_1', \ldots, \mathcal{G}_n'\} = \{\mathcal{G}_1, \mathrm{Ad}_{g_{b1}} \mathcal{G}_2, \ldots, \mathrm{Ad}_{g_{b(n-1)}} \mathcal{G}_n\}. \tag{1.27}$$

When $\mathcal{M}_P$ does not allow any motion after the joint failure, we have

$$D_m = 0 \xRightarrow{FSJF} D_{m-1} = 0 \tag{1.28}$$

and the mechanism remains equilibrated with respect to all external forces. When $\mathcal{M}_P$ allows a 1 DOF motion as a result of the joint failure, i.e.

$$D_m = 0 \xRightarrow{FSJF} D_{m-1} = 1, \tag{1.29}$$

the mechanism is not fault tolerant. In this case the mechanism can at best be conditionally equilibrated.

1.4.2.1 Overconstrained Mechanisms

Grübler formula (1.30) is used to determine the degree of freedom of a kinematic chain (Angeles [1989]):

$$M = 6(N - 1 - j) + \sum_{i=1}^{j} f_i \tag{1.30}$$

where N is the number of links including the fixed link, j is the number of joints, f_i is degrees of freedom of joint i.

Overconstrained mechanisms are linkages that violate the mobility formula by using special geometric features and dimensions to provide more mobility than would by predicted by this formula (Mavroidis and Roth [1994]). The first overconstrained mechanism is Sarrus system (Sarrus [1853]) that shown in Fig. 1.11. The Sarrus system has 6 links and 6 joints so it has mobility $M = 0$ following the Grübler formula. However the Sarrus mechanism has mobility $M = 1$, which means it allow movement in one dimension.

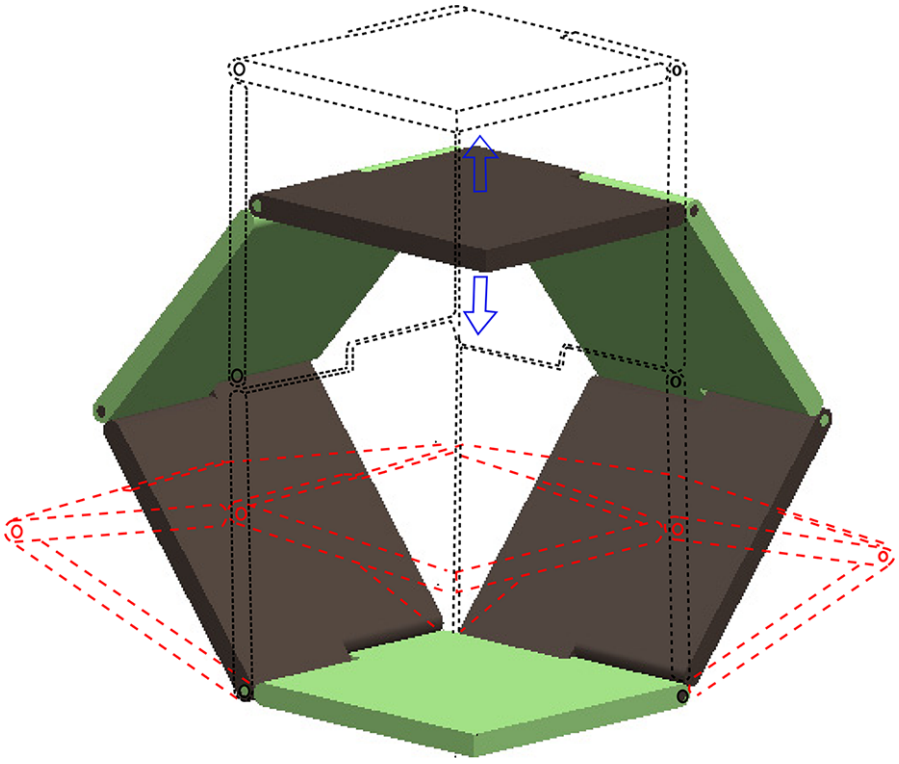

Figure 1.11: The Sarrus system. Courtesy of Chen et al. [2013].

1.4.3 State-of-the-Art of Joint Failure in Manipulators

Passive joints in serial manipulators are treated only briefly in literature, (Oriolo and Nakamura [1991], Arai and Tachi [1990]), and case studies such as the Acrobot in Hauser

and Murray [1990]. Arai and Tachi [1990] proposed an approach that control passive joints with holding brakes by using dynamic coupling.

The mobility of parallel manipulators and the relation between the active and passive joints can be found in literature. The Jacobian of the parallel manipulator is investigated in Liu et al. [1999] and Bicchi and Prattichizzo [2000] where the passive joint accelerations are found from the active joint accelerations by dividing the Jacobian into an active and a passive part. For non-overconstrained mechanisms, i.e. when there are no redundant constraints, we can find the mobility by the well known Grübler formula in Murray et al. [1994].

For overconstrained mechanisms there are many approaches to determine the mobility. In Dai et al. [2006] the mobility of the mechanism is found from the constraint space. The constraints of the system are found systematically and the redundant constraints are identified. The mobility is then found by adding the degrees of freedom represented by these redundant constraints to the Grübler formula for non-overconstrained mechanisms. This approach illustrates well the effect of redundant constraints in the mechanism.

The mobility can also be found by the motion space as in Rico et al. [2003], Rico et al. [2006]. The degree of freedom of the motion of the end effector is first found. Then the degree of freedom of the self-motion manifold of each chain is added. By this approach the redundant constraints are not found directly, but this approach gives valuable in-sight into where to place redundant actuators in the mechanism.

1.4.4 Contribution

We suggest an approach to analyse serial and parallel manipulators with passive joints, presented in the following papers:

- **A Geometric Approach to the Design of Serial and Parallel Manipulators with Passive Joints**
  C. D. Pham, P. J. From and J. T. Gravdahl
  Applied Mathematics, 2014.

- **Fault Tolerance of Parallel Manipulators with Passive Joints**
  P. J. From, C. D. Pham and J. T. Gravdahl
  Proceedings in Applied Mathematics and Mechanics, 2014.

The approach does not only to deal with parallel manipulators like previous work (From and Gravdahl [2008]) but also with serial manipulators. We can find the configuration of serial manipulators in case of joint failure to prevent the robot from collapsing. The approach also gives a global solution to the mobility of parallel manipulators that depends on active joint positions only.

1.5 Part IV - Agricultural Robots

Conventional farming has several unfortunate drawbacks that may be resolved by replacing heavy agricultural machinery with lightweight robots. Robotic swarms have

been proposed as an efficient solution to farming which may eliminate one or more of the drawbacks found in conventional farming such as soil compaction, high fuel consumption, low precision, extensive use of pesticides and fertilizers, and so on.

1.5.1 Thorvald

Thorvald is a novel robotic platform that is powerful enough to perform energy-demanding operation in the soil, and at the same time has the beneficial properties of lightweight, autonomous robots (Grimstad et al. [2015a]).

The Thorvald platform was designed and built at the Norwegian University of Life Sciences. It has a low center of gravity, and a total mass of approx. 150 kg. It uses four 600 W brushless motors connected via toothed belts to in-wheel gearboxes for propulsion, which is believed to sufficient to perform the most critical tasks in the field. Even though the robot itself is lightweight, the tools that are attached to the robot will add the necessary weight to perform each task. Thus, for monitoring and surveillance, the robot is sufficiently light weight not to damage the plants and the soil and to maintain a long operation time, while for more energy-demanding tasks, such as seeding, the seeding tool will add the necessary weight to obtain the required traction and stability.

The robot has individual steering motors for each wheel, which makes it highly maneuverable, and the frame members and frame joints are made somewhat flexible to ensure that all wheels will remain in contact with the ground, even in rough terrain. This is critical for traction, which is especially important on Norwegian farms, where the fields often are uneven and hilly. The flexible frame design was chosen as it is lighter, less expensive and less complex than traditional suspension systems.

Thorvald has a waterproof on-board computer from Small PC, which runs ROS (Robotic Operating System) on Linux Ubuntu. A heavy-duty, weather-proof, high brightness touch screen from Small PC has been installed for easy operation together with an emergency stop button. The steering motors from JVL have built in motor controllers while the four propulsion motors are connected to two dual channel motor controllers from Roboteq. All motor controllers are connected to, and communicate with the on-board computer via a CANopen network. The Thorvald platform is depicted in Fig. 1.12.

1.5.2 Controller Area Network

In this section, we will study briefly the Controller Area Network (CAN) and CANopen that are used in our robot.

1.5.2.1 Controller Area Network

Controller Area Network (CAN) is a serial network technology that was originally designed for the automotive industry but has also become a popular bus in industrial automation as well as other applications (Voss [2005]).

Figure 1.12: The Thorvald platform.

CAN specifies physical layer and data link layer in the ISO 7-layer reference model. CAN is a broadcast type of bus (Fig. 1.13). All nodes can "hear" all transmissions. There is no way to send a message to just a specific node; all nodes will invariably pick up all traffic. The CAN hardware, however, provides local filtering so that each node may react only on the “interesting” messages (Voss [2005]).

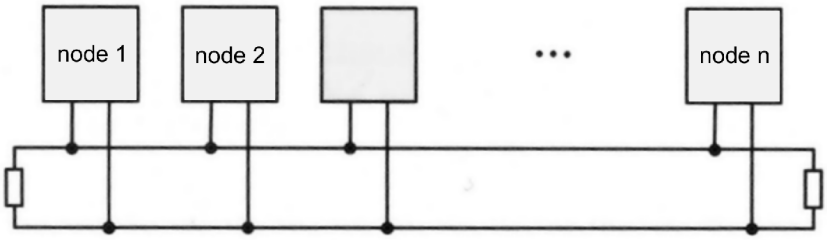

Figure 1.13: A CAN Bus example. Courtesy of BÖHNKE + PARTNER.

1.5.2.2 CANopen

CANopen is a higher-level CAN protocol that is developed by CiA. CANopen has been developed as a standardized embedded network with highly flexible configuration capabilities (Pfeiffer et al. [2008]).

CANopen is free and does not require any license fees. It can combine both CANopen and CAN nodes in one network. CANopen can easily be extended or customized towards a specific application (Pfeiffer et al. [2008]).

1.5.3 The Robot Operating System

The Robot Operating System (ROS) is an open-source robot operating system. It is a flexible framework for writing robot software. It is a collection of tools, libraries, and

conventions that aim to simplify the task of creating complex and robust robot behavior across a wide variety of robotic platforms (Quigley et al. [2009]).

The primary goal of ROS is to reuse the code developed by the robotic community. Everyone can share their work when they create a new package which lets others integrate and reuse it (Quigley et al. [2009]).

1.5.4 State-of-the-Art of Agricultural Robots

There has been an increasing interest in small agricultural robotic platforms, and several robotic solutions have emerged in recent years. Both task specific and modular robots with exchangeable implements exist. One group of robots focus on surveillance and monitoring. The BoniRob, (Ruckelshausen et al. [2009]), is for example developed for phenotyping and mapping of plants in the field. Hortibot, (Jørgensen et al. [2007]), is a robotic tool carrier for high-tech plant nursing for e.g. organic grown vegetables. Armadillo, (Jensen et al. [2012]), a field robot that can be configurable and adaptable to a wide range of precision agriculture research projects. Some robots have a specific purpose like autonomous weeding (Bakker et al. [2010]) and weed detection robots, (Bak and Jakobsen [2004]). Other robots are capable of doing physical work in the field. One such robot is the Robotti from Kongskilde, (Green et al. [2014]), which can do field operations such as mechanical weeding.

1.5.5 Contribution

We suggest an new agricultural platform. The whole system is described in the following papers:

- **On the design of a low-cost, light-weight, and highly versatile agricultural robot**
  L. Grimstad, C. D. Pham, H. N. T. Phan and P. J. From
  IEEE International Workshop on Advanced Robotics and its Social Impacts, Lyon, France, 2015.

- **Initial field-testing of Thorvald, a versatile robotic platform for agricultural applications**
  L. Grimstad, H. N. T. Phan, C. D. Pham and P. J. From
  IROS Workshop on Agri-Food Robotics: dealing with natural variability, 2015.

This is a flexible platform. My main contributions in the system are:

- Applying CANopen with ROS to communicate and control with an onboard computer. All of devices are connected to CAN network. The sytem is very open and it is easy to add new sensors or new devices to extend applications.

- Implementing control of the whole system.

Part I

Control Allocation for Teleoperation of Kinematically Dissimilar Robots

Chapter 2

Control Allocation for Mobile Manipulators with On-board Cameras

2.1 Abstract

This paper presents a new set of approaches for teleoperation of mobile manipulators with on-board cameras. Mobile manipulators consist of a robotic arm which provides for interaction and manipulation, and a mobile base which extends the workspace of the arm. While the position of the on-board camera is determined by the base motion, the principal control objective is the motion of the manipulator arm. This calls for intelligent control allocation between the base and the manipulator arm in order to obtain intuitive control of both the camera and the arm. We implement virtual mass-spring-damper forces between the end-effector and the camera so that the camera follows the end-effector with an overdamped characteristics. The operator therefore only needs to control the end-effector motion, while the vehicle with the camera will follow naturally. The operator is thus able to control the more than six degrees of freedom of the vehicle and manipulator through a standard haptic device. The control allocation problem, i.e., whether the vehicle or manipulator arm actuation is applied, is then performed automatically so that the operator can concentrate on the manipulator motion.

2.2 Introduction

Teleoperation allows operators to control remotely located objects from a safe and comfortable location. The main motivations for remotely operated robots is to relieve humans from entering hostile and dangerous environments and to utilize robots in areas where humans do not have access.

Teleoperated robotic manipulators have long been an active field of research. Passivity-based controllers are commonly used to control bilateral teleoperation systems with two-port network representations Hokayem and Spong [2006], Jee-Hwan et al. [2004a], Jee-Hwan et al. [2004b]. Energy-based approaches have also been proposed to obtain

stable behavior of the two systems, for example in Hannaford [1989], Franken et al. [2011]. Over the last years, however, we have seen an increased interest also in teleoperation of mobile manipulators, i.e., a robotic manipulator mounted on a mobile base. This setup has great potential because it combines two important properties: the mobility of the mobile base and the dexterity and manipulability of the manipulator arm Park and Khatib [2006], Seraji [1998], Farkhatdinov and Jee-Hwan [2008].

Combining mobility and dexterity in one system in this way does not only present us with possibilities—it also leads to challenges when it comes to control: It is difficult to obtain intuitive behavior when controlling two kinematically different systems using only one type of haptic device.

Several solutions have been proposed for intuitive control of mobile manipulators. One simple approach is to use two haptic devices, one joystick-like device to control the vehicle, and a serial chain master manipulator to control the manipulator arm. This does, however, lead to a more complicated setup for the operator, as it has shown difficult to control two different haptic devices at the same time, and also because the vehicle typically uses rate control while the manipulator is position controlled.

A different set of approaches commonly implemented uses the concept of operation modes to control either the manipulator base or the vehicle but with only one haptic device. Instead of using two devices the user switches between controlling the manipulator and mobile base. The switching between the two modes, referred to as manipulation and locomotion modes, is performed manually using a simple switch or button on the haptic device, i.e., the operator can choose either locomotion mode in which he/she controls the mobile base or manipulation mode where the manipulator arm is controlled.

Farkhatdinov and Jee-Hwan [2008] propose a teleoperation system, where the human operator remotely controls several different objects—such as several mobile robots or a manipulator arm mounted on a mobile base (a 2-robot system)—or to control several properties of the same robot using only one master device. A switch is used to choose what object to control, for example whether to control the mobile base or the manipulator. Similarly, Farkhatdinov et al. [2008] use a switch to control either the speed of mobile platform for efficient locomotion or the position of manipulator for fine manipulation. A passivity-based approach is implemented for stability. Also Lasnier and Murakami [2010] propose two operation modes: a standard bilateral mode to control the manipulator and a joystick-like rate control mode for the mobile base. Andaluz et al. [2011] switch between controlling the velocity of the entire vehicle-manipulator system, or the position of the robotic arm only.

In all the work presented above the human operator needs to manually select the control strategy. This switching is often confusing for the operator because he/she needs to switch between two operation modes that are very different in nature. It is therefore believed that more efficient control can be obtained if switching is avoided. One solution is presented in Wrock and Nokleby [2011] where control of the vehicle-manipulator system is performed using a single 3-DoF haptic device. Two separate modes are defined which allows the operator to control either the manipulator or the base. The system automatically switches between the two states based on the configuration of the slave manipulator. The controller will enter locomotion mode when the end effector breaches

the predefined limits of the manipulator's workspace. When in locomotion mode, the system returns to manipulation mode when the master robot has been left in the dead-band defined in the middle of the master's workspace for more than three seconds. A similar idea is presented in Farkhatdinov and Jee-Hwan [2008] where automatic switching between two different locomotion modes of a mobile base is used to increase accuracy. For small displacements in the master device a position-to-position control scheme is applied for accurate control, while for large displacements, a position-to-velocity control scheme is used for fast locomotion.

The switching between the operation modes described above, whether it occurs manually or automatically, is very apparent to the operator. In this paper we suggest that this apparent switching is not necessary for efficient control. In fact, switching in this way may take the attention of the operator away from the task that he is to perform and decrease the overall performance. The method proposed in this paper thus aims at reducing the differences between the two modes, allowing for smoother and more efficient control, as well as faster and more intuitive operation.

In this paper we introduce an artificial force between the manipulator end effector and the camera attached to the mobile base. The main idea is to let the operator control the end-effector motion only, in the normal way, and we then let the camera follow the end-effector with an artificial force dragging it towards the end-effector. We give this force an overdamped mass-spring-damper characteristics to avoid oscillations. Our approach allows the operator to focus only on the end-effector motion while the motion of the mobile base is taken care of by the control allocation.

In addition we also use the concepts of operation modes. When the master robot is inside a pre-defined workspace, a standard position-to-position control is applied. In this mode the vehicle is kept still, which allows for accurate and fine manipulation. This is normally necessary because the vehicle motion is not sufficiently smooth, for example due to vibrations and low accuracy. When the master is taken out of this area we enter locomotion mode where the end-effector motion is controlled using a position-to-velocity scheme and the mobile base will follow as described above. It is important to note that, differently from the approaches described above, the manipulator arm does not stop to move as we enter a locomotion mode. Rather, we obtain a more intuitive motion by moving both the vehicle and the arm.

Moreover, we use an on-board camera for visual feedback, which leads to several challenges compared to direct visual contact between the operator and the robot. One of the main challenges is the limited view that the operator has of the workspace. The camera can only see in one direction so the operator will miss a lot of information about the environment. This needs to be taken care of by the on-board sensors. Ideally, safe operation is obtained by proper control allocation, for example to avoid collisions, or if this is not possible, the system needs to override the operator.

The main problem when it comes to intuitive operation of the robot is that the camera is fixed to the vehicle so that the images change with the vehicle's motion. As the camera is the operator's eyes at the remote location, this motion affects his perception of the remote environment. This needs to be taken into account in the control allocation. We propose a continuous control allocation method that simultaneously

allows for intuitive operation of the end-effector motion and positioning of the camera.

2.3 System Setup and Problem Formulation

The system to be studied consists of a standard bilateral teleoperation setup with a haptic device controlled by a human operator which is used to control a remotely located robot. The robot consists of a wheeled vehicle with a manipulator arm attached to it. We will attach a frame $\mathcal{F}_b$ to the vehicle and denote the location of $\mathcal{F}_b$ with respect to the inertial frame $\mathcal{F}_0$ by the homogeneous homogeneous matrix g_{0b} and its velocity by the body velocity twist $\hat{V}_{0b}^B = g_{0b}^{-1}\dot{g}_{0b}$. The configuration of the robotic arm is given by the joint variables $q \in \mathbb{R}^n$ in the normal way, and the joint velocities as $\dot{q} = \frac{\mathrm{d}q}{\mathrm{d}t} \in \mathbb{R}^n$. The position of the end-effector frame $\mathcal{F}_e$ in the world frame is found as $g_{0e} = g_{0b}g_{be}(q)$ From et al. [2010a]. We refer to From et al. [2014a] for a detailed formulation of the kinematics of vehicle-manipulator systems.

We consider bilateral teleoperation of a mobile manipulator which consists of a Pioneer 3-AT mobile base with a 7 degrees freedom manipulator, as seen in Fig. 2.1. The mobile robot is a small four-wheel, four-motor skid-steer robot with non-hololonomic motion constraints. The operator gives commands through the master haptic manipulator which is connected to a personal computer. We use Phantom Omni haptic device from SensAble Technologies which allows for force feedback. The control signals are sent from the PC to the on-board computer through a wireless network. Obstacle range information is obtained from the robot's sonars.

2.3.1 Problem Formulation

The setup described above calls for the integration of two rather distinct operation modes: i) accurate manipulation of objects using the robotic arm in the relatively limited workspace of the manipulator; and ii) locomotion of the vehicle in a possibly very large workspace. The main challenge is therefore to obtain a control allocation between the vehicle and the manipulator in such a way that the motion of both the vehicle and the manipulator arm can be controlled intuitively using the manipulator-like haptic device.

The distribution of control forces between the manipulator and the base to obtain both manipulation and locomotion is obtained through the control allocation algorithm. The main topic discussed in this paper is thus how to interpret the master (6 DoF) reference as both position and velocity references and how to distribute the control forces between the vehicle and the base (3+6 DoF), i.e., the control allocation problem for vehicle-manipulator systems.

In this paper we take the master reference and generate position or velocity references for the vehicle and manipulator, and we denote this the control allocation problem because the motion is distributed between the two systems. It is important to note, however, that we assume that the low-level controllers of the vehicle and manipulators are such that these references are followed, i.e., we are only concerned with kinematic control. Once the control allocation is in place, any method for stable teleoperation can be used, such as passivity- and energy-based approaches. The control of teleoperated

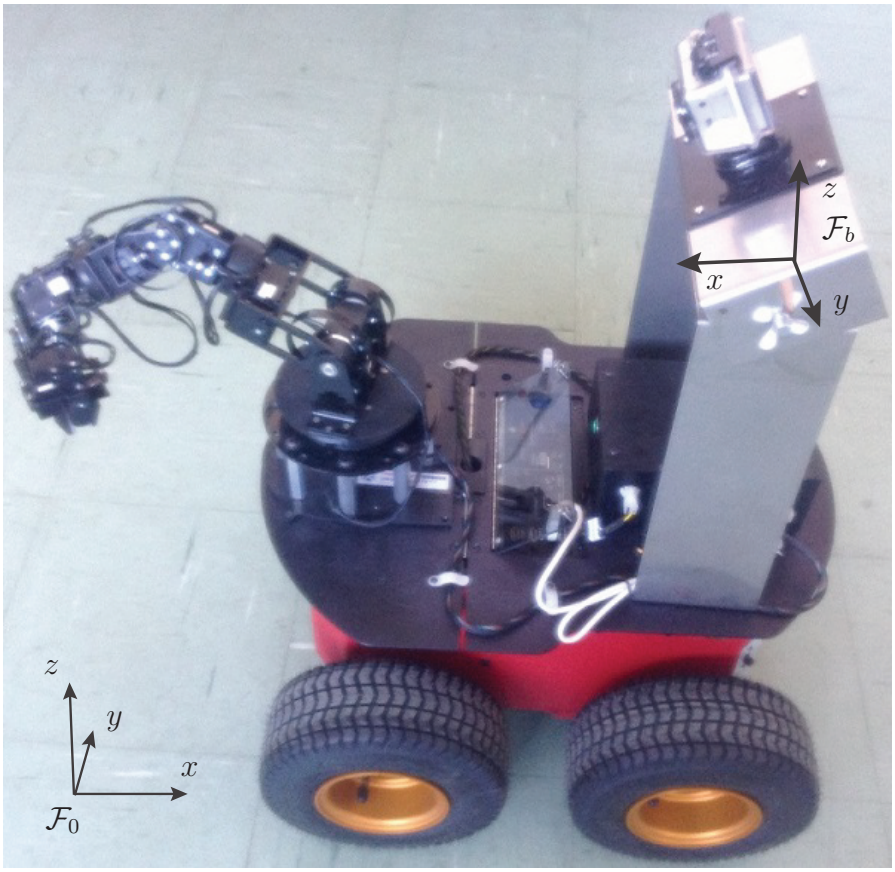

Figure 2.1: The coordinates of mobile manipulator

systems is not discussed in detail in this paper, but we present some comments on the control architecture below.

2.3.2 Control Architecture

The general idea presented in this paper is to control both the vehicle and the manipulator using a single haptic device. This calls for some kind of control allocation to decide whether the vehicle, the manipulator arm, or both are to be actuated given a reference from the master device. We will implement this control objective in intermediate layers (IL) between the master and the slave as illustrated in Fig. 2.2 and discussed in detail in Cho et al. [2012].

Teleoperation systems are often modeled as two-port networks where both the master and the slave are represented by two-ports, and the human operator and the environment are represented by one-ports (Hannaford [1989]). In addition we introduce intermediate layers between the master and the slave for control implementation. The sub-layers can then be serially connected to obtain the required overall performance.

This control architecture allows us to implement a layer between the master and the slave for control allocation and control objectives. In addition to the conventional control we can also implement other sub-layers, for example for increased safety and enhanced operator awareness. The control architecture with intermediate layers is described in more detail in Cho et al. [2012]. A simple implementation with intermediate layers for

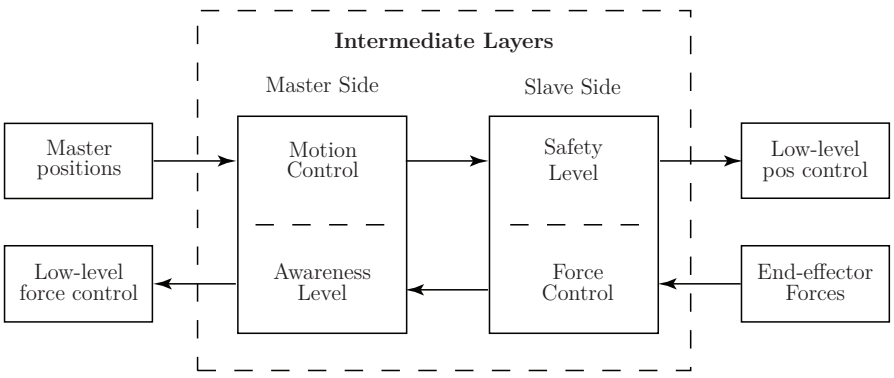

Figure 2.2: The intermediate layer architecture represented by several sub-layers used in this paper for safe haptic teleoperation of vehicle-manipulator systems.

improved safety and enhanced awareness is illustrated in Fig. 2.2.

In the next section we will study several different intermediate layers that are designed specifically for vehicle-manipulator systems, and we derive each of these in detail. We will use the control architecture described above to implement each layer as two-ports to obtain the required overall performance of the system. The four intermediate layers discussed below are illustrated in Fig. 2.2.

2.4 Motion Control

In this section, we will study what we refer to as the control allocation problem for vehicle-manipulator systems, i.e., how a reference trajectory is allocated between the vehicle and the arm.

2.4.1 Control Modes

The controller will use control modes to decide whether the trajectory is realized through the vehicle, the manipulator, or both. There are two control modes—manipulation mode and locomotion mode—that can be used only as internal modes for the controller or be communicated to the operator as two distinct operation modes:

2.4.1.1 Manipulation Mode

This mode is used for fine manipulation and interaction tasks. This is normally implemented as a position-to-position or velocity-to-velocity control scheme. Because the manipulator arm is generally much more accurate than the vehicle, manipulation mode is realized through the manipulator arm only while the vehicle is fixed. Thus, as the vehicle is fixed and we only control the slave robot which is kinematically similar to the master robot, we can apply any control scheme for haptic teleoperation in this mode. If larger motions are desired, vehicle actuation is required and we switch to locomotion mode.

2.4.1.2 Locomotion Mode

Whenever a large displacement of the robot is needed the vehicle needs to take care of this motion. Normally a position-to-velocity control scheme is chosen to allow for an infinitely large slave workspace. In locomotion mode the vehicle and the arm are used to obtain large displacements of the end-effector. As the master robot is to control both the vehicle and the slave arm, we have two kinematically dissimilar systems. We solve this by virtually connecting the master end effector to the slave end effector, which is our primary control objective.

2.4.2 Switching Strategies

2.4.2.1 Manual strategy

A simple control scheme is simply to let the operator choose the operation mode directly Farkhatdinov and Jee-Hwan [2008], Farkhatdinov et al. [2008], Lasnier and Murakami [2010], Andaluz et al. [2011]. The operator then decides what operation mode should be used, for example by pushing a button on the haptic device. In manipulation mode the speed of the vehicle is set to zero while in locomotion mode the position of the slave manipulator is normally kept constant or retracted.

2.4.2.2 Master workspace strategy

With this strategy, the robot will automatically change between the two modes depending on the master position. If the robot is far from the goal, the operator will move the haptic device far and fast. It is thus natural to define a limit area in the master manipulator's workspace so that whenever the master is inside this area, the robot will be controlled in manipulation mode while we switch to locomotion mode when it moves out of the area.

$$\text{Mode} = \begin{cases} \text{Manipulation} & \text{if} \begin{cases} |z_m| \leq z_0 \\ |x_m| \leq x_0 \\ |v_z| \leq v_0 \end{cases} \\ \text{Locomotion} & \text{otherwise} \end{cases} \tag{2.1}$$

where z_m and x_m are the master positions in the zx-plane of the haptic device and v_z is the master speed in the z-axis of the master frame. z_0, x_0 and v_0 are user designed constant parameters defining the manipulation mode.

When in locomotion mode we allow only for motion of the vehicle which is given by

$$\begin{bmatrix} v_s \\ \phi_s \end{bmatrix} = \begin{bmatrix} -k_v & 0 \\ 0 & -k_\phi \end{bmatrix} \begin{bmatrix} d_1 \\ d_2 \end{bmatrix} \tag{2.2}$$

where k_v and k_ϕ are proportionality constants; v_s and ϕ_s are the velocity and the heading angle of the vehicle in the body frame; and d_1 and d_2 are defined by the position of the haptic device, as shown in Fig. 2.3. They are the distances from the master's tip position to the limit area that is used to define the manipulation mode.

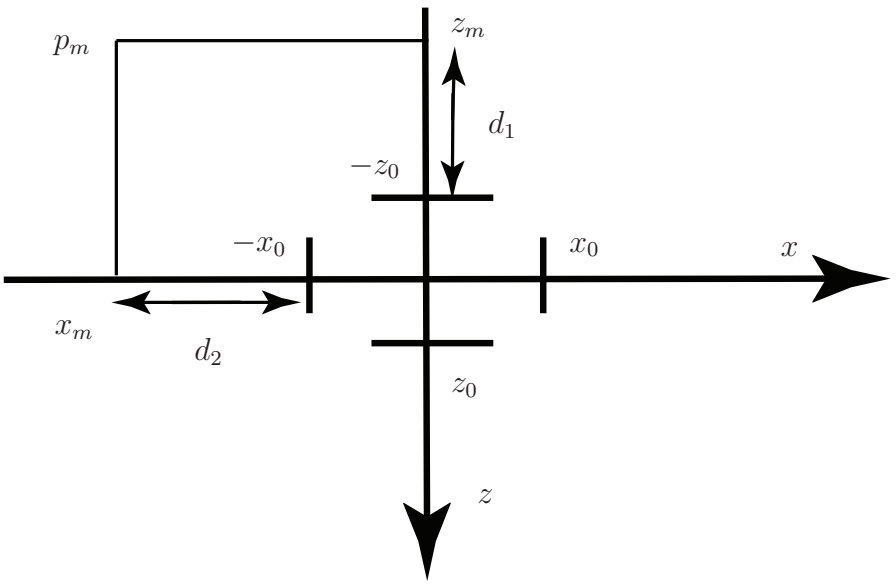

Figure 2.3: Determining d_1 and d_2 from the haptic position.

2.4.2.3 Slave workspace strategy

Alternatively we can use the slave workspace to determine the operation mode. Like in Wrock and Nokleby [2011], the system changes automatically from the manipulation mode to the locomotion mode when the slave manipulator reaches the limit of the workspace. However, the condition that is used to change back from the locomotion mode to the manipulation mode is different from that in Wrock and Nokleby [2011] where the change back to manipulation mode occurs after the master goes back in the dead-band for more than 3 seconds, in that our system changes back when the master goes back far enough so that a desired slave position can be defined in the slave workspace. We thus have

$$\text{Mode} = \begin{cases} \text{Locomotion} & \text{if} \begin{cases} |x_s| \geq x_l \text{ or } |y_s| \geq y_l \\ |x_{sd}| \geq x_l \\ |y_{sd}| \geq y_l \end{cases} \\ \text{Manipulation} & \text{otherwise} \end{cases}$$

where x_s and y_s are the actual slave positions in the $x-$ and $y-$ axes of the robot frame; x_{sd} and y_{sd}, that are computed from actual master positions, are the desired slave manipulator position; and x_l and y_l are the slave limit positions in the $x-$ and $y-$ axes of the robot frame, respectively. The locomotion mode using this approach is similar to the master workspace strategy presented in 2.4.2.2.

The differences of the master workspace strategy and the slave workspace strategy are hard to recognize from the equations, but result in very different user experience for the operator. For example, when the operators move the master device slow enough, the master workspace strategy and the slave workspace strategy are similar because the slave manipulator can tightly follow the master manipulator. However, the difference between the two modes becomes apparent in real life when the operator tends to move

the master very quickly, and often through the whole workspace so that the slave is not able to follow the master. This is very noticeable, for example, when operators want to reverse motion of the mobile base. In the master workspace strategy, operators can reverse the motion immediately by moving the haptic device fast. In the slave workspace, however, the slave manipulator has to move to the limit of the slave workspace before the mobile base can reverse the motion. This may lead slower execution of the task.

2.4.3 Control Allocation

A vehicle-manipulator system needs to be able to perform both interaction tasks with the environment using the end-effector tool and at the same time be able to move freely in its large working environment using the vehicle actuation. Ideally the switching between these two modes should be performed as intuitively as possible and in such a way that the operator performs this switching subconsciously. In this section we will propose a new framework that interprets the operator's input as either vehicle or manipulator motion without the need for actively choosing the operation mode, nor be aware of what mode we are in.

The location of the end effector with respect to the base is given by the forward kinematics in the normal way,

$$x_{0e} = \begin{bmatrix} p_m \\ \Theta_m \end{bmatrix} = f_{fk}(q) \tag{2.3}$$

where p_m is the position and Θ_m is the orientation of the master end-effector and f_{fk} is the forward kinematics map. The operator is concerned with the location of the end effector and not the base, but because the camera is mounted on the vehicle, its location affects the operator's perception of the remote environment. We thus seek a control law that allows the operator to control the end effector in the inertial space, and for which the vehicle and camera follow naturally. A change in the master position should therefore be interpreted as a position or velocity reference for the slave's end-effector. Note, however that a change in the slave's end-effector position can be obtained either through the vehicle, the manipulator arm, or both, which defines the control allocation problem. We solve this control allocation problem in three different ways: either we interpret the position of the master as a reference for the velocity of the slave end-effector, or as the position of the slave with respect to the camera (the vehicle), or as both position and velocity using operation modes.

2.4.3.1 Position-velocity Control

Let the position of the master correspond to a velocity of the slave end-effector in the inertial space. The desired end-effector velocity is given by $V^B_{0e,d}$ which can be obtained *by the robotic arm* through the Jacobian as $V^B_{0e,d} = J(q)\dot{q}$. In order to obtain an infinite workspace we do, however, need this motion to be realized also through the vehicle. Let the displacement of the end-effector from the home position be given by $\delta = x_{0e} - x^0_{0e}$ in Equation (2.3). Assume that we want the end effector to follow the desired reference

$V^B_{0e,d}$ and the vehicle to follow the end effector with a mass-spring-damper characteristic between the camera and the end-effector given by

$$F = \ddot{\delta} + d\dot{\delta} + k\delta. \tag{2.4}$$

The following references will give the above characteristics:

- Manipulator arm reference:

$$V^B_{0e,r} = V^B_{0e,d} - \frac{1}{d_b}F, \tag{2.5}$$

- Vehicle reference:

$$V^B_{0b,r} = \frac{1}{d_b}F. \tag{2.6}$$

This control law is to be interpreted in the following way: The desired end-effector velocity in the inertial space is given by $V^B_{0e,d}$. The manipulator reference is obtained by the Adjoint map Ad_g (From et al. [2014a]) and subtracting the vehicle motion $V^B_{0b,r}$, i.e.,

$$V^B_{be,r} = V^B_{0e,d} - \mathrm{Ad}_{g_{eb}} V^B_{0b,r} \tag{2.7}$$

so it only remains to find the reference for the vehicle motion from the desired end-effector motion. The position, velocity, and acceleration of the end effector with respect to the vehicle generates a force F given by (2.4) that acts on the vehicle. This force is transferred into a vehicle motion, or rather the vehicle velocity by (2.6) where d_b can be interpreted as the damping on the vehicle. Note that this is different from d which is the desired damping characteristics as observed from the camera when watching the end effector. Finally the motion of the vehicle is removed from the desired motion passed on to the manipulator controller. Note that the constants in the mass-spring-damper system (2.4) need to be tuned to avoid saturation in the manipulator workspace.

2.4.3.2 Position-position Control

Alternatively we can use position-position control. We can still obtain an infinite workspace by choosing the slave position to be chosen with respect to the base and not the inertial frame, and let the vehicle approach the end effector as above. In this case the desired vehicle velocity $V^B_{0b,r}$ and manipulator position δ_r are obtained from the desired manipulator position δ_d by the following law:

- Manipulator arm reference: $\delta_r = \delta_d - \int \frac{1}{d_b}F$,
- Vehicle reference: $V^B_{0b,r} = \frac{1}{d_b}F$.

We see that in this case the vehicle takes velocity as reference, which is necessary to obtain an infinite workspace and the manipulator arm takes position as reference which allows for fine manipulation. Also in this case the vehicle motion is subtracted from the manipulator motion so that the operator always controls the manipulator as seen from the on-board camera.

2.4.3.3 Position-position and Position-velocity Control

For the two approaches presented above the vehicle will always move, even for small desired end-effector motions used for fine interaction tasks. This is not always desirable because the vehicle is generally less fine-tuned than the manipulator arm. In this section we thus present a combination of the switching approaches presented in Sections 2.4.2.2 and 2.4.2.3 and the approaches presented in Sections 2.4.3.1 and 2.4.3.2 above.

The first thing that the control scheme checks is whether the position or velocity control is to be applied. We do this by first defining the manipulator workspace $\mathcal{W}_M$ with respect to the vehicle frame $\mathcal{F}_b$. We will define the workspace for position control as a workspace $\mathcal{W}_P$, somewhat smaller than the manipulator workspace $\mathcal{W}_M$, as illustrated in Fig. 2.4. Whenever the manipulator is inside this workspace position control is applied. This is equivalent to the manipulation mode in the previous sections. This allows the operator to perform accurate manipulation and interaction tasks, possibly with force feedback.

If the master manipulator is outside the workspace $\mathcal{W}_P$, velocity control is applied. In this case the slave manipulator remains fixed at the limit of the workspace, while the vehicle velocity is so that the vehicle follows the master end-effector with a mass-spring-damper characteristics.

We note that the vehicle might continue to move also when the master manipulator is in manipulation mode, i.e., inside the position workspace $\mathcal{W}_P$. However, because we choose on overdamped characteristic this motion will die out relatively quickly and is also compensated for by the manipulator arm moving in the opposite direction. The reason that we choose this characteristic is that this will take the vehicle to a position which gives improved manipulability to the manipulator arm because it moves away from the limits. The system is tuned so that the artificial forces of the mass-spring-damper die out after approximately 20 cm which takes the manipulator to the middle of its workspace.

The locomotion mode is thus similar to the approach in the previous section with the exception that we use the distance from the limit of the workspace instead of the home position. Denote by $\bar{x}_s$ the position of the end effector projected into the position workspace $\mathcal{W}_P$, as illustrated in Fig. 2.4. Then the slave position with respect to this projected position is given by $\Delta = x_s - \bar{x}_s$ and we will let the vehicle be governed by Equation (2.4) by replacing δ with Δ, which is substituted into the control schemes presented above.

For a wheeled robot no instantaneous motion in the direction of the y-axis is allowed, in which case the torques that act on the vehicle will take the form

$$\tau_V = \begin{bmatrix} m\ddot{\Delta}_x + d\dot{\Delta}_x + k\Delta_x \\ 0 \\ m\ddot{\Delta}_{y,\psi} + d\dot{\Delta}_{y,\psi} + k\Delta_{y,\psi} \end{bmatrix}. \tag{2.8}$$

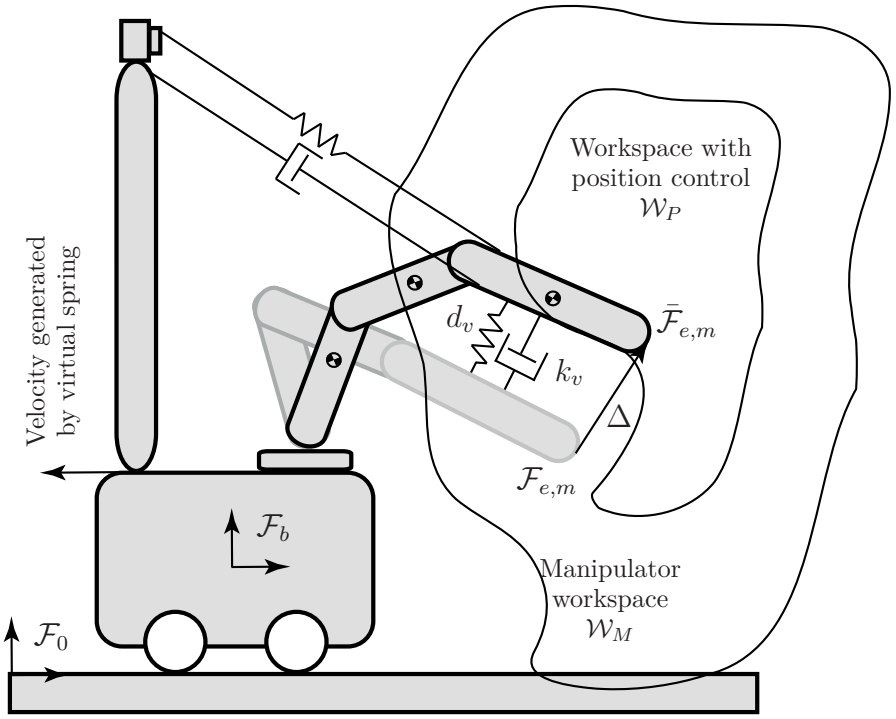

Figure 2.4: Definition of the workspaces in which the robot is controlled in the locomotion and manipulation modes. Note that the workspace is defined for the manipulator arm with respect to the vehicle frame $\mathcal{F}_b$, and not the world frame $\mathcal{F}_0$. The velocity is generated by the virtual spring between the master manipulator (gray) and the slave manipulator (black). The intuitive interpretation of the virtual spring is illustrated by the spring between the master manipulator and the vehicle.

2.5 Empirical Studies

To verify the efficiency of the proposed approach a simple setup with a mobile manipulator was used. Several inexperienced operators were asked to control the robot to perform a simple task which required both fine manipulation and locomotion, as well as switching between the two modes.

2.5.1 Experimental Setup

A standard 6-DoF Phantom haptic device from Sensable was used to control a mobile manipulator consisting of a Pioneer 3-AT mobile robot with a 7-DoF Cyton arm attached to it. The local computer communicates with the remotely located on-board computer via a wireless network. The time delay is minimal and not treated in this paper. The control is, however, implemented so that it is robust with respect to time delays.

2.5.2 Experimental Results

To verify the control scheme presented we let several inexperienced operators control the robot. We let the operators perform several different tasks using three different approaches:

1. automatic changing between locomotion and manipulation mode using master workspace, Section 2.4.2.2;

2. automatic changing between locomotion and manipulation mode using slave workspace, Section 2.4.2.3;

3. control allocation approach, Section 2.4.3.3.

During the experiments, the sequence of the control schemes are randomized to eliminate the effects of learning the task. The operators were to drive the robot to the other side of the room, grasp an object, and then drive back. This requires switching between the operation modes several times, especially for inexperienced operators.

For the master workspace strategy, almost all operators are confused whether it is the vehicle or the arm that is controlled. This makes it difficult to control the system, which can also be seen from the execution times and number of failures in Table 2.1.

With the slave workspace, the operators know exactly when the vehicle will move because the arm has to move to the limit before the vehicle can move. They can perform the task easily, but since this is a rather simple task—just to grasp an object—they almost only use the locomotion mode. They have to control the robot so that it passes the object and take the arm back if they want to control the arm to grasp the object. Because the arm is at the limit of its workspace when the system moves towards the object, some operators find it difficult to position the system close enough to the object.

The operators report that the control allocation approach is the most intuitive and find it fairly simple once they manage to think of the task as controlling the end-effector motion. They also report that they are able to disregard the vehicle motion when performing manipulation tasks and also when the vehicle is moving slowly. This makes the operation more efficient because the switching is hidden from the operator. With this approach, the operator can easily drive the system close enough to the object to execute the task. At this position, the arm is close to the center of its workspace so that it can be controlled in the manipulation mode. This strategy thus takes advantage of the slave workspace strategy and also eliminates some of the drawbacks of the same strategy.

To get a more quantitative evaluation the different approaches we timed the operators performing the task using the three approaches. The average times, number of failures, and average manipulability of three approaches are shown in Table 2.1. The executing times of 12 operators are shown in Fig. 2.5 and we see that the control allocation is the approach that performs the best quite consistently.

	Strategy		
	Master workspace	Slave workspace	Control allocation
Average duration	71,25 s	64,25 s	52,25 s
Number of fails	21	18	10
Manipulability	0,80	0,68	1

Table 2.1: Average execution times, number of filures, and average manipulability (normalized) to complete the task using the three strategies for 12 inexperienced operators.

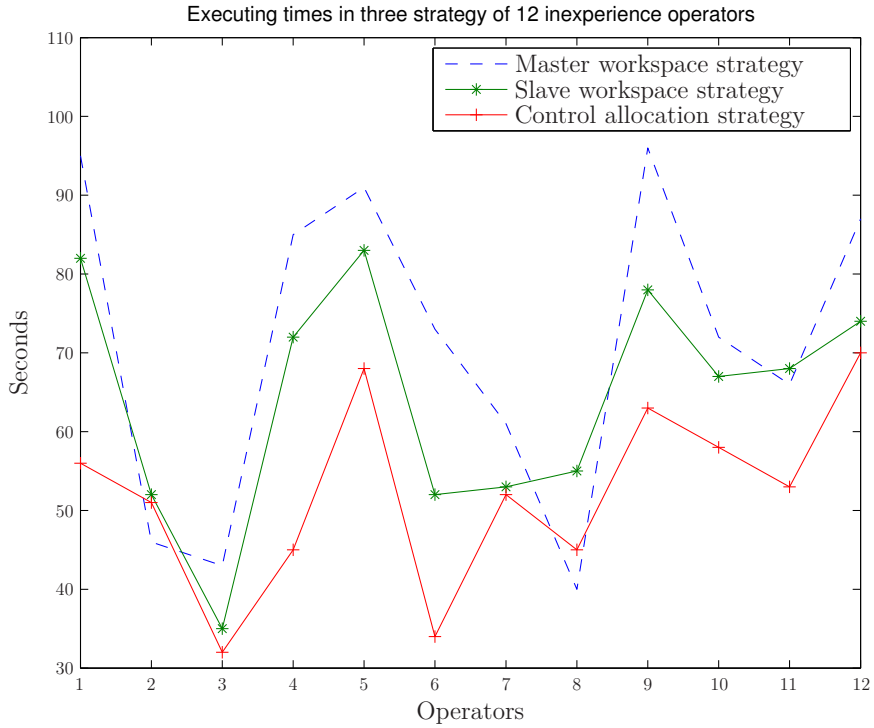

Figure 2.5: Executing times in three strategy of 12 inexperienced operators

We see that the control allocation strategy needs the shortest time to complete the task, in fact this is the case with almost all the operators. There are two operators that perform the operation fastest with the master workspace strategy. There are no users who take the shortest time with the slave workspace strategy. However, almost all the operators take the longest time in the master workspace strategy and there are three operators that take the longest time with slave workspace strategy. No-one takes the longest time with the control allocation strategy.

It seems that the control allocation strategy is the easiest strategy for controlling the robot. For the master workspace it takes longer to complete the task because the users found it difficulties to feel the area that separates the two modes.

For future work we will perform a more thorough study of the user experience of the different approaches and evaluate which approach performs best also for more complicated tasks and in the presence of time delays.

2.6 Conclusion

This paper presents a novel approach for haptic teleoperation of mobile manipulators. The main contribution of the paper is to allow the operator to control the end-effector motion in such a way the vehicle will follow automatically and result in a natural and simple way to control both the manipulator arm and the on-board camera. The operator does not need to worry about whether the master reference is to be interpreted as position control of the manipulator or velocity control of the vehicle, as this is handled by

the control allocation. Experimental work verify the efficiency of the proposed solution.

Chapter 3

Evaluation of Subjective and Objective Performance Metrics for Haptically Controlled Robotic Systems

3.1 Abstract

This paper studies in detail how different evaluation methods perform when it comes to describing the performance of haptically controlled mobile manipulators. Particularly, we investigate how well subjective metrics perform compared to objective metrics. To find the best metrics to describe the performance of a control scheme is challenging when human operators are involved; how the user perceives the performance of the controller does not necessarily correspond to the directly measurable metrics normally used in controller evaluation. It is therefore important to study whether there is any correspondence between how the user perceives the performance of a controller, and how it performs in terms of directly measurable metrics such as the time used to perform a task, number of errors, accuracy, and so on.

To perform these tests we choose a system that consists of a mobile manipulator that is controlled by an operator through a haptic device. This is a good system for studying different performance metrics as the performance can be determined by subjective metrics based on feedback from the users, and also as objective and directly measurable metrics. The system consists of a robotic arm which provides for interaction and manipulation, which is mounted on a mobile base which extends the workspace of the arm. The operator thus needs to perform both interaction and locomotion using a single haptic device. While the position of the on-board camera is determined by the base motion, the principal control objective is the motion of the manipulator arm. This calls for intelligent control allocation between the base and the manipulator arm in order to obtain intuitive control of both the camera and the arm. We implement three different approaches to the control allocation problem, i.e., whether the vehicle or manipulator arm actuation is applied to generate the desired motion. The performance

of the different control schemes is evaluated, and our findings strongly suggest that objective metrics better describe the performance of the controller, even though there is a clear correlation between subjective and objective performance metrics.

3.2 Introduction

Teleoperation and haptic control allow operators to control remotely located objects from a safe and comfortable location. The main motivation for remotely operated robots is to relieve humans from entering hostile and dangerous environments and to utilize robots in areas where humans do not have access. This kind of systems poses several challenges when it comes to the evaluation of the control scheme, as it is not only the directly measurable metrics that define the performance of the controller, but also how the operator perceives the controller.

All teleoperated systems have one thing in common; they are controlled by a human operator, so how the human operator perceives the controller performance should thus be an important criterion when designing the controller. It is not straightforward, however, to find suitable metrics for this kind of subjective performance evaluations. In this paper we will use the NASA-TLX evaluation scheme to get feedback from the operators. In addition we will compare the results of the NASA-TLX with that of the objective metrics, which in this paper are i) the time used to perform a given task, ii) the number of errors/failures, and iii) the manipulability of the manipulator arm during the task. The main objective of comparing the subjective and objective metrics is to gain insight into to what extent these correlate. It is interesting to investigate whether or not the actual performance of the system is reflected in the feedback that we get from the operator.

Human factor is an important part in human-robot interaction (HRI) (Goodrich and Schultz [2007]). NASA-TLX has been widely used to study operators performance and workload in HRI (Steinfeld et al. [2006]). Measuring human mental workload when operators perform tasks with telerobotics, has been treated in for example Kiselev and Loutfi [2012], Adams and Kaymaz-Keskinpala [2004], Kaber et al. [2000a], and Stefanidis et al. [2010]. Grane and Bengtsson [2005] compare how different types of interfaces perform in terms of mental workload and Rook and Hogema [2005] used NASA-TLX to evaluate the effect of human-machine interface design. A relevant work on evaluating the HRI in vehicle navigation systems has been studied in Ross and Burnett [2001], and Kaber et al. [2000b] evaluate the effects of workload in a teleoperation task. Goodrich et al. [2004] proposed behavioral entropy as a technique to estimate human workload in HRI.

In this paper we use a haptically controlled mobile manipulator to perform the evaluation tests. The mobile manipulator allows for both locomotion and interaction tasks, both of which are challenging tasks for the operator and require the controller to efficiently transmit information about the remote environment to the operator in order to perform the task. In addition to the manipulator arm the mobile robot is equipped with a camera that is fixed in one direction in the robot frame, so the operator will have

a restricted amount of visual information about the environment.

Teleoperated robotic manipulators have long been an active field of research and a wide variety of controllers have been proposed. Passivity-based controllers are commonly used to control bilateral teleoperation systems with two-port network representations (Hokayem and Spong [2006], Jee-Hwan et al. [2004a], Jee-Hwan et al. [2004b]). Energy-based approaches have also been proposed to obtain stable behavior of the two systems, for example in Hannaford [1989] and Franken et al. [2011]. Over the last years, however, we have seen an increased interest also in teleoperation of mobile manipulators, i.e., a robotic manipulator mounted on a mobile base. This setup has great potential because it combines two important properties: the mobility of the mobile base and the dexterity and manipulability of the manipulator arm (Park and Khatib [2006], Seraji [1998], Farkhatdinov and Jee-Hwan [2008]).

We implement three different control schemes that cannot straightforwardly be separated in terms of performance and user evaluation, and find the correlation between the different performance metrics. As the control is implemented on the slave side, the actual difference between the approaches is rather subtle from the operator's point of view, so good performance metrics are essential to be able to distinguish between them. The main objective is to investigate whether objective and/or subjective metrics can distinguish between these control schemes, to find any correlation between the metrics, and to suggest a set of metrics that in a decisive way can quantify the performance of haptically controlled robotic systems.

3.3 System Setup and Problem Formulation

The system to be studied consists of a standard bilateral teleoperation setup with a haptic device controlled by a human operator which is used to control a remotely located robot. The robot consists of a wheeled vehicle with a manipulator arm attached to it. We will attach a frame $\mathcal{F}_b$ to the vehicle and denote the location of $\mathcal{F}_b$ with respect to the inertial frame $\mathcal{F}_0$ by the homogeneous matrix g_{0b} and its velocity by the body velocity twist $\hat{V}_{0b}^B = g_{0b}^{-1}\dot{g}_{0b}$. The configuration of the robotic arm is given by the joint variables $q \in \mathbb{R}^n$ in the normal way, and the joint velocities as $\dot{q} = \frac{\mathrm{d}q}{\mathrm{d}t} \in \mathbb{R}^n$. The position of the end-effector frame $\mathcal{F}_e$ in the world frame is found as $g_{0e} = g_{0b}g_{be}(q)$ (From et al. [2010a]). We refer to From et al. [2014a] for a detailed formulation of the kinematics of vehicle-manipulator systems.

3.3.1 The Control Allocation Problem for Mobile Manipulators

The setup described above calls for the integration of two rather distinct operation modes: i) accurate manipulation of objects using the robotic arm in the relatively limited workspace of the manipulator; and ii) locomotion of the vehicle in a possibly very large workspace. The main challenge is therefore to obtain a control allocation between the vehicle and the manipulator in such a way that the motion of both the vehicle and the

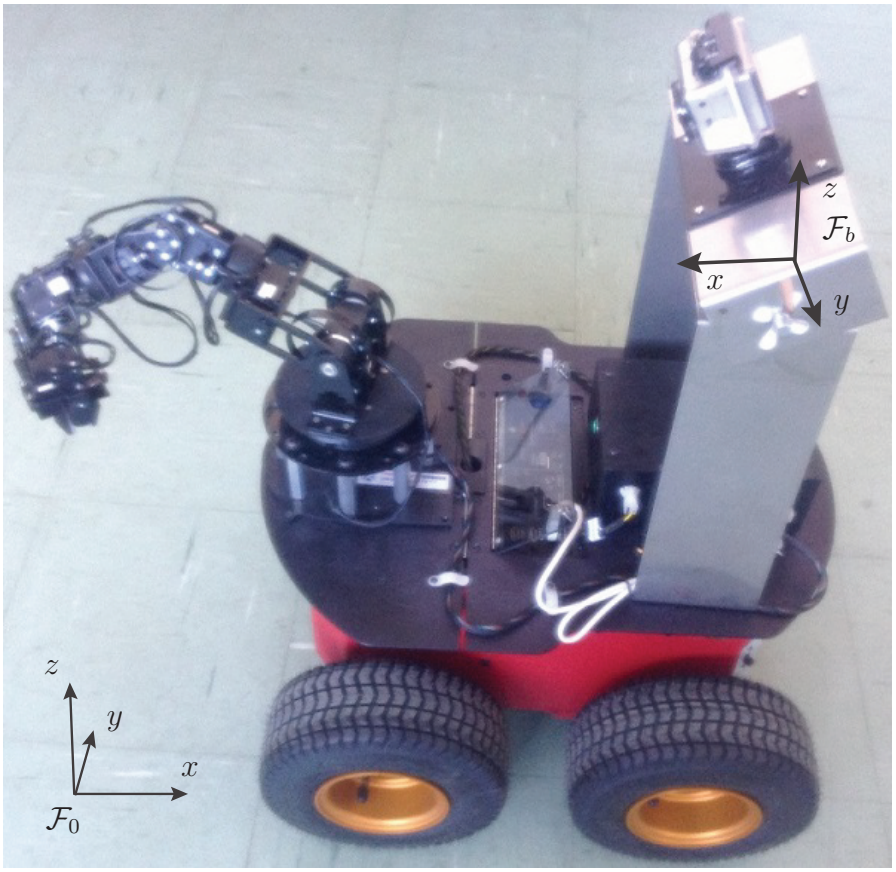

Figure 3.1: The coordinates of a mobile manipulator with on-board camera

manipulator arm can be controlled intuitively using the manipulator-like haptic device. We denote this the control allocation problem for mobile manipulators.

The distribution of control forces between the manipulator and the base to obtain both manipulation and locomotion is obtained through the control allocation algorithm, i.e., how to interpret the master reference (6 DoF) as both position and velocity references and how to distribute the control forces between the vehicle and the base (3+6 DoF), i.e., the control allocation problem for vehicle-manipulator systems.

In this paper we take the master reference and generate position or velocity references for the vehicle and manipulator, and we denote this the control allocation problem because the motion is distributed between the two systems. It is important to note, however, that we assume that the low-level controllers of the vehicle and manipulators are such that these references are followed, i.e., we are only concerned with kinematic control. Once the control allocation is in place, any method for stable teleoperation can be used, such as passivity- and energy-based approaches.

3.3.2 Problem Formulation

The main motivation of this paper is to gain more insight into how well different metrics describe the performance of user controlled mechanical systems. The main objective is to understand whether or not the way the user perceives the controller is reflected in the actual behavior of the robot in terms of objective and directly measurable metrics.

We study the correlation between

1. Objective performance metrics
   (a) execution time
   (b) number of failures
   (c) arm manipulability
2. Subjective performance metrics
   (a) NASA-TLX
   (b) interview.

We will compare three control schemes with similar characteristics and endeavor to determine whether the objective or subjective metrics best describe the performance of the system, and in particular if they give the same result.

3.4 Motion Control

In this section, we will briefly introduce what we refer to as the control allocation problem for vehicle-manipulator systems, i.e., how a reference trajectory is allocated between the vehicle and the arm. This problem has been studied in detail in Pham and From [2013].

3.4.1 Control Modes

All of the approaches presented in this paper use the notion of control modes to determine distribution of control forces. The control modes are described in brief below.

3.4.1.1 Manipulation Mode

This mode is used for fine manipulation and interaction tasks. This is normally implemented as a position-to-position or velocity-to-velocity control scheme. Because the manipulator arm is generally much more accurate than the vehicle, manipulation mode is realized through the manipulator arm only while the vehicle is fixed. Thus, as the vehicle is fixed and we only control the slave robot which is kinematically similar to the master robot, we can apply any standard control scheme for haptic teleoperation in this mode. If larger motions are desired, vehicle actuation is required and we switch to locomotion mode.

3.4.1.2 Locomotion Mode

Whenever a large displacement of the robot is needed the vehicle needs to take care of this motion. Normally a position-to-velocity control scheme is chosen to allow for an infinitely large slave workspace. In locomotion mode the vehicle and the arm are used to obtain large displacements of the end-effector. As the master robot is to control both

the vehicle and the slave arm, we have two kinematically dissimilar systems. We solve this by virtually connecting the master end effector to the slave end effector, which is our primary control objective.

3.4.2 Control Strategies

In this section we present in brief the three control strategies used for the experiments in this paper. We refer to Pham and From [2013] for a more detailed description of the control laws.

3.4.2.1 Strategy I - Master workspace strategy

With this strategy, the robot will automatically change between the two control modes depending on the master position. If the robot is far from the goal, the operator will move the haptic device far and fast. It is thus natural to define a limit area in the master manipulator's workspace so that whenever the master is inside this area, the robot will be controlled in manipulation mode while we switch to locomotion mode when it moves out of the area. Using the limits as defined in Fig. 2.3 the mode is chosen corresponding to the following law:

$$\text{Mode} = \begin{cases} \text{Manipulation} & \text{if} \begin{cases} |z_m| \leq z_0 \\ |x_m| \leq x_0 \\ |v_z| \leq v_0 \end{cases} \\ \text{Locomotion} & \text{otherwise} \end{cases} \tag{3.1}$$

where z_m and x_m are the master positions in the zx-plane of the haptic device and v_z is the master speed in the z-axis of the master frame. z_0, x_0 and v_0 are constant parameters that define when switching will occur.

When in locomotion mode we allow only for motion of the vehicle which is given by

$$\begin{bmatrix} v_s \\ \phi_s \end{bmatrix} = \begin{bmatrix} -k_v & 0 \\ 0 & -k_\phi \end{bmatrix} \begin{bmatrix} d_1 \\ d_2 \end{bmatrix} \tag{3.2}$$

where k_v and k_ϕ are proportionality constants; v_s and ϕ_s are the velocity and the heading angle of the vehicle in the body frame; and d_1 and d_2 are defined by the position of the haptic device, as shown in Fig. 2.3, i.e., the distances from the master's tip position to the limit area that is used to define the manipulation mode.

3.4.2.2 Strategy II - Slave workspace strategy

Alternatively we can use the slave workspace to determine the control mode. Like in Wrock and Nokleby [2011], the system changes automatically from the manipulation mode to the locomotion mode when the slave manipulator reaches the limit of the

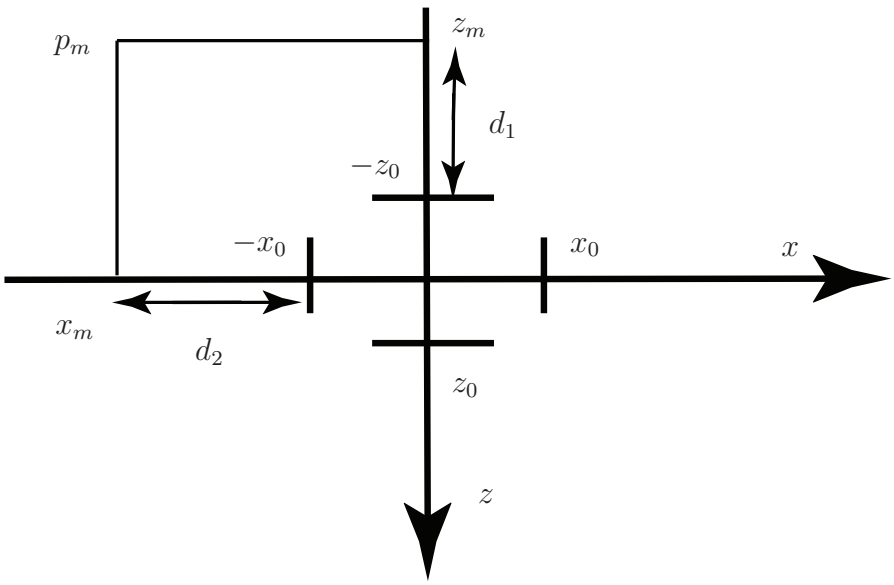

Figure 3.2: Determining d_1 and d_2 from the haptic position.

workspace. We thus have

$$\text{Mode} = \begin{cases} \text{Locomotion} & \text{if} \begin{cases} |x_s| \geq x_l \text{ or } |y_s| \geq y_l \\ |x_{sd}| \geq x_l \\ |y_{sd}| \geq y_l \end{cases} \\ \text{Manipulation} & \text{otherwise} \end{cases} \tag{3.3}$$

where x_s and y_s are the actual slave positions in the x- and y- axes of the robot frame; x_{sd} and y_{sd}, that are computed from actual master positions, are the desired slave manipulator position; and x_l and y_l are the slave limit positions in the x- and y- axes of the robot frame, respectively. The locomotion mode using this approach is similar to the master workspace strategy presented in 3.4.2.1.

3.4.2.3 Strategy III - Control Allocation

In this section we describe the third control scheme, first presented in Pham and From [2013], which introduces artificial forces between the end-effector and the base.

First we find the manipulator workspace $\mathcal{W}_M$ with respect to the vehicle frame $\mathcal{F}_b$. We define the workspace for position control as a workspace $\mathcal{W}_P$, somewhat smaller than the manipulator workspace $\mathcal{W}_M$, as illustrated in Figure 2.4. Whenever the manipulator is inside this workspace, position control is applied. This is equivalent to the manipulation mode in the previous sections.

If the master manipulator is outside the workspace $\mathcal{W}_P$, velocity control is applied. In this case the slave manipulator remains fixed at the limit of the workspace, while the vehicle velocity is so that the vehicle follows the master end-effector with a mass-spring-damper characteristics.

Denote by $\bar{x}_s$ the position of the end effector projected into the position workspace $\mathcal{W}_P$, as illustrated in Figure 2.4. Then the slave position with respect to this projected

position is given by $\Delta = x_s - \bar{x}_s$ and we will let the vehicle be governed by

$$F = \ddot{\Delta} + d\dot{\Delta} + k\Delta. \tag{3.4}$$

The following references will give the above characteristics:

- Manipulator arm reference:

$$V^B_{0e,r} = V^B_{0e,d} - \frac{1}{d_b}F, \tag{3.5}$$

- Vehicle reference:

$$V^B_{0b,r} = \frac{1}{d_b}F. \tag{3.6}$$

This control law is to be interpreted in the following way: The desired end-effector velocity in the inertial space is given by $V^B_{0e,d}$. The manipulator reference is obtained by the Adjoint map Ad_g (From et al. [2014a]) and subtracting the vehicle motion $V^B_{0b,r}$, i.e.,

$$V^B_{be,r} = V^B_{0e,d} - \mathrm{Ad}_{g_{eb}} V^B_{0b,r} \tag{3.7}$$

so it only remains to find the reference for the vehicle motion from the desired end-effector motion. The position, velocity, and acceleration of the end effector with respect to the vehicle generates a force F given by (3.4) that acts on the vehicle. This force is transferred into a vehicle motion, or rather the vehicle velocity by (3.6) where d_b can be interpreted as the damping on the vehicle. Note that this is different from d which is the desired damping characteristics as observed from the camera when watching the end effector. Finally the motion of the vehicle is removed from the desired motion passed on to the manipulator controller. Note also that the constants in the mass-spring-damper system (3.4) need to be tuned to avoid saturation in the manipulator workspace.

For a wheeled robot no instantaneous motion in the direction of the y-axis is allowed, in which case the torques that act on the vehicle will take the form

$$\tau_V = \begin{bmatrix} m\ddot{\Delta}_x + d\dot{\Delta}_x + k\Delta_x \\ 0 \\ m\ddot{\Delta}_{y,\psi} + d\dot{\Delta}_{y,\psi} + k\Delta_{y,\psi} \end{bmatrix}. \tag{3.8}$$

3.5 Experiments—Rationale and Methods

Several inexperienced operators were asked to control the robot to perform a simple task which required both fine manipulation and locomotion. Even though the task itself is simple, it is hard to perform because the operator only sees the remote workspace through a narrow camera window. It is further complicated by the kinematic dissimilarity of the master and the slave.

Due to these difficulties, particularly for inexperienced operators, we experience a high number of failures and long execution times for most operators. It is therefore difficult to compare the performance of the different approaches. The experiments are

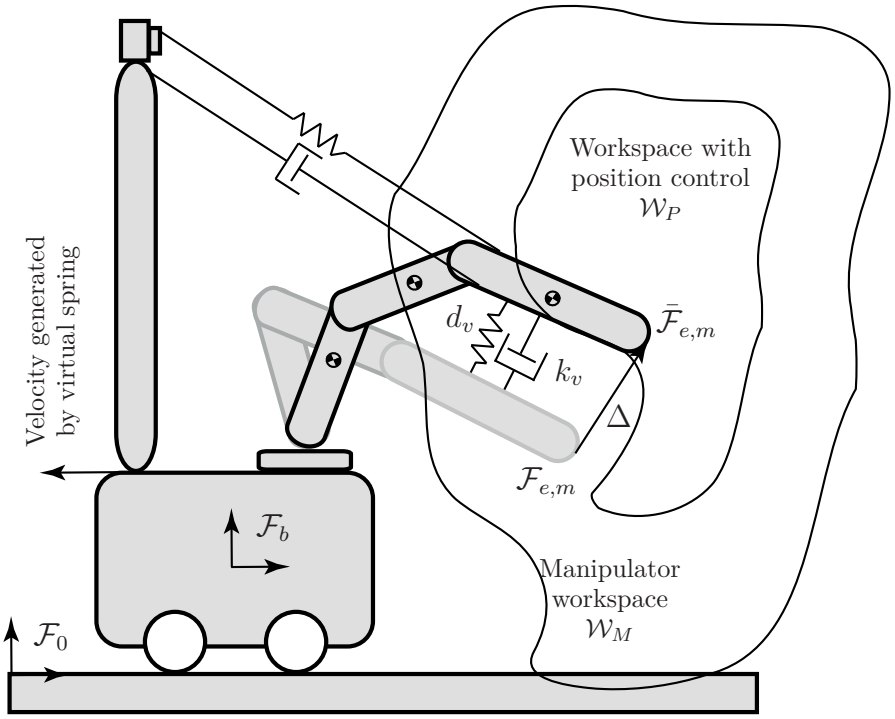

Figure 3.3: Definition of the workspaces in which the robot is controlled in the locomotion and manipulation modes. Note that the workspace is defined for the manipulator arm with respect to the vehicle frame $\mathcal{F}_b$, and not the world frame $\mathcal{F}_0$. The velocity is generated by the virtual spring between the master manipulator (gray) and the slave manipulator (black). The intuitive interpretation of the virtual spring is illustrated by the spring between the master manipulator and the vehicle.

motivated by the observation that it is hard to distinguish the performance of a control law based on the feedback from the operators, and we would like to investigate further whether this low discrepancy is due to similar performance of the approaches or because it is not captured by simply interviewing the operators. To this end, we use subjective and objective measures to see what best captures the performance of the control laws, and if the two approaches of measuring performance give the same result.

We perform a series of experiments and measure the performance using both a subjective workload assessment and measurable metric values to characterize the performance of the control laws. For the subjective evaluation we use the NASA-TLX test which gives us an overall workload score calculated from the weighted average of six subcategories. This will give us an idea of how mentally challenging the operators find the task. The objective evaluation of the task is performed based on execution time, number of failures, and the mobility of the robot arm during task execution. Our main objective is to discover discrepancies between the approaches and, if such a discrepancy exists, evaluate what is the best way to evaluate the performance of an interaction task using a mobile manipulator.

3.5.1 Robotic Setup

A standard 6-DoF Phantom haptic device from Sensable was used to control a mobile manipulator consisting of a Pioneer 3-AT mobile robot with a 7-DoF Cyton arm attached to it. The local computer communicates with the remotely located on-board computer via a wireless network. The time delay is minimal and not treated in this paper. The control is, however, implemented so that it is robust with respect to time delays.

The operator's view of the remote workspace is through a video image displayed on a screen only, i.e., there is no direct visual of the robot. The video is captured by a camera and transmitted to a screen.

3.5.2 Methods

The participants were asked to conduct a specific task which consisted in traversing a room to pick up an object and put it into a bin. We also placed several obstacles between the starting point and the destination to enforce a change of direction during the locomotion. The operators have to control the robot to cross the room and avoid all obstacles to complete the task. When they arrive at the final destination they have to pick up an object and place it into the bin, which completes the task. The task is constructed to force switching between the two control modes.

To verify the control scheme presented we let several inexperienced operators control the robot. We let the operators perform several different tasks using three different strategies:

S1. Automatic changing between locomotion and manipulation mode using master workspace, Section 3.4.2.1;

S2. Automatic changing between locomotion and manipulation mode using slave workspace, Section 3.4.2.2;

S3. Control allocation approach, Section 3.4.2.3.

To avoid learning effects the sequence of the control schemes is randomized:

- 1/3 of the operators perform the experiments with the sequence of the control schemes S1-S2-S3
- 1/3 of the operators perform the experiments with the sequence of the control schemes S2-S3-S1
- 1/3 of the operators perform the experiments with the sequence of the control schemes S3-S1-S2

To evaluate the performance of the operators the following metrics were used:

Subjective metrics

The following subjective metrics were used:

- **Interview -** the operators were asked to describe how each control law performed.
- **NASA-TLX -** the operators filled in the NASA Task Load Index (NASA-TLX). The NASA-TLX uses six dimensions to assess mental workload: mental demand, physical demand, temporal demand, performance, effort, and frustration Rubio et al. [2004]. After performing each task, the operators provide ratings on each of the six subscales. The operator is also asked to rate which factors he/she considers the most important.

Objective metrics

The following objective metrics were used:

- **Number of failures -** the number of failures for each approach was registered.
- **Execution time -** the time needed to complete the task (when successful) was recorded.
- **Manipulability -** the manipulability of the robot arm during the manipulation task was recorded, i.e., for the time interval starting when the gripper closes (when the object is grasped) and until the gripper opens (when the object is dropped into the bin), and not for the first part of the experiment when only locomotion mode is used. This gives us an idea of the mobility of the arm and the distance from singularities during motion.

3.6 Experimental Results and Discussion

In this section we first present the experimental results in Section 3.6.1, followed by a discussion in Section 3.6.2.

3.6.1 Experimental Results

3.6.1.1 General Feedback

All the operators were interviewed during and after the experiments which gave valuable feedback regarding their "feel" during the experiments. This is important information when we later are to evaluate the teleoperation schemes and compare them.

For the master workspace strategy, almost all operators are confused whether it is the vehicle or the arm that is controlled. The reason for this is probably that the arm (which is visible for the operator on the screen) does not follow the master, i.e., it can stop moving as the master enters the locomotion mode. The operators report that this makes it difficult to control the system.

With the slave workspace, on the other hand, the operators know exactly when the vehicle will move because the arm has to move to the limit before the vehicle can move.

They therefore report that they can perform the task more easily. However, since this is a rather simple task—just to grasp an object—they almost only use the locomotion mode. The slave workspace strategy allows for this as the manipulator arm is stretched forward during locomotion mode. The master workspace strategy, on the other hand, does not necessarily allow for this as the arm may be retracted during locomotion mode. In principle the operators have to control the robot so that the end effector passes the object and then move the arm back to grasp the object. Because the arm is at the limit of its workspace when the system moves towards the object, some operators find it difficult to position the system close enough to the object. This motivates leaving the manipulator more in the middle of its workspace during locomotion mode.

The operators report that the control allocation approach is the most intuitive and find it fairly simple once they manage to think of the task as controlling the end-effector motion. They also report that they are able to disregard the vehicle motion when performing manipulation tasks and also when the vehicle is moving slowly. This makes the operation more efficient because the switching is hidden from the operator. With this approach, the operator can easily drive the system close enough to the object to execute the task. At this position, the arm is close to the center of its workspace so that it can be controlled in the manipulation mode. This strategy thus takes advantage of the slave workspace strategy and also eliminates some of the drawbacks of the same strategy.

3.6.1.2 Quantitative Metrics

To get a more quantitative evaluation of the different approaches we measured the median execution times, number of failures, and median manipulability for each operator performing the task. We also asked the operators to fill in the NASA-TLX form. A summary of the results is shown in Table 2.1.

	Strategy		
	Master workspace	Slave workspace	Control allocation
Execution times	206 s	202 s	174 s
Number of failures	61	48	23
Manipulability	0.727	0.829	1.000
NASA-TLX	60.67	56.83	53.67

Table 3.1: Median execution times, number of failures, median manipulability (normalized), and median NASA-TLX for the three strategies for 24 inexperienced operators.

The executing times of the 24 operators are shown in Fig. 2.5 and Figure 3.5. We see that the control allocation is the approach that performs the best quite consistently. There are three operators that perform the operation fastest with the master workspace strategy and one user who takes the shortest time with the slave workspace strategy. Figure 3.5 shows the overall performance in terms of execution times and we see that the control allocation has better performance. This confirms the feedback from the operators that the third method is the most intuitive.

The number of failures for the three strategies is shown in Figure 3.6 and Figure 3.7. The highest number of failures occurs for the master strategy. This corresponds

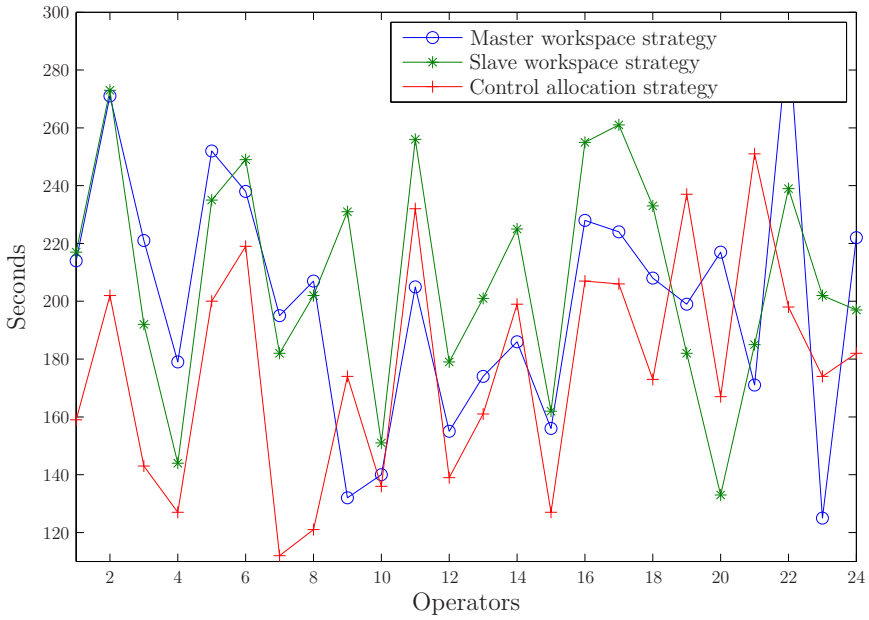

Figure 3.4: The executing times for 24 inexperienced operators performing the three strategies

Figure 3.5: The median, the maximum, 75th percentile, 25th percentile and minimum values of executing times.

well with the operators' "feel"; they reported that they felt confused when they control the robot using this strategy because the robot can change quite suddenly between the two control modes when the master moves in or out of the limit area, which can cause failures. Also the slave strategy has a high number of fail tries. Recall that the slave manipulator is at the limit of its workspace (stretched out) when the robot moves towards the object so that it is difficult for operators to put the robot in a good position to interact with the object. The control allocation strategy has the lowest number of failures. Also this is natural as the manipulator arm is drawn towards the center of its

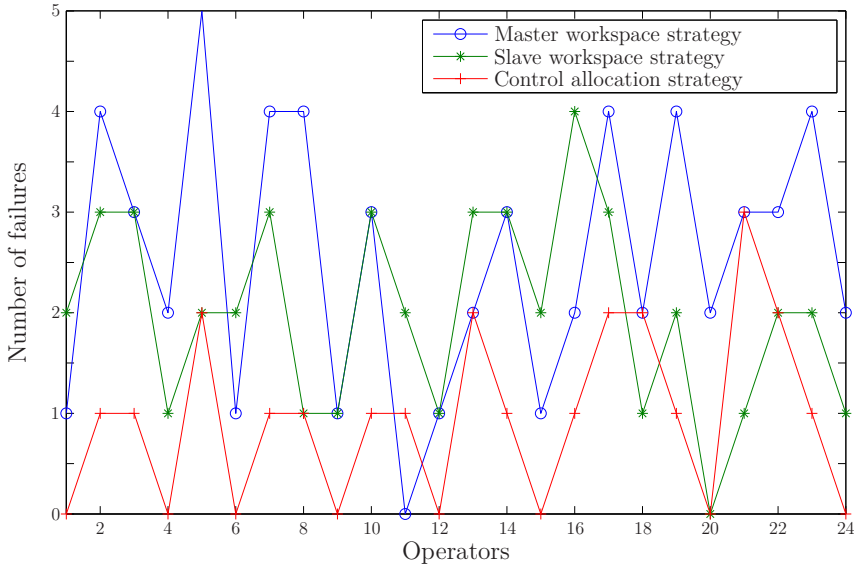

Figure 3.6: The number of failures for 24 inexperienced operators performing the three strategies

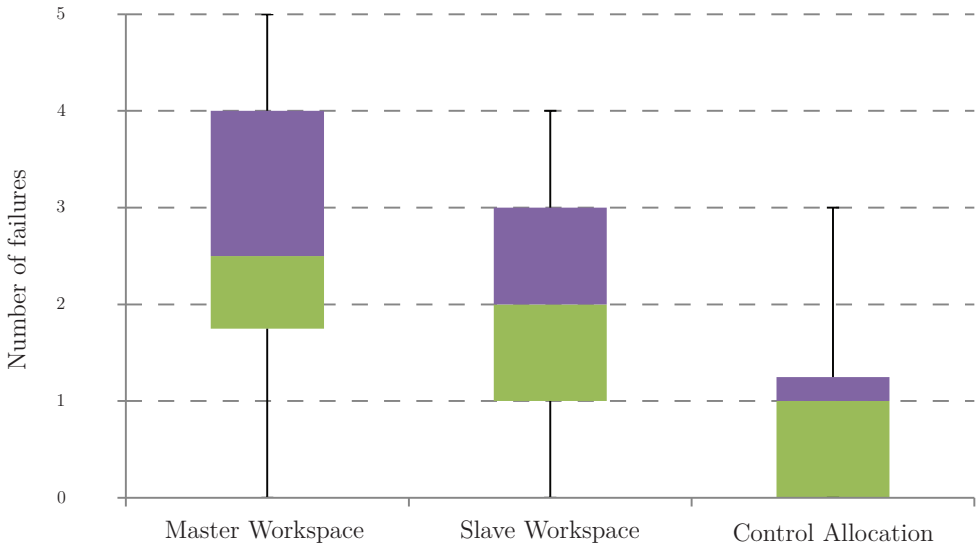

Figure 3.7: The median, the maximum, 75th percentile, 25th percentile and minimum values of number of failures.

workspace and also corresponds well with the feedback from the operators.

For the manipulability metric the control allocation maintains good manipulability during the grasping operation, as can be seen from Figure 3.8 and Figure 3.9. The control allocation maintains its high manipulability due to the virtual spring. The master workspace has a little bit better manipulability than the slave workspace. We will not put too much into this, however, as the positioning of the arm for the master workspace approach is random. The slave workspace strategy has the lowest manipulability because the slave manipulator is normally fixed at the limit of the workspace when in locomotion mode, which is the main drawback of this strategy.

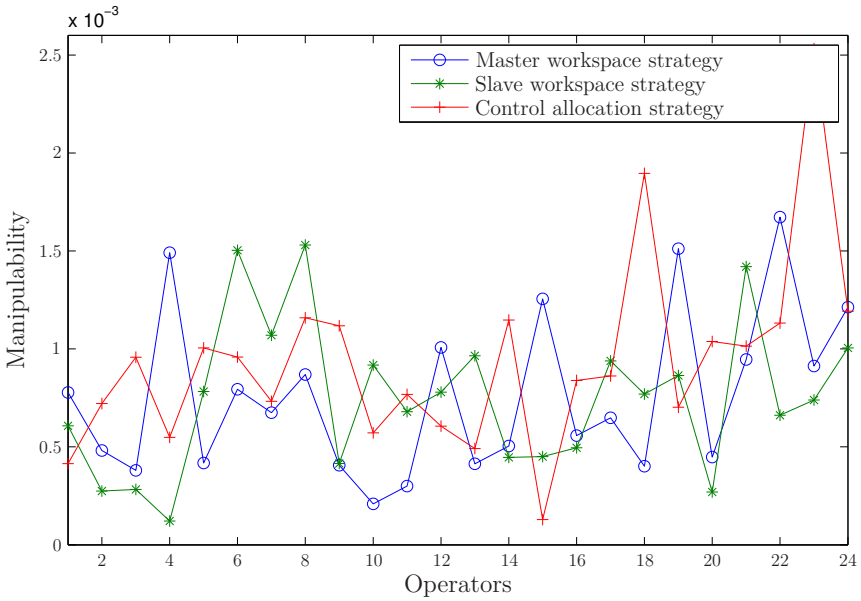

Figure 3.8: The manipulability in three strategy of 24 inexperienced operators

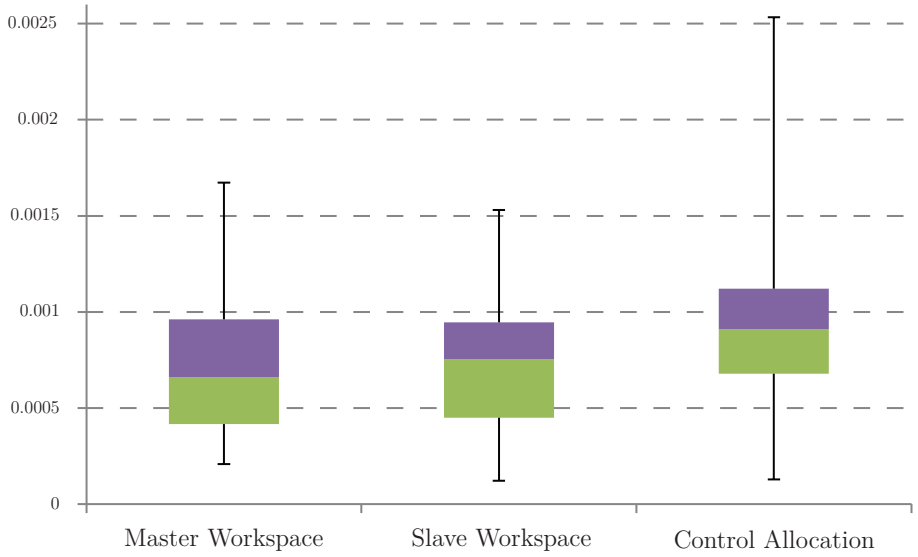

Figure 3.9: The median, the maximum, 75th percentile, 25th percentile and minimum values of manipulability.

Also for the NASA-TLX the control allocation performs slightly better than the other approaches, as can be seen from Table 2.1, Figure 3.10 and Figure 3.11. Once again the control allocation strategy has the best performance with a slight advantage over the other approaches. There are some minor variations in performance for the different subcategories, for example the operators clearly feel a higher level of frustration when using the slave and master workspace strategy compared to the control allocation, while they feel more stress on temporal demand with the control allocation.

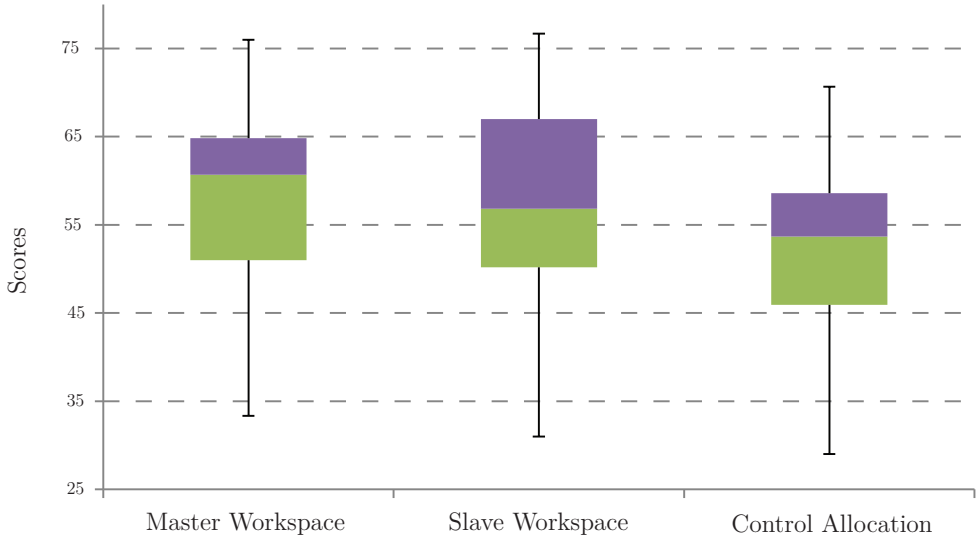

Figure 3.10: The median, the maximum, 75th percentile, 25th percentile and minimum values of NASA TLX scores.

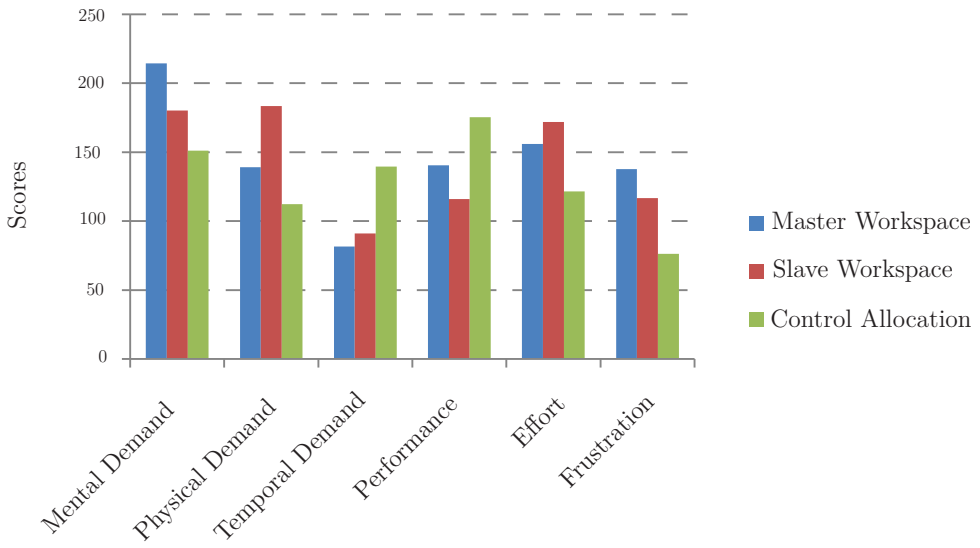

Figure 3.11: Six different categories evaluated in measuring workload

3.6.2 Discussion

Several different metrics for evaluating the performance of the proposed control schemes were presented. We divide the metrics into theoretical and directly measurable performance metrics on one hand, and subjective metrics such as stress and frustration on the other. The main purpose of this paper is to evaluate whether objective or subjective performance metrics best describe the performance of a control law for teleoperation of mobile manipulators with limited visual feedback from the remote environment, and whether there is any discrepancy between the approaches.

The results presented in the previous section all suggest that the control allocation performs better than the other approaches. In this sense the results are fairly consistent,

even though the number of experiments performed was quite low. It is fair to conclude from this that the number of experiments performed is sufficient to distinguish between the different control approaches.

The experiments suggest that the operator actually has a fairly good intuition when it comes to what control scheme that performs the best, which is not obvious as the operator only has limited knowledge of what happens on the slave side. In fact, we get more useful information from the interview process than the NASA-TLX. While the operator certainly has a good notion of how well he does in terms of failures, the execution times are in many cases very similar and it is probably fair to say that the operator will not give much thought to the manipulability during the operation. It is therefore not obvious that these results are mirrored in the interview process and the NASA-TLX. On the other hand, we believe that the theoretical metrics such as number of failures, execution time, and manipulability give a better measure of the actual performance; the number of failures, for example, tells us that the control allocation approach clearly outperforms the other methods, but this is not clear from the NASA-TLX test. We see that there is a clear correspondence between the general feedback and the objective metrics, but this is only partially seen from the results of the NASA-TLX test.

The preliminary results give some early predictions regarding the usefulness of the evaluation metrics presented and the discrepancy between these. More importantly it serves as a motivation to investigate this further and shows the importance of being aware of two rather different ways of measuring the performance of different teleoperation control schemes. The number of operators that performed the test in this paper is limited, but sufficient to obtain a preliminary conclusion. Although we need more experiments to get a strong statistical foundation, the results presented give us a clear indication of the performance of the metrics.

3.7 Conclusion

In this paper we have compared subjective and objective performance metrics for evaluating the performance of different controllers for mechanical systems that are haptically controlled by human operators. We find that even though subjective metrics based on the NASA-TLX and interviews give a fair indication of the performance of a control scheme, the objective and directly measurable evaluation methods represent better metrics of performance evaluation. In fact we find that objective metrics such as execution time, number of failures, and arm manipulability correspond better with the feedback during the interview than the NASA-TLX, which may come as a surprise, as the intention of the NASA-TLX is to capture the mental workload during operation. Even though the feedback from the operators is important to get a good understanding of how a controller performs, the results strongly suggest that objective metrics do better when it comes to evaluating the performance of different control schemes of systems controlled by a human operator.

Part II

Kinematically Constrained Serial Manipulators

Chapter 4

An Analytical Approach to Operational Space Control of Robotic Manipulators with Kinematic Constraints

4.1 Abstract

This paper presents a novel control architecture for operational space control when the end effector or the robotic chain is kinematically constrained. Particularly, we address kinematic control of robots operating in the presence of obstacles such as point, plane, or barrier constraints imposed on a point on the manipulator. The main advantage of the proposed approach is that we are able to control the end-effector motion in the normal way using conventional operational space control schemes, and by re-writing the Jacobian matrix we also guarantee that the constraints are satisfied. The most challenging problem of obstacle avoidance of robotic manipulators is the extremely complex structure that arises when the obstacles are mapped from the operational space to joint space. We solve this by first finding a new set of velocity variables for a point on the robot in the vicinity of the obstacle, and on these new variables we impose a structure which guarantees that the robot does not hit the obstacle. We then find a mapping denoted the Constrained Jacobian Matrix from the joint variables to these new velocity variables and use this mapping to find a trajectory in joint space for which the constraints are not violated. We present for the first time the Constrained Jacobian Matrix which imposes a kinematic constraint on the manipulator chain and show the efficiency of the approach through experiments on a real robot.

4.2 Introduction

Efficient solutions to collision avoidance for complex kinematic chains in the presence of obstacles of different shape and form is an extremely challenging problem. The obstacles impose constraints of different shape and dimension on one or several points

on the kinematic chain which results in very complex kinematics when the constraints are taken into account. Particularly, the mapping from the joint velocities to the end-effector velocities cannot be found in the standard way by the manipulator Jacobian when constraints are present.

The main objective of robot control, whether the trajectory is computer generated or given by an operator through a haptic device, is to control the end-effector motion to achieve a certain task or obtain a desired behavior. The control signal sent to the robot is therefore often a joint velocity reference calculated from the desired end-effector velocity by the inverse of the Jacobian matrix. This mapping does not, however, take into account the constraints imposed by obstacles in the robot's workspace. In this paper we thus propose a *Constrained Jacobian Matrix (CJM)* that maps the joint velocities to the end-effector velocities *subject to the constraints imposed by the obstacles*. The Constrained Jacobian Matrix gives us a velocity reference for the joints which guarantees that the constraints are not violated.

In this paper we solve the constrained kinematics problem by first defining a new set of velocity variables from the desired end-effector velocity in such a way that the reduced dimensionality due to the constraints are cast into the velocity variables by imposing a certain structure on these new variables. The velocity variables define a motion of a point on the robot that is close to the obstacle and the new structure guarantees that the constraints imposed by the obstacle are obtained. Secondly, we find the Jacobian matrix, denoted the Constrained Jacobian Matrix, which maps the *new* velocity variables into the joint velocities, and thus allows us to find a *trajectory in joint space for which the constraints are not violated*. Finally the control is obtained in the standard way by replacing the standard Jacobian matrix with the Constrained Jacobian Matrix. Early results were presented in From [2013b]. In this paper we present for the first time the Constrained Jacobian Matrix when the constraints are imposed on a point on the kinematic chain and verify the formulation empirically.

As the main control objective of the great majority of the applications found in robotics is to obtain a desired behavior of the tool, the control law needs to be defined in the operational space. We thus require a framework which allows the control law to be formulated in the end-effector frame and at the same time satisfies the kinematic constraints defined in the inertial frame. The Constrained Jacobian Matrix allows us to derive such a control law because it maps the joint velocities to the end-effector velocities subject to the constraints imposed on the robot.

Defining the control law in the end-effector frame allows us to apply control schemes such as impedance and hybrid control in the tool frame. Hybrid control in the end-effector space has been studied in detail by many authors and lets the end-effector space be divided into directions which require stiff control and directions that require soft compliant control (Natale [2003], Mason [1981], Craig and Raibert [1979], Abbati-Marescotti et al. [1990], Bruyninckx and De Schutter [1996], Lipkin and Duffy [1988]). One example in which hybrid or compliant control is required at the end effector and for which the kinematic chain is constrained is Robotics-assisted Minimally Invasive Surgery (RAMIS). The constraints imposed by the entry point where the robot enters the human body require zero lateral velocity in order to not damage the patient (Funda et al. [1996],

Li et al. [2005], Ortmaier and Hirzinger [2000], Locke and Patel [2007], Lenarčič and Galletti [2004], Azimian et al. [2010]). Other examples are robot manipulators in a cluttered environment or mobile manipulators for which the mobile base needs to avoid hitting obstacles while following a desired trajectory for the end effector.

The paper is organized as follows: In Section 4.4 and 4.5 we present the overall idea of how the kinematics of a constrained kinematic chain is calculated. The mathematical representation of the different kinematic constraints are presented in Section 4.6 and the corresponding Jacobian matrices are found in Section 4.7. A simple study case with constraints on the chain is presented in Section 4.8 where we also show how the results from Sections 4.6 and 4.7 are used and how the calculations are carried out in practice. The experimental results are presented in Section 4.9 and the relevant research and concluding remarks are presented in Sections 4.3 and 4.10, respectively.

4.3 Related Research

The motion planning problem has been studied by several researchers over the last decades and a wide variety of approaches have been developed to solve this problem. In general the problem is quite different for mobile robots and robotic manipulators. For mobile robots the motion planning problem normally reduces to finding a point trajectory in a cluttered environment. Even though the problem is easy to formulate it has shown to be a difficult problem to solve and still remains an active area of research. However, several results have been obtained over the last three-four decades for efficient obstacle avoidance of mobile robots. For robotic manipulators on the other hand, the complex kinematics, the collision avoidance of several bodies, and in particular the complex geometry of the obstacles when mapped to the high-dimensional joint space make motion planning extremely hard to solve.

Motion planning for vehicles and mobile robots is the problem of finding a continuous path from an initial to a final position and orientation without colliding with objects in the robot's workspace. This problem is very simple to formulate, but has turned out to be rather difficult to solve. The very first attempts to solve this problem use the notion of configuration space (Lozano-Perez [1983], Siciliano et al. [2011]) and use roadmaps to connect the initial and final position through collision-free paths. Generalized Veroni diagrams can be used efficiently to solve this problem in an optimal manner in the sense that the distance to the obstacles is minimized ODunlaing and Yap [1985]. Another early approach decomposes the collision-free workspace into cells and then find a collision-free path by connecting the cells so that a collision-free path from the initial to the final position is found (Schwartz and Sharir [1983a,b]). We refer to LaValle [2006], Canny [1988] and Latombe [1991] for more details on motion planning of mobile robots and vehicles.

In the case of robotic manipulators the problem of obstacle avoidance is normally solved by introducing a potential field pushing the manipulator away from the obstacle (Khatib [1986]). Normally two types of potential fields are applied to the robot: i) an attractive potential U_a that pushes the robot end effector towards its desired position

and a repulsive field U_{ri} that pushes each link of the robot and the robot end effector away from the obstacles. The total potential field is given by

$$U_t = U_a + \sum U_{ri} \tag{4.1}$$

which can be realized either as a joint torque

$$\tau_t = -(J_e^S(q))^\mathsf{T} \Delta U_t(p_e) - \sum (J_i^S(q))^\mathsf{T} \Delta U_t(p_i) \tag{4.2}$$

or as joint velocity

$$\dot{q}_t = -(J_e^S(q))^\mathsf{T} \Delta U_t(p_e) - \sum (J_i^S(q))^\mathsf{T} \Delta U_t(p_i) \tag{4.3}$$

where p_i for $i = 1, \ldots, m$ are the points of the manipulator that are checked for collision and J_i^S is the Jacobian matrix of the same points. The main advantage of Equation (4.2) is smooth motion obtained as the forces are filtered through the manipulator dynamics. Equation (4.3), on the other hand, has a quicker response and responds quicker to trajectory errors or moving objects.

We see that the potential field in principle guarantees that the robot does not hit the obstacles, as the artificial force pushes the robot away from the obstacle with a higher force as the distance to the obstacle reduces. Although the strength of the potential field can be tuned, the formulation does not allow for exact positioning of the robot with respect to the obstacles. For more complex obstacles like holes and planes we need to be able to position the robot more accurately in the presence of the obstacle which calls for an analytical approach to the problem. Furthermore, obstacles such as forcing a point to lie between two planes are not solved very efficiently by potential fields as they require two potential fields pushing in opposite directions which may cause unstable and oscillating behavior. When several forces are present these can also eliminate each other and the robot can encounter local minima in which it gets blocked.

4.4 System Overview and Problem Formulation

The system discussed in this paper consists of a redundant robotic manipulator in the presence of obstacles. The redundancy is obtained either by placing a standard manipulator on a moving base, by utilizing a manipulator with a higher mobility than the task space, or a combination of these. At some given points in the Cartesian space we will require that the velocities of the links are eliminated in certain directions to prevent the robot from hitting an obstacle. The system setup together with the most important configuration spaces used in this paper are shown in Fig. 4.1. We denote the frame of the joint located before the constraint located at $\mathcal{F}_c$ in the chain by $\mathcal{F}_a$ and the joint that is located after the constraint is denoted $\mathcal{F}_b$. The desired end-effector motion is given by the frame $\mathcal{F}_e$. We will denote the velocity variables in the following way

$$V_{0e}^{B,S} = \begin{bmatrix} v_x^e & v_y^e & v_z^e & \omega_x^e & \omega_y^e & \omega_z^e \end{bmatrix}^\mathsf{T} \tag{4.4}$$

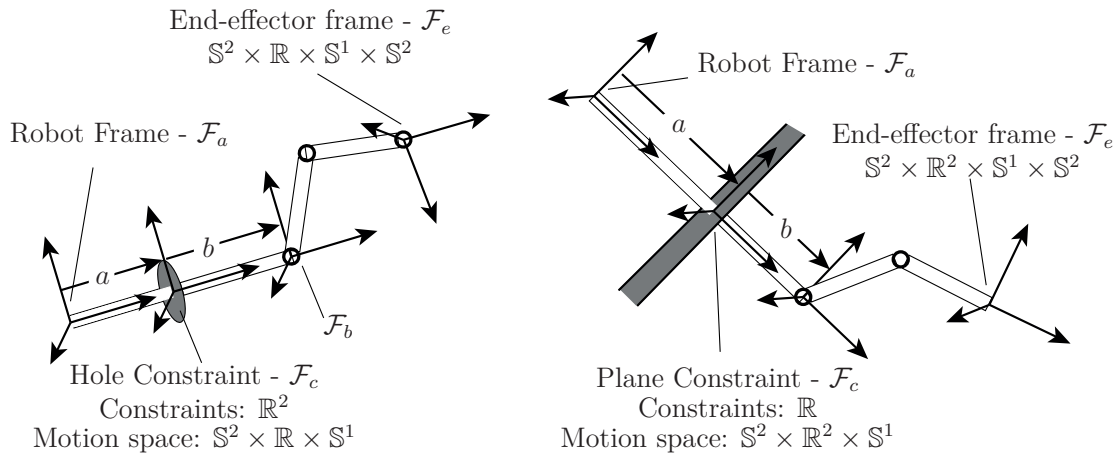

Figure 4.1: Two examples of the constraints discussed in this paper: on the left, a hole constraint which prevents any lateral motion of a specific point on the manipulator chain; and on the right, a plane constraint that restricts the linear motion of a point to a given direction in the plane. The constrained link is constrained at the point $\mathcal{F}_c$ which in turn results in a reduced motion space at $\mathcal{F}_a$. The motion spaces of the different frames are subgroups of $SE(3)$ defined by linear motion $\mathbb{R}$, circular motion $\mathbb{S}$, and the sphere $\mathbb{S}^2$.

and similarly for the other frames. $V_{ij}^{B,S}$ is thus the velocity in body or spatial coordinates of a rigid body with frame $\mathcal{F}_j$ with respect to the frame $\mathcal{F}_i$. V_{ij}^B is an element of the Lie algebra $se(3)$ of the Special Euclidean Group SE(3), and is found as $V_{ij}^B = g_{ij}^{-1}\dot{g}_{ij}$ where g_{ij} is the homogeneous transformation matrix describing the location of $\mathcal{F}_j$ in $\mathcal{F}_i$.

The problem considered consists of maintaining a stiff control of zero velocity in certain directions in the presence of obstacles while the end effector follows the desired trajectory. The objective is to obtain a formulation that allows us to control the end effector using any of the conventional control schemes without violating the constraints. The approach should thus allow for control schemes such as trajectory following, impedance control, or a combination of stiff and compliant control of the end effector. Common for all these control schemes is that a formulation which allows the controller to act on the end effector variables directly is required, and not for example on the joint variables.

4.5 Constrained Kinematics

The overall goal of this paper is to derive the motion of a kinematic chain given a desired end-effector motion $\mathcal{F}_e$ and a kinematic constraint at a point represented by $\mathcal{F}_c$. In the next sections we will find the admissible velocities at $\mathcal{F}_c$ for different types of constraints and the corresponding admissible velocities at the last joint prior to the constrained link, i.e., at $\mathcal{F}_a$. In this section we will present the overall idea of how these relations are used to find the kinematics of a constrained kinematic chain.

The main idea is to find the velocity V_{0a}^B in terms of a set of new velocity variables parametrized in such a way that these variables can be chosen freely and at the same time

guarantee that the constraints at $\mathcal{F}_c$ are satisfied. This means that certain directions in the velocity space are reduced from a higher to a lower-dimensional space represented by new velocity variables v_i.

As our main objective is to follow a desired end-effector motion V_{0e}^B we need to find the mapping from V_{0e}^B to the free variables, i.e., V_{0a}^B with the reduction in dimensionality represented by v_i. This is obtained in the following way:

1. Define a desired end-effector velocity V_{0e}^B.

2. Given a constraint at $\mathcal{F}_c$, define the velocities at this point which satisfy the constraints, i.e., the velocities at the previous joint $\mathcal{F}_a$ are given by

   - the free variables $\{v_x^a,\, v_y^a,\, v_z^a,\, \omega_x^a,\, \omega_y^a,\, \omega_z^a\}$, and
   - the constrained variables $\{v_1,\, v_2,\, v_3,\, \dots\}$.

   The free variables are the ones that can be chosen freely and do not affect the constraint. The constraint variables require a specific form and structure for the constraints to be satisfied. We therefore replace some of the free variables with the constraint variables which gives us the required structure. These variables thus represent a freedom, but in a space with reduced dimensionality that satisfies the constraint. The constrained variables are thus written in terms of the free variables v as
   $$V_{0a}^B = V_{0a}^B(v). \tag{4.5}$$

3. Eliminate the redundant variables that arise as a result of the reduced dimensionality and denote the minimal representation of the velocity variables by $\bar{V}_{0a}^B$.

4. Find a mapping from the end-effector velocities V_{0e}^B to the new reduced velocity variables $\bar{V}_{0a}^B$, which take the form
   $$v_m^a = \begin{bmatrix} \bar{V}_{0a}^B \\ \dot{q} \end{bmatrix} = \begin{bmatrix} \text{constrained variables} \\ \text{free variables} \\ \text{joint velocities} \end{bmatrix}. \tag{4.6}$$

   The mapping is given by the Constrained Jacobian Matrix J_{ea}^m that gives the important relation $V_{0e}^B = J_{ea}^m v_m^a$, i.e., the transformation from the new reduced velocity variables v_m^a to the desired end-effector velocities V_{0e}^B.

   The *joint velocities* represent the joints that are determined by the end-effector velocity V_{0e}^B only and do not depend on the constraints. These are typically the joints that are situated between the constraint and the end effector. The *free variables* are the velocities of $\mathcal{F}_a$ that do not depend on the constraint, but differently from the *joint velocities*, they depend on the joints between the base and the constraint. Finally, the *constrained variables* are constraint dependent and give the velocity at $\mathcal{F}_a$ the required structure so that the constraints are satisfied.

5. From the new variables, find the robot velocity at $\mathcal{F}_a$.

We note that there are two main steps. Firstly, we need to find a suitable representation of the velocity variables, which is discussed in Section 4.6. Secondly, we need to define the Constrained Jacobian Matrix, which treated in Section 4.7.

4.6 Constraint Kinematics

In this section we derive the kinematics of the constraints. This is used in the next section to derive the constrained kinematics of the robotic manipulator in the velocity space, i.e., the Constrained Jacobian Matrix.

4.6.1 Plane Constraint

For a plane-shaped constraint we want to eliminate the velocity at $\mathcal{F}_c$ in one direction. Lets assume that we allow no velocity in the direction of v_y^c. As this can be written in terms of the velocities at $\mathcal{F}_a$ (prior to the entry point) as

$$v_y^c = v_y^a - a\omega_x^a \tag{4.7}$$

the constraint $v_y^c = 0$ can be transformed to the frame $\mathcal{F}_a$ as

$$v_y^a = a\omega_x^a. \tag{4.8}$$

We can now introduce a new variable v_1 which describes the one degree of freedom represented by (4.8). The constrained variables v_y^a and ω_x^a then take the form

$$v_y^a = v_1 \qquad\qquad \omega_x^a = \frac{1}{a}v_1 \tag{4.9}$$

which forces a point $\mathcal{F}_c$ on the robot to avoid lateral motion in the direction of the y-axis. The constrained velocity variables at $\mathcal{F}_a$ can now be written as

$$\begin{bmatrix} v_x^a \\ v_y^a \\ v_z^a \\ \omega_x^a \\ \omega_y^a \\ \omega_z^a \end{bmatrix} = \begin{bmatrix} v_x^a \\ v_1 \\ v_z^a \\ \frac{1}{a}v_1 \\ \omega_y^a \\ \omega_z^a \end{bmatrix} \tag{4.10}$$

which have five degrees of freedom, as expected. We see that we impose a certain structure on the velocities at $\mathcal{F}_a$ which guarantees that the constraints are satisfied.

4.6.2 Entry Hole

Assume a robotic chain that is inserted through a hole. This add a 2-DoF constraint to the point of entry, represented by $\mathcal{F}_c$, which is a point on the link penetrating the

hole. This is for example the case in minimally invasive surgery where the robot is to be inserted into the abdomen through a trocar.

Similarly with Section 4.6.1, we can incorporate these constraints in the kinematics by introducing new variables v_1 and v_2 such that

$$v_x^a = v_1 \qquad \omega_y^a = -\frac{1}{a}v_1 \tag{4.11}$$

$$v_y^a = v_2 \qquad \omega_x^a = \frac{1}{a}v_2 \tag{4.12}$$

which for any choice of v_1 and v_2 will result in zero lateral velocity at the entry point. The constrained velocities can now be given as

$$\begin{bmatrix} v_x^a \\ v_y^a \\ v_z^a \\ \omega_x^a \\ \omega_y^a \\ \omega_z^a \end{bmatrix} = \begin{bmatrix} v_1 \\ v_2 \\ v_z^a \\ \frac{1}{a}v_2 \\ -\frac{1}{a}v_1 \\ \omega_z^a \end{bmatrix}. \tag{4.13}$$

The expressions are found similarly for other types of constraints.

4.7 Constrained Jacobian Matrix

In this section we will find the relation between the desired end-effector velocities and the corresponding joint velocities subject to the constraints described in the previous section. Given the end-effector velocity we want to find the free and constrained velocity variables of the robot. We will find the Constrained Jacobian Matrix J_{ea}^m which gives the relation $V_{0e}^B = J_{ea}^m v_m^a$ and the required velocities v_m^a are found from the desired end-effector velocities by the inverse of the Constrained Jacobian Matrix.

The standard body Jacobian matrix gives the mapping from the joint velocities to the end-effector velocities in body coordinates and is given by From et al. [2014a]

$$\begin{aligned} J_e^B &= \begin{bmatrix} X_1^\dagger & X_2^\dagger & \cdots & X_n^\dagger \end{bmatrix} \\ &= \begin{bmatrix} \mathrm{Ad}_{g_{1e}}^{-1} X_1^1 & \mathrm{Ad}_{g_{2e}}^{-1} X_2^2 & \cdots & X_n^n \end{bmatrix} \in \mathbb{R}^{n\times 6} \end{aligned} \tag{4.14}$$

where X_i^i is the constant twist in frame $\mathcal{F}_i$ and $\mathrm{Ad}_{g_{ie}}^{-1}$ is the Adjoint matrix that transforms X_i^i from frame $\mathcal{F}_i$ to $X_i^\dagger$ represented in the end-effector frame $\mathcal{F}_e$. The body Jacobian matrix can also be found for other links than the end effector, in which case it is denoted J_i^B which gives the velocities of link i. Particularly, the Jacobian matrix that gives the velocity of the link $\mathcal{F}_a$ located before the constraint is denoted J_a^B.

In this section we will find the body Jacobian matrices, as above, but subject to the constraints, i.e., we find the mapping from the joint velocity variables to the respective links subject to a constraint on the velocity at the constraint frame $\mathcal{F}_c$. We will see that for a large class of constraints the Constrained Jacobian Matrix can be written in the

form

$$\bar{J}_a^B = \begin{bmatrix} \sum \alpha_i X_i^\dagger & \sum \alpha_j X_j^\dagger & \cdots & \sum \alpha_k X_k^\dagger \end{bmatrix} \in \mathbb{R}^{m\times 6} \tag{4.15}$$

for some $(n-m)$-dimensional constraint. Where the bar in $\bar{J}_a^B$ distinguishes the Constrained Jacobian Matrix from the standard Jacobian J_a^B. $X_i^\dagger$ are the manipulator twists while α_i are configuration-dependent functions of the manipulator and constraint kinematics. The form of the Constrained Jacobian Matrix depends on the type of constraint. We will now look at what the constrained Jacobian matrices look like for different types of constraints.

4.7.1 Plane Constraint

Following the approach in From [2013b] we see from (4.10) that the Constrained Jacobian Matrix can be found by adding columns two and four of the standard Jacobian, i.e.,

$$\begin{aligned} \bar{J}_a^B &= \begin{bmatrix} \sum \alpha_i X_i^\dagger & \sum \alpha_j X_j^\dagger & \cdots & \sum \alpha_k X_k^\dagger \end{bmatrix} \\ &= \begin{bmatrix} X_1^\dagger & X_2^\dagger + \frac{1}{a} X_4^\dagger & X_3^\dagger & X_5^\dagger & X_6^\dagger & X_7^\dagger \end{bmatrix} \in \mathbb{R}^{6\times 6}. \end{aligned} \tag{4.16}$$

For a manipulator like the one in Fig. 4.1 with one joint after the constraint the required expression is given by the expression $V_{0e}^B = \bar{J}_a^B v_m^a$ which is found as

$$V_{0e}^B = \mathrm{Ad}_{g_{eb}} V_{0b}^B + V_{be}^B \tag{4.17}$$

with

$$\begin{aligned} \mathrm{Ad}_{g_{eb}} = \mathrm{Ad}_{g_{be}^{-1}} &= \begin{bmatrix} R_{be}^\mathsf{T} & -R_{be}^\mathsf{T} \hat{p}_{be} \\ 0 & R_{be}^\mathsf{T} \end{bmatrix} \\ &= \begin{bmatrix} 1 & 0 & 0 & 0 & l_7 c q_7 & l_7 s q_7 \\ 0 & c q_7 & s q_7 & -l_7 & 0 & 0 \\ 0 & -s q_7 & c q_7 & 0 & 0 & 0 \\ 0 & 0 & 0 & 1 & 0 & 0 \\ 0 & 0 & 0 & 0 & c q_7 & s q_7 \\ 0 & 0 & 0 & 0 & -s q_7 & c q_7 \end{bmatrix} \end{aligned} \tag{4.18}$$

$$V_{0b}^B = \begin{bmatrix} 1 & 0 & 0 & 0 & (a+b) & 0 \\ 0 & 1 & 0 & -(a+b) & 0 & 0 \\ 0 & 0 & 1 & 0 & 0 & 0 \\ 0 & 0 & 0 & 1 & 0 & 0 \\ 0 & 0 & 0 & 0 & 1 & 0 \\ 0 & 0 & 0 & 0 & 0 & 1 \end{bmatrix} \begin{bmatrix} v_x^a \\ v_1 \\ v_z^a \\ \frac{1}{a} v_1 \\ \omega_y^a \\ \omega_z^a \end{bmatrix} \tag{4.19}$$

$$V_{be}^B = \begin{bmatrix} 0 \\ -l_7 \\ 0 \\ 1 \\ 0 \\ 0 \end{bmatrix} \dot{q}_7. \tag{4.20}$$

so that $V_{0e}^B = \bar{J}_a^B v_m^a$ can be written as

$$V_{0e}^B = \begin{bmatrix} 1 & 0 & 0 & \beta_1 + l_7 c q_7 & l_7 s q_7 & 0 \\ 0 & \alpha_1 & s q_7 & 0 & 0 & -l_7 \\ 0 & \frac{b}{a} s q_7 & c q_7 & 0 & 0 & 0 \\ 0 & \frac{1}{a} & 0 & 0 & 0 & 1 \\ 0 & 0 & 0 & c q_7 & s q_7 & 0 \\ 0 & 0 & 0 & -s q_7 & c q_7 & 0 \end{bmatrix} \begin{bmatrix} v_x^a \\ v_1 \\ v_z^a \\ \omega_y^a \\ \omega_z^a \\ \dot{q}_7 \end{bmatrix} \tag{4.21}$$

where we have defined $\alpha_1 = -\frac{b}{a}\cos q_7 - \frac{1}{a} l_7$ and $\beta_1 = (a + b)$.

The new velocity variables are then found from the inverse of this expression as

$$v_m^a = (\bar{J}_a^B)^{-1} V_{0e}^B. \tag{4.22}$$

4.7.2 Entry Hole

Similarly, the Constrained Jacobian Matrix can be found as

$$\bar{J}_a^B = \begin{bmatrix} X_1^\dagger - \frac{1}{a} X_5^\dagger & X_2^\dagger + \frac{1}{a} X_4^\dagger & X_3^\dagger & X_6^\dagger & X_7^\dagger & X_8^\dagger \end{bmatrix} \in \mathbb{R}^{6\times 6} \tag{4.23}$$

for a hole-shaped constraint. We have

$$V_{0e}^B = \mathrm{Ad}_{g_{eb}} V_{0b}^B + V_{be}^B \tag{4.24}$$

which for a robot like the one in Fig. 4.1 with two joints after the constraint gives

$$\begin{aligned} \mathrm{Ad}_{g_{eb}} = \mathrm{Ad}_{g_{be}^{-1}} &= \begin{bmatrix} R_{be}^\mathsf{T} & -R_{be}^\mathsf{T} \hat{p}_{be} \\ 0 & R_{be}^\mathsf{T} \end{bmatrix} \\ &= \begin{bmatrix} 1 & 0 & 0 & 0 & l_7 c q_7 & l_7 s q_7 \\ 0 & c q_{78} & s q_{78} & -l_7 c q_8 & 0 & 0 \\ 0 & -s q_{78} & c q_{78} & l_7 s q_8 & 0 & 0 \\ 0 & 0 & 0 & 1 & 0 & 0 \\ 0 & 0 & 0 & 0 & c q_{78} & s q_{78} \\ 0 & 0 & 0 & 0 & -s q_{78} & c q_{78} \end{bmatrix} \end{aligned} \tag{4.25}$$

$$V_{0b}^{B} = \begin{bmatrix} 1 & 0 & 0 & 0 & (a+b) & 0 \\ 0 & 1 & 0 & -(a+b) & 0 & 0 \\ 0 & 0 & 1 & 0 & 0 & 0 \\ 0 & 0 & 0 & 1 & 0 & 0 \\ 0 & 0 & 0 & 0 & 1 & 0 \\ 0 & 0 & 0 & 0 & 0 & 1 \end{bmatrix} \begin{bmatrix} v_1 \\ v_2 \\ v_z^a \\ \frac{1}{a}v_2 \\ -\frac{1}{a}v_1 \\ \omega_z^a \end{bmatrix} \tag{4.26}$$

$$V_{be}^{B} = \begin{bmatrix} 0 & 0 \\ -l_7 cq_8 & 0 \\ l_7 sq_8 & 0 \\ 1 & 1 \\ 0 & 0 \\ 0 & 0 \end{bmatrix} \begin{bmatrix} \dot{q}_7 \\ \dot{q}_8 \end{bmatrix} \tag{4.27}$$

The expression $V_{0e}^{B} = \bar{J}_a^B v_m^a$ is found as

$$\begin{bmatrix} v_x^e \\ v_y^e \\ v_z^e \\ \omega_x^e \\ \omega_y^e \\ \omega_z^e \end{bmatrix} = \begin{bmatrix} -\alpha_1 & 0 & 0 & l_7 sq_7 & 0 & 0 \\ 0 & -\beta_1 & sq_{78} & 0 & -l_7 cq_8 & 0 \\ 0 & \beta_2 & cq_{78} & 0 & l_7 sq_8 & 0 \\ 0 & \frac{1}{a} & 0 & 0 & 1 & 1 \\ -\frac{1}{a}cq_{78} & 0 & 0 & sq_{78} & 0 & 0 \\ \frac{1}{a}sq_{78} & 0 & 0 & cq_{78} & 0 & 0 \end{bmatrix} \begin{bmatrix} v_1 \\ v_2 \\ v_z^a \\ \omega_z^a \\ \dot{q}_7 \\ \dot{q}_8 \end{bmatrix}. \tag{4.28}$$

Here we have defined $\alpha_1 = \frac{1}{a}(b + l_7 cq_7)$, $\beta_1 = \frac{1}{a}(bcq_{78} + l_7 cq_8)$ and $\beta_2 = \frac{1}{a}(bsq_{78} + l_7 sq_8)$.

4.8 Case Study - Hole Constraint on the Chain

We will see how the calculations are carried out through a simple example.

Assume a robotic manipulators as the one pictured to the left in Fig. 4.1 with 6 degrees of freedom before and another 2 degrees of freedom after the constraint. Assume further that the constraint is a hole, i.e., a 2-DoF constraint given by (4.13). The kinematic relations are then found as follows:

1. The end-effector velocity is given by V_{0e}^{B}.

2. The lateral velocities at $\mathcal{F}_c$ are required to be zero, which for our choice of reference

frame gives $v_x^c = v_y^c = 0$. The corresponding velocities at $\mathcal{F}_a$ are then found as

$$\begin{bmatrix} v_x^a \\ v_y^a \\ v_z^a \\ \omega_x^a \\ \omega_y^a \\ \omega_z^a \end{bmatrix} = \begin{bmatrix} v_1 \\ v_2 \\ v_z^a \\ \frac{1}{a} v_2 \\ -\frac{1}{a} v_1 \\ \omega_z^a \end{bmatrix}. \tag{4.29}$$

3. The reduced variables are then found by eliminating the dependent variables ω_x^a and ω_y^a:

$$\bar{V}_{0a}^B = \begin{bmatrix} v_1 \\ v_2 \\ v_z^a \\ \omega_z^a \end{bmatrix}. \tag{4.30}$$

4. The mapping from the end-effector velocities to these new velocity variables can now be found as

$$\begin{bmatrix} v_x^e \\ v_y^e \\ v_z^e \\ \omega_x^e \\ \omega_y^e \\ \omega_z^e \end{bmatrix} = \begin{bmatrix} -\alpha_1 & 0 & 0 & l_7 s q_7 & 0 & 0 \\ 0 & -\beta_1 & s q_{78} & 0 & -l_7 c q_8 & 0 \\ 0 & \beta_2 & c q_{78} & 0 & l_7 s q_8 & 0 \\ 0 & \frac{1}{a} & 0 & 0 & 1 & 1 \\ -\frac{1}{a} c q_{78} & 0 & 0 & s q_{78} & 0 & 0 \\ \frac{1}{a} s q_{78} & 0 & 0 & c q_{78} & 0 & 0 \end{bmatrix} \begin{bmatrix} v_1 \\ v_2 \\ v_z^a \\ \omega_z^a \\ \dot{q}_7 \\ \dot{q}_8 \end{bmatrix}. \tag{4.31}$$

We see that we have found a mapping from the 6-DoF end-effector space to the another 6-DoF space represented by a 6-DoF manipulator, a 2-DoF wrist and a 2-DoF hole constraint.

This is suitable for workspace control and at the same time guarantees that the entry point velocity constraints are satisfied.

5. Finally the robot velocities are found from Equations (4.11-4.12) as

$$\begin{bmatrix} v_x^a \\ v_y^a \\ v_z^a \\ \omega_x^a \\ \omega_y^a \\ \omega_z^a \end{bmatrix} = \begin{bmatrix} 1 & 0 & 0 & 0 \\ 0 & 1 & 0 & 0 \\ 0 & 0 & 1 & 0 \\ 0 & \frac{1}{a} & 0 & 0 \\ -\frac{1}{a} & 0 & 0 & 0 \\ 0 & 0 & 0 & 1 \end{bmatrix} \begin{bmatrix} v_1 \\ v_2 \\ v_z^a \\ \omega_z^a \end{bmatrix} \tag{4.32}$$

and the corresponding joint velocities are found from the manipulator Jacobian in the standard way and fed to the controller together with the joint velocities found in point (4).

4.8.1 Singularity Avoidance

We cannot, in general, guarantee that there exists a set of joint velocities v_m^a which generates the desired end-effector velocities V_{0e}^B. For instance, if the Constrained Jacobian Matrix $\bar{J}_a^B$ is singular, the end-effector motion cannot be generated.

The damped least square (DLS) method to avoid singularities for the manipulator Jacobian J_a^B can be written as Siciliano et al. [2011].

$$V_{0e}^B = \left(J_a^B\right)^T \left(J_a^B \left(J_a^B\right)^T + \lambda^2 I\right)^{-1} \dot{q}. \tag{4.33}$$

We can use the same idea to avoid singularities in the CJM. Assume that we want to minimize the cost function

$$f(v_m^a) = \left\| \bar{J}_a^B v_m^a - V_{0e}^B \right\| + \lambda^2 \left\| v_m^a \right\| \tag{4.34}$$

We can rewrite this as

$$\begin{aligned}
\left\| \begin{bmatrix} \bar{J}_a^B \\ 0 \end{bmatrix} v_m^a - \begin{bmatrix} V_{0e}^B \\ 0 \end{bmatrix} \right\| &= 0 \\
\left[\left(\bar{J}_a^B\right)^T \quad \lambda I \right] \begin{bmatrix} \bar{J}_a^B \\ \lambda I \end{bmatrix} v_m^a &= \left[\left(\bar{J}_a^B\right)^T \quad \lambda I \right] \begin{bmatrix} V_{0e}^B \\ 0 \end{bmatrix} \\
\left(\left(\bar{J}_a^B\right)^T \bar{J}_a^B + \lambda^2 I \right) v_m^a &= \left(\bar{J}_a^B\right)^T V_{0e}^B \\
v_m^a &= \left(\bar{J}_a^B\right)^T \left(\bar{J}_a^B \left(\bar{J}_a^B\right)^T + \lambda^2 I\right)^{-1} V_{0e}^B.
\end{aligned} \tag{4.35}$$

Our DLS has the same form as for the standard approach, but the interpretation is somewhat different. We restrict the velocities in the new variables v_m^a while following the desired end effector trajectory V_{0e}^B as tightly as possible, which differs from the standard formulation which restrict the joint velocities directly. We thus avoid the singularities that arise as a result of the constraints imposed on the chain, and not the kinematic singularities of the robot arm itself.

4.9 Experiments

To verify the proposed theory a simple setup with a manipulator was used.

4.9.1 Experimental Setup

To verify this theory, we control a manipulator by a haptic device. A standard 6-DoF Phantom haptic device from Sensable was used to control a Motoman DIA-10, which is a dual-arm robot. Each arm on the Motoman DIA-10 has 7 axes of motion and a "human-like" structure. The robot also has a 1-DoF base. We want the robot end effector to follow the reference, so workspace control is required. The time delay is minimal and not treated in this paper. The control is, however, implemented so that it

Figure 4.2: The robot and the constraint

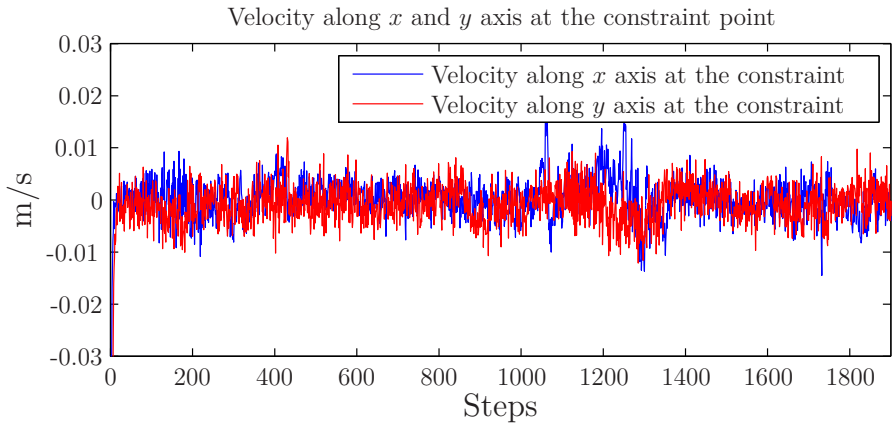

Figure 4.3: Velocity along x and y axis at the constraint point

is robust with respect to time delays.

4.9.2 Experimental Results

The end effector of the Motoman is to follow the reference from the master without violating the constraint. We use one arm of the Motoman and the base so the arm has 8 degrees of freedom. We apply the hole constraint on link 6. So we have 6 degrees of freedom before the constraint and 2 degrees of freedom after the constraint.

The velocities at the constraint are shown in Fig. 4.3. We can see the velocities v_x^c and v_y^c along $x-$ and $y-$axes, respectively, that are, except for the noise, very close to zero, which shows that the entry point constraint is satisfied.

In Fig. 4.4, we see how well the actual velocities at the end effector follow the desired velocities. From Fig. 4.3 and Fig. 4.4, we can conclude that our manipulator satisfies

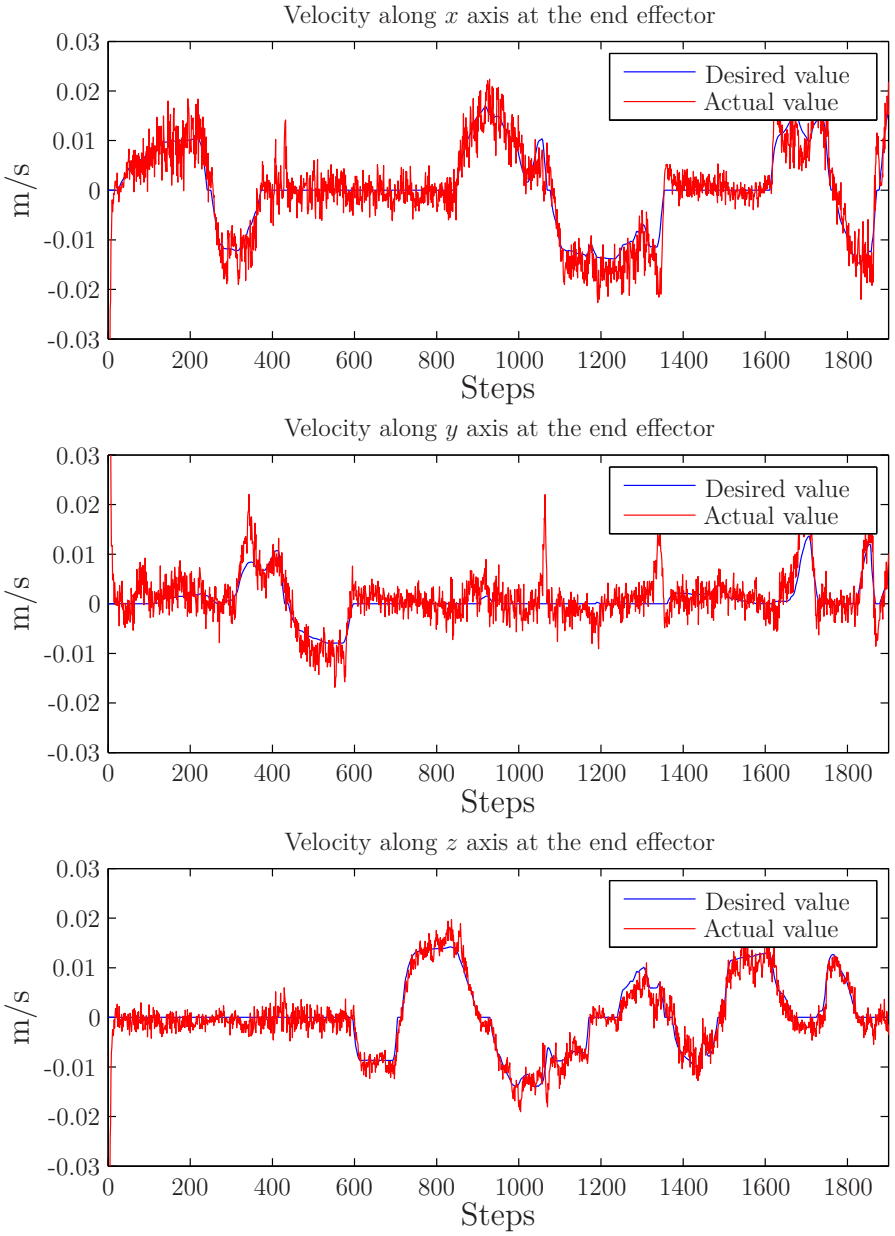

Figure 4.4: Linear velocities at the end effector

the constraint while the end effector still follow the desired values. The variances of the velocities at the constraint and the end effector are calculated to approximately 2.10^{-6} so we conclude that this is noise in both cases.

An illustration of the robot showing overlaid images is shown in Fig. 4.2. We see that for a single point on the arm there is no motion in the direction of the $x-$ and $y-$ axes. A video of the experiments can also be found by following the following link: *http://youtu.be/BiLiiD1MR6o*.

4.10 Conclusion

This paper solves the constrained motion problem for a robotic manipulator by mapping the end-effector velocities to the joint velocities in such a way that the constraints are guaranteed to be satisfied. We solve this at a kinematic level, i.e., we force the velocities in certain directions to vanish in order to avoid hitting obstacles. The reduced dimensionality due to the constraints are cast into a reduced velocity space by introducing a new set of velocity variables. The Jacobian is rewritten so that it finds the mapping to the new velocity variables instead of the joint velocities, and as a result the constraints are always satisfied. This mapping is denoted the *Constrained Jacobian Matrix* and presents us with a solution to the inverse kinematics problem for constrained manipulators. Experimental results show the efficiency of the approach.

Chapter 5

Dynamic Manipulability of Velocity-constrained Serial Robotic Manipulators

5.1 Abstract

This paper presents a new performance metric for serial manipulators with velocity constraints on the chain. These systems arise in several different applications such as serial manipulators in the presence of obstacles and in robotics-assisted minimally invasive surgery. It is important to know how constraints on the chain affect the mobility of the end effector and we therefore present a reformulation of the dynamic manipulability of the end effector for serial manipulators with velocity constraints on the chain. In this paper we propose to use the Constrained Jacobian Matrix, i.e., an analytical mapping between the end-effector and joint velocities that also takes the chain constraints into account. The approach allows us to compare the dynamic manipulability of serial manipulators with and without constraints and we show through a simple planar example how the dynamic manipulability is reduced as a result of the trocar constraint in minimally invasive surgery.

5.2 Introduction

The performance and characteristics of constrained robotic systems differ fundamentally from their non-constrained counterparts. Parallel robots, for example, have several advantageous properties such as speed and accuracy compared to serial manipulators. Velocity constraints, on the other hand, tend to reduce the overall performance of the robotic system, for example when a serial manipulator is inserted into a human body through a trocar during minimally invasive surgery. This paper endeavors to find an exact quantification of how much the performance of a robot is reduced in the presence of these constraints.

Robot control laws are often designed or evaluated based on performance metrics. One such metric is what is referred to as the manipulability of the robotic arm. The

manipulability of a robotic manipulator tells us in what directions the end effector can move and how much effort it requires to move in each direction. The manipulability is often measured by the condition number or the maximum singular value of the Jacobian matrix, or more illustratively by the manipulability ellipsoid. For redundant systems the objective is generally to take advantage of the null-space of the robot to find a trajectory for which the manipulability remains high, or at least above some limit, while for non-redundant robots the objective is to avoid singular configurations by modifying the trajectory.

The concept of manipulability of serial manipulators was introduced in Yoshikawa [1985b] where the kinematic manipulability was defined as the end-effector velocities that can be realized by a set of joint velocities belonging to a unit sphere. The manipulability has also been studied in the case of parallel manipulators, in which case the length in one or more directions of the manipulability ellipsoid can become either zero or infinite (Wen and Wilfinger [1999] and Park and Kim [1998]). If one direction is zero it means that a velocity cannot be realized in this direction, this is often referred to as an unmanipulable singularity. On the other hand, if the length approaches infinity the manipulator cannot prevent the end effector to move in a certain direction. In this case the passive joints will move even though all the active joints are locked, which is referred to as an unstable singularity (Wen and Wilfinger [1999] and From and Gravdahl [2008]).

In Yoshikawa [1985a] the manipulability index was developed further and also the manipulator dynamics was taken into account. In this case a metric of how well a unit sphere of joint torques are able to generate end-effector accelerations was derived. The dynamic manipulability has been developed further in Chiacchio et al. [1992] where the effects of gravity was included in the formulation and in Chiacchio and Concilio [1998] where an improved formulation of the redundant case was presented.

In the case of minimally invasive surgery there is a great need to include the dynamics in the performance metric. As the trocar can be thought of as a pivoting point for the robot arm, a small motion on one side of the trocar can generate a large motion on the other side. In a dynamic system, this motion cannot always be realized by the available torques in the system, which motivates studying the dynamic manipulability for these systems.

For serial manipulators the Jacobian is defined as the mapping from joint space velocities to the velocity of the end effector, i.e., the standard analytical or geometric Jacobian matrix. Similarly, for the dynamic manipulability the mapping from the joint torques to the end-effector accelerations is used. For parallel manipulators the manipulability Jacobian is normally found as the mapping from the active joints to the end-effector space. To find the manipulability of velocity-constrained serial manipulators, however, we need to find a mapping that also takes these constraints into account as they may have great influence on the dynamic manipulability. In this case, the dynamic manipulability cannot be determined in terms of the standard Jacobian matrix so in this paper we propose to use a modified Jacobian to determine the dynamic manipulability. More specifically we use the Constrained Jacobian Matrix (CJM) introduced in From [2013a] as a candidate for analyzing the dynamic manipulability of a serial robotic manipulator subject to one or more velocity constraints on the kinematic chain. The

CJM finds the mapping between the end-effector velocities and a new set of velocity variables which again has a one-to-one relation to the joint velocities. As this mapping takes the constraints into account we can use this to find the dynamic manipulability of a robotic manipulator subject to these constraints directly.

The paper is organized as follows: Section 5.3 gives an overview of the problem discussed and sets the framework. Section 5.4 briefly introduces the most relevant concepts of differential kinematics and introduce the Constrained Jacobian Matrix. The new dynamic manipulability index for constrained serial manipulators is introduced in Section 5.5 and a simple example related to robotics-assisted minimally invasive surgery is shown in Section 5.6.

5.3 System Overview and Problem Formulation

The system discussed in this paper consists of a serial robotic manipulator with one or more velocity constraints on the kinematic chain. The manipulator arm is normally redundant to maintain the full mobility of the end effector under chain constraints. The system setup for these constraints together with the most important configuration spaces used in this paper are shown in Fig. 5.1. We denote the frame of the joint located before the constraint at $\mathcal{F}_c$ in the chain by $\mathcal{F}_a$ and the joint that is located after the constraint is denoted $\mathcal{F}_b$. The desired end-effector motion is given by the frame $\mathcal{F}_e$. In this paper we are concerned with the dynamic manipulability of the frame $\mathcal{F}_e$. We will denote the body velocity variables representing the velocities of $\mathcal{F}_e$ with respect to the base frame $\mathcal{F}_0$ in the following way

$$V_{0e}^{B} = \begin{bmatrix} v_x^e & v_y^e & v_z^e & \omega_x^e & \omega_y^e & \omega_z^e \end{bmatrix}^{\mathsf{T}}, \tag{5.1}$$

and similarly for the other frames.

We consider robotic manipulators with n joints so that the unconstrained motion is an n-DoF motion. Furthermore we assume that the constrained motion has m degrees of freedom so the constraint has dimension $n-m$. The end-effector space has dimension r. Denote the joints so that the joint closest to the base is joint 1 and in increasing order until we reach the last joint and the end effector. We will divide the joints into two groups where the first group q_a consists of all joints that come before the constraint $\mathcal{F}_c$ in the kinematic chain and the second group q_b consists of all joints after the constraints.

The problem considered in this paper is to find the dynamic manipulability of these kinds of kinematic structures, i.e., serial robotic manipulators with "free" end-effector motion—which means there are no constraints imposed on the end effector itself—but with one or more kinematic constraints on the kinematic chain. Intuitively this kind of constraints will potentially drastically reduce the mobility of the system and thus leads to reduced performance. In this paper we derive a performance metric for thorough analysis of these systems and study in detail the effects that these constraints have on the dynamic manipulability of constrained serial manipulator.

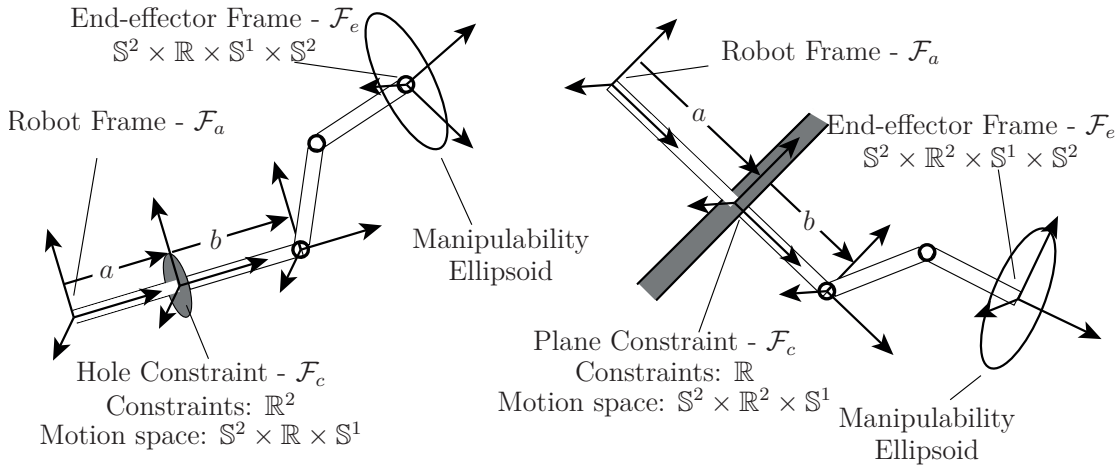

Figure 5.1: We study the dynamic manipulability of the end-effector frame $\mathcal{F}_e$ in the presence of a constraint at $\mathcal{F}_c$. The figure shows two examples of the constraints discussed in this paper: on the left, a hole constraint which prevents any lateral motion of a specific point on the manipulator chain; and on the right, a plane constraint that restricts the linear motion of a point to a given direction in the plane. The motion spaces of the different frames are subgroups of $SE(3)$ defined by linear motion $\mathbb{R}$, circular motion $\mathbb{S}$, and the sphere $\mathbb{S}^2$.

5.4 Manipulator Kinematics and Dynamics

Dynamics is the study of how joint torques relate to the end-effector accelerations. Manipulability can be thought of as a measure of how well defined this mapping is for a given configuration of the robot arm.

5.4.1 Manipulator Jacobian

In this section we will find the relation between the desired end-effector velocities and the corresponding joint velocities for serial manipulators. The standard body Jacobian matrix gives the mapping from the joint velocities $\dot{q}$ to the end-effector velocities V_{0e}^B in body coordinates which is the mapping From et al. [2014a]

$$V_{0e}^B = J_{0e}^B(q)\dot{q}. \tag{5.2}$$

The body Jacobian matrix $J_{0e}^B(q)$ is found by representing the twist of each joint i in the end-effector frame, i.e.,

$$\begin{aligned} J_{0e}^B(q) &= \begin{bmatrix} X_1^\dagger & X_2^\dagger & \cdots & X_n^\dagger \end{bmatrix} \\ &= \begin{bmatrix} \mathrm{Ad}_{g_{1e}}^{-1} X_1^1 & \mathrm{Ad}_{g_{2e}}^{-1} X_2^2 & \cdots & X_n^n \end{bmatrix} \in \mathbb{R}^{6\times n}, \end{aligned} \tag{5.3}$$

where X_i^i is the constant twist in frame $\mathcal{F}_i$ and $\mathrm{Ad}_{g_{ie}}^{-1}$ is the Adjoint matrix that transforms X_i^i from frame $\mathcal{F}_i$ to $X_i^\dagger$ represented in the end-effector frame $\mathcal{F}_e$. The body Jacobian matrix can also be found for other links than the end effector, in which case

it is denoted J^B_{0i} which gives the velocities of link i. Particularly, the Jacobian matrix that gives the velocity of the link $\mathcal{F}_a$ located before the constraint is denoted J^B_{a0}.

5.4.2 Constrained Jacobian Matrix

In this section we will find the body Jacobian matrices, as above, but subject to the constraints, i.e., we find the mapping from the joint velocity variables to the end effector subject to a constraint on the velocity at the constraint frame $\mathcal{F}_c$. For a large class of constraints the Constrained Jacobian Matrix can be written in the form From [2013a]

$$\bar{J}^B_{0e} = \begin{bmatrix} \sum \alpha_i X_i^\dagger & \sum \alpha_j X_j^\dagger & \cdots & \sum \alpha_k X_k^\dagger \end{bmatrix} \in \mathbb{R}^{6\times m}, \tag{5.4}$$

for some $(n-m)$-dimensional constraint. The bar in $\bar{J}^B_{e0}$ distinguishes the Constrained Jacobian Matrix from the standard Jacobian J^B_{e0}. $X_i^\dagger$ are the manipulator twists (represented in $\mathcal{F}_a$) while α_i are configuration-dependent functions of the manipulator and constraint kinematics. We refer to From [2013a] for examples of what this matrix looks like for different types of constraints.

Given the end-effector velocity we want to find the free and constrained velocity variables of the robot. We will find the Constrained Jacobian Matrix $\bar{J}^B_{e0}$ which gives the relation $V^B_{0e} = \bar{J}^B_{e0} v^a_m$ and the required velocities v^a_m are found from the desired end-effector velocities by the inverse of the Constrained Jacobian Matrix. These new velocity variables and the form of the Constrained Jacobian Matrix depends on the type of constraint. For plane and hole constraints shown in Fig. 5.1, for example, the new velocity variables are found as

$$\begin{bmatrix} v^a_x \\ v^a_y \\ v^a_z \\ \omega^a_x \\ \omega^a_y \\ \omega^a_z \end{bmatrix} = \begin{bmatrix} v^a_x \\ v_1 \\ v^a_z \\ \frac{1}{a} v_1 \\ \omega^a_y \\ \omega^a_z \end{bmatrix} \qquad \begin{bmatrix} v^a_x \\ v^a_y \\ v^a_z \\ \omega^a_x \\ \omega^a_y \\ \omega^a_z \end{bmatrix} = \begin{bmatrix} v_1 \\ v_2 \\ v^a_z \\ \frac{1}{a} v_2 \\ -\frac{1}{a} v_1 \\ \omega^a_z \end{bmatrix}, \tag{5.5}$$

respectively. We can now write the reduced velocity variables as

$$\bar{V}^B_{0a} = \begin{bmatrix} v_1 & v^a_x & v^a_z & \omega^a_y & \omega^a_z \end{bmatrix}^\mathsf{T}, \; \bar{V}^B_{0a} = \begin{bmatrix} v_1 & v_2 & v^a_z & \omega^a_z \end{bmatrix}, \tag{5.6}$$

respectively. v_1 and v_2 are the constrained variables while the remaining variables are denoted the free variables. We now present in brief the main idea of how to find the new velocity variables and derive the Constrained Jacobian Matrix. The following is taken from From [2013a]:

The main idea is to find the velocity V^B_{0a} in terms of a set of new velocity variables parametrized in such a way that these variables can be chosen freely and at the same time guarantee that the constraints at $\mathcal{F}_c$ are satisfied. This means that certain directions in the velocity space are reduced from a higher to a lower-dimensional space represented by new velocity variables v_i.

As our main objective is to follow a desired end-effector motion V_{0e}^B we need to find the mapping from V_{0e}^B to the free variables, i.e., V_{0a}^B with the reduction in dimensionality represented by v_i. This is obtained in the following way From [2013a]:

1. Define a desired end-effector velocity V_{0e}^B.

2. Given a constraint at $\mathcal{F}_c$, define the velocities at this point which satisfy the constraints, i.e., the velocities at the previous joint $\mathcal{F}_a$ are given by

   - the free variables $\{v_x^a,\, v_y^a,\, v_z^a,\, \omega_x^a,\, \omega_y^a,\, \omega_z^a\}$, and
   - the constrained variables $\{v_1,\, v_2,\, v_3,\, \dots\}$.

   The free variables are the ones that can be chosen freely and do not affect the constraint. The constrained variables require a specific form and structure for the constraints to be satisfied. We will therefore replace some of the free variables with the constrained variables which gives us the required structure. These variables thus represent a freedom, but in a space with reduced dimensionality that satisfies the constraint. The constrained variables are thus written in terms of the free variables v as
   $$V_{0a}^B = V_{0a}^B(v). \tag{5.7}$$

3. Eliminate the redundant variables that arise as a result of the reduced dimensionality and denote the minimal representation of the velocity variables by $\bar{V}_{0a}^B$. The variables will now take the form shown in (5.6).

4. Find a mapping from the end-effector velocities V_{0e}^B to the new reduced velocity variables $\bar{V}_{0a}^B$, which will take the form
   $$v_m^a = \begin{bmatrix} \bar{V}_{0a}^B \\ \dot{q}_b \end{bmatrix} = \begin{bmatrix} \text{constrained variables} \\ \text{free variables} \\ \text{joint velocities} \end{bmatrix}. \tag{5.8}$$

   The mapping is given by the Constrained Jacobian Matrix $\bar{J}_{e0}^B$ that gives the important relation $V_{0e}^B = \bar{J}_{e0}^B v_m^a$, i.e., the transformation from the new reduced velocity variables v_m^a to the desired end-effector velocities V_{0e}^B. The *joint velocities* represent the joints that are determined by the end-effector velocity V_{0e}^B only and do not depend on the constraints. These are typically the joints q_b that are situated between the constraint and the end effector. The *free variables* are the velocities of $\mathcal{F}_a$ that do not depend on the constraint, but differently from the *joint velocities*, they depend on the joints q_a between the base and the constraint. Finally, the *constrained variables* are constraint dependent and give the velocity at $\mathcal{F}_a$ the required structure so that the constraints are satisfied.

5. From the new variables, find the robot velocity at $\mathcal{F}_a$.

We refer to From [2013a] for details on this topic.

We note that there are two main steps: First we need to find a suitable representation of the velocity variables and define the Constrained Jacobian Matrix which gives us $\bar{V}_{0a}^B$ and $\dot{q}_b$. Then we find V_{0a}^B from $\bar{V}_{0a}^B$ and finally the joint velocities $\dot{q}_a$ from V_{0a}^B by the standard Jacobian matrix.

The kinematics of a serial robotic manipulator with chain constraints is now found by the two kinematic relations

$$V_{0e}^B = \bar{J}_{0e}^B(q) v_m^a \tag{5.9}$$
$$V_{0a}^B = J_{0a}^B(q)\dot{q}_a, \tag{5.10}$$

where $\bar{J}_{e0}^B(q)$ is the Constraint Jacobian Matrix and $J_{a0}^B(q)$ is the standard body geometric Jacobian that gives the mapping from the (first m) joints $\dot{q}_a$ to joint $\mathcal{F}_a$. We will see examples of these matrices in Section 5.6.

For robotics-assisted minimally invasive surgery with hole constraints, for example, the variables become

$$\bar{V}_{0a}^B = \begin{bmatrix} v_1 \\ v_2 \\ v_z^a \\ \omega_z^a \end{bmatrix} = \bar{J}_{0a}^B(q)\dot{q}_a. \tag{5.11}$$

Using (5.10) we can rewrite the (5.9) as

$$\begin{aligned} V_{0e}^B &= \bar{J}_{0e}^B(q) v_m^a \\ &= \bar{J}_{0e}^B(q) \begin{bmatrix} \bar{J}_{0a}^B(q)\dot{q}_a \\ \dot{q}_b \end{bmatrix} \\ &= \bar{J}_{0e}^B(q) \begin{bmatrix} \bar{J}_{0a}^B(q) & 0 \\ 0 & I \end{bmatrix} \dot{q} \\ &= \bar{J}_{0e}^B(q) J_A(q)\dot{q} \\ &= J(q)\dot{q} \end{aligned} \tag{5.12}$$

where

$$J_A(q) = \begin{bmatrix} \bar{J}_{0a}^B(q) & 0 \\ 0 & I \end{bmatrix} \tag{5.13}$$

is found directly from Equation (5.12) and we define

$$J(q) = \bar{J}_{0e}^B(q) J_A(q). \tag{5.14}$$

5.4.3 Manipulator Dynamics

The dynamic equation of a robotic manipulator is given by

$$M(q)\ddot{q} + C(q,\dot{q})\dot{q} + N(q) = \tau, \tag{5.15}$$

where q represents the joint variables, $M(q)$ is the inertia matrix, $C(q, \dot{q})$ represent the Coriolis and centrifugal forces, $N(q)$ the potential forces, and τ is the joint torques. We will omit the dependencies on q to reduce notation.

5.5 Manipulability

In this section we briefly review the kinematic and dynamic manipulability measures of robots as presented in literature.

5.5.1 Manipulability

Given the manipulability Jacobian $J_M \in \mathbb{R}^{r\times n}$, the (kinematic) manipulability matrix is given by

$$W = J_M J_M^{\mathsf{T}}, \tag{5.16}$$

and the manipulability measure as

$$w = \sqrt{\det\left|J_M J_M^{\mathsf{T}}\right|}. \tag{5.17}$$

For non-redundant robots where $r = n$, the manipulability measure is given simply by

$$w = \left|\det J_M\right|. \tag{5.18}$$

The manipulability ellipsoid is found by the eigenvalues and Eigenvectors of the manipulability matrix W. Let the singular value decomposition of J_M be written as Yoshikawa [2003]

$$J_M = U\Sigma V^{\mathsf{T}} \tag{5.19}$$

where

$$\Sigma = \begin{bmatrix} \sigma_1 & 0 & \cdots & 0 & \vdots & 0 \\ 0 & \sigma_2 & \cdots & 0 & \vdots & 0 \\ \vdots & \vdots & \ddots & 0 & \vdots & 0 \\ 0 & 0 & \cdots & \sigma_r & \vdots & 0 \end{bmatrix} \tag{5.20}$$

with $\sigma_1 \geq \sigma_2 \geq \cdots \geq \sigma_r$. The manipulability measure can now be written as

$$w = \sigma_1\sigma_2\sigma_3\cdots\sigma_r. \tag{5.21}$$

Furthermore the manipulability ellipsoid is the ellipsoid with principal axes $\sigma_1 u_1$, $\sigma_2 u_2$, $\ldots$, $\sigma_r u_r$ where u_i are the columns of U.

We can find the manipulability measure for constrained robotic arms. The manipulability measure is found by (1.16), so it only remains to find the manipulability Jacobian, which is found in the following way:

- Serial manipulators: The standard Jacobian matrix $J_{0e}^{\mathcal{B}}(q)$.

- Parallel manipulators: The Jacobian map from the active joint velocities to the end-effector velocities.
- Constrained serial manipulators: The Jacobians $\bar{J}^B_{e0}(q)$ and $J^B_{a0}(q)$ found in Equations (5.9) and (5.10).

5.5.2 Dynamic Manipulability

The dynamic manipulability was studied in detail in Yoshikawa [1985a] and Chiacchio and Concilio [1998]. In the general case, if the bounds of each joint torque are not equal, we scale the torques to obtain the unit sphere by

$$\bar{\tau} = L^{-1}\tau, \tag{5.22}$$

where $L = diag(\tau_1^{max}, \ldots, \tau_n^{max})$ is the scaling matrix.

Differentiating Equation (5.12), we obtain

$$\dot{V}^B_{0e} = J\ddot{q} + \dot{J}\dot{q}. \tag{5.23}$$

Following the procedure in Yoshikawa [1985b], Chiacchio and Concilio [1998], we have the dynamic manipulability measure given by

$$\omega_d = \sqrt{\det |J(Q^TQ)^{-1}J^T|}, \tag{5.24}$$

with $Q = L^{-1}M$.

5.5.3 The Manipulability Measure for Constrained Kinematic Chains

The manipulability of constrained serial manipulators needs to be found in two steps. We first look at the manipulability of the end effector assuming the first joints q_a can generate the required motion. This mapping depends only on the geometry of the constraint and the links q_b located after the constraint. This is given by (5.9).

The Constraint Jacobian Matrix $\bar{J}^B_{e0}(q)$ tells us whether it is possible to generate an end-effector velocity $\bar{V}^B_{0e}$ using the new velocity variables v^a_m, i.e., whether the constrained velocities V^B_{0a} and the joints after the constraint can generate the desired end-effector velocities. The condition number and singularity analysis of this matrix thus gives the effects of the constraints on the manipulability. This depends only on the kinematics of the constraint itself and the kinematics of the joints after the constraint.

The manipulability ellipsoid is given by choosing $J_M = \bar{J}^B_{e0}(q)$, and thus gives the manipulability in the directions of the end-effector frame V^B_{0e}. The interpretation of this is as follows:

It gives us the mobility of V^B_{0e} given V^B_{0a} and $\dot{q}_b$. We see that because we use V^B_{0a} the mobility depends on the constraint. We thus interpret this as the constraint-dependent manipulability of the system, and denote this the Constrained Manipulability Measure (CMM).

In the above we have assumed that the robot can always generate the desired motion V_{0a}^B. This is of course not always the case. We thus need to find the same performance measure for V_{0a}^B. This is similar to the standard manipulability measure for non-constrained serial manipulators.

The manipulability of the standard geometric Jacobian $J_{a0}^B(q)$ is a measure of how efficiently the manipulator can generate the motion V_{0a}^B required to generate the desired end-effector motion V_{0e}^B. This is thus equivalent to the standard manipulability analysis of a serial manipulator, but with respect to joint $\mathcal{F}_a$ as opposed the the end effector $\mathcal{F}_e$. We will denote this the Manipulator Manipulability Measure (MMM).

The CMM and MMM together give a measure of the manipulability of a constrained serial manipulator. If the manipulability ellipsoid of both these are non-vanishing we know that an arbitrary motion can be realized in the end-effector space, even though there are constraints on the kinematic chain. Furthermore, the manipulability ellipsoids gives us valuable information about the cause of the singularity and how it can be resolved.

5.5.4 The Dynamic Manipulability Measure for Constrained Kinematic Chains

In the general case the Jacobian matrix J is not a square matrix and it does not take into account the constraints, as these are only implemented in Equation (5.5) and not the Jacobian itself. We need to add constrained equations in this matrix to have a new Jacobian matrix. From Equations (5.5) and (5.10), for example, we can have constrained equations for hole constraints in the form

$$v_x^a + a\omega_y^a = 0 \quad \text{and} \quad v_y^a - a\omega_x^a = 0, \tag{5.25}$$

where

$$\begin{bmatrix} v_x^a \\ v_y^a \\ \omega_x^a \\ \omega_y^a \end{bmatrix} = \begin{bmatrix} J_{v_x^a} \\ J_{v_y^a} \\ J_{\omega_x^a} \\ J_{\omega_y^a} \end{bmatrix} \dot{q}_a. \tag{5.26}$$

From this we find the relation

$$\begin{bmatrix} J_{v_x^a} + aJ_{\omega_y^a} \\ J_{v_y^a} - aJ_{\omega_x^a} \end{bmatrix} \dot{q}_a = 0. \tag{5.27}$$

Extend the above equation from $\dot{q}_a$ to $\dot{q}$, and we have

$$\begin{bmatrix} J_{v_x^a} + aJ_{\omega_y^a} & 0 \\ J_{v_y^a} - aJ_{\omega_x^a} & 0 \end{bmatrix} \dot{q} = 0, \tag{5.28}$$

and the constraints are defined by the matrix

$$J_c = \begin{bmatrix} J_{v_x^a} + aJ_{\omega_y^a} & 0 \\ J_{v_y^a} - aJ_{\omega_x^a} & 0 \end{bmatrix}. \tag{5.29}$$

To find dynamic manipulability of constrained manipulator, we have to combine J in (5.12) and J_c in (5.29) into one Jacobian J_C describing the whole system

$$J_C = \begin{bmatrix} J \\ J_c \end{bmatrix}. \tag{5.30}$$

Here, J_C has two parts: i) J gives us information about the end-effector velocities, and ii) J_c gives us information about the velocities at the constraints.

We will now use J_C to compute the dynamic manipulability measure for the constrained manipulator. In the constrained case Equation (5.24) thus becomes

$$\omega_d = \sqrt{\det |J_C(Q^TQ)^{-1}J_C^T|}. \tag{5.31}$$

It is important to note that ω_d gives us more information than just the overall manipulability of the system. The first entries of the manipulability ellipsoid that correspond to Equation (5.31) above give us the manipulability of the end-effector in the normal way. The last entries give us the manipulability at the entry point. This thus tells us whether we are able to maintain zero velocity at this point. Thus, in order to be able to follow the end-effector trajectory and also maintain zero velocity at the incision point ω_d must be non-zero.

5.6 Case Study—Dynamic Manipulability of a Serial Manipulator with Hole Constraints

In this section we study a simple and intuitive example of a planar robot. We compare the manipulability of a 3-DoF robot without constraints on the chain, and a 4-DoF robot with a 1-DoF constraint imposed on the chain. The two systems are not equal or directly comparable, so to get an idea of how the constraint affects the manipulability we find the manipulability index for several different joint positions in both cases and compare these.

The 4-DoF manipulator has 3 joints before and 1 joint after a hole constraint. Assume further that all joints rotate around the z-axes, both for the constrained and unconstrained case. In both cases we only use joint positions that do not violate the constraint, i.e., around the zero pose $q = 0$. The two robots are shown in Figures 5.2 and 5.3.

The kinematic manipulability is shown in Fig. 5.4 where we can see that the two surfaces have the same shape with and without constraint, but the manipulability is about three times lower with the constraint imposed on the chain. Recall that we use the body velocity of the end effector. Thus, the manipulability in this frame will not be

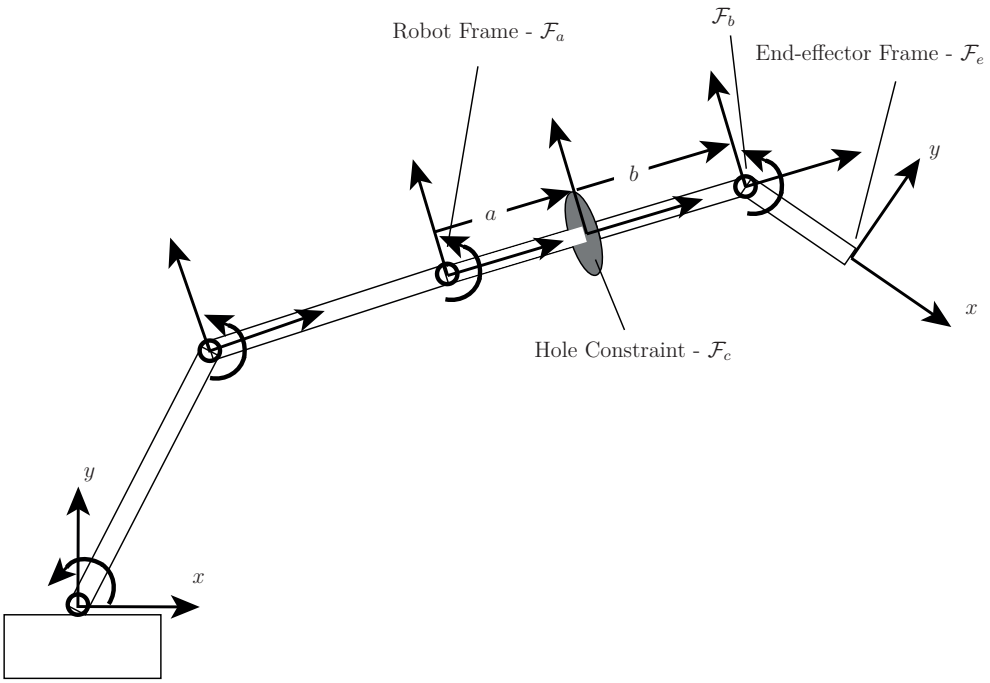

Figure 5.2: The constrained case: a 4-DoF planar robot with a 1-DoF constraint on the third link

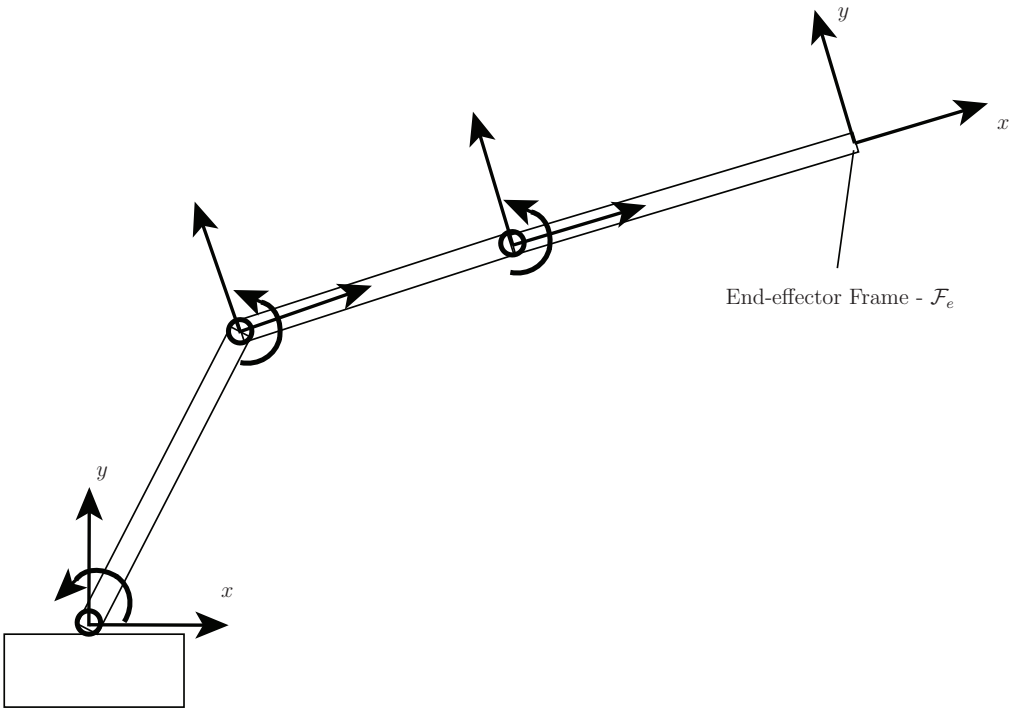

Figure 5.3: The non-constrained case: a 3-DoF planar robot with no constraints on the links

affected to a large extent by small changes in the position of this joint around the home position. This is true both for the constrained and non-constrained case.

For the dynamic manipulability shown in Fig. 5.5 we also note that the manipulability is generally higher for the non-constrained case, as expected. We also note that in

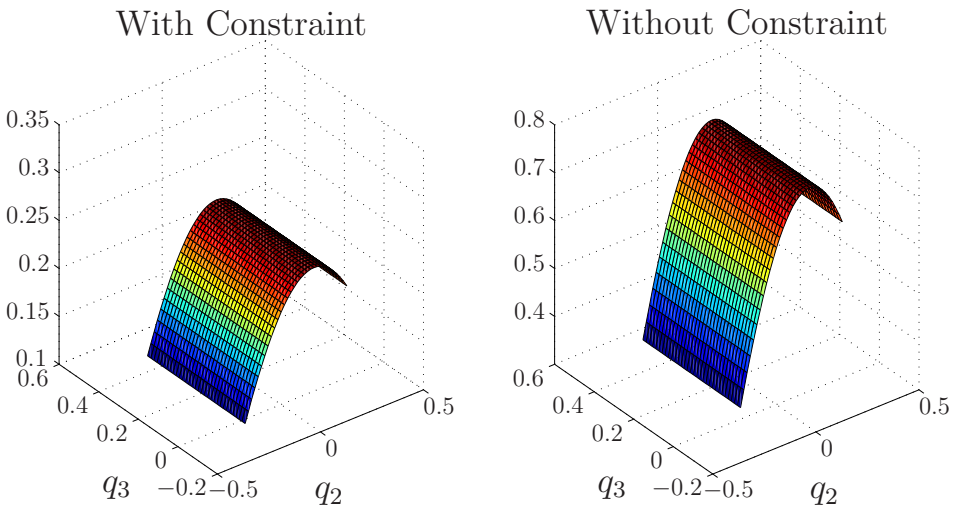

Figure 5.4: The kinematic manipulability index for a robotic manipulator with and without hole constraint

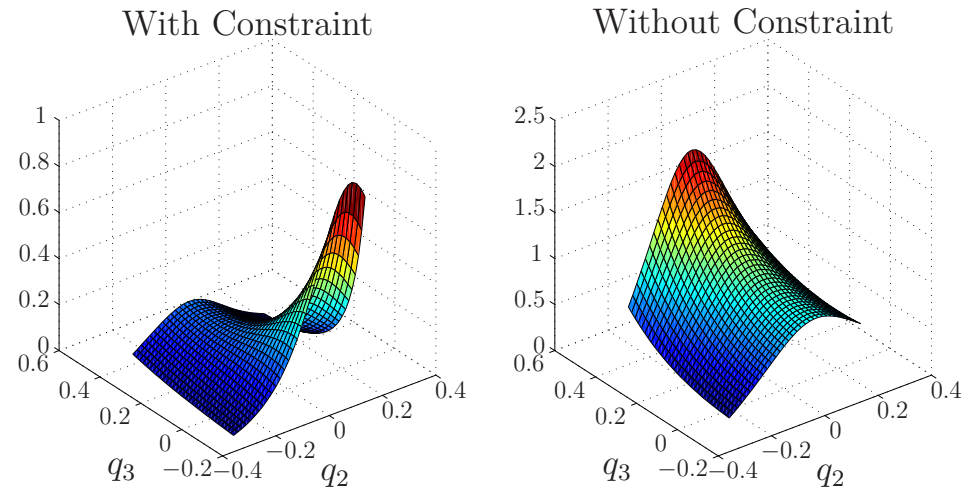

Figure 5.5: The dynamic manipulability index for a robotic manipulator with and without hole constraint

addition to having a lower maximum manipulability measure, the constrained case also decreases faster than the non-constrained case. The dynamic manipulability depends on both joints, which is reasonable because the joints are not free, but related through the new variables v_1, $v_2, \ldots$ due to the constraint.

More interestingly we note that the maximum manipulability is located at different joint position when the chain constraint is imposed. This means that we need to take the constraint into account not only when considering the robot's workspace, but also when it comes to maintaining a sufficiently high manipulability and avoiding singularities. The optimal trajectory in the constrained case will deviate from the optimal trajectory in the non-constrained case, and as can be seen from Fig. 5.5 the two can actually be quite different.

5.7 Conclusion

In this paper we have proposed a new dynamic manipulability measure for constrained serial manipulators. The manipulability measure allows us to study the performance of several important robotic systems such as the ones used for minimally invasive surgery. Through simple examples we have shown how the kinematic and dynamic manipulability changes when a hole constraint is imposed on the kinematic chain. While the kinematic manipulability changes mainly in size and maintains its shape for different joint positions, the dynamic manipulability is completely changed both in size and shape when the constraint is introduced, so the trajectory planner and control law should take these considerations into account to maintain good manipulability at all times.

Chapter 6

Analysis of a Moving Remote Center of Motion for Robotics-Assisted Minimally Invasive Surgery

6.1 Abstract

This paper presents a novel control architecture for controlling a moving remote center of motion in addition to the end-effector motion during robotic surgery. In minimally invasive surgery, it is common to require that the point at which the robot enters the body, called the incision point or the trocar, does not allow for any lateral motion. It is generally considered that no motion should be applied to this point in order to avoid inflicting damage to the patient's skin. However, in surgery, the patient's body may be moving, for example due to breathing or the beating of the heart. In order to compensate for this motion—or if we for some other reason want to leverage the possible motion of the incision point to improve performance in any other way—we derive a new framework which allows us to actively control the motion both at the incision point and the end effector. The novelty of the approach lies in the possibility of controlling both the incision point and the end effector to follow a trajectory, and that we find a Jacobian matrix that satisfies the velocity constraints in both the end-effector and the incision point frames. This allows us to formulate a framework that is not only suited for control, but also for analyzing the condition number of the Jacobian and avoid any singular configurations that may arise either as a result of the constrained motion or the manipulator geometry. The approach is verified experimentally on a redundant industrial manipulator.

6.2 Introduction

Robotic surgery has become one of the most promising applications of robotic technology in health care. In particular we have seen a growing interest in minimally invasive surgery

(MIS) using robots, which is characterized by the tools being inserted through small holes in the patient body. MIS leads to less patient trauma, shorter recovery times and lower overall risk compared to conventional open surgery. In robotics-assisted minimally invasive surgery (RAMIS) the end effector is attached to a long and thin shaft used to penetrate the skin through a small opening called the trocar, or the incision point. To avoid damaging the patients' tissues at the incision point, it is common to require that the lateral displacements at this point is kept to a minimal.

The constraints imposed by the entry point are commonly referred to as the Remote Center of Motion (RCM), which has been studied by several researchers. Early results solved the motion constraints as a general optimization problem, for example in Funda et al. [1996]. In Ortmaier and Hirzinger [2000], the RCM kinematics was derived and used to estimate the position of the entry point for a robot with passive joints. The passive joints guarantee that no forces are exerted to the entry point. In Locke and Patel [2007] the kinematic model was used to derive an optimization technique that allows isotropy of the surgical tool to be evaluated subject to the RCM constraint. Trocar kinematics was also discussed in Mayer et al. [2004].

In the setting of minimally invasive surgery, Deal et al. [2012] presented a method for stiff control at the entry point and compliant control at the end effector. A combination of hybrid force/position control and Natural Admittance Control (NAC), Glosser and Newman [1994], was used to satisfy the portal constraints and at the same time allows for compliant behavior at the end-effector. The resulting controller divided the control efforts into a 2-DoF stiff control at the entry point and a 4-DoF NAC controller at the end effector.

Azimian et al. [2010] used the concept of task priority and restricted Jacobian to derive the constrained motion in terms of the trocar and manipulator geometry. The end-effector motion was found in the standard way from the manipulator Jacobian, which was taken from the null space of the constraint Jacobian of the entry point. The constraint Jacobian was found in the normal way by the mapping from the joint space velocities to the lateral linear velocities of the RCM point. The constraints at the incision point were given first priority and the end-effector motion was given a secondary priority as this was taken from the null space of the first Jacobian Nakamura [1991]. The approach depended on the kinematics of both the robotic manipulator and the trocar.

Marinho et al. [2014] used a dual quaternion-based kinematic controller to maintain the RCM while the tool movement references are generated by surgeons. Aghakhani et al. [2013] proposed a formalization of the RCM constraint that explicitly models translation along the link axis and therefore allows direct control of a variable representing a link penetration into a patient's body.

The main motivation in all of the above work is to guarantee zero lateral motion at the incision point, which was obtained either through the control loop, or by a dual parallelogram design of the robot. There are, however, situations where we do not necessarily want the velocity at this point to be zero, but to follow a given trajectory. Heavy breathing and a strong heartbeat cause the patient's skin to move, which one might want to compensate for in extreme situations. Kapoor et al. [2006] used the concept of a "soft" customized virtual fixture and the entry port be constrained within

a region. If the tool is outside of the region, the surgeon experiences some resistances and no motion that moves the tool outside of the outer region is permitted. The approach allows the tool move freely in a defined region that is just a bigger entry port.

In this paper we thus propose an alternative approach to the RCM problem where we actively control the velocity both at the trocar and at the end effector. The approach is particularly useful when the operator controls the end effector through a haptic device, while the incision point is controlled by a computer, for example to follow the patient's breathing. We show through experimental results that we are able to control the end effector using a haptic device and at the same time are able to let the incision point follow a pre-planned trajectory, that for example simulates the effects of a heavily breathing patient. In the more general case we note that the same approach can be applied to obstacle avoidance of a point on a robotic arm while following an end-effector velocity. Furthermore we show that we can predict singular configurations by studying the condition number of the novel Jacobian matrix. This Jacobian matrix is obtained in a similar way as the Constrained Jacobian Matrix presented by the authors in previous publications Pham et al. [2014a] for a non-moving RCM, but we modify it to also take into consideration a moving incision point.

The paper is organized as follows: nn Section 6.3 we present the overall idea of how the kinematics of a constrained kinematic chain is calculated. The mathematical representation of the different kinematic constraints is shown in Section 6.4 and the corresponding Jacobian matrices are found in Section 6.5. Singularity of the system is studied and dealt with in Section 6.6. The experimental results are presented in Section 6.7 and concluding remarks are presented in Section 6.8.

6.3 System Overview and Problem Formulation

The system discussed consists of a redundant robot manipulator we want to control the motion at the end effector and an additional point at the robotic chain named the trocar point. The system setup together with the most important configuration spaces used in this paper are shown in Fig. 6.1. We denote the frame of the joint located before the incision point, that is located at $\mathcal{F}_c$ in the chain, by $\mathcal{F}_a$ and the joint that is located after the incision point is denoted $\mathcal{F}_b$.

We want to control the lateral velocities at the incision point, i.e., the velocity variables v_x^c and v_y^c in the frame $\mathcal{F}_c$. This is illustrated in Fig. 6.1 for a one- and two-dimensional motion at $\mathcal{F}_c$.

The desired end-effector motion is given by the frame $\mathcal{F}_e$. We will denote the velocity variables in the following way

$$V_{0e}^B = \begin{bmatrix} v_x^e & v_y^e & v_z^e & \omega_x^e & \omega_y^e & \omega_z^e \end{bmatrix}^\mathsf{T} \tag{6.1}$$

and similarly for the other frames. V_{ij}^B is thus the velocity in body coordinates of a rigid body with frame $\mathcal{F}_j$ with respect to the frame $\mathcal{F}_i$. V_{ij}^B is an element of the Lie algebra $se(3)$ of the Special Euclidean Group SE(3), and is found as $V_{ij}^B = g_{ij}^{-1}\dot{g}_{ij}$ where g_{ij} is the homogeneous transformation matrix describing the location of $\mathcal{F}_j$ in $\mathcal{F}_i$.

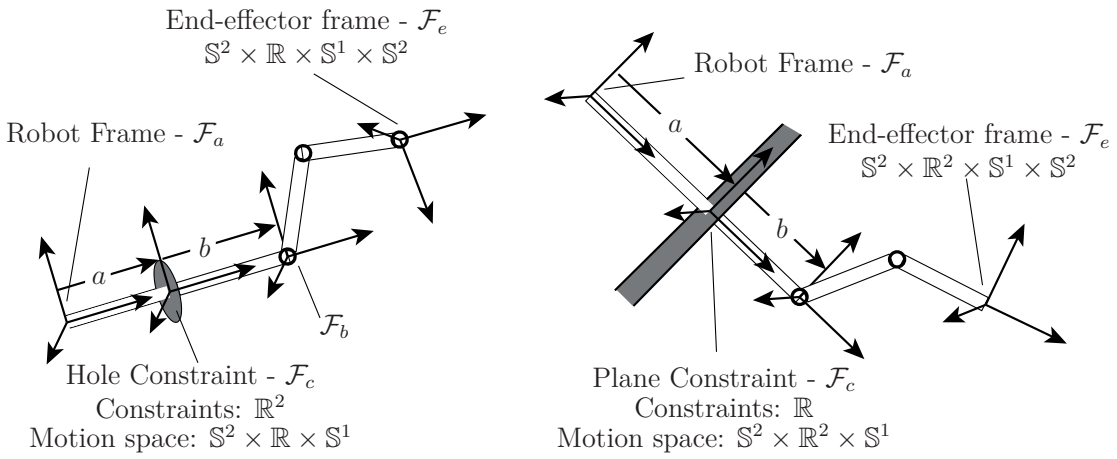

Figure 6.1: Two examples of the constraints discussed in this paper: on the left, a hole constraint which prevents any lateral motion of a specific point on the manipulator chain; and on the right, a plane constraint that restricts the linear motion of a point to a given direction in the plane. The constrained link is constrained at the point $\mathcal{F}_c$ which, in turn, results in a reduced motion space at $\mathcal{F}_a$. The motion spaces of the different frames are subgroups of $SE(3)$ defined by linear motion $\mathbb{R}$, circular motion $\mathbb{S}$, and the sphere $\mathbb{S}^2$.

In this paper we consider a redundant robot with eight revolute joints, so that six DoF are used for controlling the end effector and the remaining two DoF are used to control the incision point. All the equations to be presented stand for a robot whose the last two joints located inside the human body are assumed to rotate around the x-axis.

The problem considered is similar to the remote center of motion problem which consists of maintaining a stiff control of zero velocity in certain directions while the end effector follows the desired trajectory. For RCM we normally allow all motions at $\mathcal{F}_c$ to be chosen freely, except the linear motion in the x- and y-directions. The rotational motion around all axes and the linear motion in the direction of the z-axis (which is chosen parallel to the shaft) can thus be chosen freely as these do not affect the RCM. In this paper, differently from conventional RCM found in literature, we also allow a linear motion in the x- and y-directions. We do not allow any motion, however, because these directions do affect the RCM, but we allow either a small motion to improve the overall performance, or to follow the trajectory of $\mathcal{F}_c$ when this is moving.

6.4 Constraint Kinematics

In this section, we derive the kinematics of the robot manipulator in order to control the velocity at two points on the manipulator chain. We first find the kinematics for the conventional RCM, i.e., when the lateral motion is required to have zero velocity. This is similar to the approach presented in From [2013b]. We then find the formulation when the lateral velocities are required to follow a pre-defined trajectory, while the other directions at the incision point can be chosen freely, which together with Section 6.5 represents the main contribution of the paper.

6.4.1 Fixed Point

Assume a robotic chain that is inserted through a hole. This adds a 2-DoF constraint to the point of entry, represented by $\mathcal{F}_c$, which is a point on the link penetrating the hole. The velocities at the entry point and the zero velocity constraint can be written in terms of the velocities at $\mathcal{F}_a$ as

$$v_x^c = v_x^a + a\omega_y^a, \qquad v_x^a = -a\omega_y^a, \tag{6.2}$$
$$v_y^c = v_y^a - a\omega_x^a, \qquad v_y^a = a\omega_x^a, \tag{6.3}$$

where we need to know the distance a from the joint prior to the constraint to the entry point (see Fig. 4.1). We can incorporate these constraints in the kinematics by introducing new variables v_1 and v_2 such that

$$v_x^a = v_1\,, \quad \omega_y^a = -\frac{1}{a}v_1\,, \qquad v_y^a = v_2\,, \quad \omega_x^a = \frac{1}{a}v_2\,, \tag{6.4}$$

which for any choice of v_1 and v_2 will result in zero lateral velocity at the entry point. The constrained velocities can now be given as

$$\begin{bmatrix} v_x^a \\ v_y^a \\ v_z^a \end{bmatrix} = \begin{bmatrix} v_1 \\ v_2 \\ v_z^a \end{bmatrix}, \quad \begin{bmatrix} \omega_x^a \\ \omega_y^a \\ \omega_z^a \end{bmatrix} = \begin{bmatrix} \frac{1}{a}v_2 \\ -\frac{1}{a}v_1 \\ \omega_z^a \end{bmatrix}. \tag{6.5}$$

6.4.2 Trajectory Following

This is similar to Section 6.4.1 with the difference that v_x^c and v_y^c are not zero but equal desired values v_{xd}^c and v_{yd}^c. So we have

$$v_x^c = v_{xd}^c\,, \qquad v_x^c = v_x^a + a\omega_y^a, \tag{6.6}$$
$$v_y^c = v_{yd}^c\,, \qquad v_y^c = v_y^a - a\omega_x^a. \tag{6.7}$$

We can incorporate these constraints in the kinematics by introducing new variables v_1 and v_2 in (6.6)-(6.7) such that

$$v_x^a = v_1\,, \qquad \omega_y^a = -\frac{1}{a}v_1 + \frac{1}{a}v_{xd}^c, \tag{6.8}$$
$$v_y^a = v_2\,, \qquad \omega_x^a = \frac{1}{a}v_2 - \frac{1}{a}v_{yd}^c. \tag{6.9}$$

The constrained velocities can now be given as

$$\begin{aligned}
\begin{bmatrix} v_x^a \\ v_y^a \\ v_z^a \\ \omega_x^a \\ \omega_y^a \\ \omega_z^a \end{bmatrix} &= \begin{bmatrix} v_1 \\ v_2 \\ v_z^a \\ \frac{1}{a}v_2 - \frac{1}{a}v_{yd}^c \\ -\frac{1}{a}v_1 + \frac{1}{a}v_{xd}^c \\ \omega_z^a \end{bmatrix} \\
&= \begin{bmatrix} 1 & 0 & 0 & 0 & 0 & 0 \\ 0 & 1 & 0 & 0 & 0 & 0 \\ 0 & 0 & 1 & 0 & 0 & 0 \\ 0 & \frac{1}{a} & 0 & 0 & 0 & -\frac{1}{a} \\ -\frac{1}{a} & 0 & 0 & 0 & \frac{1}{a} & 0 \\ 0 & 0 & 0 & 1 & 0 & 0 \end{bmatrix} \begin{bmatrix} v_1 \\ v_2 \\ v_z^a \\ \omega_z^a \\ v_{xd}^c \\ v_{yd}^c \end{bmatrix} \\
&= J_c v_d^{ac}
\end{aligned} \tag{6.10}$$

6.5 Constrained Jacobian Matrix

In this section, we will find the mapping from the desired end-effector and incision point velocities to the corresponding joint velocities subject to the constraints described in the previous section. The standard body Jacobian matrix gives the mapping from the joint velocities to the end-effector velocities in body coordinates and is given by From et al. [2014a]:

$$J_e^B = \begin{bmatrix} X_1^\dagger & X_2^\dagger & \cdots & X_n^\dagger \end{bmatrix} \in \mathbb{R}^{n\times 6}$$

where $X_i^\dagger = Ad_{g_{ie}}^{-1} X_i^i$ for $i = 1, \cdots, n-1$. X_i^i is the constant twist in frame $\mathcal{F}_i$ and $\mathrm{Ad}_{g_{ie}}^{-1}$ is the adjoint matrix that transforms X_i^i from frame $\mathcal{F}_i$ to $X_i^\dagger$ represented in the end-effector frame $\mathcal{F}_e$. The body Jacobian matrix can also be found for other links than the end effector, in which case it is denoted J_i^B which gives the velocities of link i. Particularly, the Jacobian matrix that gives the velocity of the link $\mathcal{F}_a$ located before the constraint is denoted J_a^B.

In this section, we also impose a constraint on the motion of $\mathcal{F}_c$. We will see that for a large class of constraints the Constrained Jacobian Matrix can be written in the form

$$\bar{J}_a^B = \begin{bmatrix} \sum \alpha_i X_i^\dagger & \sum \alpha_j X_j^\dagger & \cdots & \sum \alpha_k X_k^\dagger \end{bmatrix} \in \mathbb{R}^{m\times 6} \tag{6.11}$$

for some $(n-m)$-dimensional constraints where the bar in $\bar{J}_a^B$ distinguishes the Constrained Jacobian Matrix from the standard Jacobian J_a^B. $X_i^\dagger$ are the manipulator twists while α_i are configuration-dependent functions of the manipulator and constraint kinematics. It is worth mentioning that the form of the Constrained Jacobian Matrix depends on the type of constraint.

When the entry point is to follow a trajectory in the xy-plane (at $\mathcal{F}_c$) we will see

that we can use the same Jacobian (6.11) as above.

We have $V_{0e}^B = \mathrm{Ad}_{g_{eb}} V_{0b}^B + V_{be}^B$,

whose elements take the slightly different form

$$V_{0b}^B = \begin{bmatrix} 1 & 0 & 0 & 0 & (a+b) & 0 \\ 0 & 1 & 0 & -(a+b) & 0 & 0 \\ 0 & 0 & 1 & 0 & 0 & 0 \\ 0 & 0 & 0 & 1 & 0 & 0 \\ 0 & 0 & 0 & 0 & 1 & 0 \\ 0 & 0 & 0 & 0 & 0 & 1 \end{bmatrix} \begin{bmatrix} v_1 \\ v_2 \\ v_z^a \\ \frac{1}{a}v_2 - \frac{1}{a}v_{yd}^c \\ -\frac{1}{a}v_1 + \frac{1}{a}v_{xd}^c \\ \omega_z^a \end{bmatrix}$$

$$V_{be}^B = \begin{bmatrix} 0 & 0 \\ -l_7 cq_8 & 0 \\ l_7 sq_8 & 0 \\ 1 & 1 \\ 0 & 0 \\ 0 & 0 \end{bmatrix} \begin{bmatrix} \dot{q}_7 \\ \dot{q}_8 \end{bmatrix}, \tag{6.12}$$

where sq_8 and cq_8 are $sin\,(q_8)$ and $cos\,(q_8)$, respectively. Finally, the expression for V_{0e}^B can now be written as

$$\begin{bmatrix} v_x^e \\ v_y^e \\ v_z^e \\ \omega_x^e \\ \omega_y^e \\ \omega_z^e \end{bmatrix} = \begin{bmatrix} -\alpha_1 & 0 & 0 & l_7 sq_7 & 0 & 0 \\ 0 & -\beta_1 & sq_{78} & 0 & -l_7 cq_8 & 0 \\ 0 & \beta_2 & cq_{78} & 0 & l_7 sq_8 & 0 \\ 0 & \frac{1}{a} & 0 & 0 & 1 & 1 \\ -\frac{1}{a}cq_{78} & 0 & 0 & sq_{78} & 0 & 0 \\ \frac{1}{a}sq_{78} & 0 & 0 & cq_{78} & 0 & 0 \end{bmatrix} \begin{bmatrix} v_1 \\ v_2 \\ v_z^a \\ \omega_z^a \\ \dot{q}_7 \\ \dot{q}_8 \end{bmatrix} + \begin{bmatrix} 1+\alpha_1 & 0 \\ 0 & cq_{78}+\beta_1 \\ 0 & sq_{78}-\beta_2 \\ 0 & -\frac{1}{a} \\ \frac{1}{a}cq_{78} & 0 \\ -\frac{1}{a}sq_{78} & 0 \end{bmatrix} \begin{bmatrix} v_{xd}^c \\ v_{yd}^c \end{bmatrix}. \tag{6.13}$$

Here, we have defined $\alpha_1 = \frac{1}{a}(b+l_7 cq_7)$, $\beta_1 = \frac{1}{a}(bcq_{78}+l_7 cq_8)$ and $\beta_2 = \frac{1}{a}(bsq_{78}+l_7 sq_8)$. Moreover, sq_7, sq_{78} and cq_{78} are $sin\,(q_7)$, $sin\,(q_7+q_8)$ and $cos\,(q_7+q_8)$, respectively. We now introduce the new variable

$$V_{0em}^{B} = \underbrace{\begin{bmatrix} v_x^e \\ v_y^e \\ v_z^e \\ \omega_x^e \\ \omega_y^e \\ \omega_z^e \end{bmatrix}}_{V_{0e}^{B}} - \underbrace{\begin{bmatrix} 1+\alpha_1 & 0 \\ 0 & cq_{78}+\beta_1 \\ 0 & sq_{78}-\beta_2 \\ 0 & -\frac{1}{a} \\ \frac{1}{a}cq_{78} & 0 \\ -\frac{1}{a}sq_{78} & 0 \end{bmatrix}}_{J_{vc}} \begin{bmatrix} v_{xd}^c \\ v_{yd}^c \end{bmatrix} . \tag{6.14}$$

Combining (6.13) and (6.14) gives

$$V_{0em}^{B} = \bar{J}_a^B \, v_m^a \, , \tag{6.15}$$

where $\bar{J}_a^B$ is the matrix in (6.13). We thus see that we first find V_{0em}^B from (6.14) which allows us to find the required velocities v_m^a by inverting the expression in (6.15).

6.6 Dealing with Singularities

Considering our robot geometry, the singularity appears at $q_7 = 0$. This joint position is almost impossible to avoid, and we thus need to deal with this in a different manner.

According to the kinematic control approach, the required velocities v_m^a in (6.15) are the velocity control signals u that could be applied to the robot joints as $u = (\bar{J}_a^B)^{-1} V_{0em}^B$. This open-loop control law can be computed only when the Jacobian matrix $\bar{J}_a^B$ has full rank, i.e., when the robot is away from singular configurations. In addition, the inversion of the Jacobian may represent a problem in the vicinity of a singularity, as ill-conditioning of the matrix can produce unwanted large joint velocities.

A well-known solution to deal with the problem of inverting the Jacobian matrix in the vicinity of a singularity is given by the so-called Damped Least-Squares (DLS) inverse method proposed by Nakamura and Hanafusa [1986].

The main idea behind the DLS method is to attenuate the non-feasible joint velocities in the neighborhood of a singular configuration, allowing the robot end effector to deviate from the desired reference trajectory. The performance of the DLS method for the MRC motion control problem was investigated in our recently published work Pham et al. [2014a].

An alternative solution to overcome the performance degradation of the kinematic control in the vicinity of singular configurations is to employ the recently proposed Filtered Inverse (FI) method Vargas et al. [2014]. From the FI method, we consider that the control law u uses a dynamically updated matrix $\Theta(t)$ instead of its inverse computed instantaneously as $(\bar{J}_a^B)^{-1}$ such that $\bar{J}_a^B \, \Theta = I$. The dynamics of the matrix $\Theta(t)$ can be established from the error signals based on the right and left inverses, S_r

and S_l, suitably defined as:

$$S_r = \bar{J}_a^B \Theta - I\,, \qquad S_l = \Theta\, \bar{J}_a^B - I\,. \tag{6.16}$$

Considering the Lyapunov function candidate $V_c(S_r, S_l) = \mathrm{tr}(S_r^\mathsf{T} S_r) + \mathrm{tr}(S_l^\mathsf{T} S_l)$, where $\mathrm{tr}(\cdot)$ denotes the trace function of a matrix. As can be seen, this Lyapunov function candidate is positive definite and decrescent. From the time-derivative of V_c and (6.16), the following composite update law can be obtained:

$$\dot{\Theta} = -\Gamma \left[(\bar{J}_a^B)^\mathsf{T} S_r + S_l (\bar{J}_a^B)^\mathsf{T} \right], \tag{6.17}$$

where $\Gamma = \Gamma^\mathsf{T} > 0$ in the update gain matrix. Notice that, in the particular case where the matrix to be inverted is constant, Θ can be interpreted as the output of a linear filter where the input is the true inverse. Finally, resorting to the FI method Vargas et al. [2014], the velocity control signal u can be defined in terms of the filtered inverse matrix Θ as:

$$u = \Theta\, \Theta^\mathsf{T}\, \bar{J}_a^B\, V_{0em}^B. \tag{6.18}$$

It is worth mentioning that, compared to other inversion solutions based on the differential kinematics equation described in the literature, the main advantages of the FI method are twofold: the *number of design parameters to be tuned*, i.e., only the update gain matrix Γ, and the *computational efficiency*, since it does not require matrix inversion, singular value decomposition or computation of manipulability measures.

6.7 Experiments and Results

In this section, we describe the experimental setup used to carry out the experiments. We also present preliminary results to demonstrate the performance and feasibility of the proposed methodology.

6.7.1 Experimental Setup

In the experimental tests, we control a Motoman DIA10 dual-arm robot using a Phantom Omni haptic device to perform the tracking of a previously planned trajectory. The control diagram is shown in Fig. 6.2. The DIA10 robot has 15-DoF or axes of motion, with 7-DoF per each arm plus 1-DoF for the base rotation. For the sake of simplicity, we employ only the left arm and the robot base to execute the experimental tests, which results in 8-DoF to be controlled in the joint space. The experimental setup also consists of a low-level industrial controller NX100 and an HSC system (High-speed Synchronous Controller) as shown in Fig. 6.3. The reference signals for the DIA10 robot are generated by an external computer (User PC) running the user application developed in Matlab/Simulink on Windows OS. The signals are then sent to a position control loop, built-in Simulink blocks (Server) and executed at the frequency of 500 Hz. The User PC is connected to the NX100 controller through the HSC system and the access is given by a Matlab server running a proper communication protocol provided

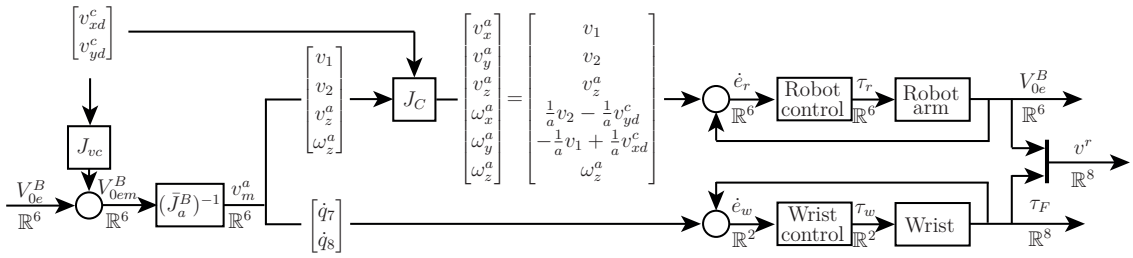

Figure 6.2: Block diagram for the proposed control scheme.

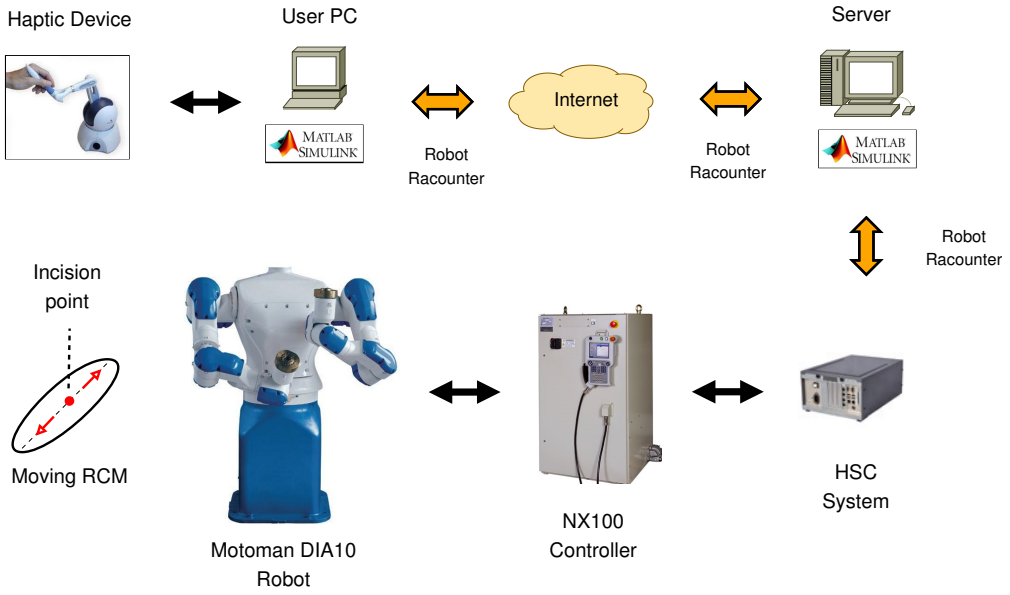

Figure 6.3: Schematic diagram of the experimental setup.

by the Robot Racounter architecture Wason and Wen [2011].

6.7.2 Experimental Results

Two sets of experiments were carried out using a kinematic control scheme for the end-effector pose. The Cartesian position and orientation control laws are based on a fixed-gain proportional plus feedforward term which can ensure the asymptotic convergence of the output tracking errors.

In the first set, the key idea is to evaluate the behavior of the robot end effector in the vicinity of a singular configuration, when the joint angle q_7 varies in the range $[-\frac{\pi}{36}, \frac{\pi}{4}]$ passing through zero. To achieve this aim, we consider that the robot end effector is performing a programmable tracking task of a time-varying desired position and orientation simultaneously. The reference trajectories for the robot end effector are given respectively by $r_p(k) = c_1 \sin(\omega k)$ and $r_o(k) = c_2 \cos(\omega k) + d_2$. In these experiments, the incision point has to follow a sinusoidal motion in the direction of the x-axis with linear velocity of 10 $cm\, s^{-1}$. The time-varying velocity for the incision point is given by $v_c(k) = \sin(c_3 \omega k)$. It is worth mentioning that, c_1, c_2, c_3 are constant parameters which define the motion direction, d_2 is a phase shift parameter, ω is the signal frequency and k is the number of iterations. The control parameters used in all experiments were: $\Gamma = 5$,

$K_p = 270\ s^{-1}$, $K_o = 1500\ s^{-1}$. Other parameters are: $c_1 = 0.03$, $c_2 = \frac{\pi}{18}$, $d_2 = -\frac{\pi}{18}$, $c_3 = 8$, $\omega = 2\pi/7000\ rad\, s^{-1}$. The execution time of the programmable trajectory tracking was about 60 s with $k = 7000$, whereas the trajectory tracking task with the haptic device takes about 40 s with $k = 5000$.

We have investigated the singularity issue from the practical point of view, since it is not always possible to perform in advance a singularity-free trajectory planning for the robot arm. In addition, the main goal of the proposed methodology is to allow the task execution by means of a haptic device, considering that the operator does not have prior knowledge of the singularity-free regions of the robot workspace. This motivates us to run a second set of experiments to investigate the performance of the haptic control for the end-effector pose in the vicinity of singular configurations.

6.7.2.1 Singularity Analysis

The results of the first set of experiments are depicted in Figs. 6.4-6.8. For comparative purposes, we also present the signals obtained with the DLS inverse method and the filtered-inverse method during the tracking of a desired time-varying position and orientation. Fig. 6.4 shows the behavior in time of the velocity signals along the x- and z-axis of the constraint frame. We can observe that a satisfactory tracking performance was achieved using the singularity avoidance methods. However, as expected, the kinematic control scheme based on the inverse Jacobian matrix was not able to ensure the trajectory tracking for the incision point. The time history of the manipulability index for the DLS inverse and FI methods is illustrated in Fig. 6.5, where it is possible to observe the occurrence of two singularity points. Fig. 6.6 and Fig. 6.7 illustrate the behavior in time of the position and orientation errors of the robot end effector along the x-, y- and z-axis respectively. The time history of the joint velocity signals generated by the kinematic control scheme is illustrated in Fig. 6.8. We can observe the lower magnitude of the control signals obtained from the singularity avoidance methods compared to the conventional inverse Jacobian-based controller, which demonstrate the feasibility of the proposed methodology.

6.7.2.2 Haptic Control

In the second set of experiments, we control the end effector using a haptic device and we let the velocities at the incision point follow the same pre-defined trajectory. The key idea here is to evaluate the performance of the FI method in the neighbourhood of singular configurations. The time history of the velocities of the incision point along the x- and z-axis are shown in Fig. 6.9. We can observe that a remarkable tracking performance for the incision point was achieved even for the haptic-based teleoperation of the robot end effector. Fig. 6.10 and Fig. 6.11 illustrate the behavior in time of the trajectory tracking for the end-effector pose along the x-, y- and z-axis respectively. The time history of the error norm for the end-effector pose is illustrated in Fig. 6.12, (a) and (b), where we can observe the low magnitude of the signal thanks to the use of a singularity avoidance method. The behavior in time of the manipulability index and the joint control signals are illustrated in Fig. 6.13, where it is possible to note the

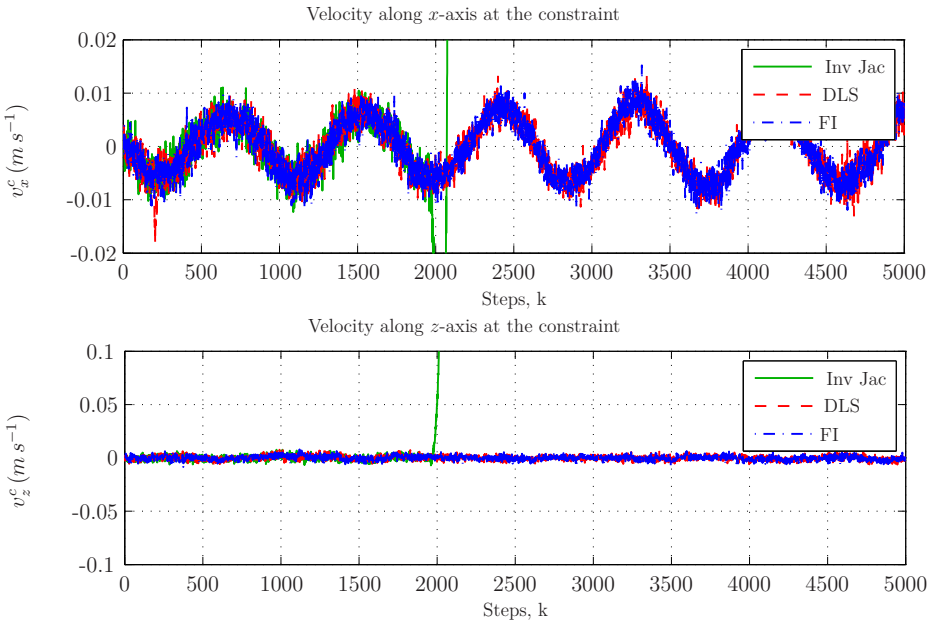

Figure 6.4: Velocity signal along the x- and z-axis at the incision point.

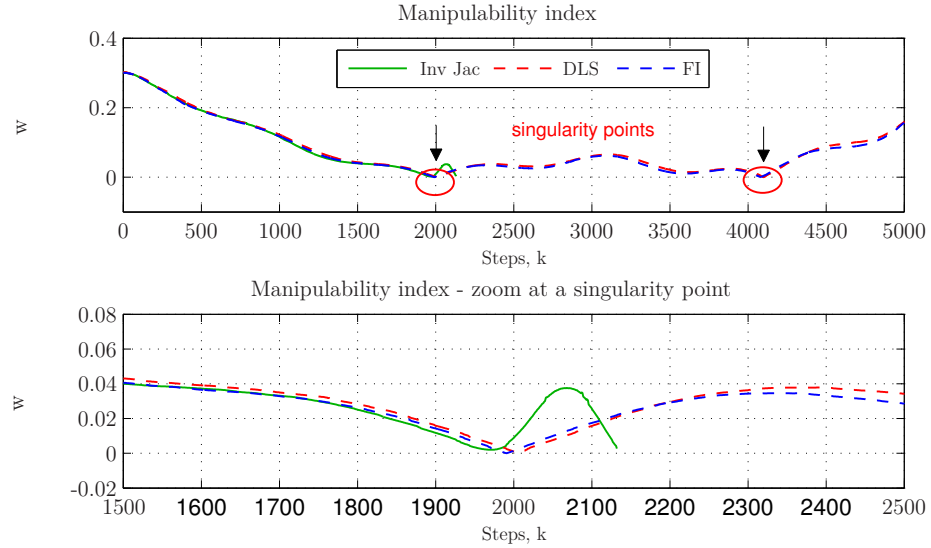

Figure 6.5: Manipulability index: near to zero indicates a singularity point.

occurrence of two singularity points. The kinematic control scheme based on the FI method is able to avoid large joint control signals even in the presence of singularities.

It is worth mentioning that, for the sake of saving space, we do not present the graphic results obtained with the DLS method for the haptic control. In addition, it is quite difficult to reproduce the robot motion for a particular singularity avoidance method using the Phantom Omni device. In fact, the motion repeatability and accuracy depend on the operator's maneuverability performance in the haptic teleoperation task. A simple and direct way to compare the performance of the singularity avoidance methods is to record the robot motion for the first task and then apply it as the reference trajectory for the second task. Moreover, it was observed during the experiments that in most attempts to perform the tracking task with the haptic device, the operator

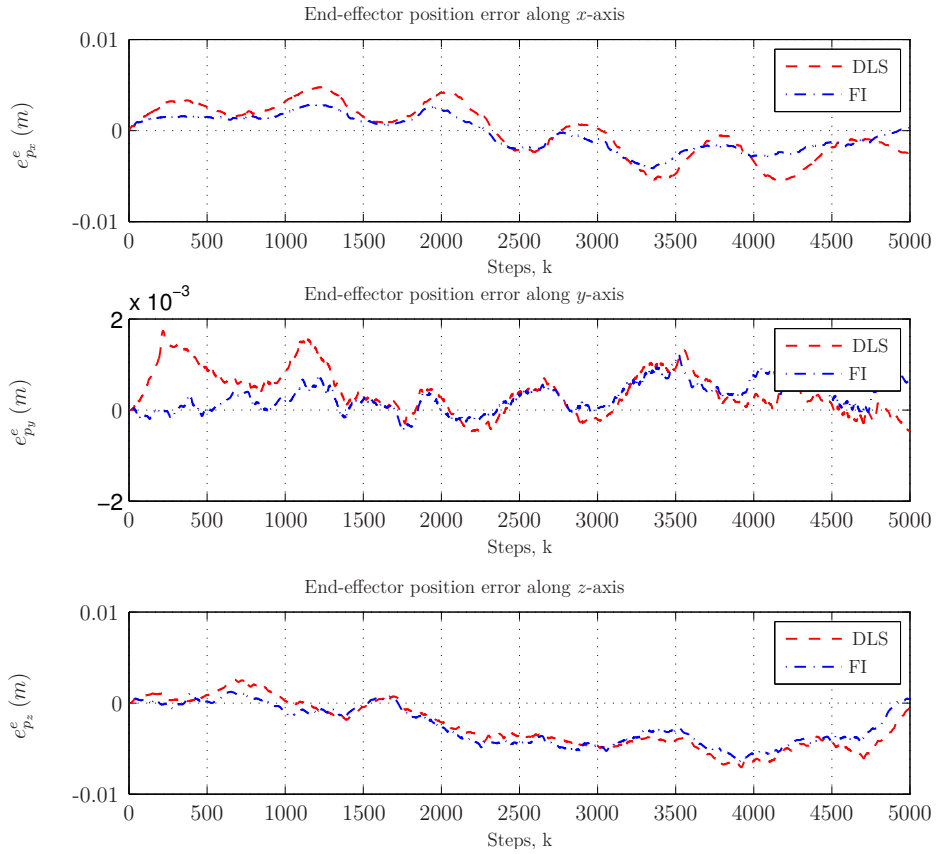

Figure 6.6: Position error of the robot end effector.

was not able to cross the singularity points without the aid of the singularity avoidance methods, even for operations at low speed and/or low acceleration.

6.8 Conclusion

This paper solved the problem of actively controlling the remote center of motion for robotics-assisted minimally invasive surgery. We derived a framework that allows us to follow both the end-effector and the incision point trajectories. The results were verified through experimental results on an industrial manipulator.

We have also shown how to deal with singularities and presented a methodology that allows us to pass through the singular configuration while keeping the error low and without blowing up the control signals. These kinds of constrained systems, being minimally invasive surgery or other constrained systems, tend to have singularities at configurations that are difficult to avoid, which may make it necessary to pass through or close to the singularity.

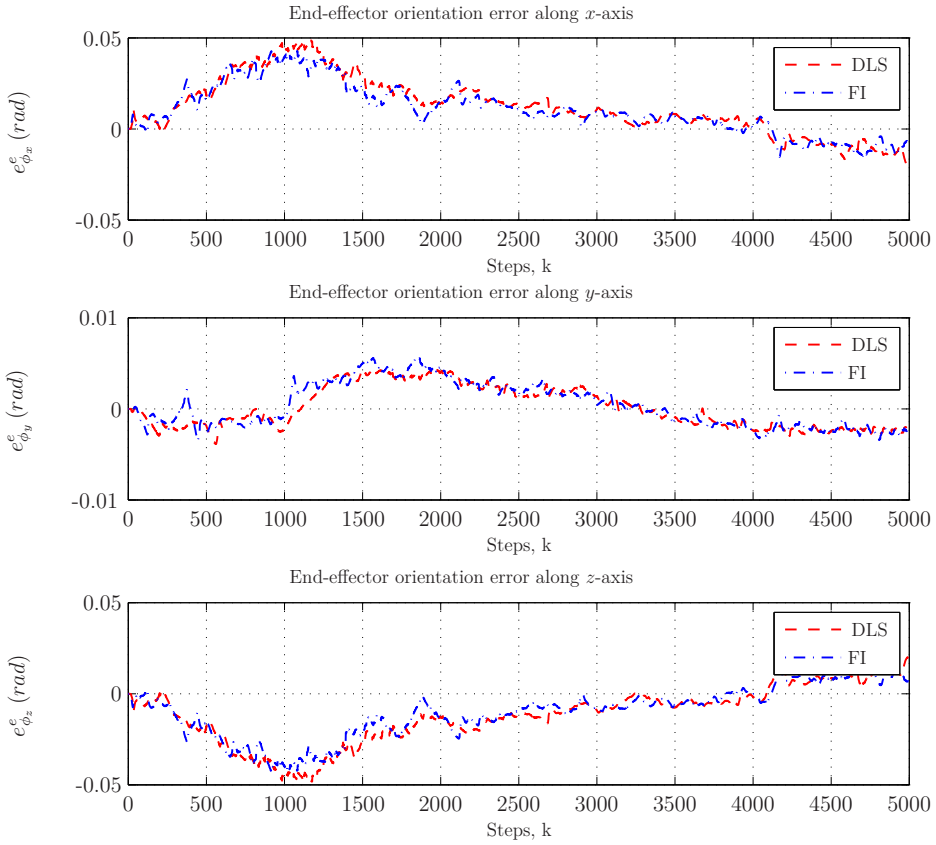

Figure 6.7: Orientation error of the robot end effector.

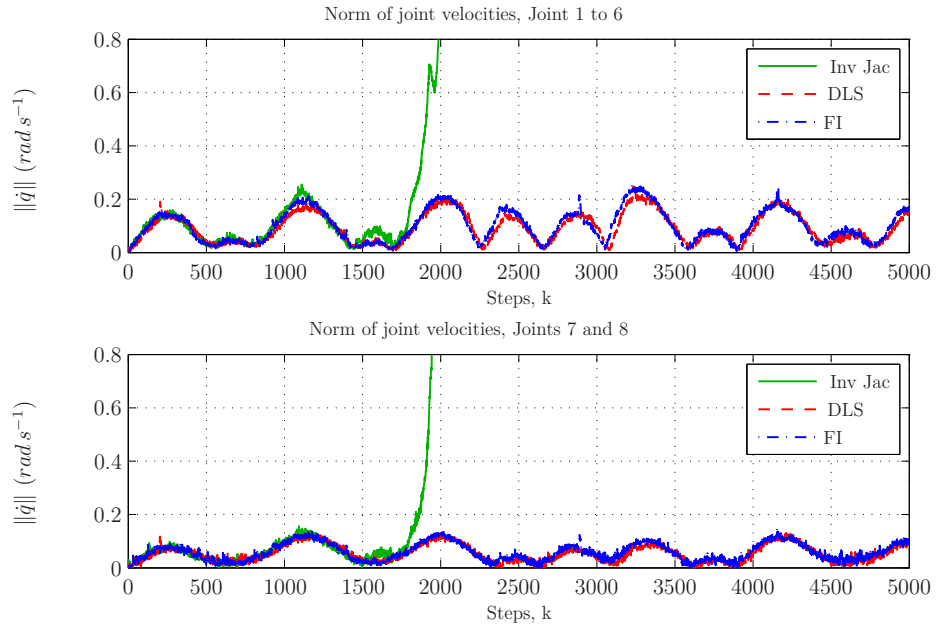

Figure 6.8: Norm of the velocity control signals applied to the robot joints.

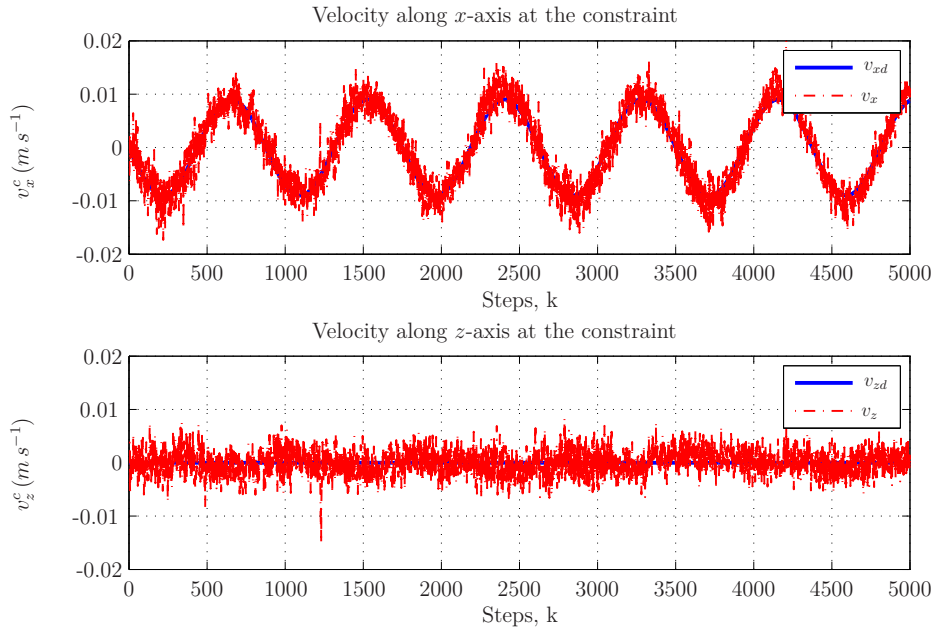

Figure 6.9: Velocity signals along the x- and z-axis at the incision point.

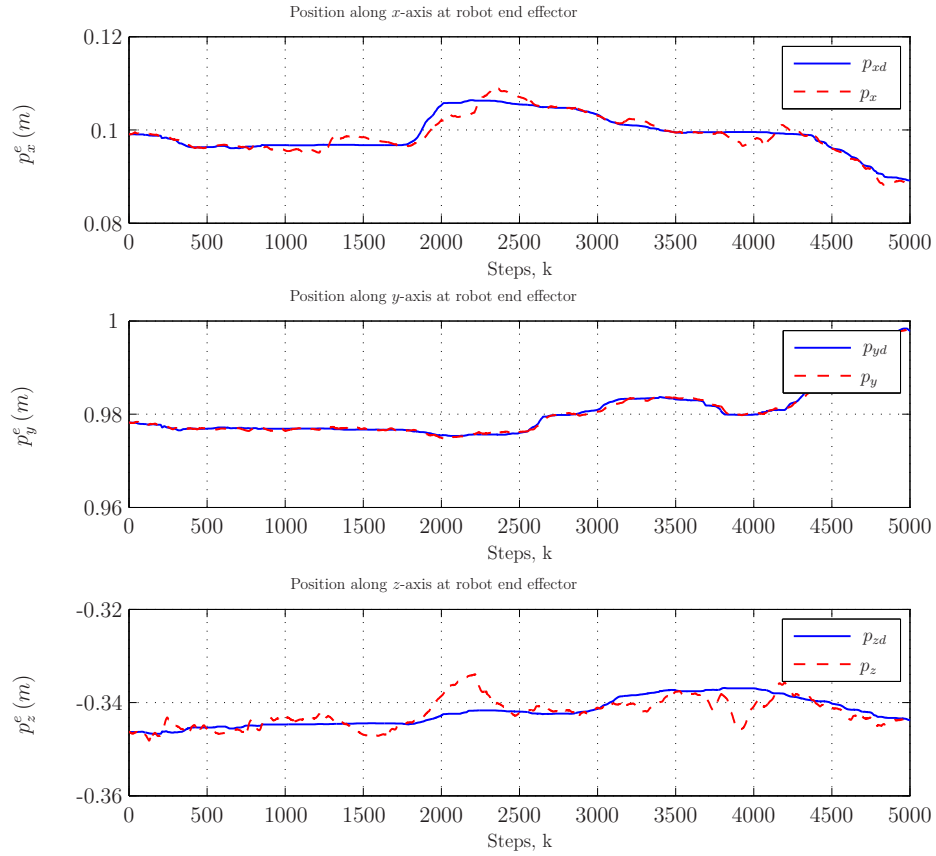

Figure 6.10: Position tracking for the robot end effector.

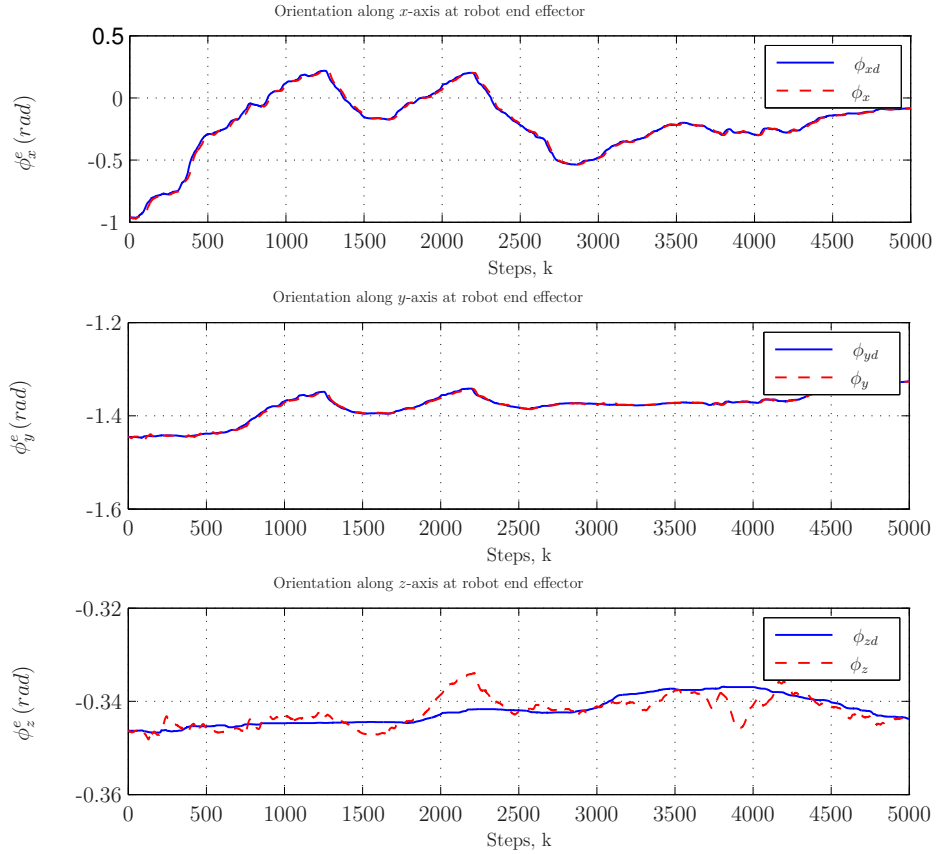

Figure 6.11: Orientation tracking for the robot end effector.

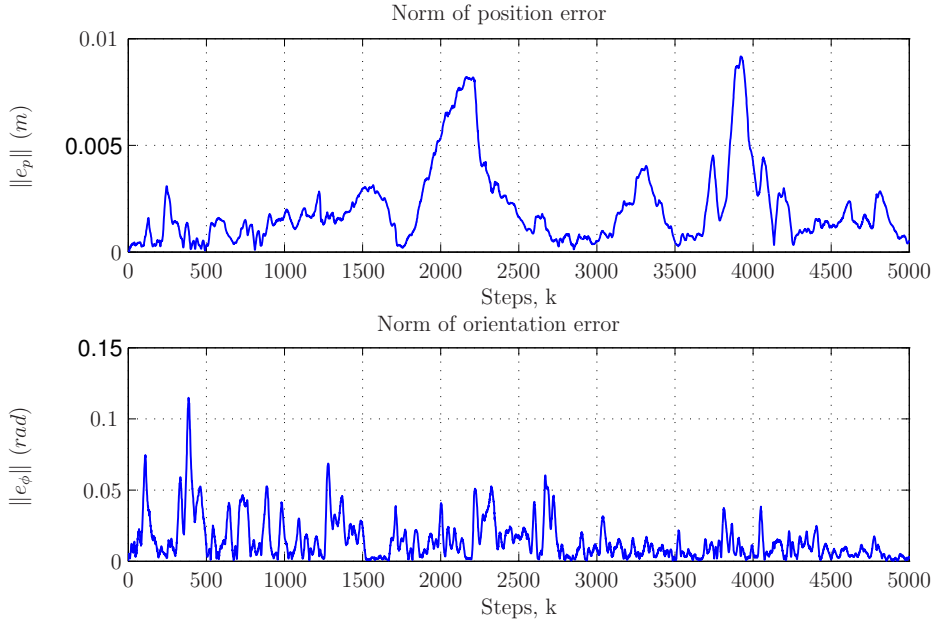

Figure 6.12: Norm of position and orientation errors of the robot end effector.

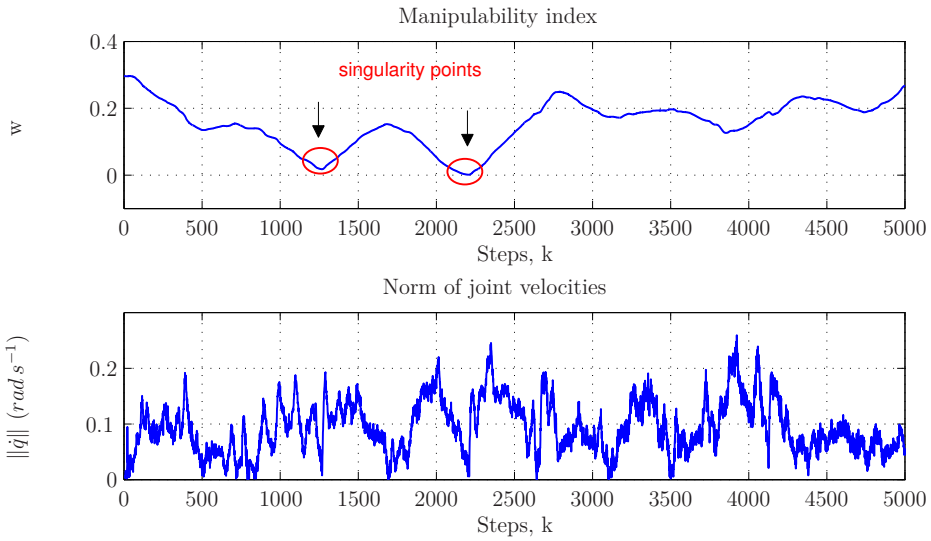

Figure 6.13: Manipulability index and norm of the velocity control signals.

Chapter 7

Singularity Analysis of Robotic Manipulators with Velocity-Constraints for Minimally Invasive Surgery

7.1 Abstract

This paper presents a novel framework for analyzing the mobility of constrained serial manipulators. We focus on the type of constraints that arise in minimally invasive surgery, where a long shaft is inserted into the human body through a incision point, or trocar. The trocar constraint will in this case change the mobility of the manipulator and the location and nature of the singularities. For minimally invasive surgery both the mobility and the singularities of the system need to be known to obtain safe and reliable operation.

Velocity constraints on the chain will in general complicate the mobility analysis of the manipulator as conventional methods such as manipulability and other methods that require the manipulator Jacobian cannot be applied because these methods do not take the constraints into account. The main contribution of the paper is to find the end-effector velocity by adding the velocity at the constraint and the velocity of the joints after the constraint (often called the wrist) and observing that these velocities need to span the whole end-effector velocity space. We then use this new representation of the end-effector velocity to find the mobility of the constrained manipulators. The framework can be used both to determine the optimal manipulator geometry in the presence of chain constraints and, once the manipulator geometry is chosen, to control the robot such that the mobility is maintained high and singularities avoided. The first property of the presented framework can for example be used to find the optimal geometry of the wrist of a surgical robot subjects to incision point constraints, and the latter can be used to control the robot so that singularities are avoided. The singularities typically take a very different form than for the unconstrained case.

7.2 Introduction

Constraints imposed on the manipulator chain poses great challenges to both the analysis and control. We know that kinematic constraints can take a very complex form when mapped to the joint space of the manipulator, and it can therefore be challenging to find control laws to avoid these singularities. In this paper, we present a framework that allows us to analyze in detail how the constraints affect the singularities. These singularities are different from the manipulator singularities found in open chain robots as they are greatly dependent on the geometry of the constraint and on the geometry of the joints located after the constraints on the manipulator chain. We do, however, find that there are several similarities to the analysis of unconstrained manipulators.

There are several approaches to analyze the singularities of serial manipulators. The concept of manipulability was introduced in Yoshikawa [1985b]. For the six degrees of freedom of the end-effector space, the manipulability was found and a 6-DoF ellipsoid was constructed to define the manipulability. When a motion in one direction of the ellipsoid cannot be realized, the length of this axis becomes zero and the manipulability ellipsoid has no volume. This is referred to as a singular configuration. Chen and Chen [1994], Boudreau and Podhorodeski [2010] analyze the singularity of serial unconstrained manipulators by using the theory of reciprocal screws while Hao and McCarthy [1998] considers singular configurations of a robotic system that can be modeled as a platform supported by serial robotic chains.

The manipulability can also be found for parallel manipulators (Wen and Wilfinger [1999], Park and Kim [1998]). In this case the length in one or more directions of the manipulability ellipsoid can become either zero or infinite. If one direction is zero it means that a velocity cannot be realized in this direction, this is often referred to as an unmanipulable singularity. On the other hand, if the length approaches infinity the manipulator cannot prevent the end effector to move in a certain direction. In this case the passive joints will move even though all the active joints are locked, which is referred to as an unstable singularity (Wen and Wilfinger [1999], From and Gravdahl [2008]). The analysis of singularities for closed kinematic chains was studied in Park and Kim [1999], Gosselin and Angeles [1990].

We just take a different approach to the problem as the analysis normally applied to serial manipulators cannot be applied as these do not take the constraints into account, and the analysis used for parallel manipulators cannot be applied to serial manipulators, even in the constrained case. The proposed approach is to study how well the end-effector motion can be generated given a specific constraint. We observe that by adding the motion allowed by the constraint and the motion generated by the joints after the constraint we can easily determine the mobility. We can do this either by simple geometric reasoning, or by constructing a Constrained Jacobian Matrix and analyze this in the same way as the manipulator Jacobian normally used for singularity analysis.

The main contribution of this paper is that we recognize that we can use the Constrained Jacobian Matrix previously presented by the authors to perform a singularity and mobility analysis of different geometric structures and to find the optimal geometry of a robot given the constraint geometry. We present for the first time a detailed anal-

ysis of how velocity constraints on the chain affect the mobility of different geometric structures. In addition we show how this can be used to avoid singular configurations that arise due to the chain constraints.

The paper is organized as follows: In Section 7.3 and 7.4 we present the overall idea of how the kinematics of a constrained kinematic chain, the mathematical representation of the different kinematic constraints and the corresponding Jacobian matrices are calculated. We study the singularities of constrained planar and spatial manipulators in Section 7.5 and 7.6, respectively. The conclusion is presented in Section 7.7.

7.3 System Overview and Problem Formulation

The system discussed in this paper consists of a redundant robotic manipulator in the presence of kinematic constraints.

At some given points in the Cartesian space we will require that the velocities of the links are eliminated in certain directions to prevent the robot from hitting an obstacle. The system setup together with the most important configuration spaces used in this paper are shown in Fig. 7.1. We denote the frame of the joint located before the incision point, that is located at $\mathcal{F}_c$ in the chain, by $\mathcal{F}_a$ and the joint that is located after the incision point is denoted $\mathcal{F}_b$. The desired end-effector motion is given by the frame $\mathcal{F}_e$. We will denote the velocity variables in the following way

$$V_{0e}^B = \begin{bmatrix} v_x^e & v_y^e & v_z^e & \omega_x^e & \omega_y^e & \omega_z^e \end{bmatrix}^\mathsf{T} \tag{7.1}$$

and similarly for the other frames. V_{ij}^B is thus the velocity in body coordinates of a rigid body with frame $\mathcal{F}_j$ with respect to the frame $\mathcal{F}_i$. V_{ij}^B is an element of the Lie algebra $se(3)$ of the Special Euclidean Group SE(3), and is found as $V_{ij}^B = g_{ij}^{-1}\dot{g}_{ij}$ where g_{ij} is the homogeneous transformation matrix describing the location of $\mathcal{F}_j$ in $\mathcal{F}_i$.

7.4 Constrained Kinematics

The first step of the mobility and singularity analysis is to find the required velocity mappings and at the same time take the constraints into account. This section presents a short summary of Pham et al. [2014a].

We first derive the motion of a kinematic chain given a desired end-effector motion $\mathcal{F}_e$ and a kinematic constraint at a point represented by $\mathcal{F}_c$. In this section we will present the overall idea of how these relations are used to find the kinematics of a constrained kinematic chain.

The main idea is to find the velocity V_{0a}^B in terms of a set of new velocity variables parametrized in such a way that these variables can be chosen freely and at the same time guarantee that the constraints at $\mathcal{F}_c$ are satisfied. This means that certain directions in the velocity space are reduced from a higher to a lower-dimensional space represented by new velocity variables v_i.

As our main objective is to follow a desired end-effector motion V_{0e}^B we need to find

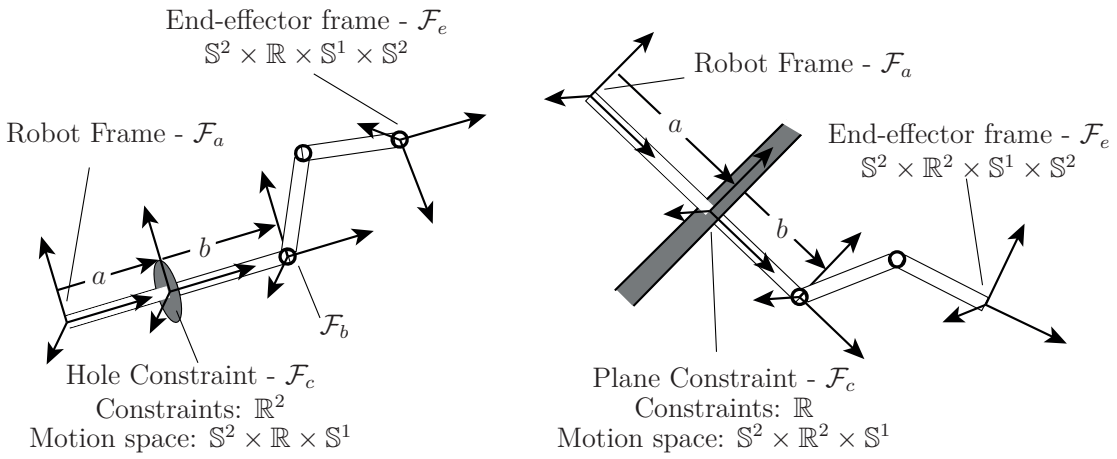

Figure 7.1: Two examples of the constraints discussed in this paper: on the left, a hole constraint which prevents any lateral motion of a specific point on the manipulator chain; and on the right, a plane constraint that restricts the linear motion of a point to a given direction in the plane. The constrained link is constrained at the point $\mathcal{F}_c$ which in turn results in a reduced motion space at $\mathcal{F}_a$. The motion spaces of the different frames are subgroups of $SE(3)$ defined by linear motion $\mathbb{R}$, circular motion $\mathbb{S}$, and the sphere $\mathbb{S}^2$.

the mapping from V_{0e}^B to the free variables, i.e., V_{0a}^B with the reduction in dimensionality represented by v_i. This is obtained in the following way Pham et al. [2014a]:

1. Define a desired end-effector velocity V_{0e}^B.

2. Given a constraint at $\mathcal{F}_c$, define the velocities at this point which satisfy the constraints, i.e., the velocities at the previous joint $\mathcal{F}_a$ are given by

   - the free variables $\{v_x^a,\, v_y^a,\, v_z^a,\, \omega_x^a,\, \omega_y^a,\, \omega_z^a\}$, and
   - the constrained variables $\{v_1,\, v_2,\, v_3,\, \dots\}$.

   The free variables are the ones that can be chosen freely and do not affect the constraint. The constraint variables require a specific form and structure for the constraints to be satisfied. We will therefore replace some of the free variables with the constraint variables which gives us the required structure. These variables thus represent a freedom, but in a space with reduced dimensionality that satisfies the constraint. The constrained variables are thus written in terms of the free variables v as
   $$V_{0a}^B = V_{0a}^B(v). \tag{7.2}$$

3. Eliminate the redundant variables that arise as a result of the reduced dimensionality and denote the minimal representation of the velocity variables by $\bar{V}_{0a}^B$.

4. Find a mapping from the end-effector velocities V_{0e}^B to the new reduced velocity

variables $\bar{V}_{0a}^B$, which will take the form

$$v_m^a = \begin{bmatrix} \bar{V}_{0a}^B \\ \dot{q} \end{bmatrix} = \begin{bmatrix} \text{constrained variables} \\ \text{free variables} \\ \text{joint velocities} \end{bmatrix}. \tag{7.3}$$

The mapping is given by the Constrained Jacobian Matrix J_{ea}^m that gives the important relation $V_{0e}^B = J_{ea}^m v_m^a$, i.e., the transformation from the new reduced velocity variables v_m^a to the desired end-effector velocities V_{0e}^B.

The *joint velocities* represent the joints that are determined by the end-effector velocity V_{0e}^B only and do not depend on the constraints. These are typically the joints that are situated between the constraint and the end effector. The *free variables* are the velocities of $\mathcal{F}_a$ that do not depend on the constraint, but differently from the *joint velocities*, they depend on the joints between the base and the constraint. Finally, the *constrained variables* are constraint dependent and give the velocity at $\mathcal{F}_a$ the required structure so that the constraints are satisfied.

5. From the new variables, find the robot velocity at $\mathcal{F}_a$.

7.4.1 Constrained Jacobian Matrix

In this section we will find the relation between the desired end-effector velocities and the corresponding joint velocities subject to the constraints described in the previous section. Given the end-effector velocity we want to find the free and constrained velocity variables of the robot. We will find the Constrained Jacobian Matrix J_{ea}^m which gives the relation $V_{0e}^B = J_{ea}^m v_m^a$ and the required velocities v_m^a are found from the desired end-effector velocities by the inverse of the Constrained Jacobian Matrix.

The standard body Jacobian matrix gives the mapping from the joint velocities to the end-effector velocities in body coordinates and is given by (From et al. [2014a])

$$\begin{aligned} J_{0e}^B &= \begin{bmatrix} X_1^\dagger & X_2^\dagger & \cdots & X_n^\dagger \end{bmatrix} \\ &= \begin{bmatrix} \mathrm{Ad}_{g_{1e}}^{-1} X_1^1 & \mathrm{Ad}_{g_{2e}}^{-1} X_2^2 & \cdots & X_n^n \end{bmatrix} \in \mathbb{R}^{n\times 6} \end{aligned} \tag{7.4}$$

where X_i^i is the constant twist in frame $\mathcal{F}_i$ and $\mathrm{Ad}_{g_{ie}}^{-1}$ is the Adjoint matrix that transforms X_i^i from frame $\mathcal{F}_i$ to $X_i^\dagger$ represented in the end-effector frame $\mathcal{F}_e$. The body Jacobian matrix can also be found for other links than the end effector, in which case it is denoted J_{0i}^B which gives the velocities of link i. Particularly, the Jacobian matrix that gives the velocity of the link $\mathcal{F}_a$ located before the constraint is denoted J_{0a}^B.

In this section we will find the body Jacobian matrices, as above, but subject to the constraints, i.e., we find the mapping from the joint velocity variables to the respective links subject to a constraint on the velocity at the constraint frame $\mathcal{F}_c$. We will see that for a large class of constraints the Constrained Jacobian Matrix can be written in the form

$$\bar{J}_{0a}^B = \begin{bmatrix} \sum \alpha_i X_i^\dagger & \sum \alpha_j X_j^\dagger & \cdots & \sum \alpha_k X_k^\dagger \end{bmatrix} \in \mathbb{R}^{m\times 6} \tag{7.5}$$

for some $(n-m)$-dimensional constraint. Here the bar in $\bar{J}^B_{0a}$ distinguishes the Constrained Jacobian Matrix from the standard Jacobian J^B_{0a}. $X_i^\dagger$ are the manipulator twists while α_i are configuration-dependent functions of the manipulator and constraint kinematics. The form of the Constrained Jacobian Matrix depends on the type of constraint. We will now look at what the Constrained Jacobian matrices look like for different types of constraints.

7.4.2 Plane Constraint

For a plane-shaped constraint we want to eliminate the velocity at $\mathcal{F}_c$ in one direction. Lets assume that we will allow no velocity in the direction of v_y^c. As this can be written in terms of the velocities at $\mathcal{F}_a$ (prior to the entry point) as

$$v_y^c = v_y^a - a\omega_x^a \tag{7.6}$$

the constraint $v_y^c = 0$ can be transformed to the frame $\mathcal{F}_a$ as

$$v_y^a = a\omega_x^a. \tag{7.7}$$

We can now introduce a new variable v_1 which describes the one degree of freedom represented by (4.8). The constrained variables v_y^a and ω_x^a then take the form

$$v_y^a = v_1 \qquad\qquad \omega_x^a = \frac{1}{a}v_1 \tag{7.8}$$

which forces a point $\mathcal{F}_c$ on the robot to avoid lateral motion in the direction of the y-axis. The constrained velocity variables at $\mathcal{F}_a$ can now be written as

$$\begin{bmatrix} v_x^a \\ v_y^a \\ v_z^a \\ \omega_x^a \\ \omega_y^a \\ \omega_z^a \end{bmatrix} = \begin{bmatrix} v_x^a \\ v_1 \\ v_z^a \\ \frac{1}{a}v_1 \\ \omega_y^a \\ \omega_z^a \end{bmatrix} \tag{7.9}$$

which have five degrees of freedom, as expected. We see that we impose a certain structure on the velocities at $\mathcal{F}_a$ which guarantees that the constraints are satisfied.

7.4.3 Entry Hole

Assume a robotic chain that is inserted through a hole. This will add a 2-DoF constraint to the point of entry, represented by $\mathcal{F}_c$, which is a point on the link penetrating the hole. This is for example the case in minimally invasive surgery where the robot is to be inserted into the abdomen through a trocar.

The velocities at the entry point can be written in terms of the velocities at $\mathcal{F}_a$ as

$$v_x^c = v_x^a + a\omega_y^a \tag{7.10}$$
$$v_y^c = v_y^a - a\omega_x^a \tag{7.11}$$

and the constraint of zero velocity can therefore be cast into the following simple form

$$v_x^a = -a\omega_y^a \tag{7.12}$$
$$v_y^a = a\omega_x^a \tag{7.13}$$

where we need to know the distance from the joint prior to the constraint to the entry point. We can incorporate these constraints in the kinematics by introducing new variables v_1 and v_2 such that

$$v_x^a = v_1 \qquad \omega_y^a = -\frac{1}{a}v_1 \tag{7.14}$$
$$v_y^a = v_2 \qquad \omega_x^a = \frac{1}{a}v_2 \tag{7.15}$$

which for any choice of v_1 and v_2 will result in zero lateral velocity at the entry point. The constrained velocities can now be given as

$$\begin{bmatrix} v_x^a \\ v_y^a \\ v_z^a \\ \omega_x^a \\ \omega_y^a \\ \omega_z^a \end{bmatrix} = \begin{bmatrix} v_1 \\ v_2 \\ v_z^a \\ \frac{1}{a}v_2 \\ -\frac{1}{a}v_1 \\ \omega_z^a \end{bmatrix}. \tag{7.16}$$

The expressions are found similarly for other types of constraints.

7.5 Singularity analysis of planar manipulators

We consider a 4-DoF planar manipulator with a 1-DoF constraint on the third link, see Fig. 7.2. We assume that all four joints rotate around the z-axis. Following Section 4.5 we find the Constrained Jacobian Matrix for this manipulator as

$$\bar{J}_{0a1}^B = \begin{bmatrix} cq_4 & sq_4 - \frac{1}{a}l_3 sq_4 & 0 \\ -sq_4 & cq_4 - \frac{1}{a}\left(l_4 + l_3 cq_4\right) & l_4 \\ 0 & -\frac{1}{a} & 1 \end{bmatrix} \tag{7.17}$$

which gives the mapping

$$\begin{bmatrix} v_x^e \\ v_y^e \\ \omega_z^e \end{bmatrix} = \bar{J}_{0a1}^B \begin{bmatrix} v_1 \\ v_x^a \\ \dot{q}_4 \end{bmatrix}. \tag{7.18}$$

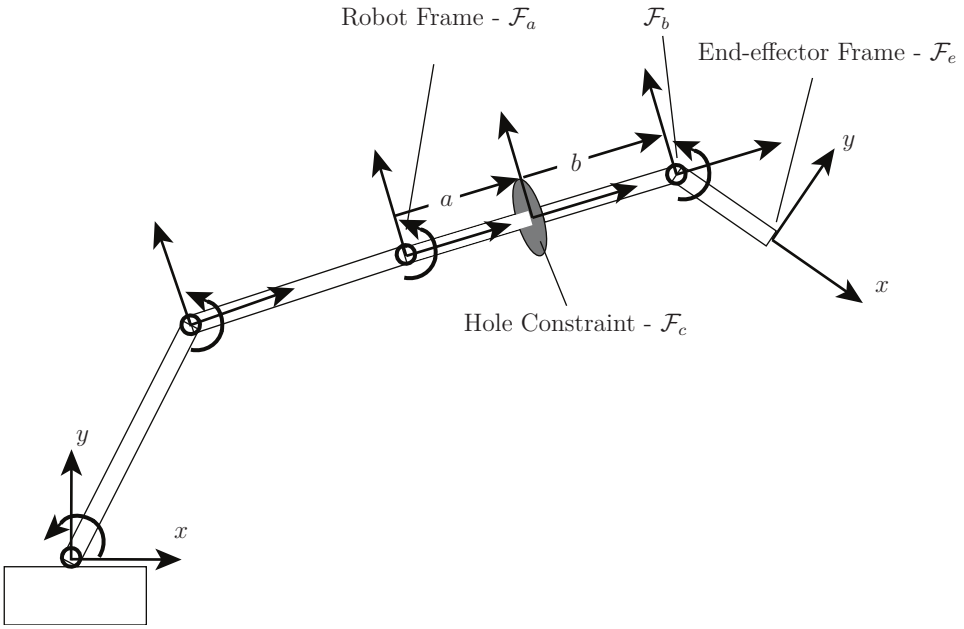

Figure 7.2: The planar case: a 4-DoF planar robot with a 1-DoF constraint on the third link.

We find the determinant of the Constrained Jacobian Matrix as

$$\det\left(\bar{J}^B_{0a1}\right) = \frac{a - l_3}{a}. \tag{7.19}$$

From this we can see that the Constrained Jacobian Matrix is never singular except when the constraint is located exactly at the fourth joint. At this point the Constrained Jacobian Matrix reduces to

$$\bar{J}^B_{0a1} = \begin{bmatrix} cq_4 & 0 & 0 \\ -sq_4 & -\frac{l_4}{a} & l_4 \\ 0 & -\frac{1}{a} & 1 \end{bmatrix} \tag{7.20}$$

and we see that we cannot control both v^e_y and ω^e_z independently once v_1 is chosen to obtain v^e_x. The singularity arises as one of the degrees of freedom allowed by the constraint, the rotation around the constraint point, is exactly the same as the degree of freedom represented by the last joint q_4, which results in a reduced mobility.

We note that mathematically this is identically the analysis of non-constrained serial manipulators, i.e., the singularity occurs when two intersecting axes occur. However, the geometric interpretation is rather different, as in our case the singularity occurs when the axes of the last manipulator joint intersects with the axes of the constraint velocities. The singularity thus depends on the geometry of the constraint, and not only on the geometry of the robot, which is the case when the singularity arises as a result of two intersecting joint axes.

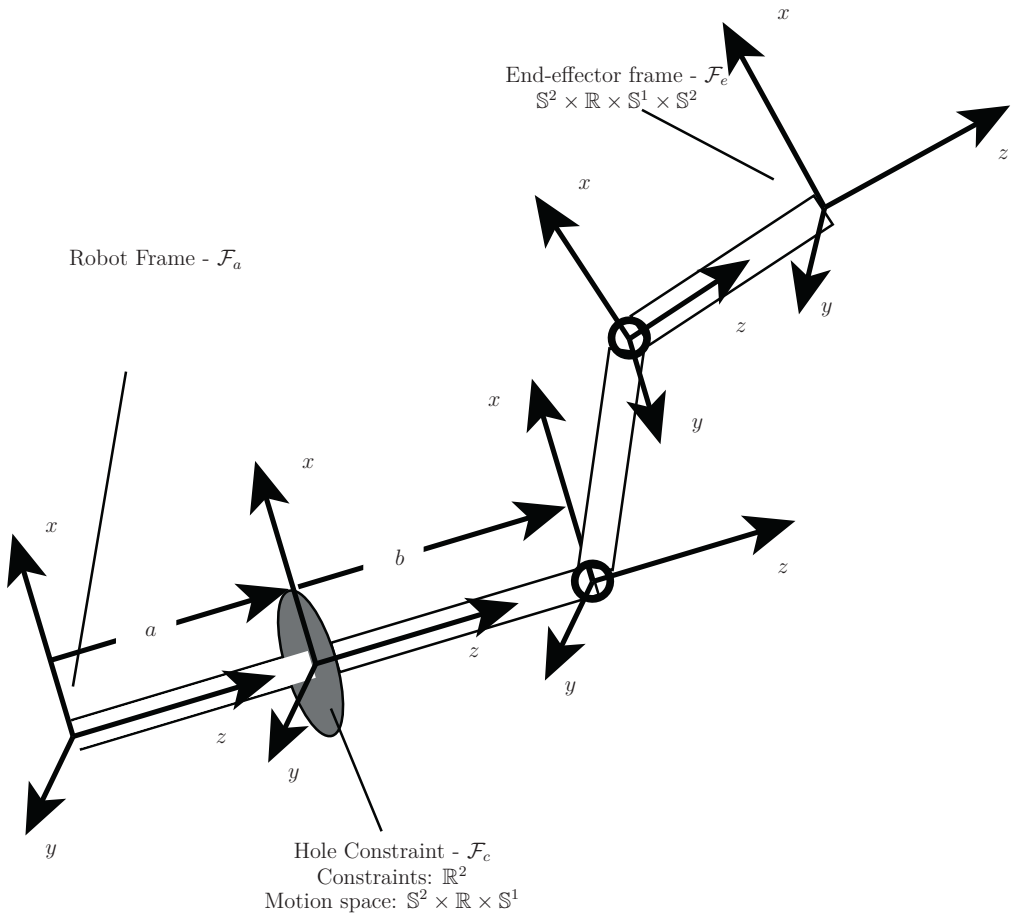

Figure 7.3: A constrained manipulator where both joints after the constraint rotate around the y-axis.

7.6 Singularity Analysis of spatial manipulators

In this section we consider spatial manipulators with a total of eight joints and with two joints after a hole constraint. We will divide the problem into four different cases and analyze each case separately. In all the cases, we consider 8-DoF manipulators with a constraint on the sixth link. So the manipulators have 6 joints before the constraint and 2 joints after the constraint. We use the notation $cq_7 = cos\,(q_7)$, $sq_7 = sin\,(q_7)$, $cq_8 = cos\,(q_8)$, $sq_8 = sin\,(q_8)$, $cq_{78} = cos\,(q_7 + q_8)$, $sq_{78} = sin\,(q_7 + q_8)$.

7.6.1 Both joints after the constraint rotate around the same axis

We first assume that both joints after the constraint rotate around the y-axis, as shown in Fig. 7.3. The analysis for the x-axis is similar.

We have the Constrained Jacobian Matrix in this case as

$$\bar{J}^B_{0a2} = \begin{bmatrix} \chi_1 & 0 & -sq_{78} & 0 & l_7cq_8 & 0 \\ 0 & \delta_1 & 0 & l_7sq_7 & 0 & 0 \\ \chi_2 & 0 & cq_{78} & 0 & l_7sq_8 & 0 \\ 0 & \frac{1}{a}cq_{78} & 0 & -sq_{78} & 0 & 0 \\ -\frac{1}{a} & 0 & 0 & 0 & 1 & 1 \\ 0 & \frac{1}{a}sq_{78} & 0 & cq_{78} & 0 & 0 \end{bmatrix}. \tag{7.21}$$

Here we have defined $\chi_1 = -\frac{1}{a}(b\,cq_{78} + l_7cq_8)$, $\chi_2 = -\frac{1}{a}(b\,sq_{78} + l_7sq_8)$ and $\delta_1 = -\frac{1}{a}(b + l_7cq_7)$.

The determinant of the Constrained Jacobian Matrix is

$$\det\left(\bar{J}^B_{0a2}\right) = 0. \tag{7.22}$$

We see that in this case the matrix is always singular. The reason is that ω^c_y, v^c_z, $\dot{q}_7$, and $\dot{q}_8$ all generate motion in the xz-plane of $\mathcal{F}_c$. It thus requires 4 DoF to control the three variables in the plane. In other words the manipulator has only 2 DoF left to control the remaining three degrees of freedom which is what leads to the singular configuration.

Following the same line of arguments, we also find that the manipulator is always singular when the two last joints after the constraint rotate around x-axis of $\mathcal{F}_c$.

7.6.2 The last joint rotate around the z-axis

We will consider two cases where the first joint after the constraint rotates around x- or y-axis and the last joint rotate around z-axis. The two cases are similar. The y-axis case is shown in Fig. 7.4.

The Constrained Jacobian Matrix for the x-axis case is found as

$$\bar{J}^B_{0a3} = \begin{bmatrix} \alpha_1 & \beta_1 & sq_7sq_8 & \gamma_1 & \varphi_1 & 0 \\ \alpha_2 & \beta_2 & cq_8sq_7 & \gamma_2 & \varphi_2 & 0 \\ 0 & \frac{b}{a}sq_7 & cq_7 & 0 & 0 & 0 \\ -\frac{1}{a}cq_7sq_8 & \frac{1}{a}cq_8 & 0 & sq_7sq_8 & cq_8 & 0 \\ -\frac{1}{a}cq_7cq_8 & -\frac{1}{a}sq_8 & 0 & cq_8sq_7 & -sq_8 & 0 \\ \frac{1}{a}sq_7 & 0 & 0 & cq_7 & 0 & 1 \end{bmatrix}. \tag{7.23}$$

Here we have defined $\alpha_1 = -\frac{1}{a}cq_8(b + l_7cq_7 + l_8cq_7)$, $\alpha_2 = \frac{1}{a}sq_8(b + l_7cq_7 + l_8cq_7)$, $\beta_1 = -\frac{1}{a}sq_8(l_7 + l_8 + b\,cq_7)$, $\beta_2 = -\frac{1}{a}cq_8(l_7 + l_8 + b\,cq_7)$, $\gamma_1 = cq_8sq_7(l_7 + l_8)$, $\gamma_2 = -sq_7sq_8(l_7 + l_8)$, $\varphi_1 = -sq_8(l_7 + l_8)$ and $\varphi_2 = -cq_8(l_7 + l_8)$.

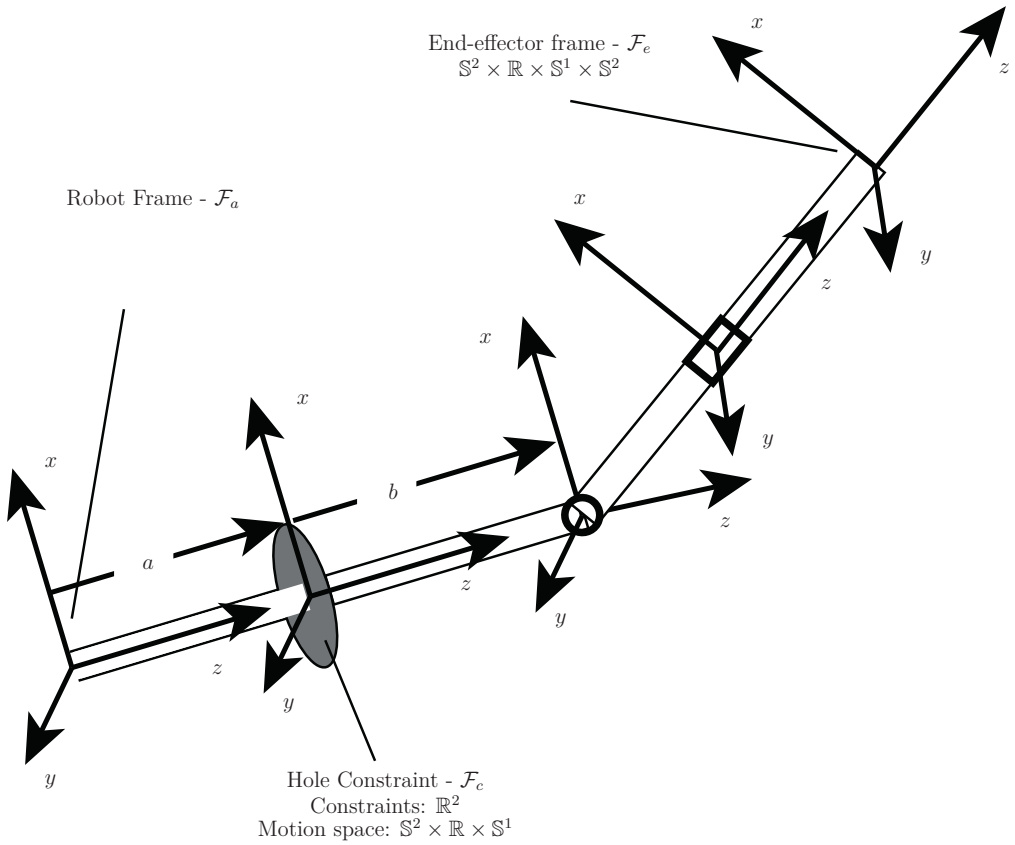

Figure 7.4: An example of constrained manipulator with the first joint after the constraint rotate around y-axis and the last joint rotate around z-axis.

For the y-axis case the Constrained Jacobian Matrix is found as

$$\bar{J}^B_{0a4} = \begin{bmatrix} \alpha_3 & \beta_3 & -cq_8sq_7 & \gamma_3 & \varphi_3 & 0 \\ \alpha_4 & \beta_4 & sq_7sq_8 & \gamma_4 & \varphi_4 & 0 \\ -\frac{b}{a}sq_7 & 0 & cq_7 & 0 & 0 & 0 \\ -\frac{1}{a}sq_8 & \frac{1}{a}cq_7cq_8 & 0 & -cq_8sq_7 & sq_8 & 0 \\ -\frac{1}{a}cq_8 & -\frac{1}{a}cq_7sq_8 & 0 & sq_7sq_8 & cq_8 & 0 \\ 0 & \frac{1}{a}sq_7 & 0 & cq_7 & 0 & 1 \end{bmatrix}. \tag{7.24}$$

Here we have defined $\alpha_3 = -\frac{1}{a}cq_8\,(l_7 + l_8 + b\,cq_7)$, $\alpha_4 = \frac{1}{a}sq_8\,(l_7 + l_8 + b\,cq_7)$, $\beta_3 = -\frac{1}{a}sq_8\,(b + l_7\,cq_7 + l_8\,cq_7)$, $\beta_4 = -\frac{1}{a}cq_8\,(b + l_7\,cq_7 + l_8\,cq_7)$, $\gamma_3 = sq_7sq_8\,(l_7 + l_8)$, $\gamma_4 = cq_8sq_7\,(l_7 + l_8)$, $\varphi_3 = cq_8\,(l_7 + l_8)$ and $\varphi_4 = -sq_8\,(l_7 + l_8)$.

The determinants of the Constrained Jacobian matrices in both cases are found as

$$\det\left(\bar{J}^B_{0a3}\right) = \det\left(\bar{J}^B_{0a4}\right) = -\frac{b^2}{a^2}sq_7. \tag{7.25}$$

We see that the matrix is singular when $sq_7 = 0$, i.e., for $q_7 = 0; \pi$. The reason is that ω^c_z and $\dot{q}_8$ rotate around the same axis and the manipulator loses 1 DoF. We note that this type of singularity resembles the singularity found in open chain manipulators when two

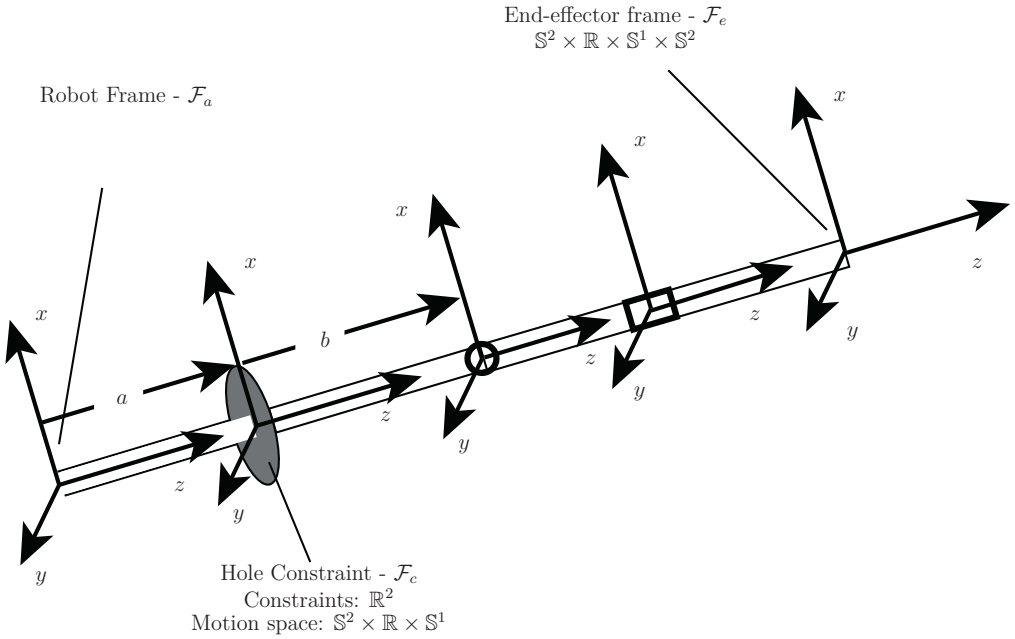

Figure 7.5: Singularity analysis of the manipulator where the first joint rotate around the y-axis and the last joint around z-axis. The manipulator is singular when $q_7 = 0$.

joints rotate around the same axis. The difference is that in this case the singularity arises when joint seven rotates around one of the axes for which the constraint allows motion, which in our case was ω_z^c. The singular configuration is shown in Fig. 7.5.

7.6.3 The first joint after the constraint rotate around $z-$axis

Similarly to the result of Section 7.6.2, we can easily conclude that if the first joint after the constraint rotates around the z-axis it will coincide with ω_z^c, and the manipulator will lose 1 DoF and always be singular.

7.6.4 No joint after the constraint rotate around z-axis

We will now consider two cases where the first joint after the constraint rotates around y-axis, the last joint rotates around x-axis and the vice versa. The Constrained Jacobian Matrix for the first case is

$$\bar{J}^B_{0a5} = \begin{bmatrix} \alpha_5 & \beta_5 & -sq_7 & l_8 cq_7 sq_8 & \theta_5 & 0 \\ \alpha_6 & \beta_6 & cq_7 sq_8 & \gamma_5 & 0 & -l_8 \\ \alpha_7 & \beta_7 & cq_7 cq_8 & -l_7 sq_7 sq_8 & 0 & 0 \\ 0 & \frac{1}{a} cq_7 & 0 & -sq_7 & 0 & 1 \\ -\frac{1}{a} cq_8 & \frac{1}{a} sq_7 sq_8 & 0 & cq_7 sq_8 & cq_8 & 0 \\ \frac{1}{a} sq_8 & \frac{1}{a} cq_8 sq_7 & 0 & cq_7 cq_8 & -sq_8 & 0 \end{bmatrix}. \tag{7.26}$$

Here we have defined $\alpha_5 = -\frac{1}{a}(l_7 + b\, cq_7 + l_8 cq_8)$, $\alpha_6 = -\frac{b}{a} sq_7 sq_8$, $\alpha_7 = -\frac{b}{a} cq_8 sq_7$,

$\beta_5 = \frac{1}{a} l_8 sq_7 sq_8$, $\beta_6 = -\frac{1}{a}\left(b\, cq_8 + l_8 cq_7 + l_7 cq_7 cq_8\right)$, $\beta_7 = \frac{1}{a} sq_8\left(b + l_7 cq_7\right)$, $\gamma_5 = sq_7\left(l_8 + l_7 cq_8\right)$, $\theta_5 = l_7 + l_8 cq_8$.

For the second case, the Constrained Jacobian Matrix is found as

$$\bar{J}^B_{0a6} = \begin{bmatrix} \alpha_8 & \beta_8 & -cq_7 sq_8 & \gamma_8 & 0 & l_8 \\ \alpha_9 & \beta_9 & sq_7 & l_8 cq_7 sq_8 & \theta_8 & 0 \\ \alpha_1 0 & \beta_1 0 & cq_7 cq_8 & l_7 sq_7 sq_8 & 0 & 0 \\ -\frac{1}{a} sq_7 sq_8 & \frac{1}{a} cq_8 & 0 & -cq_7 sq_8 & cq_8 & 0 \\ -\frac{1}{a} cq_7 & 0 & 0 & sq_7 & 0 & 1 \\ \frac{1}{a} cq_8 sq_7 & \frac{1}{a} sq_8 & 0 & cq_7 cq_8 & sq_8 & 0 \end{bmatrix}. \tag{7.27}$$

Here we have defined $\alpha_8 = -\frac{b}{a}\left(cq_8 + l_8 cq_7 + l_7 cq_7 cq_8\right)$, $\alpha_9 = \frac{1}{a}\left(l_8 sq_7 sq_8\right)$, $\alpha_1 0 = -\frac{1}{a} sq_8\left(b + l_7 cq_7\right)$, $\beta_8 = -\frac{b}{a}\left(sq_7 sq_8\right)$, $\beta_9 = -\frac{1}{a}\left(l_7 + b\, cq_7 + l_8 cq_8\right)$, $\beta_1 0 =$ $fracba\left(cq_8 sq_7\right)$, $\gamma_8 = sq_7\left(l_8 + l_7 cq_8\right)$, $\theta_8 = -l_7 - l_8 cq_8$.

The determinants of the Constrained Jacobian Matrices in the two cases are found that

$$\det\left(\bar{J}^B_{0a5}\right) = \det\left(\bar{J}^B_{0a6}\right) = -\frac{b}{a^2}\left(l_7 + b\, cq_7\right). \tag{7.28}$$

and the manipulator is singular when $cq_7 = -\frac{l_7}{b}$. This configuration is illustrated in Fig. 7.6, where we can see that the axis of joint 8 at this configuration intersects with the constraint point. At this configuration we note that the axes of $\dot{q}_8$, ω^c_x, ω^c_y, and ω^c_z all intersect at the constraint point $\mathcal{F}_c$. The screws represented by these degrees of freedom are thus linearly dependent, which is the reason for the singularity. This is same type of singularity that arises in open chain manipulators with intersecting axes, as studied in Chen and Chen [1994].

A table summarizing the results found in this section is found in Table 7.1.

First joint, q_7	Second joint, q_8	Singularity
x	x	$\forall\, q_7,\ q_8$
y	y	$\forall\, q_7,\ q_8$
x	z	$q_7 = 0; \pi$
y	z	$q_7 = 0; \pi$
z	x	$\forall\, q_7,\ q_8$
z	y	$\forall\, q_7,\ q_8$
z	z	$\forall\, q_7,\ q_8$
x	y	$\cos q_7 = -\frac{l_7}{b}$
y	x	$\cos q_7 = -\frac{l_7}{b}$

Table 7.1: Summary of the results found in this section. The singularities for the different manipulator structures discussed in this paper with two joints after the constraints.

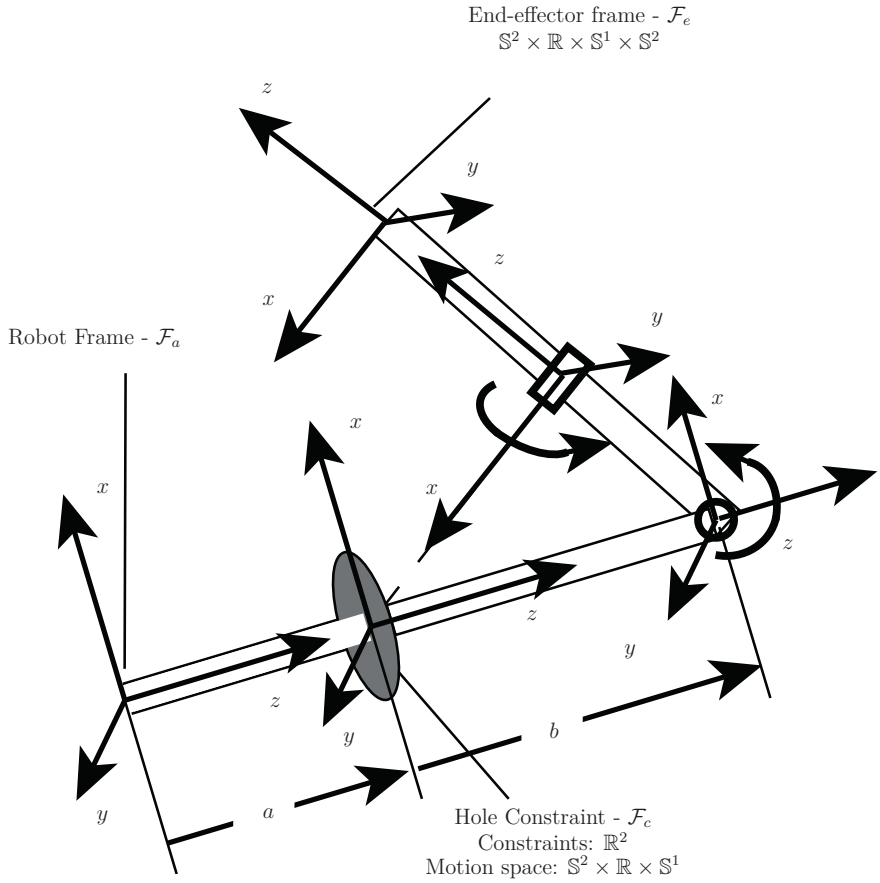

Figure 7.6: Singularity analysis of the manipulator where the first joint rotate around the y-axis and the last joint around x-axis. The manipulator is singular when the axis of joint 8 intersect with the constraint point

.

7.7 Conclusion

This paper presents a detailed analysis of the presence of singularities in open-chain manipulators with velocity constraints on a point on the chain. We find that the analysis has several similarities with the well-known analysis of open-chain manipulators without constraints, but that the geometric interpretation is rather different. We find that we need to look at the velocity space generated by the last joints after the constraint and the directions of the velocities allowed at the constraint point. Once these velocity spaces are found, the singularity analysis resembles the conventional non-constrained case in that the singularities arises in the same situations, i.e., at the limit point and when axes intersect. However, in the constrained case the analysis cannot be performed by studying the axes of the robot joints as in the standard Jacobian matrix, as this does not take the constraints into account. When constraints are present, we need to study the allowed velocities at the constraint and the velocities generated by the joints after the constraints and find how these spaces span the end-effector space.

Part III

Kinematic Analysis of Parallel Manipulators

Chapter 8

A Geometric Approach to the Design of Serial and Parallel Manipulators with Passive Joints

8.1 Abstract

The use of robotic manipulators in remote and sensitive areas calls for more robust solutions when handling joint failure, and the industry demands mathematically robust approaches to handle even the worst case scenarios. For both serial and parallel manipulators torque failure is indeed a worst case scenario. Thus, a systematic analysis of the effects of external forces on manipulators with passive joints is presented.

For serial manipulators we find under what conditions the robot is conditionally equilibrated, that is, equilibrated with respect to a specific external force. These conditions are, as expected, very restrictive. The serial, or subchain, case serves as a good platform for analysing parallel manipulators. In parallel manipulators passive joints can appear as a design choice or as a result of torque failure. In both cases a good understanding of the effects that passive joints have on the mobility and motion of the parallel manipulator is crucial. We first look at the effects that passive joints have on the mobility of the mechanism. Then, if the mobility considering passive joints only is not zero we find a condition similar to the serial case for which the parallel manipulator is conditionally equilibrated with respect to a specific external force.

8.2 Introduction

Serial and parallel robots are widely used in remote and harsh environments where humans cannot or do not want to operate. The need for a rigorous theory on what happens when joint failure occurs is thus important to be able to cope with unforeseen events such as actuation failure. This paper endeavors to convey a complete theory of the effects that passive joints have on serial and parallel manipulators when external forces are present. We start by looking at how joint failure affects the mobility of closed chain manipulators. We are interested in the undesired motion generated by the passive joints

that cannot be compensated for by the active joints. For parallel manipulators, joint failure may or may not allow a motion generated by the passive joints. If the manipulator does not allow such a passive motion, we will denote it equilibrated. In this case it can resist a wrench in an arbitrary direction either through kinematic constraints or through actuator torques. We obtain this if the manipulator, considering the passive joints only, has mobility equal to zero, i.e. we do not want the passive joints to allow any motion when the active joints are locked. If this property is satisfied the manipulator does not have an unstable singularity, following the classification in Matone and Roth [1999]. On the other hand, for serial manipulators joint failure will always result in an undesired motion if an arbitrary external force is present. In this case we investigate under what conditions, i.e. for what external forces and for what configurations, the external forces do not affect the motion of the passive joints. We will say that the manipulator is conditionally equilibrated with respect to an external force at all configurations for which the passive joints are not affected by the given force.

Many papers discussing the mobility of parallel manipulators and the relation between the active and passive joints can be found in literature. The Jacobian of the parallel manipulator is investigated in Liu et al. [1999] and Bicchi and Prattichizzo [2000] where the passive joint accelerations are found from the active joint accelerations by dividing the Jacobian into an active and a passive part. For non-overconstrained mechanisms, i.e. when there are no redundant constraints, we can find the mobility by the well known Grübler formula Murray et al. [1994]. For overconstrained mechanisms there are many approaches to determine the mobility. In Dai et al. [2006] the mobility of the mechanism is found from the constraint space. The constraints of the system are found systematically and the redundant constraints are identified. The mobility is then found by adding the degrees of freedom represented by these redundant constraints to the Grübler formula for non-overconstrained mechanisms. This approach illustrates well the effect of redundant constraints in the mechanism.

The mobility can also be found by the motion space as in Rico et al. [2003],Rico et al. [2006]. The degree of freedom of the motion of the end effector is first found. Then the degree of freedom of the self-motion manifold of each chain is added. By this approach the redundant constraints are not found directly, but this approach gives valuable in-sight into where to place redundant actuators in the mechanism.

Even though the mobility of closed chain manipulators is given a lot of attention in literature, there does not seem to be a thorough treatment of mobility in the light of joint failure. In this paper we are mainly concerned with the effects of torque failure Matone and Roth [1999], also known as free-swinging joint faults (FSJF), see English and Maciejewski [1998] and Tinós and Terra [2002], Tinós et al. [2007]. This occurs when an active joint suddenly loses its actuation and starts behaving like a passive joint. For a comprehensive treatment on how to identify joint failures see Tinós et al. [2007]. Once these are identified the appropriate control actions should be applied to minimise damage to the surroundings.

Passive joints will in general not be an intrinsic property of an open chain manipulator as this would make the manipulator collapse due to gravity or other external forces. In the case of free-swinging joint faults, however, the study of passive joints is

important also for serial manipulators in order to prevent damage from the free-swinging joint. FSJF may occur for any joint and for any configuration of the manipulator. A systematic and rigorous description is thus essential in order to find a good and fast solution and to prevent damage to the surroundings. For serial manipulators the strongest property we can obtain is that the robot is conditionally equilibrated, i.e. a set of configurations for which the manipulator is equilibrated with respect to a given external force. Passive joints in serial manipulators are treated only briefly in literature, see for example Oriolo and Nakamura [1991] and Arai and Tachi [1990], and case studies such as the Acrobot Hauser and Murray [1990].

Parallel manipulators can be designed such that all the degrees of freedom of the motion remain controllable when joint failure occurs for an arbitrary joint. This will, however, require more active joints than necessary to control the degrees of freedom of the manipulator. This actuator redundancy is in many cases undesirable due to manufacturing and maintenance costs, weight, performance, and so on. If the fault tolerance problem is not addressed in the design process it must be handled in the control of the manipulator in the case of such an occurrence. In this case the serial and parallel manipulators are treated in a similar manner and we search the configuration space of the manipulator for a set of joint positions for which the manipulator remains equilibrated for a given external force.

The approach presented in this paper is in itself very simple. First, we use Grübler's formula or a generic method based on the results in Rico et al. [2003, 2006] to verify whether the manipulator, considering the passive joints only, generates a non-trivial motion. This is based on the results found in From and Gravdahl [2008]. Then, if the passive joints of the manipulator allow a motion, we investigate what kind of motion it implements. From this we can conclude the two main results of this paper; (i) given a mechanism, with respect to what kind of external forces is the manipulator equilibrated; and (ii) given an external force, what kind of mechanism and for what configurations is the mechanism equilibrated with respect to the external force.

In Meng et al. [2007], a precise geometric theory for analysis and synthesis of sub-6 DOF manipulators was presented. The low dimensional subgroups or submanifolds of $SE(3)$ were used to represent the lower pairs, or primitive generators, while the high dimensional subgroups were used to represent the desired end-effector motion types. Given a desired end-effector motion type as a Lie subgroup or a submanifold, the synthesis problem was solved for serial and parallel manipulators. Then, from a pre-specified list of primitive generators, all possible serial and parallel arrangements of the primitive generators so that the resulting manipulator has the desired end-effector motion type were found. Using the formalism of Meng et al. [2007], we find that a mechanism is conditionally equilibrated with respect to an external force if the mechanism considering the passive joints only, is a motion generator of a motion for which the reciprocal product with the external force vanishes. Thus, while Meng et al. [2007] uses the general concept of motion type (reference frame not specified) in their definition of motion generator, we will use a motion defined in a specific coordinate frame in our definitions. This allows us to verify resistance with respect to a specific external force, as opposed to a type or class of forces.

8.3 Preliminaries

This section presents a brief overview of mathematical modelling of rigid body motion and the definition of motion type. For a detailed treatment of the topic, the reader is referred to Murray et al. [1994], Meng et al. [2007], and From et al. [2014a].

8.3.1 Rigid Body Motion

The special Euclidean group $SE(3)$ represents the configuration space of a rigid body. In addition to its group structure, $SE(3)$ is a differentiable manifold, and is what is known as a *Lie group*. $SE(3)$ as a matrix Lie group can be written by homogeneous coordinates

$$SE(3) = \left\{ \begin{bmatrix} R & p \\ 0 & 1 \end{bmatrix} \mid p \in \mathbb{R}^3, R \in SO(3) \right\} \tag{8.1}$$

where $SO(3)$ is the 3-dimensional special orthogonal group. An element $g \in SE(3)$ represents a rotation and a displacement of a rigid body relative to a reference configuration. Associated with every Lie group G is its *Lie algebra* $\mathfrak{g}$ which is defined as the tangent space of G at the identity e and is written as $\mathfrak{g} \triangleq T_eG$. The Lie algebra $se(3)$ of $SE(3)$ consists of all 4×4 matrices

$$se(3) = \begin{bmatrix} \hat{\omega} & v \\ 0 & 0 \end{bmatrix} \tag{8.2}$$

where $v \in \mathbb{R}^3$ and $\hat{\omega}$ is the skew-symmetric matrix representation of $\omega \in \mathbb{R}^3$ given by

$$\hat{\omega} = \begin{bmatrix} 0 & -\omega_3 & \omega_2 \\ \omega_3 & 0 & -\omega_1 \\ -\omega_2 & \omega_1 & 0 \end{bmatrix} \in so(3). \tag{8.3}$$

An element of $se(3)$ can be represented by the twist coordinates $\xi = \begin{bmatrix} v^\mathsf{T} & \omega^\mathsf{T} \end{bmatrix}^\mathsf{T} \in \mathbb{R}^6$ which can be identified with the twist $\hat{\xi} \in se(3)$ by the map[1]

$$\wedge : \xi = \begin{bmatrix} v \\ \omega \end{bmatrix} \in \mathbb{R}^6 \mapsto \hat{\xi} = \begin{bmatrix} \hat{\omega} & v \\ 0 & 0 \end{bmatrix} \in se(3). \tag{8.4}$$

Let Q be the configuration space of the constrained system. In our case $Q \in SE(3)$ so an element $\hat{\xi} \in se(3)$ can be represented by $\xi = \begin{bmatrix} v^\mathsf{T} & w^\mathsf{T} \end{bmatrix}^\mathsf{T}$. Then T_gQ defines the set of allowed velocities of the constrained system at g. We will write an element of the constraint forces as $F = \begin{bmatrix} f^\mathsf{T} & \tau^\mathsf{T} \end{bmatrix}^\mathsf{T}$. The set of constraint forces at g is then defined as the vanishing of the reciprocal product with ξ, i.e.

$$T_g^*Q^\perp = \{F \in \mathbb{R}^6 | \, \langle \xi, F \rangle = 0, \forall \, \xi \in T_gQ\} \tag{8.5}$$

where $\langle \xi, F \rangle = v \cdot f + \omega \cdot \tau$.

[1] For simplicity we will write twist for both twist coordinates and twists.

Denote by L_g and R_g the left and right translation maps, respectively. The differential L_{g*} of L_g defines the body velocity and the differential R_{g*} of R_g defines spatial[2] velocity of a rigid body. Then for a trajectory $g(t) \in SE(3), t \in (-\epsilon, \epsilon)$, the body velocity of the rigid body is given by

$$\hat{V}^b = L_{g(t)^{-1}} \cdot \dot{g}(t) = \begin{bmatrix} R^\mathsf{T}\dot{R} & R^\mathsf{T}\dot{p} \\ 0 & 0 \end{bmatrix} = \begin{bmatrix} \hat{\omega} & v \\ 0 & 0 \end{bmatrix} \tag{8.6}$$

while the spatial velocity is given by $\hat{V}^s = \dot{g} \cdot R_{g^{-1}}$. The body and spatial velocities are related by the Adjoint map

$$V^s = \mathrm{Ad}_g V^b \tag{8.7}$$

where $g = (R, p)$ and

$$\mathrm{Ad}_g = \begin{bmatrix} R & \hat{p}R \\ 0 & R \end{bmatrix}. \tag{8.8}$$

For a robotic mechanism with several sub-chains $j = 1...k$, we will write the twist of joint i as $\mathcal{G}_i$ and the *twist system* of chain j as

$$\overline{\mathcal{M}}_j = (\mathcal{G}_1, \mathcal{G}_2, \ldots, \mathcal{G}_n) = (\overline{\mathcal{M}}_{j1}, \overline{\mathcal{M}}_{j2}, \ldots, \overline{\mathcal{M}}_{jn}). \tag{8.9}$$

where we use the second notation $\mathcal{M}_{ji}$ when we need to clarify what chain the joints belong to in a parallel mechanism. We use the same notation for the joint positions, i.e. θ_{ji}. The twist system describes the motion of the end effector for the open chain.

Let the parallel manipulator

$$\mathcal{M} = \mathcal{M}_1 || \mathcal{M}_2 || \cdots || \mathcal{M}_k \tag{8.10}$$

consist of k serial manipulator sub-chains that share a common base and a common end effector. The set of end-effector motions is defined as Meng et al. [2007]

$$C_\mathcal{M} = C_{\mathcal{M}_1} \cap C_{\mathcal{M}_2} \cap \cdots \cap C_{\mathcal{M}_k}, \tag{8.11}$$

where $C_{\mathcal{M}_j}$ is the set of rigid transformations that the subchain $\mathcal{M}_j$ generates without loop constraints. $C_\mathcal{M}$ defines the configurations of the end effector with the loop constraints imposed.

We are interested in the *passive motion*, i.e. the motion due to the passive joints when the active joints are fixed. We denote this by

$$\mathcal{M}_P = \mathcal{M}_{P1} || \mathcal{M}_{P2} || \cdots || \mathcal{M}_{Pk} \tag{8.12}$$

where $\mathcal{M}_{Pj}$ consists of only the passive joints of chain j.

Although only the passive joints are considered, the twists of the passive joints

[2]In this context, *spatial* means that the velocity is given with respect to a globally defined coordinate system. We will also use spatial for the 3-dimensional space, as opposed to the 2-dimensional space.

depend on the configuration of the active joints. The twist of joint i is given by

$$\mathcal{G}_i' = \mathrm{Ad}_{g_{b(i-1)}} \mathcal{G}_i \tag{8.13}$$

where $g_{bi} \in SE(3)$ is the transformation from the base to joint i. We will assume it implicitly understood that the twists, as written in (8.9), are transformed according to (8.13), and thus write $\mathcal{G}$ for $\mathcal{G}'$. Similarly when we write $\mathrm{Ad}_g \overline{\mathcal{M}}$, we mean

$$\mathrm{Ad}_{g(\theta)} \overline{\mathcal{M}} := \{\mathcal{G}_1', \ldots, \mathcal{G}_n'\} = \{\mathcal{G}_1, \mathrm{Ad}_{g_{b1}} \mathcal{G}_2, \ldots, \mathrm{Ad}_{g_{b(n-1)}} \mathcal{G}_n\}. \tag{8.14}$$

8.3.2 Motion Type

We now define motion type as in Meng et al. [2007]. Motion type describes a class of motions, that is the conjugacy class of a normal form subgroup or submanifold of $SE(3)$ under the similarity transformation.

Definition 8.1. *The group of similarity transformations of $\mathbb{R}^3$, denoted $Sim^+(3)$, consists of matrices of the form*

$$\{g \cdot s_\lambda := g \begin{bmatrix} \frac{1}{\lambda} I & 0 \\ 0 & 1 \end{bmatrix} \mid g \in SE(3), \lambda > 0\} \tag{8.15}$$

Under the group of similarity transformations, helical motion with distinct pitches belong to the same conjugacy class. This is desirable in the definition of motion type as defined in Meng et al. [2007].We will need the following definition from Meng et al. [2007].

Definition 8.2. *Let $\mathcal{M}$ be a mechanism that consists of a system of coupled rigid bodies, one of which is identified with the base and one as the end-effector. Choose a reference configuration of $\mathcal{M}$ and identify the joint variables with zero. Attach a coordinate frame to the end-effector and denote by $C_\mathcal{M}$ the set of rigid motions generated (or attainable) by the end-effector relative to the reference configuration, i.e. $e \in C_\mathcal{M}$. Let Q_0 be a normal form subgroup or submanifold of $SE(3)$ and Q, the conjugacy class of Q_0 under $Sim^+(3)$. $\mathcal{M}$ is said to have the motion type (or finite motion property) of Q if there exists $g_r \in Sim^+(3)$ such that $g_r^{-1} C_\mathcal{M} g_r$ agrees with Q_0 in an open neighbourhood $U \subset SE(3)$ of e, i.e.*

$$(g_r^{-1} C_\mathcal{M} g_r) \cap U = Q_0 \cap U. \tag{8.16}$$

Equivalently we can write

$$C_\mathcal{M} \cap U = (g_r Q_0 g_r^{-1}) \cap U. \tag{8.17}$$

We are now ready to give the conditions for which serial and parallel manipulators have the motion type of Q.

Definition 8.3. *We will denote a serial manipulator $\mathcal{M}$ a* motion generator *of a subgroup or submanifold Q of $SE(3)$ if $\mathcal{M}$ contains an open neighbourhood of e in Q. If Q is*

a subgroup[3] *of* $SE(3)$*, then* $\mathcal{M}$ *is a motion generator of* Q *if there exists a configuration such that* $\overline{\mathcal{M}} = (\mathcal{G}_1, \cdots, \mathcal{G}_n) = T_eQ$.

For parallel manipulators the corresponding definition of a *Parallel Motion (PM) generator* is given by

Definition 8.4. *A parallel manipulator* $\mathcal{M} = \mathcal{M}_1 || \cdots || \mathcal{M}_k$ *is a* Parallel Motion (PM) generator *of* Q *if there exists an open neighbourhood* U *of* e *in* $SE(3)$ *such that* $C_{\mathcal{M}} \cap U = Q \cap U$*, where* $C_{\mathcal{M}} = C_{\mathcal{M}_1} \cap \cdots \cap C_{\mathcal{M}_k}$.

The conditions for which $\mathcal{M}$ is a PM generator of the subgroup Q is given in the following proposition Meng et al. [2007]:

Theorem 8.1. *Given a motion type* $Q \in SE(3)$*. Assume that each* $C_{\mathcal{M}_j}, j = 1, ..., k$ *contains a connected open subset* Q_U *of* Q *around* e*,*

$$Q_U \subseteq C_{\mathcal{M}_j}, \quad j = 1, ..., k \tag{8.18}$$

and consequently $Q_U \subseteq C_{\mathcal{M}}$*. If the following condition*

$$T_eQ = \overline{\mathcal{M}}_1 \cap \cdots \cap \overline{\mathcal{M}}_k \tag{8.19}$$

or the dual condition

$$T_e^*Q^\perp = (T_e^*C_{\mathcal{M}_1})^\perp + \cdots + (T_e^*C_{\mathcal{M}_k})^\perp \tag{8.20}$$

holds, where

$$T_e^*Q^\perp = \{ F \in \mathbb{R}^6 \Big| \langle \xi, F \rangle = 0, \forall \xi \in T_eQ \} \tag{8.21}$$

denotes the set of constraint forces for T_eQ*, then,* $\mathcal{M} = \mathcal{M}_1 || \cdots || \mathcal{M}_k$ *is a PM generator of* Q.

Proof. The proof is given in Meng et al. [2007]. □

In the setting of this paper the following is also important. If for every $g \in W$,

$$R_{g^{-1}*}T_gQ = R_{g^{-1}*}T_gC_{\mathcal{M}_{P1}} \cap \cdots \cap R_{g^{-1}*}T_gC_{\mathcal{M}_{Pk}} \tag{8.22}$$

or its dual holds, then there exists a connected open subset W of $SE(3)$ around e such that $Q_U = C_{\mathcal{M}} \cap W$, i.e. $C_{\mathcal{M}}$ agrees with Q_U in W.

Thus, alternatively we can write (8.19) in the transformed form as

$$R_{g^{-1}*}T_gQ = \mathrm{Ad}_g \overline{\mathcal{M}}_1 \cap \mathrm{Ad}_g \overline{\mathcal{M}}_2 \cap \cdots \cap \mathrm{Ad}_g \overline{\mathcal{M}}_k. \tag{8.23}$$

[3]The case when Q is a submanifold of $SE(3)$ is treated in detail in Meng et al. [2007].

8.4 Equilibrated and Conditionally Equilibrated Serial and Parallel Manipulators

A parallel manipulator for which the mobility of $\mathcal{M}_P$ is zero, can resist any external force. Specifically, we will denote a mechanism equilibrated if the following is satisfied:

Definition 8.5. *A parallel manipulator $\mathcal{M}$ is denoted* equilibrated *if $\mathcal{M}$, either through kinematic constraints or through actuator torques, can resist an arbitrary external wrench $F_{ext} = \begin{bmatrix} f^\mathsf{T} & \tau^\mathsf{T} \end{bmatrix}^\mathsf{T}$. In the case that an arbitrary wrench can be accommodated by the kinematic constraints, we will say that the manipulator is* passively sustained. *When an arbitrary wrench can be produced by the actuation torque, we will denote it* actively equilibrated.

A parallel manipulator is equilibrated with respect to an arbitrary wrench if and only if the mobility is equal to zero. To guarantee fault tolerance the mobility needs to remain zero when torque failure occurs for an arbitrary joint. This will require redundant actuators to be implemented. We note that a serial manipulator with passive joints can never be equilibrated.

When the mobility is not zero, the best result we can obtain is that the mechanism is *conditionally equilibrated* with respect to a given external wrench. This applies both to serial and parallel manipulators.

Definition 8.6. *A manipulator $\mathcal{M}$ is denoted* conditionally equilibrated *with respect to a given external wrench $F_{ext} = \begin{bmatrix} f^\mathsf{T} & \tau^\mathsf{T} \end{bmatrix}^\mathsf{T}$, if $\mathcal{M}$, either through kinematic constraints or through actuator torques, can produce a wrench opposite to F_{ext}, i.e. $\mathcal{M}$ can produce the wrench $-kF_{ext}$ for some $k > 0$.*

Note that in this case we do not require that the manipulator can resist any external wrench, only that it can produce a wrench of a given type and direction. This can for example be used to verify if a mechanism can resist forces in the direction of the gavitational forces, but not necessarily gravitational forces of an arbitrary magnitude.

We see that we will need a different definition of motion than the one given in Section 8.3. While Definition 8.2 requires the existence of some $g_r \in Sim^+(3)$, we need to check for stability of an external force in one given direction, i.e. an external disturbance fixed in one given frame. Hence, we will define *motion*, as opposed to *motion type*, as all $g_s C_\mathcal{M} g_s^{-1}$ that agree with Q_{S0} for a specific $g_s \in SE(3)$.

Definition 8.7. *Let Q_{S0} be a normal form subgroup or submanifold of $SE(3)$ and $Q_S = g_s Q_{S0} g_s^{-1}$ the homogeneous transformation of Q_{S0} for a given $g_s \in SE(3)$. $\mathcal{M}$ is said to have the* motion *of Q_S if $g_s^{-1} C_\mathcal{M} g_s$ agrees with Q_{S0} in an open neighbourhood $U \subset SE(3)$ of e, i.e.*

$$(g_s^{-1} C_\mathcal{M} g_s) \cap U = Q_{S0} \cap U \tag{8.24}$$

or equivalently

$$\begin{aligned} C_\mathcal{M} \cap U &= (g_s Q_{S0} g_s^{-1}) \cap U \\ C_\mathcal{M} \cap U &= Q_S \cap U. \end{aligned} \tag{8.25}$$

Note that Q_{S0} is a motion type while g_s determines in what coordinate frame the motion is given, i.e. the "direction" of the motion. Hence, like Q_0 in Definition 8.2, Q_{S0} is a motion type. However, while Q (in Definition 8.2) is the conjugacy class of Q_0 under $Sim^+(3)$, Q_S is a homogeneous transformation of Q_{S0} under $SE(3)$. We then get the following important result.

Definition 8.8. *A manipulator $\mathcal{M}$ is conditionally equilibrated with respect to external forces F_{ext} if and only if $\mathcal{M}_P$ is not a motion generator of any component of F_{ext}, i.e. $\mathcal{M}_P$ is a motion generator of some $Q'_S \subseteq Q_S$ where $\langle F_{ext}, Q_S \rangle = 0$. We write this as $C_{\mathcal{M}_P} \in Q_S$.*

Thus we want the mechanism $\mathcal{M}$ to generate the required motion Q and at the same time we want the passive mechanism $\mathcal{M}_P$ to generate motions that lie in Q_S. We can summarise this as follows:

To get the desired properties for a parallel manipulator, we choose $\mathcal{M}$ such that

- $\mathcal{M}$ is a motion generator of (the motion type) Q,
- $\mathcal{M}_P$ is a motion generator of (the motion) $Q'_S \subseteq Q_S$.

When joint failure occurs in a parallel mechanism we want the second property to remain true. We note that $\mathcal{M}$ includes both passive and active joints and will thus not change if torque failure occurs. $\mathcal{M}_P$, however, will change and therefore, to guarantee fault tolerance, the mobility of $\mathcal{M}_P$ must be checked against joint failure in all joints. If the manipulator allows any motion we need to look into if we can guarantee that the mechanism remains conditionally stable with respect to a given external force.

For parallel manipulators we start the analysis by finding the mobility D considering the passive joints only. If the mobility of the mechanism is zero we can conclude that the mechanism is equilibrated with respect to any external force. Mobility in the setting of fault tolerance is discussed briefly in Section 8.5, and examples are given in From and Gravdahl [2008]. On the other hand, if the mobility $D > 0$ for parallel manipulators and similarly for serial manipulators with passive joints, an additional condition needs to be satisfied for the mechanism to be equilibrated. The requirement for which $\mathcal{M}$ is conditionally equilibrated is treated in Section 8.6 for serial manipulators and Section 8.7 for parallel manipulators together with several examples.

8.5 Fault Tolerance

In this section, we look into the effect of free-swinging joint failure (FSJF), or torque failure, in parallel manipulators and in particular how the results found in From and Gravdahl [2008] can be used to prevent that the mechanism turns unequilibrated when this occurs. For a general treatment and an approach on how to identify joint failure see Tinós et al. [2007]. In this case, as the number of passive joints in the manipulator increases by one, the mobility of $\mathcal{M}_P$ may remain zero or increase by one. Let m be

the number of active joints in $\mathcal{M}$. When $\mathcal{M}_P$ does not allow any motion after the joint failure, we have

$$D_m = 0 \xRightarrow{FSJF} D_{m-1} = 0 \tag{8.26}$$

and the mechanism remains equilibrated with respect to all external forces. When $\mathcal{M}_P$ allows a 1 DOF motion as a result of the joint failure, i.e.

$$D_m = 0 \xRightarrow{FSJF} D_{m-1} = 1, \tag{8.27}$$

the mechanism is not fault tolerant. In this case the mechanism can at best be conditionally equilibrated, this is discussed in the remainder of the paper.

8.6 Robustness to external forces for serial manipulators

The results presented in Section 8.3 let us quickly verify if a given serial or parallel manipulator has the desired type of end-effector motion. We will now use the same approach to analyse if a manipulator allows an undesired motion due to passive joints. We will start with a motivating example for the serial case.

Example 1. *Consider a serial manipulator with one passive revolute joint at the end of the manipulator chain in Fig. 8.1.*

Attach a coordinate frame at the base of the manipulator and choose the reference configuration so that the revolute axis of the last joint and the y-axis of the inertial frame are parallel. Assume that the joint revolutes about the y-axis with unit velocity, i.e. $\omega_y = \begin{bmatrix} 0 & 1 & 0 \end{bmatrix}^\mathsf{T}$*, and let* $p \in \mathbb{R}^3$ *be a point on the y-axis* $p = \begin{bmatrix} p_x & p_y & p_z \end{bmatrix}^\mathsf{T}$*. Then the twist is given by*

$$\xi = \begin{bmatrix} p \times \omega_y \\ \omega_y \end{bmatrix} = \begin{bmatrix} -p_z & 0 & p_x & 0 & 1 & 0 \end{bmatrix}^\mathsf{T}. \tag{8.28}$$

Assume further two external (linear) forces

$$F_y = \begin{bmatrix} 0 & 1 & 0 & 0 & 0 & 0 \end{bmatrix}^\mathsf{T}, \quad F_z = \begin{bmatrix} 0 & 0 & 1 & 0 & 0 & 0 \end{bmatrix}^\mathsf{T}. \tag{8.29}$$

For the chosen reference configuration the set of constraint forces for the twist ξ *is given by all forces* F_ξ *that satisfy* $\langle \xi, F_\xi \rangle = 0$*, and we conclude that*

$$F_y \in F_\xi, \quad F_z \notin F_\xi. \tag{8.30}$$

Thus, for the twist describing a joint that revolutes about the y-axis and an external force F_y *the reciprocal product vanishes and the joint is not affected by the external force* F_y*. For a force in the direction of the z-axis, however, this is not the case and the configuration of the last joint is affected by this external force. We see that for a serial manipulator the set of external forces for which the passive joint maintains its posture is, as already noted, very limited.*

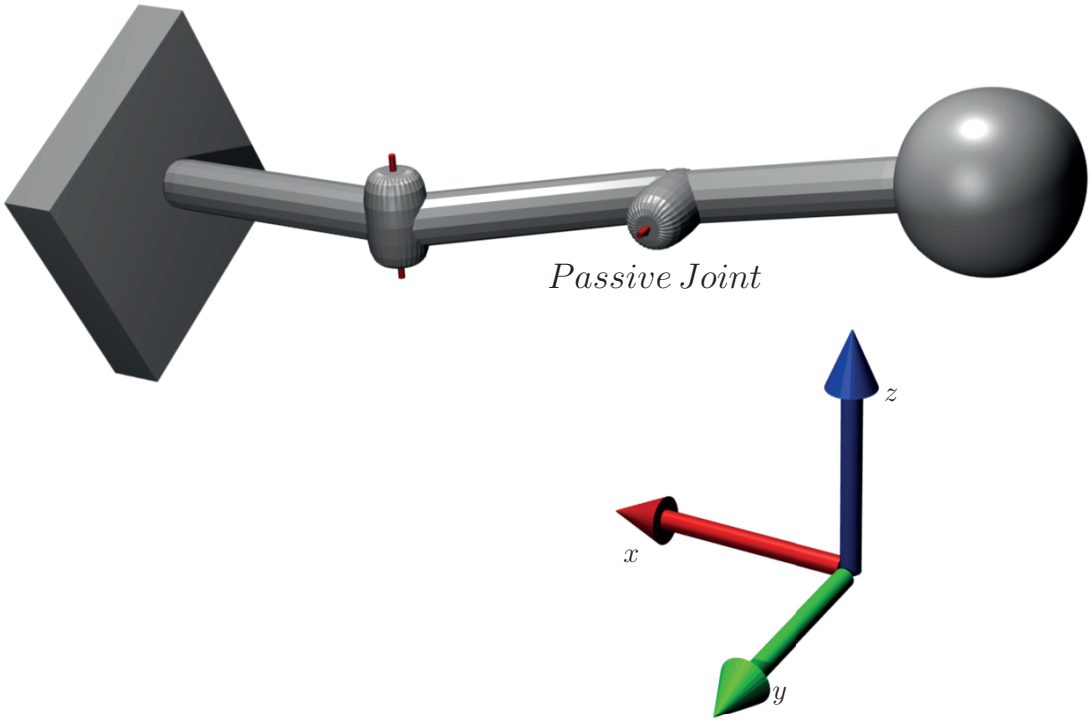

Figure 8.1: A serial manipulator with one passive revolute joint at the end of the manipulator chain.

From the simple example presented above, we see that the end-effector configuration is equilibrated with respect to one "type" or group of external forces, but not to others. We will denote the mechanism *conditionally equilibrated* when it is equilibrated with respect to a specific type of external force, e.g. gravity. In the following we will generalise this using the formalism presented in Meng et al. [2007].

We will restrict ourselves to $F_{ext} = \begin{bmatrix} f^\mathsf{T} & 0 \end{bmatrix}^\mathsf{T}$, i.e. linear forces and the moments that result from these. The extension to $F_{ext} = \begin{bmatrix} 0 & \tau^\mathsf{T} \end{bmatrix}^\mathsf{T}$ is straight forward. This is for example the case when the base moves with an angular velocity, for example ships or a moving vehicle (From et al. [2010b]).

Example 1 is special in the sense that the axis of the passive joint is constant. This is obviously not always the case, for example when the passive joint is at the end of a manipulator chain. Thus, we will divide the problem into two parts; i) when the mechanism is locally equilibrated (at reference configuration); and ii) when the mechanism is globally equilibrated (for any position of the active joints). A mechanism can be equilibrated with respect to an external disturbance for one configuration but not for another. We will start by looking at the local case and look at how external disturbances affect the mechanism at the reference configuration. In Section 8.6.2 we will extend this to the entire workspace of the manipulator.

8.6.1 A Local Solution

To analyse the manipulator when it is in the reference configuration is very much related to the work presented in Meng et al. [2007], and their results can be applied with a few simple modifications. From Example 1 we see that another definition of motion than the one given in Definition 8.2 is needed. We need to define the motion with respect to a given reference frame.

Thus, for a given external wrench, the equilibrated motion represents all the "directions" in which we can allow the manipulator to move, i.e. the directions that are not affected by the external force. This is formalised in the following.

Definition 8.9. *For a given nominal external wrench* $F_0 = \begin{bmatrix} f_0^\mathsf{T} & 0 \end{bmatrix}^\mathsf{T}$ *the* set of equilibrated motions *is defined as all twists for which the reciprocal product with* F_0 *vanishes, i.e.*

$$Q_{S0} = F_0^\perp = \{\xi \mid \langle F, \xi \rangle = 0, \forall F \in F_0\}. \tag{8.31}$$

We see that Q_{S0} gives us a complete description of all the motions the mechanism can generate and still be conditionally equilibrated with respect to the external wrench. The complete description of the equilibrated motion is then given by choosing the external wrench F_0 represented in the inertial frame, i.e. the type of the disturbance, and the coordinate frame g_s of F_0 and we write $F_{ext} = \mathrm{Ad}_{g_s} F_0$. Similarly, we get $Q_{Sg} = \mathrm{Ad}_{g_s} Q_{S0}$.

Assume now a manipulator with m joints, which of l are passive. Without loss of generality we assume that the passive joints are at the end of the manipulator chain. We denote by $\mathcal{M}_A$ the $n-l$ first active joints and by $\mathcal{M}_P$ the last l passive joints of the manipulator, so we have

$$\mathcal{M} = \mathcal{M}_A \cdot \mathcal{M}_P. \tag{8.32}$$

For a mechanism to be resistant to an external force it can only allow motions in Q_{Sg}. From this observation and the fact that active joints themselves are always equilibrated with respect to external forces, we conclude the following:

Definition 8.10. *Given* $F_{ext} = \begin{bmatrix} f^\mathsf{T} & 0 \end{bmatrix}^\mathsf{T}$ *and a corresponding equilibrated motion* Q_S*. A serial manipulator* $\mathcal{M}$ *is equilibrated with respect to external forces* F_{ext} *if and only if* $\mathcal{M}_P$ *generates a motion* $Q \subseteq Q_{Sg}$*.*

This becomes clearer with the following proposition:

Proposition 1. *Let* $\overline{\mathcal{M}}_P := \{\mathcal{G}_{P(n-l+1)}, \ldots, \mathcal{G}_{Pn}\}$ *and* $\overline{F}_{ext} = \{\mathcal{H}_{ext1}, \ldots, \mathcal{H}_{extm}\}$ *so that each* $\mathcal{G}_{Pi}$ *represents the twist of joint* i *and the* $\mathcal{H}_{extj}$*'s are* m *external forces. Then* $\mathcal{M}$ *is conditionally equilibrated with respect to* F_{ext} *if and only if*

$$\langle \mathcal{G}_{Pi}, \mathcal{H}_{extj} \rangle = 0, \quad \text{for} \begin{cases} i = (n-l+1) \ldots n, \\ j = 1 \ldots m. \end{cases} \tag{8.33}$$

This proposition states that the external force must lie in the constraint motion of each joint and that each joint can be looked at independently. We will write this on a more compact form as

$$\left\langle \overline{\mathcal{M}}_P, \overline{F}_{ext} \right\rangle = 0. \tag{8.34}$$

We will say that when Equation (8.34) is satisfied, $\mathcal{M}_P$ is conditionally equilibrated with respect to all external forces in $\overline{F}_{ext}$.

8.6.2 A Global Solution

The results presented in the previous section give a simple condition for the mechanism to be equilibrated with respect to an external force around the reference configuration. We now expand this to the entire workspace, i.e. for what positions of the active joints is the mechanism conditionally equilibrated. We start with a simple example.

Example 2. *Assume we want to check if a mechanism is equilibrated with respect to the gravitational forces, i.e.* $F_{ext} = \begin{bmatrix} 0 & 0 & 1 & 0 & 0 & 0 \end{bmatrix}^{\mathsf{T}}$. *Let the last passive joint revolute around the inertial y-axis at reference configuration Fig. 8.2.*

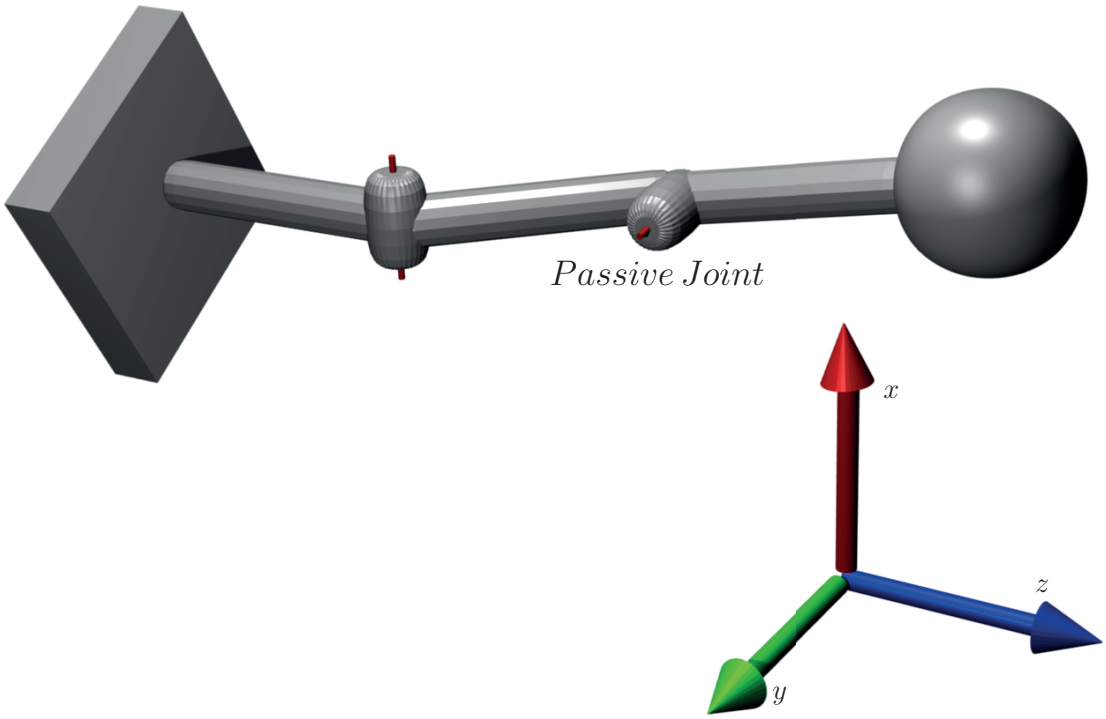

Figure 8.2: A serial manipulator with one passive revolute joint at the end of the manipulator chain.

We have

$$\xi_y = \begin{bmatrix} p \times y \\ y \end{bmatrix} = \begin{bmatrix} -p_z & 0 & p_x & 0 & 1 & 0 \end{bmatrix}^{\mathsf{T}}. \tag{8.35}$$

Then the problem amounts to finding all configurations θ *for which*

$$\langle \mathrm{Ad}_{g_\theta} \xi_y, F_{ext} \rangle = 0. \tag{8.36}$$

where

$$Ad_{g_\theta}\xi_y = \begin{bmatrix} 1 & 0 & 0 & 0 & p_{ya}s\theta - p_{za}c\theta & p_{ya}c\theta + p_{za}s\theta \\ 0 & c\theta & -s\theta & p_{za} & -p_{xa}s\theta & -p_{xa}c\theta \\ 0 & s\theta & c\theta & -p_{za} & p_{xa}c\theta & -p_{xa}s\theta \\ 0 & 0 & 0 & 1 & 0 & 0 \\ 0 & 0 & 0 & 0 & c\theta & -s\theta \\ 0 & 0 & 0 & 0 & s\theta & c\theta \end{bmatrix} \begin{bmatrix} -p_z \\ 0 \\ p_x \\ 0 \\ 1 \\ 0 \end{bmatrix}$$

$$= \begin{bmatrix} p_{ya}s\theta - p_{za}(c\theta + 1) - p_z \\ -(p_{xa} + p_x)s\theta \\ (p_{xa} + p_x)c\theta \\ 0 \\ c\theta \\ s\theta \end{bmatrix} \tag{8.37}$$

where $c\theta$ *means* $\cos(\theta)$ *and* $s\theta$ *means* $\sin(\theta)$.

The solution is obtained by a rotation $\pm\frac{\pi}{2}$ *around the* x*-axis. We see that the mechanism is equilibrated with respect to forces working in the same direction as the axis of the revolute joint only. Note in addition to these there are certain positions of the passive joint for which the external forces do not affect the configuration, such as the stable and unstable equilibrium of a pendulum, but we require that the mechanism can resist external forces for* all *positions in order to denote it conditionally equilibrated and isolated points in the configuration space are thus not included in the solution.*

For serial manipulators the formulation described can give us a restriction on the configuration of the last "active link" for the manipulator to be conditionally equilibrated. By last active link we mean the link after the last active joint. This is formalized in the following.

A transformation from the reference configuration to a joint can be given as a rigid transformation g by the Adjoint map Ad_g. We will introduce the following notation $\mathrm{Ad}_{g(\theta)}\overline{\mathcal{M}}_P$ which describes the twists of the passive joints under the influence (rigid transformation) of the active joints. Hence,

$$\mathrm{Ad}_{g(\theta)}\overline{\mathcal{M}}_P := \{\mathcal{G}'_{n-l+1}, \ldots, \mathcal{G}'_n\} = \{\mathrm{Ad}_{g_{n-l}}\mathcal{G}_{n-l+1}, \ldots, \mathrm{Ad}_{g_{n-1}}\mathcal{G}_n\} \tag{8.38}$$

where g_i is the rigid transformation from the base to joint i and thus depends on the joint positions. Further we will assume that the passive joint, if equilibrated at the reference configuration, is equilibrated for all positions of the passive joint. Note that we can only control the position of the active joints θ_A while the position of the passive joints θ_B can move freely. An example is given in the next section.

8.6.3 Free Swinging Joint Faults in Serial Manipulators

For a serial manipulator free-swinging joint fault is extremely serious and will in general cause the manipulator to collapse, or at least lose its controllability. This can cause

damage both to humans and the surroundings. In this case we will need an additional requirement on the active joint positions so that the manipulator is conditionally equilibrated.

Definition 8.11. *A serial manipulator $\mathcal{M}$ is conditionally equilibrated with respect to an external force F_{ext} (e.g gravity) if and only if the active joints θ_A are chosen such that*

$$\mathbf{\Theta} = \{\theta_A \mid \left\langle Ad_{g(\theta)}(\overline{\mathcal{M}}_P), F_{ext} \right\rangle = 0\}. \tag{8.39}$$

When joint failure occurs for any of the joints close to the base, this requirement is practically impossible to satisfy. Due to the kinematics of many commonly used manipulators such as the Motoman DIA or ABB IRB, this condition is, on the other side, quite easy to satisfy when the joint error occurs for one of the last joints. Examples of this are given below.

Example 3. *Assume a manipulator with one active and one passive revolute joint and where the passive joint is parallel to the disturbance (gravity) $F_{ext} = \begin{bmatrix} 0 & 0 & 1 & 0 & 0 & 0 \end{bmatrix}^\mathsf{T}$ at reference configuration. We have*

$$\mathcal{M} = \mathcal{M}_A \cdot \mathcal{M}_P\,, \quad \overline{\mathcal{M}} = \{\mathcal{G}_1, \mathcal{G}_2\} \tag{8.40}$$

We are to verify under what condition, i.e. for what configurations of $\mathcal{M}_A$, the mechanism remains equilibrated. We will consider two cases

- *when the active joint rotates about the z-axis Fig. 8.3,*
- *when the active joint rotates about the y-axis Fig. 8.4.*

In both cases, the twist of the passive joint is written as

$$\mathcal{G}_2 = \begin{bmatrix} p_{y_2} & -p_{x_2} & 0 & 0 & 0 & 1 \end{bmatrix}^\mathsf{T}. \tag{8.41}$$

The rotational and translational displacements due to the active joint in the two cases are given by

$$R_z = \begin{bmatrix} c\theta_1 & -s\theta_1 & 0 \\ s\theta_1 & c\theta_1 & 0 \\ 0 & 0 & 1 \end{bmatrix}, \qquad R_y = \begin{bmatrix} c\theta_1 & 0 & s\theta_1 \\ 0 & 1 & 0 \\ -s\theta_1 & 0 & c\theta_1 \end{bmatrix},$$

$$p = \begin{bmatrix} p_{x_{b1}} & p_{y_{b1}} & p_{z_{b1}} \end{bmatrix}^\mathsf{T}$$

where $c\theta$ means $\cos(\theta)$ and $s\theta$ means $\sin(\theta)$. For the first case when the active joint is parallel to the disturbance, Ad_{g_z} is given by

$$Ad_{g_z} = \begin{bmatrix} c\theta_1 & -s\theta_1 & 0 & -p_{z_{b1}}s\theta_1 & -p_{z_{b1}}c\theta_1 & p_{y_{b1}} \\ s\theta_1 & c\theta_1 & 0 & p_{z_{b1}}c\theta_1 & -p_{z_{b1}}s\theta_1 & -p_{x_{b1}} \\ 0 & 0 & 1 & p_{x_{b1}}s\theta_1 - p_{y_{b1}}c\theta_1 & p_{x_{b1}}c\theta_1 + p_{y_{b1}}s\theta_1 & 0 \\ 0 & 0 & 0 & c\theta_1 & -s\theta_1 & 0 \\ 0 & 0 & 0 & s\theta_1 & c\theta_1 & 0 \\ 0 & 0 & 0 & 0 & 0 & 1 \end{bmatrix}.$$

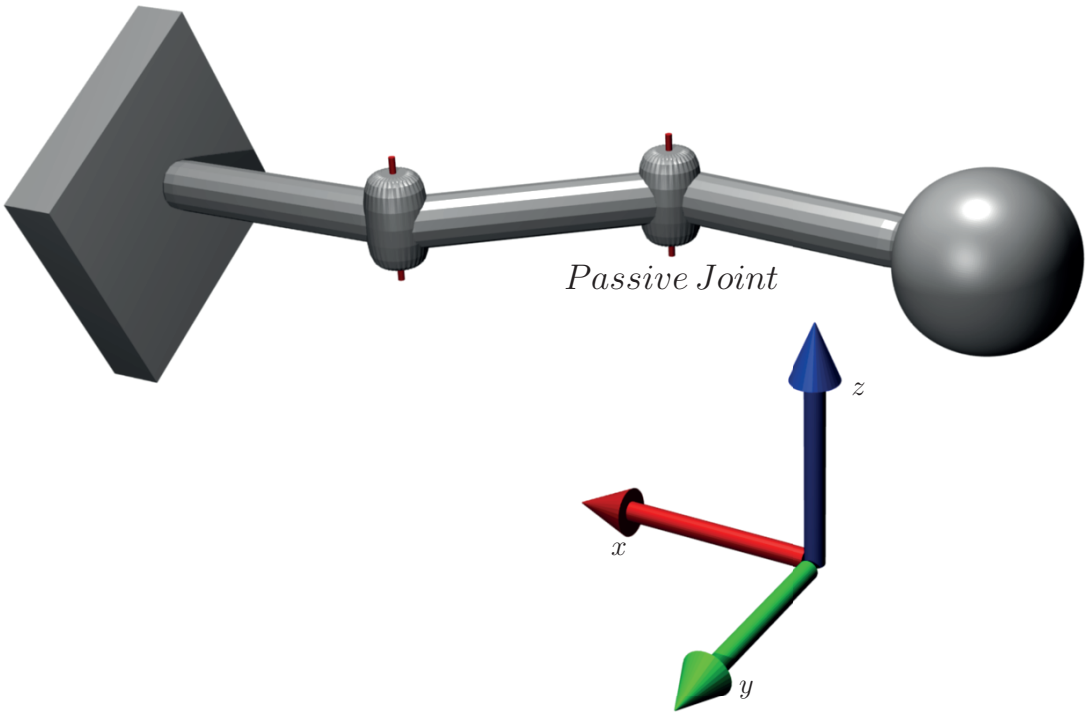

Figure 8.3: A serial manipulator with one active and one passive revolute joint.

and we get that

$$Ad_{g_z}\mathcal{G}_1 = \begin{bmatrix} p_{y_2}c\theta_1 + p_{x_2}s\theta_1 + p_{y_{b1}} \\ p_{y_2}s\theta_1 - p_{x_2}c\theta_1 - p_{x_{b1}} \\ 0 \\ 0 \\ 0 \\ 1 \end{bmatrix}. \tag{8.42}$$

As (8.39) is always satisfied, the mechanism is equilibrated for all configurations and no further action is required.

For the second case, we have

$$Ad_{g_y} = \begin{bmatrix} c\theta_1 & 0 & s\theta_1 & -p_{y_{b1}}s\theta_1 & -p_{z_{b1}} & p_{y_{b1}}c\theta_1 \\ 0 & 1 & 0 & p_{z_{b1}}c\theta_1 + p_{x_{b1}}s\theta_1 & 0 & p_{z_{b1}}s\theta_1 - p_{x_{b1}}c\theta_1 \\ -s\theta_1 & 0 & c\theta_1 & -p_{y_{b1}}c\theta_1 & p_{x_{b1}} & -p_{y_{b1}}s\theta_1 \\ 0 & 0 & 0 & c\theta_1 & 0 & s\theta_1 \\ 0 & 0 & 0 & 0 & 1 & 0 \\ 0 & 0 & 0 & -s\theta_1 & 0 & c\theta_1 \end{bmatrix}.$$

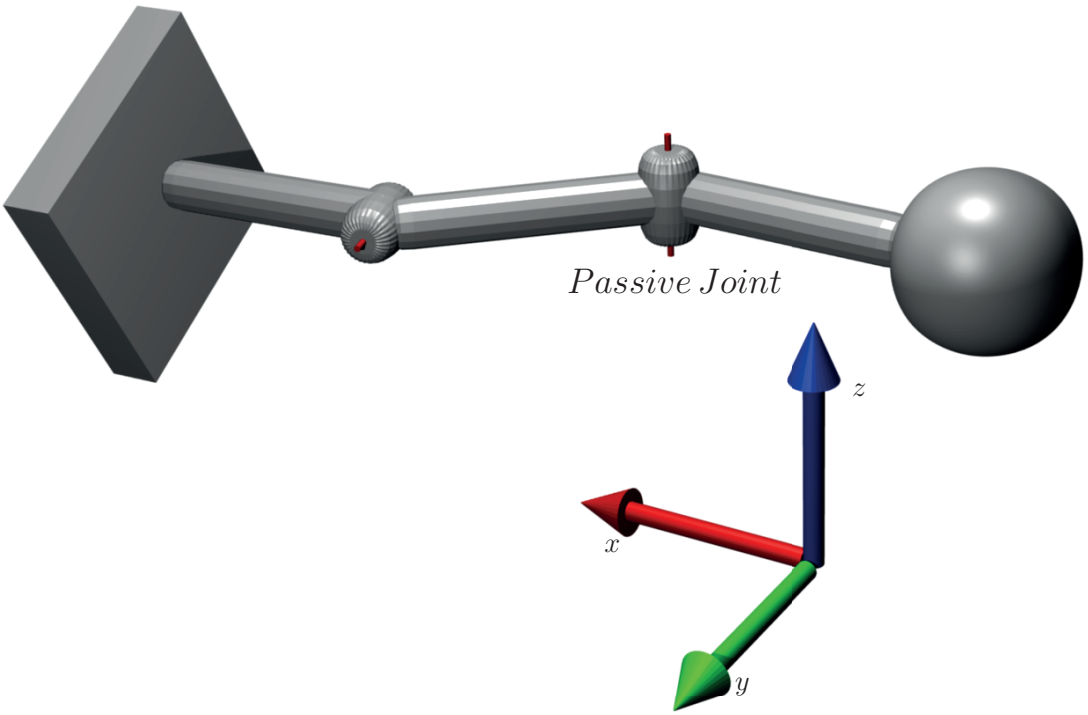

Figure 8.4: A serial manipulator with one active and one passive revolute joint.

and we get that

$$Ad_{g_y}\mathcal{G}_1 = \begin{bmatrix} (p_{y_2} + p_{y_{b1}})c\theta_1 \\ -p_{x_2} + (p_{z_{b1}}s\theta_1 - p_{x_{b1}}c\theta_1) \\ -(p_{y_2} + p_{y_{b1}})s\theta_1 \\ s\theta_1 \\ 0 \\ c\theta_1 \end{bmatrix}. \tag{8.43}$$

We see that in the second case, the manipulator is conditionally equilibrated with respect to F_{ext} if and only if

$$(p_{y_2} + p_{y_{b1}})\sin(\theta_1) = 0. \tag{8.44}$$

This is the case when $\theta_1 = 0$, which is the reference configuration and when $\theta_1 = \pm\pi$ which is when the first link points in the exact opposite direction of the reference configuration. Thus, if joint failure occurs, we should strive to reach one of the configurations represented by

$$\mathbf{\Theta}_A = \{\theta_1 = 0, \pm\pi\} \tag{8.45}$$

in order to minimise damage to the surroundings.

Example 4. *Assume a manipulator with two active (z- and y-axes in reference configuration) and one passive (z-axis) joint in Fig. 8.5.*

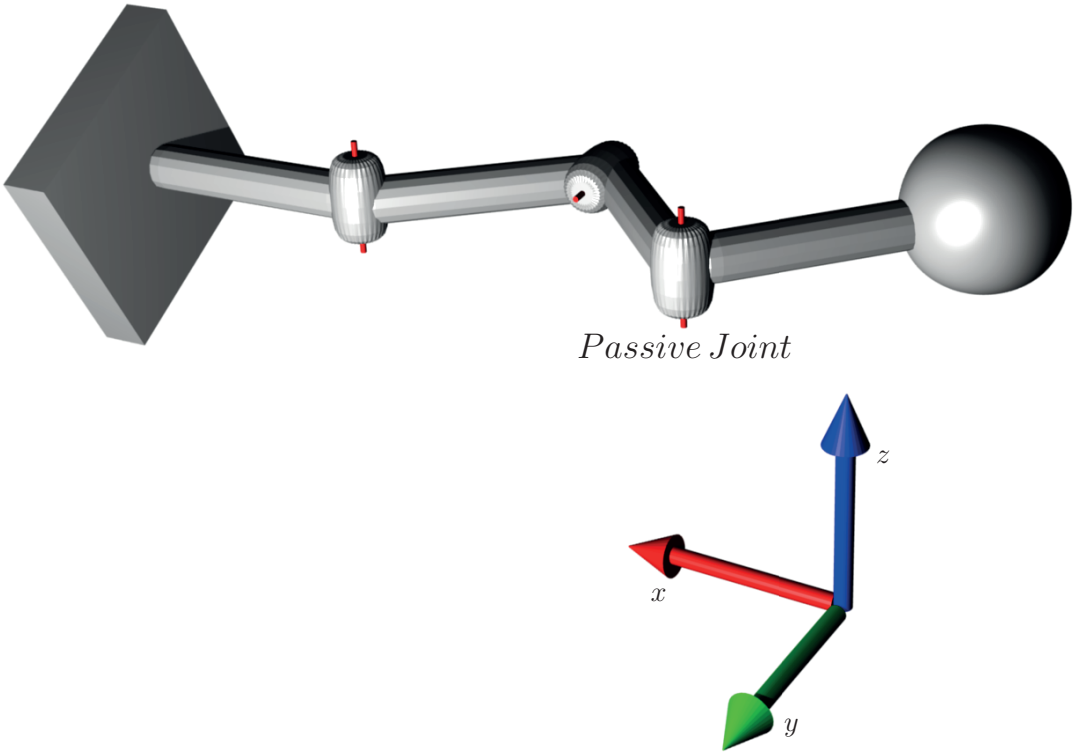

Figure 8.5: A serial manipulator with two active (z- and y-axes in reference configuration) and one passive (z-axis) joint.

In this case the set of equilibrated configurations $\mathbf{\Theta}_A = \{\theta_A \mid \left\langle Ad_{g(\theta)}(\overline{\mathcal{M}}_P), F_{ext} \right\rangle = 0\}$*, is given by*

$$\mathbf{\Theta}_A = \begin{cases} \theta_1 \text{ free,} \\ \theta_2 = 0, \pm\pi. \end{cases} \tag{8.46}$$

We see that the stability depends on the position of θ_2 *while the position of* θ_1 *can be chosen freely.*

8.7 Robustness to external forces for parallel manipulators

From From and Gravdahl [2008] and Section 8.5, we learned that when $\mathcal{M}_P$ does not allow any motion after the joint failure, i.e. we have $D_{m-1} = 0$, the mechanism is passively sustained with respect to any external force. However, when the mechanism allows a motion due to the joint failure, i.e.

$$D_m = 0 \xrightarrow{FSJF} D_{m-1} = 1, \tag{8.47}$$

an additional requirement needs to be satisfied for the mechanism to be equilibrated. In this case the mechanism cannot be equilibrated with respect to an arbitrary external force, as there will always exist a force that results in the free motion. Thus, the strongest result we can obtain in this case is to guarantee that the mechanism is passively sustained with respect to a given external force.

As for the serial case, we get that this is true when the allowed motion lies in the annihilating space of the external forces. Finally we look at the global case and find for what configurations, i.e. positions of the active joints, this is true.

8.7.1 A Local Solution

Again we start by choosing a reference configuration and identify the joint positions with zero. In this section we apply the same modifications to the results presented in Meng et al. [2007] as for serial manipulators. Recall that our definition of motion differs from the definition of motion type in Meng et al. [2007] in that Q_S relates to Q_{S0} by a (specific) homogeneous transformation and not by the conjugacy class of the similarity transformation. We need to verify if the constrained motion of the end effector $C_{\mathcal{M}_P}$ lies in the equilibrated motion Q_S. We thus assume that each $C_{\mathcal{M}_{Pj}}, j = 1, \ldots, k$ contains a connected open subset Q_U of Q_S around e,

$$Q_U \subseteq C_{\mathcal{M}_{Pj}}, j = 1, \ldots, k \tag{8.48}$$

and consequently, $Q_U \subseteq C_{\mathcal{M}_P}$. Due to the kinematic constraints, the configuration space of the end effector is forced to be

$$C_{\mathcal{M}_P} = C_{\mathcal{M}_{P1}} \cap C_{\mathcal{M}_{P2}} \cap \cdots \cap C_{\mathcal{M}_{Pk}}. \tag{8.49}$$

Recall that Q_S represents the equilibrated motions with respect to F_{ext} represented in the coordinate frame $g \in SE(3)$.

Proposition 2. *Let Q_S be the equilibrated motion with respect to F_{ext}. The parallel manipulator $\mathcal{M}$ is resistant to the external forces F_{ext} if $\overline{\mathcal{M}}_P = \overline{\mathcal{M}}_{P1} \cap \overline{\mathcal{M}}_{P2} \cap \cdots \cap \overline{\mathcal{M}}_{Pk}$ is contained in Q_S, i.e.*

$$\overline{\mathcal{M}}_P \in Q_S. \tag{8.50}$$

Alternatively we can verify that F_{ext} is contained in the constraint forces of $\mathcal{M}_P$, i.e.

$$F_{ext} \in (T_e^* C_{\mathcal{M}_{P1}})^\perp + (T_e^* C_{\mathcal{M}_{P2}})^\perp + \cdots + (T_e^* C_{\mathcal{M}_{Pk}})^\perp \tag{8.51}$$

holds, which means that every component of F_{ext} is restrained by the constraint forces of $\mathcal{M}$.

This guarantees that the end-effector motion is not affected by the external forces. Note that we also have to check for the internal motion of each chain. Hence, if joint failure occurs in chain i, we also need to verify that the internal motion of this chain is contained in Q_S.

8.7.2 A Global Solution

In this section we generalise the results from the previous section to find all configurations for which the mechanism is conditionally equilibrated with respect to a given external force. We will first assume that all the passive joints are at the end of the sub-chains

$$\mathcal{M} = \mathcal{M}_A \cdot \mathcal{M}_P. \tag{8.52}$$

Again we need to verify if the mechanism, considering the passive joints only, is equilibrated with respect to an external force F_{ext}. We denote the transformation of $\mathcal{M}_P$ by the active joints as g_A. We then need to find the set

$$\boldsymbol{G}_A = \{g_A \mid R_{g_A^{-1}*} T_{g_A} C_{\mathcal{M}_P} \in R_{g^{-1}*} T_g Q_{S0}\} \tag{8.53}$$

where

$$R_{g_A^{-1}*} T_{g_A} C_{\mathcal{M}_P} = R_{g_A^{-1}*} T_{g_A} C_{\mathcal{M}_{P1}} \cap \cdots \cap R_{g_A^{-1}*} T_{g_A} C_{\mathcal{M}_{Pk}} \tag{8.54}$$

is the attainable spatial velocities of $\mathcal{M}_P$ at g_A and $R_{g^{-1}*} T_g Q_{S0}$ is the equilibrated motion with respect to F_{ext} in a given reference frame g.

The main observation here is that the infinitesimal motions attainable by $\mathcal{M}_P$, when $\mathcal{M}_P$ is at the end of the chains, are transformed by a rigid transformation g_A which depends on the active joints only. Thus, we can write

$$\overline{\mathcal{M}}'_P = \mathrm{Ad}_{g_A} \overline{\mathcal{M}}_P \tag{8.55}$$

and we can use $\overline{\mathcal{M}}'_P$ for $\overline{\mathcal{M}}_P$ in Equation (8.50).

We will divide the motion of the mechanism into two motions. First, $C_{\mathcal{M}_P}$ is the motion due to the passive joints. This motion is affected by the external disturbances. The other motion is $C_{\mathcal{M}_A}$ which is due to the active joints. This is not affected by the external disturbance. The aim of this section is to find the configurations of the active joints so that $C_{\mathcal{M}_P} \in Q_S$.

We will write

$$\overline{\mathcal{G}}'_{ji} = \mathrm{Ad}_{g_{j,bi}} \overline{\mathcal{G}}_{ji}, \tag{8.56}$$

where $g_{j,bi}$ is the transformation from the base to joint i of chain j. In the previous sections the active joints were considered fixed. Now, the direction of the twists of the passive joints will depend on the position of the active joints, i.e. $g_{j,bi}$ depends on the position of the active joints.

We need to verify if

$$\overline{\mathcal{M}}_P \in Q_S \tag{8.57}$$

where $\overline{\mathcal{M}}_P = \overline{\mathcal{M}}_{P1} \cap \overline{\mathcal{M}}_{P2} \cap \cdots \cap \overline{\mathcal{M}}_{Pk}$ and $\overline{\mathcal{M}}_{Pj} = \{\overline{\mathcal{G}}'_{j1}, \overline{\mathcal{G}}'_{j2}, \cdots, \overline{\mathcal{G}}'_{jn_j}\}$. We will represent the set of conditionally equilibrated configurations as

$$\boldsymbol{G}_A = \{g_A \mid \overline{\mathcal{M}}_P(g(\theta)) \in Q_S\} \tag{8.58}$$

which is found by

$$\boldsymbol{G}_A = \{g_A \mid \left\langle \mathrm{Ad}_{g(\theta)}(\overline{\mathcal{M}}_P), F_{ext} \right\rangle = 0\} \tag{8.59}$$

which is the set of all equilibrated configurations for $\mathcal{M}$.

8.7.3 Free Swinging Joint Faults in Parallel Manipulators

Free swinging joint faults affect parallel manipulators differently than serial manipulators. For serial manipulators joint faults is extremely serious while this is not always the case for closed chain manipulators due to the kinematic constraints. In this section we present several examples illustrating the effects of torque failure in parallel mechanisms.

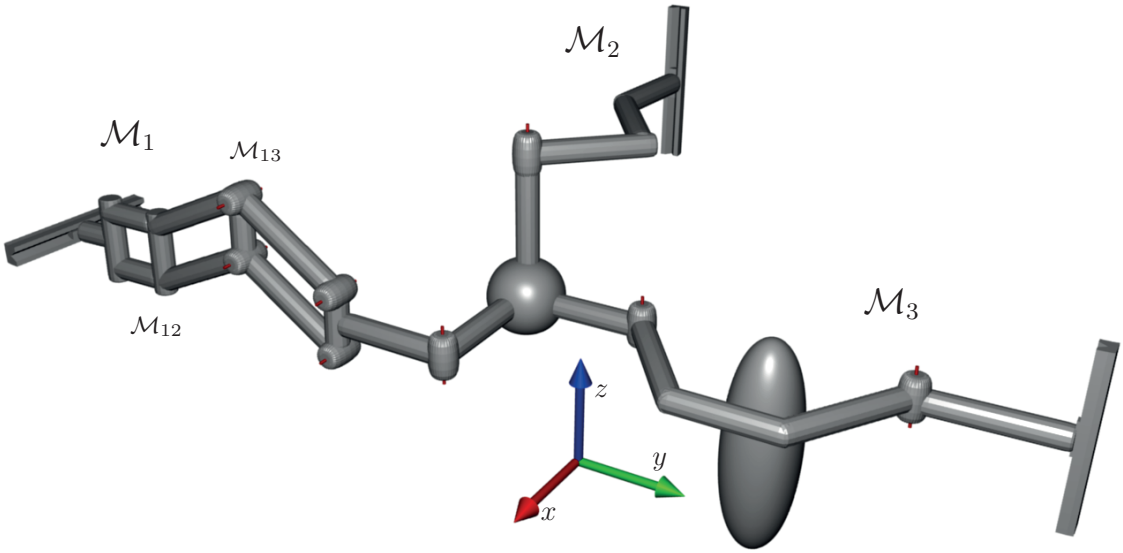

Figure 8.6: Trivial Linkage of Type I. Bad choice of active joints. If joint failure occurs in joint $\mathcal{M}_{12}$, the mechanism is no longer equilibrated with respect to forces in the direction of the z-axis, such as gravitational forces. Joints $\mathcal{M}_{12}$ and $\mathcal{M}_{13}$ are parallelogram joints that generate motion in S^1.

Consider the parallel manipulator in Fig. 8.6. We consider two cases when joint failure occurs in $\mathcal{M}_{12}$;

- the actuated joints are chosen as in Fig. 8.6,
- the actuated joints are chosen as in Fig. 8.6 but with $\mathcal{M}_{21}$ actuated instead of $\mathcal{M}_{33}$.

Example 5. *Assume that the actuated joints are chosen as in Fig. 8.6 and joint failure occurs in $\mathcal{M}_{12}$. We choose a reference configuration as in Fig. 8.6 and the twists of each chain is given by*

$$\begin{aligned}
\overline{\mathcal{M}}_{P1} &= \left\{ \begin{bmatrix} v_x \\ 0 \end{bmatrix}, \begin{bmatrix} p_{12} \times w_x \\ 0 \end{bmatrix}, \begin{bmatrix} p_{13} \times w_x \\ 0 \end{bmatrix}, \begin{bmatrix} p_{14} \times w_z \\ w_z \end{bmatrix} \right\}, \\
\overline{\mathcal{M}}_{P2} &= \left\{ \begin{bmatrix} v_z \\ 0 \end{bmatrix}, \begin{bmatrix} 0 \\ w_z \end{bmatrix} \right\}, \\
\overline{\mathcal{M}}_{P3} &= \left\{ \begin{bmatrix} v_z \\ 0 \end{bmatrix}, \begin{bmatrix} p_{32} \times w_z \\ w_z \end{bmatrix}, \begin{bmatrix} p_{35} \times w_z \\ w_z \end{bmatrix} \right\}.
\end{aligned} \tag{8.60}$$

and we get

$$\overline{\mathcal{M}}_P = \overline{\mathcal{M}}_{P1} \cap \overline{\mathcal{M}}_{P2} \cap \overline{\mathcal{M}}_{P3} = \begin{bmatrix} v_z \\ 0 \end{bmatrix}. \tag{8.61}$$

Thus for the chosen reference configuration, $\mathcal{M}_P$ is not conditionally equilibrated with respect to the gravitational forces. It is, however, conditionally equilibrated with respect to all forces in the xy-plane, e.g.

$$\left\langle \overline{\mathcal{M}}_P, \overline{F}_z \right\rangle \neq 0,$$
$$\left\langle \overline{\mathcal{M}}_P, \overline{F}_y \right\rangle = 0,$$

We now look into for what configurations this is true. This is straight forward due to the observation

$$\overline{\mathcal{M}}_{Pij} = \mathrm{Ad}_{g_{j,bi}(\theta)} \overline{\mathcal{M}}_{Pij}\,, \forall i, j, \theta \tag{8.62}$$

and thus the twists of the passive joints are independent of positions of the active joints. The set of joint positions for which the manipulator is conditionally equilibrated with respect to F_y is thus given by

$$\mathbf{\Theta}_{F_y} = \{\theta \mid \left\langle Ad_{g(\theta)}(\overline{\mathcal{M}}_P), F_y \right\rangle = 0\} = \{\forall\, \theta\} \tag{8.63}$$

Similarly, the set of joint positions for which the manipulator is conditionally equilibrated with respect to F_z is thus given by

$$\mathbf{\Theta}_{F_z} = \{\theta \mid \left\langle Ad_{g(\theta)}(\overline{\mathcal{M}}_P), F_z \right\rangle = 0\} = \{\emptyset\} \tag{8.64}$$

Example 6. *Again we assume that the actuated joints are chosen as in Fig. 8.6 and joint failure occurs in $\mathcal{M}_{12}$, but with $\mathcal{M}_{21}$ actuated instead of $\mathcal{M}_{33}$. We choose a reference configuration as in Fig. 8.6 and the twists of each chain is given by*

$$\begin{aligned}
\overline{\mathcal{M}}_{P1} &= \left\{ \begin{bmatrix} v_x \\ 0 \end{bmatrix}, \begin{bmatrix} p_{12} \times w_x \\ 0 \end{bmatrix}, \begin{bmatrix} p_{13} \times w_x \\ 0 \end{bmatrix}, \begin{bmatrix} p_{14} \times w_z \\ w_z \end{bmatrix} \right\}, \\
\overline{\mathcal{M}}_{P2} &= \left\{ \begin{bmatrix} 0 \\ w_z \end{bmatrix} \right\}, \\
\overline{\mathcal{M}}_{P3} &= \left\{ \begin{bmatrix} v_z \\ 0 \end{bmatrix}, \begin{bmatrix} p_{32} \times w_z \\ w_z \end{bmatrix}, \begin{bmatrix} p_{33} \times w_z \\ w_z \end{bmatrix}, \begin{bmatrix} p_{35} \times w_z \\ w_z \end{bmatrix} \right\}.
\end{aligned} \tag{8.65}$$

and we get

$$\overline{\mathcal{M}}_P = \overline{\mathcal{M}}_{P1} \cap \overline{\mathcal{M}}_{P2} \cap \overline{\mathcal{M}}_{P3} = \begin{bmatrix} 0 \\ w_z \end{bmatrix}. \tag{8.66}$$

Thus for the chosen reference configuration, $\mathcal{M}_P$ is conditionally equilibrated with respect to the gravitational forces only, e.g.

$$\left\langle \overline{\mathcal{M}}_P, \overline{F}_z \right\rangle = 0,$$
$$\left\langle \overline{\mathcal{M}}_P, \overline{F}_y \right\rangle \neq 0.$$

We now look into for what configurations this is true. Again we have that Equation (8.62) is true and that the twists of the passive joints are independent of positions of the active joints. The set of joint positions for which the manipulator is conditionally equilibrated with respect to F_z is thus given by

$$\mathbf{\Theta}_{F_z} = \{\theta \mid \left\langle Ad_{g(\theta)}(\overline{\mathcal{M}}_P), F_z \right\rangle = 0\} = \{\forall\, \theta\} \tag{8.67}$$

Similarly, the set of joint positions for which the manipulator is conditionally equilibrated with respect to F_y is thus given by

$$\mathbf{\Theta}_{F_y} = \{\theta \mid \left\langle Ad_{g(\theta)}(\overline{\mathcal{M}}_P), F_y \right\rangle = 0\} = \{\emptyset\} \tag{8.68}$$

This example illustrates the difference between the effects of joint failure in serial and parallel manipulators. For serial manipulators we can often take the manipulator to a certain configuration for which it is conditionally equilibrated. For parallel manipulators, however, we find that this requirement is either satisfied for all configurations, as in (8.67), or it is not satisfied at all, as in (8.68). Thus, if the parallel mechanism is conditionally equilibrated, this is an intrinsic property of the mechanical design and only in very special cases can it be taken care of in the control. For serial manipulators, however, the design of the manipulator does affect the condition to a certain extent, but we have more freedom to deal with external disturbances in the control when joint failure occurs.

8.8 Conclusion

A mathematically rigorous framework for analysing the effects of joint failure in serial and parallel manipulators is presented. For serial manipulators we find that for certain configurations the manipulator remains conditionally equilibrated with respect to a specific external force, such as gravity, even after joint failure occurs. This must thus be handled in the control algorithms as there is no way to guarantee fault tolerance through a fault tolerant design of the mechanism.

For parallel manipulators, however, we can find a set of active joints for which the design itself is fault tolerant. In this sense, the parallel manipulators are more robust than their serial counterparts. On the other hand, when actuator failure occurs and this allows for a motion in the passive joints, we have less flexibility to deal with this in the control algorithms than for serial manipulators. In general we find that the parallel manipulator is either conditionally equilibrated for all configurations, or it is never conditionally equilibrated. Fault tolerance of parallel manipulators should thus be addressed in the design of the mechanism.

Part IV

Agricultural Robots

Chapter 9

Initial field-testing of Thorvald, a versatile robotic platform for agricultural applications

9.1 Abstract

Much effort has been put into developing robotic systems for the agricultural domain that are able to perform specific tasks such as yield estimation, phenotyping, sampling, precise application of pesticides, and so on. Some robots have also been developed for more energy-demanding tasks such as seeding, but little work has been done to make more versatile systems that are able to perform tasks of great variety in energy demand, required precision, operation speed, etc. In this paper we present a novel robotic platform capable of performing both the energy-demanding tasks previously performed by heavy tractors, and in addition the more precise around-the-clock operations normally identified with agricultural robotics. We present results from a field experiment on seeding patterns and densities, and from field-tests done in cooperation with researchers working in phenotyping of cereals. We also show that the robot is well suited for monitoring tasks, and that we can obtain valuable information about the condition of the plants and weed by a standard camera and simple image analysis.

9.2 Introduction

In agricultural robotics, effort is often put into developing task-specific robots. That is, robots that are custom built to solve one specific task in the field, like mechanical weeding, crop scouting or applying herbicides by precision spraying. There are many impressive robots and concepts, but most are not designed with exchangeable tools and energy demanding tasks in mind. There are some exceptions to this though, such as Robotti by Kongskilde (Green et al. [2014]); a tracked robot which can be fitted with multiple implements. Robotti's effective traction capability is 10 hp, and it has a mass of less than 500 kg.

It is our belief that the farmer will not replace his or her tractors with robots, partially

or completely, if it does not make sense economically. Robotic solutions are generally expensive, and will probably continue to be so in the foreseeable future. Independently of the task to be performed, they need to be equipped with advanced sensory systems such as RTK GNSS, LIDAR and cameras that represent a substantial cost increase. One way to make robotic solution more economically viable, is to make them more versatile. We believe strongly in developing robotic systems that are able to perform several different tasks, and in this way represent an added value to the farmer, both economically and in increased life quality, and to the consumer, in improved food quality and lower prices.

Another important aspect in this setting is the fact that heavy machinery damages the soil by causing soil compaction (Nawaz et al. [2013], Batey [2009]). Blackmore et al. [2007] estimates that as much as 80-90 % of the energy input in the field may be eliminated by using lightweight machines. This is why efforts should be put into designing complete solutions based on lightweight robots that are capable of solving all required tasks, from seeding to harvesting, eliminating heavy machines from as much of the field as possible.

Robots that are to perform energy-demanding tasks in the field need to be constructed differently from robots that are merely made for collecting data. Even though some robots that are able to perform several different tasks are presented in literature, they are normally not capable of performing a wide variety of tasks. Robots that are constructed for monitoring are generally not powerful enough or the center of mass is too high for them to perform energy-demanding tasks in the soil. One example of such a robot is the BoniRob (Ruckelshausen et al. [2009], Bangert et al. [2013]), which can be fitted with several different tools for monitoring, data collection, and other tasks that are not too energy-demanding.

On the other end of the scale, we have large and heavy robots, or autonomous tractors for that sake, powerful enough to perform any task, but lack the benefits represented by the lightweight robots. Examples of such robots are the APU module (Oksanen [2015]) and the Spirit autonomous tractor (atc).

We present *Thorvald*, a novel robotic platform that is powerful enough to perform energy-demanding operation in the soil, and at the same time has the beneficial properties of lightweight, autonomous robots. The Thorvald platform was designed and built at the Norwegian University of Life Sciences. It has a low center of gravity, and a total mass of approx. 150 kg. It uses four 600 W brushless motors connected via toothed belts to in-wheel gearboxes for propulsion, which is believed to sufficient to perform the most critical tasks in the field. Even though the robot itself is lightweight, the tools that are attached to the robot will add the necessary weight to perform each task. Thus, for monitoring and surveillance, the robot is sufficiently light weight not to damage the plants and the soil and to maintain a long operation time, while for more energy-demanding tasks, such as seeding, the seeding tool will add the necessary weight to obtain the required traction and stability.

The robot has individual steering motors for each wheel, which makes it highly maneuverable, and the frame members and frame joints are made somewhat flexible to ensure that all wheels will remain in contact with the ground, even in rough terrain.

Table 9.1: Thorvald Key Specifications

Drive power	4 x 600 W
Battery	48 V, 30 Ah, LiFePO4 (capacity can be doubled if needed)
Mass	$\sim$ 150 kg
Payload	200 kg
Ground clerance	59 cm

Figure 9.1: The Thorvald platform. Attached is an early prototype of a precision seeding tool.

This is critical for traction, which is especially important on Norwegian farms, where the fields often are uneven and hilly. The flexible frame design was chosen as it is lighter, less expensive and less complex than traditional suspension systems.

Thorvald has a waterproof on-board computer from Small PC, which runs ROS (Robotic Operating System) on Linux Ubuntu. A heavy-duty, weather-proof, high brightness touch screen from Small PC has been installed for easy operation together with an emergency stop button. The steering motors from JVL have built in motor controllers while the four propulsion motors are connected to two dual channel motor controllers from Roboteq. All motor controllers are connected to, and communicate with the on-board computer via a CANopen network. Table 9.1 lists the robot's key specifications. The Thorvald platform is depicted in Fig. 9.1.

We are currently developing our own precision seeder as described in Grimstad et al. [2015a], which distributes the seeds evenly across the field in a hexagonal circle packing pattern. This paper presents results from a small experiment conducted in connection with the development of this tool.

The robot is equipped with all sensors required for reliable, autonomous navigation, and different tools, or implements, are attached within the robot frame according to the task that is to be performed. The tool is installed by backing the robot towards the tool until the tool is within the robot frame. The tool will then connect to the frame

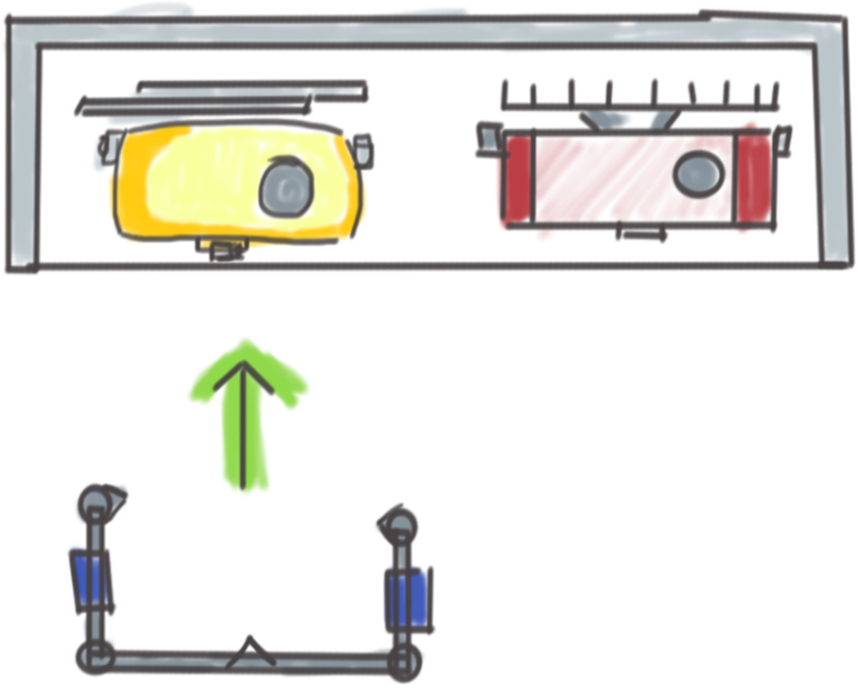

Figure 9.2: Thorvald is designed to be used with multiple implements

at three different points, as shown in Fig. 9.2. Currently the tool is fastened manually, but inn the future this will be done automatically.

We wish to show that with our simple design, we are able to perform both energy-demanding tasks and also the monitoring and information gathering part using the same robot.

The reader should note that we do not intend to plow the field, as plowing is highly energy demanding, and leaves the soil vulnerable to the elements, which in turns leads to soil erosion. Instead we wish to use no-till practices. By not plowing, there will be an increased problem with weeds. It is our belief that this problem can be reduced by seeding in a more uniform pattern, and by developing precision weeding tools to be used together with the robotic platform.

An important part of robotic farming is data collection. Modern technology allows us to do work in the field on a single-plant level, as opposed to treating all plants in a field or sub-field in the same way. The Thorvald platform will therefore be equipped with sensors for crop scouting, and the robot is currently being tested by researchers working in cereal phenotyping.

The paper is organized as follows: In Section 9.3 we discuss the effect of different seeding patterns and seeding densities, while Section 9.4 addresses crop scouting. Section 9.5 presents results from a small experiment on seeding patterns conducted at our research farm, and Section 9.6 results from field-tests conducted in cooperation with plant researchers.

9.3 Precision Seeding

Conventional seeding places seeds in rows, with short spacing within the row, and considerably larger spacing between rows. This means that inter-row weeds are free to develop while the crop is competing against itself within the rows (Fig. 9.3a). The reason the seeds are placed in this way has to do with the way the machinery works (i.e., what is most easily obtained mechanically), and not what is ideal for growth and weed suppression. Studies show that seeds that are placed in a more uniform pattern (Fig. 9.3b) are more capable of suppressing weeds, which can be directly translated into increased yield. For example, in Weiner et al. [2001b,a] it is shown that the advantages of initial size in competition among individual plants is highly favorable to the crops and that weed is considerably more suppressed when the crop density is increased and the crop is uniformly distributed in the field, as opposed to rows. Heege [2013] presents a detailed discussion on the effects of row distances from a more mechanical point of view. More resent studies show the same effects on crops normally sown with lower densities, such as maize (Marín and Weiner [2014]).

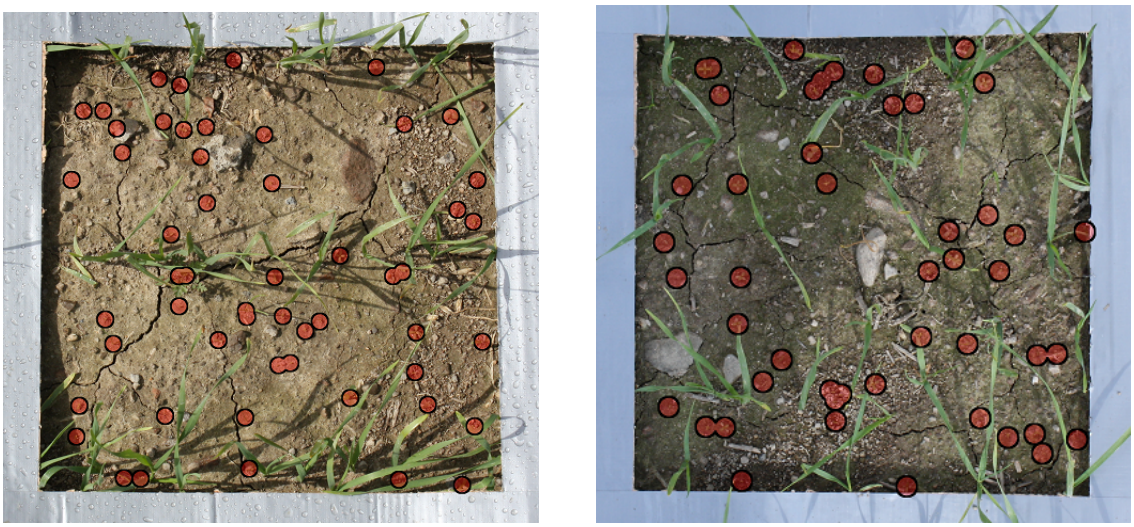

(a) Row. (b) Evenly destributed.

Figure 9.3: With conventional row seeding, weeds (red circles) are free to develop undisturbed by the crop.

Based on the the strong indications found in literature showing that crops can substantially gain from a more uniformly distributed seeding pattern, especially under high weed pressure and asymmetry, we believe there is a lot to gain from developing seeding tools that are able to place the seeds more uniformly and accurately. We are currently working on several different approaches that allow us to place seeds in this way. The main advantage, as we see it, is that by using a robot that is substantially cheaper than existing tractor-based systems, and therefore can be scaled up in numbers and not in size, and also allows for 24 hour operation, we can develop systems with less pressure on productivity (per unit) and speed. This allows for far more accurate seeding machines that are able to accurately place the seeds in a required pattern.

The first step of this process is to get a better understanding of what is the ideal

Figure 9.4: Thorvald with an early precision seeding tool prototype

density and pattern for different kinds of crops under different weed pressure. By distributing the seeds more evenly across the field, each plant will have more room to develop in all directions, not just on each side of a dense row. The plant will then be able to collect more sunlight, and of course take sunlight from slower developing plants such as most weeds. We study the effects of changing the seeding pattern in Section 9.5.

The seeder being developed for Thorvald, seeds in an hexagonal pattern. An early prototype is currently being tested with the robot (Fig. 9.4). Based on the results from the experiment described in this paper, the seeder will be modified to place seeds in the optimal pattern, and the experiments will be repeated on a larger field and under different conditions, such a weed pressure, soil structure, fertilization practices, etc.

9.4 Monitoring

An ongoing project is to enable the robot to be used for crop scouting. A downward facing camera has therefore been mounted on the robot (Fig. 9.5). The camera is connected to the on-board computer via USB. A 2D laser scanner has been acquired. This will make the robot able to measure crop height and other parameters related to crop health, and also enable the robot to identify weed, calculate plant coverage and so on. All data collected will be tagged with position using the on-board RTK-GNSS system, which is also to be used for navigation.

Fig. 9.6 shows early results from a test plot seeded with a hexagonal circle packing pattern. Image processing software, ImageJ Rasband [1997-2014] is used to separate the green plants form the surrounding ground (color thresholds in the HSB color space, no other filters are applied). Today plant coverage is often measured just by visual inspection, so the requirements for accuracy are not particularly high. With this dense pattern, we see that approx. 37 % of the ground is covered by the plants. Here the

Figure 9.5: Thorvald is taking pictures in the field

plants are still at an early stage, as the picture was captured only 16 days after seeding.

In the future we also wish to extend the robots sensor systems to include a pH-meter for measuring soil pH. If the pH gets too low, the yield will be affected in a negative manner. For best results, pH should be measured continuously and on site (Pansu and Gautheyrou [2007]). Measuring the pH across the field, will then allow us to apply the correct amount of lime where this is needed, and keep the entire field within the acceptable pH level.

9.5 Seeding Experiment

To investigate the benefits of seeding in a more uniform pattern, simple tools for seeding (by hand) was designed and 3D printed. Some of the tools are depicted in Fig. 9.7. The tools were made so that each seed would be placed at 3 cm depth with the correct spacing to neighboring seeds. Spring wheat was then seeded by hand in three different patterns using these tools:

1. Row: 12.5 cm between rows with 2 cm seed spacing (400 seeds/m^2)

2. Hexagonal circle packing pattern: 5.0 cm seed spacing (462 seeds/m^2)

3. Hexagonal circle packing pattern: 2.5 cm seed spacing (1848 seeds/m^2)

Fig. 9.8 shows examples of row and hexagonal patterns. For pattern 1 and 2, 1.5 m x 1.5 m squares were seeded. Because of the high number of seeds required for pattern 3, a smaller area was used for this plot.

Pattern 3 turned out to be difficult to seed with the aforementioned hand seeding tool, and the resulting plant pattern, although uniform, did not fully resemble the targeted hexagonal pattern.

Figure 9.6: Hexagonal pattern with 2.5 cm seed spacing (pattern 3), with plant coverage of approx. 37 %. Picture with and without highlighted plants.

Two months after seeding, four 25x25 cm squares were randomly selected for each seeding pattern, and the heights of wheat plants and weeds were measured. We also counted the number of wheat plants and weeds in each case. The results were as follows:

- The 2 cm row pattern had the highest plants, with average wheat height of 55 cm and average weed height of 11 cm.
- The uniform 5 cm pattern had medium sized plants, with average wheat height of 48 cm and average weed height of 7.4 cm.
- The uniform pattern with 2.5 cm spacing had the smallest weeds size and a sub-

Table 9.2: Number of crop and weed in a 25x25 cm area for the different sowing patterns

Pattern	Crop	Weed	Crop-weed ratio
Row, 2 cm	21	45	0.47
Uniform, 5 cm	30	47	0.64
Uniform, 2.5 cm	92	30	3.1

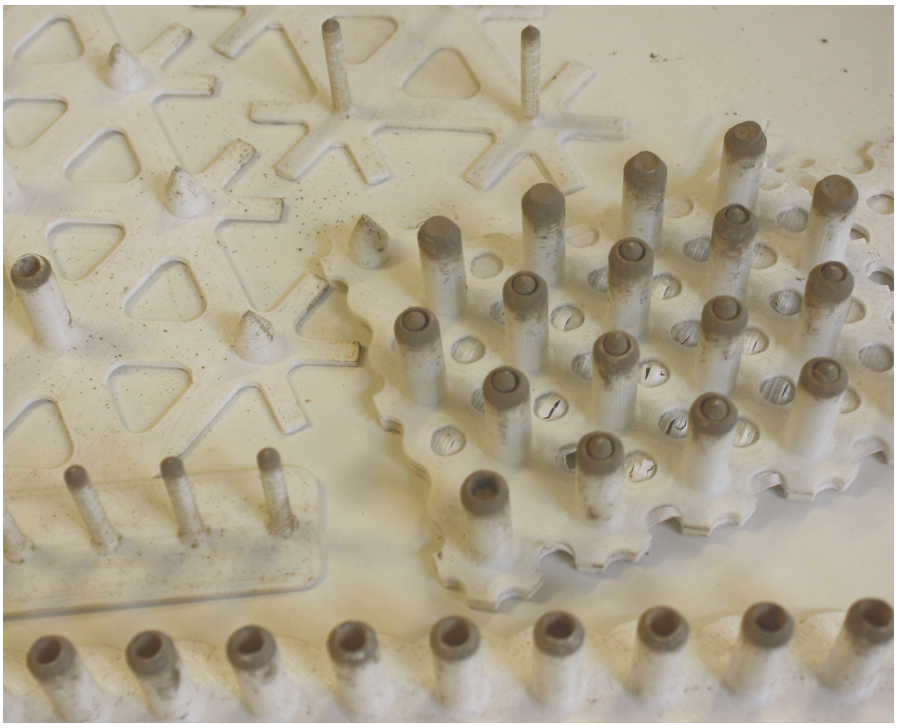

Figure 9.7: Tools used for seeding in different patterns

stantially better crop-weed ratio compared to the other plots, but it also had the smallest wheat plants.

Fig. 9.9 and 9.10 compare the wheat height and weed height of the 2 cm row pattern and the 5 cm uniform pattern in more detail, as these have approximately the same seed density. From the figures we see that the wheat plants are somewhat higher for the row pattern, but for the weed the relative difference in size is considerably larger with an average size of about 11 cm for the row pattern and 7.4 cm for the uniform pattern. This is a strong indication that the uniform pattern is better than rows when it comes to suppressing weeds. However, it is not possible to draw a conclusion that this advantage in weed suppression translates in an advantage in growing conditions for the crop. Further experiments with larger test areas and where the plant density for

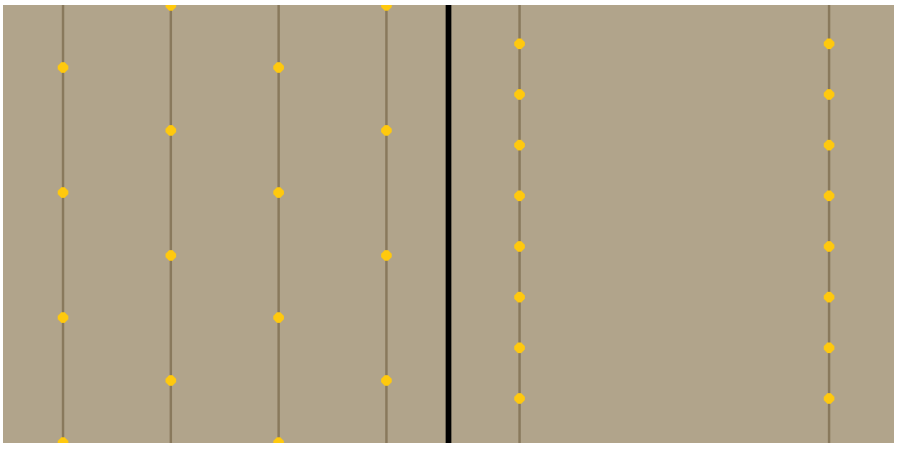

Figure 9.8: Hexagonal (left) and row seeding pattern

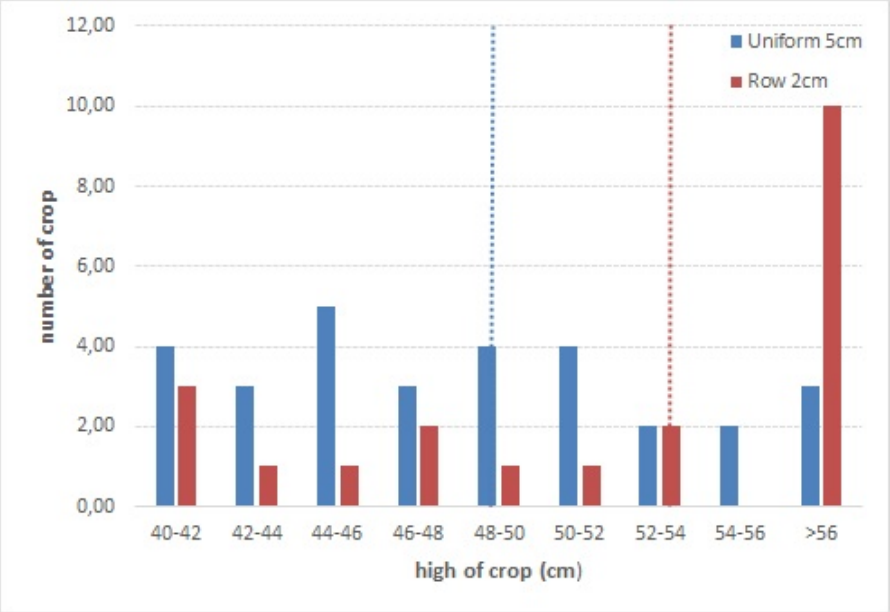

Figure 9.9: Wheat size in 25x25 cm area of 2 cm row, and 5 cm uniform patterns. The dotted lines show the average heights.

the different patterns are equal are needed to conclude on this. The number of crop plants and weeds is shown in Table 9.2. We see that the crop-weed ratio is better for the uniform patterns.

9.6 Field-Tests

In order to identify requirements for the aforementioned crop scouting system, Thorvald has been used in cooperation with researchers working with phenotyping of cereals. During these tests, the robot was teleoperated, taking pictures with the on-board camera at different locations in the test fields. Fig. 9.11 shows pictures that have been captured by the robot in the field for an experiment on seeding density and fertilization. The pictures are used to estimate the plant coverage.

The feedback regarding the robot's performance was mainly positive, but as the researchers who used it are working with cereal, they found it to be somewhat low. During the tests the plants were still young and the robot was able to drive over the crop without any danger of harming the plants, but the researchers also require the robot to be able to drive over fully grown crops. Fully grown crops are about 1 m high, and can in some cases reach heights of 1.5 m.

As Thorvald is designed to be used on farms, and not by plant researchers, a low center of gravity is more important than the ability to drive over fully grown cereal crops. The robot's ground clearance is similar to what one finds on a regular tractor, and it will be able to perform scouting and weed control tasks until the crop has grown to a size where it prevents sunlight from reaching the ground, and thus stops new weeds from developing.

The researchers also found the wheel modules to be a bit wide. Again the concern

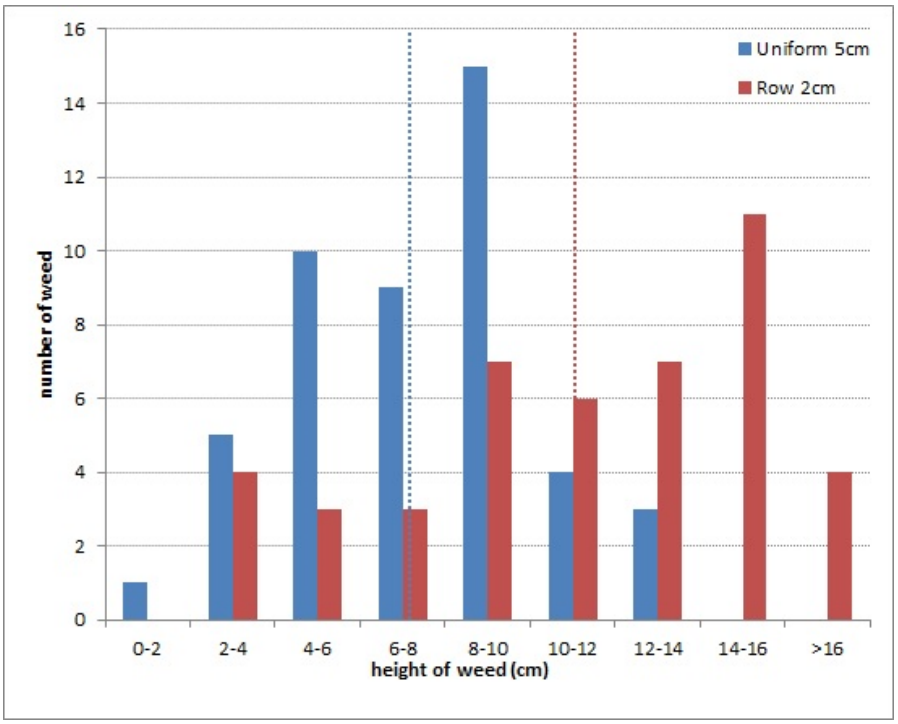

Figure 9.10: Weed size in 25x25 cm area of 2 cm row, 5 cm and uniform patterns. The dotted lines show the average heights.

was that plants could get damaged. This is an issue we will address, and improvements to the design will be made.

As for the maneuverability and traction, the robot performed better than expected. It drives up steep slopes with ease and have good traction capabilities on a range of different surfaces. In rough terrain, all four wheels maintain contact with the ground, and the robot did not get stuck once during the tests.

Thorvald is frequently out in the field to test algorithms as well as the mechanical design of the platform and the tools. It is also recording data to be used in the development of new tools and systems, e.g. recording video of cereal crops to be used as reference when developing algorithms for weed identification. The development of the Thorvald platform will continue during the fall and winter of 2015/2016, and more extensive field-tests will be carried out in the spring and summer of 2016.

9.7 Conclusion

The Thorvald project aims to develop a lightweight robot that is capable of performing all tasks in the field, also the energy demanding ones. Thus, we have constructed a powerful robot with low mass and a low center of gravity. The latter of these properties also renders it unsuited for phenotyping of cereal, as the robot is too low. However, Thorvald has a ground clearance similar to what one can find on a normal tractor, and we therefore believe the height to be adequate for the average farmer.

The results from our small experiment on seeding patterns suggest that it may be beneficial to seed in a uniform pattern as opposed to seeding in rows, as the experiments

Figure 9.11: Images captured by Thorvald's on-board camera

show that a uniform seeding pattern can suppress weed more efficiently. It is, however, not possible to draw any conclusions from the experiments whether this advantage in weed suppression translates into improved growing conditions for the crop. Large-scale experiments need to be carried out to confirm, and better quantify the potential gain by utilizing the proposed seeding patterns.

The first field-tests of the Thorvald platform show promising results. The mechanical design, maneuverability and traction capabilities are shown to be as expected and in some cases somewhat better than expected.

References

Autonomous tractor corporation. http://www.autonomoustractor.com/index.html.

A. Abbati-Marescotti, C. Bonivento, and C. Melchiorri. On the invariance of the hybrid position/force control. *J. Intell. Robot. Syst.*, 3(4):233–250, 1990. ISSN 0921-0296.

J.A. Adams and H. Kaymaz-Keskinpala. Analysis of perceived workload when using a pda for mobile robot teleoperation. In *Proceedings of IEEE International Conference on Robotics and Automation*, volume 4, pages 4128–4133 Vol.4, April 2004. doi: 10.1109/ROBOT.2004.1308919.

N. Aghakhani, M. Geravand, N. Shahriari, M. Vendittelli, and G. Oriolo. Task control with remote center of motion constraint for minimally invasive robotic surgery. In *Proc. IEEE Int. Conf. on Rob. and Aut.*, pages 5807–5812, Karlsruhe, Germany, 6-10 May 2013.

V. H. Andaluz, L. Salinas, F. Roberti, J. M. Toibero, and R. Carelli. Switching control signal for bilateral tele-operation of a mobile manipulator. In *Control and Automation (ICCA), 2011 9th IEEE International Conference on*, pages 778–783, 2011.

J. Angeles. *Rational Kinematics*. Springer Tracts in Natural Philosophy. Springer New York, 1989. ISBN 9780387968131. URL https://books.google.no/books?id=2TIwUAqQu-IC.

H. Arai and S Tachi. Dynamic control of a manipulator with passive joints - position control experiments by a prototype manipulator. *IEEE/RSJ International Conference on Intelligent Robots and Systems, Ibaraki, Japan*, pages 935–940, 1990.

H. Azimian, R. V. Patel, and M. D. Naish. On constrained manipulation in robotics-assisted minimally invasive surgery. In *Proc. of the Int. Conf. on Biomedical Robotics and Biomechatronics (BioRob)*, pages 650–655, Tokyo, Japan, 26-29 Sep. 2010.

Thomas Bak and Hans Jakobsen. Agricultural robotic platform with four wheel steering for weed detection. *Biosystems Engineering*, 87(2):125 – 136, 2004. ISSN 1537-5110. doi: http://dx.doi.org/10.1016/j.biosystemseng.2003.10.009. URL http://www.sciencedirect.com/science/article/pii/S153751100300196X.

Tijmen Bakker, Kees Asselt van, Jan Bontsema, Joachim Müller, and Gerrit Straten van. Systematic design of an autonomous platform for robotic weeding. *Journal of Terramechanics*, 47(2):63 – 73, 2010. ISSN 0022-4898. doi: http://dx.doi.org/10.1016/j.

jterra.2009.06.002. URL http://www.sciencedirect.com/science/article/pii/S0022489809000858.

W Bangert, A Kielhorn, F Rahe, A Albert, P Biber, S Grzonka, S Haug, A Michaels, D Mentrup, M Hänsel, et al. Field-robot-based agriculture: "remotefarming. 1" and "bonirob-apps". In *71th conference LAND. TECHNIK-AgEng 2013*, pages 439–446, 2013.

T Batey. Soil compaction and soil management–a review. *Soil use and management*, 25 (4):335–345, 2009.

Antonio Bicchi and Domenico Prattichizzo. Manipulability of cooperating robots with unactuated joints and closed-chain mechanisms. *IEEE Transaction of Robotics and Automation*, 16(4):336–345, 2000.

B.S. Blackmore, H.W. Griepentrog, S. Fountas, and T.A. Gemtos. A specification for an autonomous crop production mechanization system. *Agricultural Engineering International: the CIGR Ejournal*, 2007.

R. Boudreau and R. P. Podhorodeski. Singularity analysis of a kinematically simple class of 7-jointed revolute manipulators. *Transactions of the Canadian Society for Mechanical Engineering*, 34(1):105–117, 2010.

H. Bruyninckx and J. De Schutter. Specification of force-controlled actions in the "task frame formalism"-a synthesis. *IEEE Trans. Robot.*, 12(4):581 –589, aug 1996. ISSN 1042-296X.

J. Canny. *The Complexity of Robot Motion Planning*. Acm Doctoral Dissertation Awards, 1987. Mit Press, 1988. ISBN 9780262031363.

Guimin Chen, Shouyin Zhang, and Geng Li. Multistable behaviors of compliant sarrus mechanisms. *Journal of Mechanisms and Robotics*, 5(2):021005–021005, 2013. ISSN 1942-4302. doi: 10.1115/1.4023557. URL http://dx.doi.org/10.1115/1.4023557. 10.1115/1.4023557.

Y. C. Chen and C. L. P. Chen. An analysis to the singularity of serial manipulators using the theory of reciprocal screw. In *Systems, Man, and Cybernetics, 1994. Humans, Information and Technology., 1994 IEEE International Conference on*, volume 1, pages 148–153 vol.1, Oct 1994. doi: 10.1109/ICSMC.1994.399827.

P. Chiacchio and M. Concilio. The dynamic manipulability ellipsoid for redundant manipulators. In *Proceedings. 1998 IEEE International Conference on Robotics and Automation*, volume 1, pages 95–100 vol.1, 1998.

P. Chiacchio, S. Chiaverini, L. Sciavicco, and B. Siciliano. Influence of gravity on the manipulability ellipsoid for robot arms. *Journal of Dynamic Systems Measurement and Control*, 114(4):723–727, 1992.

J. H. Cho, P. J. From, M. Annerstedt, A. Robertsson, , and R. Johansson. Design of an intermediate layer to enhance operator awareness and safety in telesurgical systems. *Proceedings of IEEE/RSJ International Conference on Intelligent Robots and Systems, Vilamoura, Portugal*, 2012.

J. J. Craig and M. H. Raibert. A systematic method of hybrid position/force control of a manipulator. In *Proc. COMPSAC '79*, pages 446 – 451, 1979.

Jian S. Dai, Zhen Huang, and Harvey Lipkin. Mobility of overconstrained parallel mechanisms. *Transactions of ASME*, 128(1):220–229, 2006.

A. Deal, D. L. Chow, and W Newman. Hybrid natural admittance control for laparoscopic surgery. In *Proc. IEEE/RSJ Int. Conf. Intel. Rob. and Syst.*, pages 127–1283, Vilamoura, Portugal, 7-12 Oct. 2012.

Vincent Duindam. Port-based modeling and control for efficient bipedal walking robots. 2006.

J. D. English and A. A. Maciejewski. Fault tolerance for kinematically redundant manipulators: Anticipating free-swinging joint failures. *IEEE Transactions of Robotics and Automation*, 14(4):566–575, 1998.

I. Farkhatdinov and Ryu Jee-Hwan. Switching of control signals in teleoperation systems: Formalization and application. In *Advanced Intelligent Mechatronics, 2008. AIM 2008. IEEE/ASME International Conference on*, pages 353–358, 2008.

I. Farkhatdinov, Ryu Jee-Hwan, and J. Poduraev. A feasibility study of time-domain passivity approach for bilateral teleoperation of mobile manipulator. In *Control, Automation and Systems, 2008. ICCAS 2008. International Conference on*, pages 272–277, 2008.

M. Franken, S. Stramigioli, S. Misra, C. Secchi, and A. Macchelli. Bilateral telemanipulation with time delays: A two-layer approach combining passivity and transparency. *Robotics, IEEE Transactions on*, 27(4):741–756, 2011.

P. J. From. On the kinematics of robotic-assisted minimally invasive surgery. *Modeling, Identification and Control*, 34(2):69–82, 2013a.

P. J. From. On the Kinematics of Robotic-assisted Minimally Invasive Surgery. *Modeling, Identification and Control*, 34(2):69–82, 2013b. doi: 10.4173/mic.2013.2.3.

P. J. From and J. T. Gravdahl. On the mobility and fault tolerance of closed chain manipulators with passive joints. *Modeling, Identification and Control*, 29(4):151–165, 2008.

P. J. From, V. Duindam, K. Y. Pettersen, J. T. Gravdahl, and S. Sastry. Singularity-free dynamic equations of vehicle-manipulator systems. *Simulation Modelling Practice and Theory*, 18(6):712–731, 2010a.

P. J. From, J. T. Gravdahl, and P Abbeel. On the influence of ship motion prediction accuracy on motion planning and control of robotic manipulators on seaborne platforms. *Proceedings of International Conference of Robotics and Automation, Anchorage, Alaska, USA*, 2010b.

P. J. From, K. Y. Pettersen, and J. T. Gravdahl. *Vehicle-manipulator systems - modeling for simulation, analysis, and control*. Springer Verlag, London, UK, 2014a.

Pål Johan From, Cong Dung Pham, and Jan Tommy Gravdahl. Fault tolerance of parallel manipulators with passive joints. In *Proceedings in Applied Mathematics and Mechanics*, 2014b.

J. Funda, R. H. Taylor, B. Eldridge, S. Gomory, and K.G. Gruben. Constrained Cartesian motion control for teleoperated surgical robots. *IEEE Tran. on Rob. and Aut.*, 12(3):453–465, 1996. ISSN 1042-296X.

G.D. Glosser and W.S. Newman. The implementation of a natural admittance controller on an industrial manipulator. In *Proc. IEEE Int. Conf. on Rob. and Aut.*, pages 1209–1215, San Diego, USA, 8-13 May 1994.

Paula Gomes. Surgical robotics: Reviewing the past, analysing the present, imagining the future. *Robotics and Computer-Integrated Manufacturing*, 27(2):261 – 266, 2011. ISSN 0736-5845. doi: http://dx.doi.org/10.1016/j.rcim.2010.06.009. URL `http://www.sciencedirect.com/science/article/pii/S0736584510000608`. Translational Research – Where Engineering Meets Medicine.

Michael A Goodrich and Alan C Schultz. Human-robot interaction: a survey. *Foundations and trends in human-computer interaction*, 1(3):203–275, 2007.

Michael A Goodrich, Erwin R Boer, Jacob W Crandall, Robert W Ricks, and Morgan L Quigley. Behavioral entropy in human-robot interaction. Technical report, DTIC Document, 2004.

C. Gosselin and J. Angeles. Singularity analysis of closed-loop kinematic chains. *Robotics and Automation, IEEE Transactions on*, 6(3):281–290, Jun 1990. ISSN 1042-296X. doi: 10.1109/70.56660.

C. Grane and P. Bengtsson. Menu selection with a rotary device founded on haptic and/or graphic information. In *Eurohaptics Conference, 2005 and Symposium on Haptic Interfaces for Virtual Environment and Teleoperator Systems, 2005. World Haptics 2005. First Joint*, pages 475–476, March 2005.

Ole Green, T. Schmidt, R. Pietrzkowski, K Jensen, M. Larsen, G. Edwards, and R. Jørgensen. Commercial autonomous agricultural platform - kongskilde robotti. *Second International Conference on Robotics and associated High-technologies and Equipment for Agriculture and Forestry*, 2014.

L. Grimstad, C. D. Pham, H. T. Phan, and P. J. From. On the design of a low-cost, light-weight, and highly versatile agricultural robot. In *IEEE Workshop on Advanced Robotics and its Social Impacts (ARSO 2015)*, 2015a.

L. Grimstad, H. N. T. Phan, C. D. Pham, and P. J. From. Initial field-testing of thorvald, a versatile robotic platform for agricultural applications. In *IROS Workshop on Agri-Food Robotics: dealing with natural variability*. IEEE, 2015b.

Lars Grimstad, Cong Dung Pham, Huynh Nhat Trinh Phan, and Pål Johan From. On the design of a low-cost, light-weight, and highly versatile agricultural robot. In *IEEE International Workshop on Advanced Robotics and its Social Impacts*, 2015c.

G.S. Guthart and J.K. Salisbury Jr. The intuitive^{TM} telesurgery system: overview and application. In *Proc. IEEE Int. Conf. Rob. Aut.*, pages 618–621, 2000.

B. Hannaford. A design framework for teleoperators with kinesthetic feedback. *Robotics and Automation, IEEE Transactions on*, 5(4):426–434, 1989.

F. Hao and J. M. McCarthy. Conditions for line-based singularities in spatial platform manipulators. *Journal of Robotic Systems*, 15(1):43–55, 1998.

J. Hauser and R. M. Murray. Nonlinear controllers for non-integrable systems: the acrobot example. *American Control Conference, San Diego, CA, USA*, pages 669–671, 1990.

HermannJ. Heege. Site-specific sowing. In Hermann J. Heege, editor, *Precision in Crop Farming*, pages 171–192. Springer Netherlands, 2013. ISBN 978-94-007-6759-1.

Peter F. Hokayem and Mark W. Spong. Bilateral teleoperation: An historical survey. *Automatica*, 42(12):2035–2057, 2006.

Ryu Jee-Hwan, Kwon Dong-Soo, and B. Hannaford. Stable teleoperation with time-domain passivity control. *Robotics and Automation, IEEE Transactions on*, 20(2): 365–373, 2004a.

Ryu Jee-Hwan, Kim Yoon Sang, and B. Hannaford. Sampled- and continuous-time passivity and stability of virtual environments. *Robotics, IEEE Transactions on*, 20 (4):772–776, 2004b.

K. Jensen, S. H. Nielsen, A. Boegild, O.J. Jørgensen, N.J. Jacobsen, C.L. Jaeger-Hansen, and R.N. Jørgensen. A low cost modular robotics tool carrier for precision agriculture research. In *11th International Conference on Precision Agriculture*, July 2012.

R. N. Jørgensen, C. G. Sørensen, J. Maagaard, I. Havn, K. Jensen, H. T. Søgaard, and L. B. Sørensen. Hortibot: A system design of a robotic tool carrier for high-tech plant nursing. *Agricultural Engineering International: the CIGR Ejournal*, IX, 2007.

David B Kaber, Emrah Onal, and Mica R Endsley. Design of automation for telerobots and the effect on performance, operator situation awareness, and subjective workload. *Human Factors and Ergonomics in Manufacturing*, 10(4):409–430, 2000a.

David B Kaber, Jennifer M Riley, Rong Zhou, and John Draper. Effects of visual interface design, and control mode and latency on performance, telepresence and workload in a teleoperation task. In *Proceedings of the Human Factors and Ergonomics Society Annual Meeting*, volume 44, pages 503–506. SAGE Publications, 2000b.

Ankur Kapoor, Ming Li, and R.H. Taylor. Constrained control for surgical assistant robots. In *Proc. IEEE Int. Conf. on Rob. and Aut.*, pages 231–236, Orlando, FL, USA, 15-19 May 2006.

O. Khatib. Real-time obstacle avoidance for manipulators and mobile robots. *Int. J. Robot. Res.*, 5(1):90–98, 1986.

Andrey Kiselev and Amy Loutfi. Using a mental workload index as a measure of usability of a user interface for social robotic telepresence. In *Workshop in Social Robotics Telepresence*, 2012.

A. Lasnier and T. Murakami. Hybrid sensorless bilateral teleoperation of two-wheel mobile manipulator with underactuated joint. In *Advanced Intelligent Mechatronics (AIM), 2010 IEEE/ASME International Conference on*, pages 347–352, 2010.

J. C. Latombe. *ROBOT MOTION PLANNING.: Edition en anglais.* The Springer International Series in Engineering and Computer Science. Springer, 1991. ISBN 9780792391296.

S.M. LaValle. *Planning Algorithms.* Cambridge University Press, 2006. ISBN 9780521862059.

J. Lenarčič and C. Galletti. Kinematics and modelling of a system for robotic surgery. In *On Advances in Robot Kinematics.* Springer, 2004. ISBN 9781402022487.

M. Li, A. Kapoor, and R. H. Taylor. A constrained optimization approach to virtual fixtures. In *Proc. IEEE/RSJ Int. Conf. on Intel. Rob. and Syst.*, pages 1408–1413, Edmonton, Alberta, Canada, 2-6 Aug. 2005.

H. Lipkin and J. Duffy. Hybrid twist and wrench control for a robotic manipulator. *Trans. ASME J. Mech. Transm. Autom. Des.*, 110:138–144, 1988.

Y. H. Liu, Y. Xu, and M. Bergerman. Cooperation control of multiple manipulators with passive joints. *IEEE Transactions on Robotics and Automation*, 15(2):258–267, 1999.

R. C. O. Locke and R. V. Patel. Optimal remote center-of-motion location for robotics-assisted minimally-invasive surgery. In *Proc. IEEE Int. Conf. on Rob. and Aut.*, pages 1900–1905, Roma, Italy, 10-14 Apr. 2007.

T. Lozano-Perez. Spatial planning: A configuration space approach. *Computers, IEEE Transactions on*, C-32(2):108–120, 1983. ISSN 0018-9340.

AA Maciejewski and V Balakrishnan. Undetected locked-joint failures in kinematically redundant manipulators: A workspace analysis. In *Intelligent Robots and Systems, 1998. Proceedings., 1998 IEEE/RSJ International Conference on*, volume 1, pages 317–322. IEEE, 1998.

Anthony A Maciejewski and Charles A Klein. Obstacle avoidance for kinematically redundant manipulators in dynamically varying environments. *The international journal of robotics research*, 4(3):109–117, 1985.

C Marín and J Weiner. Effects of density and sowing pattern on weed suppression and grain yield in three varieties of maize under high weed pressure. *Weed Research*, 54 (5):467–474, 2014. ISSN 1365-3180.

M. M. Marinho, M. C. Bernardes, and A. P. L. Bo. A programmable remote center-of-motion controller for minimally invasive surgery using the dual quaternion framework. In *Proc. of the Int. Conf. on Biomedical Robotics and Biomechatronics (BioRob)*, pages 339–344, Sao Paulo, Brazil, 12-15 Aug. 2014.

Matthew T Mason. Compliance and force control for computer controlled manipulators. *IEEE Transactions on Systems, Man and Cybernetics*, 11(6):418–432, 1981.

R. Matone and B. Roth. In-parallel manipulators: A framework on how to model actuation schemes and a study of their effects on singular postures. *Transaction of ASME*, 121(1):2–8, 1999.

Constantinos Mavroidis and Bernard Roth. Analysis and synthesis of overconstrained mechanisms. In *Proceedings of the 1994 ASME Design Technical Conferences, DE-70, Minneapolis, MI, ASME, New York, NY*, pages 115–133, 1994.

H. Mayer, I. Nagy, and A. Knoll. Kinematics and modelling of a system for robotic surgery. In J. Lenarčič and C. Galletti, editors, *On Advances in Robot Kinematics*, pages 181–190. Springer Netherlands, Dordrecht, Netherlands, 2004.

Jian Meng, Guanfeng Liu, and Zexiang Li. A geometric theory for analysis and synthesis of sub-6 DoF parallel manipulators. *IEEE Transactions on robotics*, 23(4):625–649, 2007.

J.P. Merlet. *Parallel Robots*. Solid Mechanics and Its Applications. Springer Netherlands, 2012. ISBN 9789401095877. URL `https://books.google.no/books?id=GydrCQAAQBAJ`.

R. M. Murray, Z. Li, and S. S. Sastry. *A Mathematical Introduction to Robotic Manipulation*. CRC Press, Boca Raton, FL, USA, 1994. ISBN 0-8493-7981-4.

Y. Nakamura. *Advanced robotics: redundancy and optimization*. Addison-Wesley series in electrical and computer engineering: Control engineering. Addison-Wesley Longman, Incorporated, Boston, MA, USA, 1991. ISBN 9780201151985.

Y. Nakamura and H. Hanafusa. Inverse kinematics solutions with singularity robustness for robot manipulator control. *ASME Journal of Dynamic Systems, Measurement, and Control*, 108:163–171, 1986.

Yoshihiko Nakamura, Hideo Hanafusa, and Tsuneo Yoshikawa. Task-priority based redundancy control of robot manipulators. *The International Journal of Robotics Research*, 6(2):3–15, 1987.

C. Natale. *Interaction Control of Robot Manipulators: Six-degrees-of-freedom Tasks*. Springer Tracts in Advanced Robotics. Springer, 2003. ISBN 9783540001591.

MuhammadFarrakh Nawaz, Guilhem Bourrié, and Fabienne Trolard. Soil compaction impact and modelling. a review. *Agronomy for Sustainable Development*, 33(2):291–309, 2013.

S.Y. Nof. *Handbook of Industrial Robotics*. Number v. 1 in Electrical and electronic engineering. Wiley, 1999. ISBN 9780471177838. URL `https://books.google.no/books?id=7od4alFKfNMC`.

C. ODunlaing and C. K. Yap. A "retraction" method for planning the motion of a disc. *Journal of Algorithms*, 6(1):104 – 111, 1985. ISSN 0196-6774.

Timo Oksanen. Accuracy and performance experiences of four wheel steered autonomous agricultural tractor in sowing operation. In Luis Mejias, Peter Corke, and Jonathan Roberts, editors, *Field and Service Robotics*, volume 105 of *Springer Tracts in Advanced Robotics*, pages 425–438. Springer International Publishing, 2015.

G. Oriolo and Y. Nakamura. Free-joint manipulators: Motion control under second-order nonholonomic constraints. *Proceedings of IEEE International Workshop on Intelligent Robots and Systems, Osaka, Japan*, pages 1248–1253, 1991.

T. Ortmaier and G. Hirzinger. Cartesian control issues for minimally invasive robot surgery. In *Proc. IEEE/RSJ Int. Conf. on Intel. Rob. and Syst.*, pages 565–571, Takamatsu, Japan, 31 Oct. - 5 Nov. 2000.

Marc Pansu and Jacques Gautheyrou. *Handbook of soil analysis: mineralogical, organic and inorganic methods*. Springer Science & Business Media, 2007.

F. C. Park and J. W. Kim. Singularity analysis of closed kinematic chains. *Journal of Mechanical Design*, 121(1):32–38, 1999. ISSN 1050-0472. doi: 10.1115/1.2829426. URL `http://dx.doi.org/10.1115/1.2829426`. 10.1115/1.2829426.

F.C. Park and J. W. Kim. Manipulability and singularity analysis of multiple robot systems: a geometric approach. In *Robotics and Automation, 1998. Proceedings. 1998 IEEE International Conference on*, volume 2, pages 1032–1037 vol.2, 1998. doi: 10.1109/ROBOT.1998.677224.

J. Park and O. Khatib. Robust haptic teleoperation of a mobile manipulation platform, 2006.

O. Pfeiffer, A. Ayre, and C. Keydel. *Embedded Networking with CAN and CANopen*. Copperhill Technologies Corporation, 2008. ISBN 9780976511625. URL `https://books.google.no/books?id=CstN61COZe4C`.

Cong Dung Pham and Pål Johan From. Control allocation for mobile manipulators with on-board cameras. In *Proc. of IEEE/RSJ International Conference on Intelligent Robots and Systems (IROS)*, pages 5002–5008, Tokyo, Japan, 3-8 Nov. 2013.

Cong Dung Pham and Pål Johan From. Dynamic manipulability of velocity-constrained serial robotic manipulators. In *IEEE International Conference on Robotics and Biomimetics*, pages 2012–2018, 2014.

Cong Dung Pham, Fernando Coutinho, Fernando Lizarralde, Liu Hsu, and Pål Johan From. An analytical approach to operational space control of robotic manipulators with kinematic constraints. In *19th World Congress of the International Federation of Automatic Control*, pages 8509–8515, Cape Town, South Africa, 24-29 Aug. 2014a.

Cong Dung Pham, Pål Johan From, and Jan Tommy Gravdahl. A geometric approach to the design of serial and parallel manipulators with passive joints. *Applied Mathematics*, 5(16):2585–2601, 2014b. ISSN 2152-7393.

Cong Dung Pham, Huynh Nhat Trinh Phan, and Pål Johan From. Evaluation of subjective and objective performance metrics for haptically controlled robotic systems. *Modeling, Identification and Control*, 35(3):147–157, 2014c. ISSN 0332-7353.

Cong Dung Pham, Huynh Nhat Trinh Phan, and Pål Johan From. Comparison of mental and theoretical evaluations of remotely controlled mobile manipulators. In *19th World Congress of the International Federation of Automatic Control*, pages 326–331, Cape Town, South Africa, 24-29 Aug. 2014d. Elsevier IFAC Publications / IFAC Proceedings series.

Cong Dung Pham, Fernando Coutinho, Antonio Leite, Fernando Lizarralde, Pål Johan From, and Rolf Johansson. Analysis of a moving remote center of motion for robotics-assisted minimally invasive surgery. In *IEEE/RSJ International Conference on Intelligent Robots and Systems*, 2015.

Morgan Quigley, Ken Conley, Brian Gerkey, Josh Faust, Tully Foote, Jeremy Leibs, Rob Wheeler, and Andrew Y Ng. Ros: an open-source robot operating system. In *ICRA workshop on open source software*, volume 3, page 5, 2009.

M. H. Raibert and J. J. Craig. Hybrid position/force control of manipulators. *Journal of Dynamic Systems, Measurement, and Control*, 103(2):126–133, 1981. ISSN 0022-0434. doi: 10.1115/1.3139652. URL `http://dx.doi.org/10.1115/1.3139652`. 10.1115/1.3139652.

W.S. Rasband. Imagej. U. S. National Institutes of Health, Bethesda, Maryland, USA, `http://imagej.nih.gov/ij/`, 1997-2014.

J. M. Rico, J Gallardo, and B Ravani. Lie algebra and the mobility of kinematic chains. *Journal of Robotic Systems*, 20(8):477–499, 2003.

J. M. Rico, L. D. Aguilera, J. Gallardo, R. Rodriguez, H. Orozco, and J. M. Barrera. A more general mobility criterion for parallel mechanisms. *Journal of Mechanical Design*, 128(1):207–219, 2006.

Arno Rook and Jeroen Hogema. Effects of human-machine interface design for intelligent speed adaptation on driving behavior and acceptance. *Transportation Research Record: Journal of the Transportation Research Board*, 1937(-1):79–86, 2005.

Tracy Ross and Gary Burnett. Evaluating the human–machine interface to vehicle navigation systems as an example of ubiquitous computing. *International Journal of Human-Computer Studies*, 55(4):661 – 674, 2001. ISSN 1071-5819. doi: http://dx.doi.org/10.1006/ijhc.2001.0495.

S. Rubio, E. Diaz, J. Martin, and J. M. Puente. Evaluation of subjective mental workload: A comparison of swat, nasa-tlx, and workload profile methods. *Applied Psychology*, 53(1):61–86, 2004.

A. Ruckelshausen, P. Biber, M. Dorna, H. Gremmes, R. Klose, A. Linz, F. Rahe, R. Resch, M. Thiel, D. Trautz, and U. Weiss. Bonirob: an autonomous field robot platform for individual plant phenotyping. *Precision agriculture*, 9(841), 2009.

P. T. Sarrus. Note sur la transformation des mouvements rectilignes alternatifs, en mouvements circulaires; et reciproquement. *Academie des sciences, comtes rendus hebdomataires des seances*, 36:1036–1038, 1853.

J. T. Schwartz and M. Sharir. On the "piano movers" problem i. the case of a two-dimensional rigid polygonal body moving amidst polygonal barriers. *Communications on Pure and Applied Mathematics*, 36(3):345–398, 1983a.

J. T. Schwartz and M. Sharir. On the "piano movers" problem ii. general techniques for computing topological properties of real algebraic manifolds. *Advances in Applied Mathematics*, 4:298–351, 1983b.

H. Seraji. A unified approach to motion control of mobile manipulators. *International Journal of Robotics Research*, 17(2):107–118, 1998.

B. Siciliano, L. Sciavicco, L. Villani, and G. Oriolo. *Robotics: Modelling, Planning and Control*. Advanced Textbooks in Control and Signal Processing. Springer, 2011.

Bruno Siciliano and Oussama Khatib. *Springer handbook of robotics*. Springer Science & Business Media, 2008.

Dimitrios Stefanidis, Fikre Wang, James R Korndorffer Jr, J Bruce Dunne, and Daniel J Scott. Robotic assistance improves intracorporeal suturing performance and safety in the operating room while decreasing operator workload. *Surgical endoscopy*, 24(2): 377–382, 2010.

Aaron Steinfeld, Terrence Fong, David Kaber, Michael Lewis, Jean Scholtz, Alan Schultz, and Michael Goodrich. Common metrics for human-robot interaction. In *Proceedings of the 1st ACM SIGCHI/SIGART conference on Human-robot interaction*, pages 33–40. ACM, 2006.

R. Tinós and M. H. Terra. Control of cooperative manipulators with passive joints. *American Control Conference, Anchorage, Alaska, USA*, pages 1129–1134, 2002.

Renato Tinós, Marco Henrique Terra, and Marcel Bergerman. A fault tolerance framework for cooperative robotic manipulators. *Control Engineering Practice*, 15:615–625, 2007.

L. V. Vargas, A. C. Leite, and R. R. Costa. Overcoming kinematic singularities with the filtered inverse approach. In *19th World Congress of the International Federation of Automatic Control*, pages 8496–8502, Cape Town, South Africa, 24-29 Aug. 2014.

W. Voss. *A Comprehensible Guide to Controller Area Network*. Copperhill Technologies Corporation, 2005. ISBN 9780976511601. URL `https://books.google.no/books?id=PU6ppO3XbUwC`.

J.D. Wason and J.T. Wen. Robot raconteur: A communication architecture and library for robotic and automation systems. In *Prof. IEEE Conf. on Autom. Science & Eng.*, pages 761–766, Trieste, Italy, 24-27 Aug 2011. doi: 10.1109/CASE.2011.6042513.

J. Weiner, P. Stoll, H. Muller-Landau, and A. Jasentuliyana. The effects of density, spatial pattern, and competitive symmetry on size variation in simulated plant populations. *The American Naturalist*, 158(4):pp. 438–450, 2001a. ISSN 00030147.

Jacob Weiner, Hans-Werner Griepentrog, and Lars Kristensen. Suppression of weeds by spring wheat triticumaestivum increases with crop density and spatial uniformity. *Journal of Applied Ecology*, 38(4):784–790, 2001b. ISSN 1365-2664.

J. Wen and L.S. Wilfinger. Kinematic manipulability of general constrained rigid multibody systems. *Robotics and Automation, IEEE Transactions on*, 15(3):558–567, 1999. ISSN 1042-296X. doi: 10.1109/70.768187.

M. R. Wrock and S. B. Nokleby. Decoupled teleoperation of a holonomic mobile-manipulator system using automatic switching. In *Electrical and Computer Engineering (CCECE), 2011 24th Canadian Conference on*, pages 001164–001168, 2011.

T. Yoshikawa. Dynamic manipulability of robot manipulators. *International Journal of Robotics Research*, 4:3–9, 1985a. doi: 10.1177/027836498500400201.

T. Yoshikawa. Manipulability of robot manipulators. In *Robotics and Automation. Proceedings. 1985 IEEE International Conference on*, volume 2, pages 1033–1038, 1985b. doi: 10.1109/ROBOT.1985.1087277.

T. Yoshikawa. Singular-value decomposition. *Foundations of Robotics:Analysis and Control, MIT Press*, 2003.